Sites M0001–M0004[1]

Expedition 302 Scientists[2]

Chapter contents

[1]Expedition 302 Scientists, 2006. Sites M0001–M0004. *In* Backman, J., Moran, K., McInroy, D.B., Mayer, L.A., and the Expedition 302 Scientists. *Proc. IODP,* 302: College Station TX (Integrated Ocean Drilling Program Management International, Inc.). doi:10.2204/iodp.proc.302.104.2006
[2]**Expedition 302 Scientists' addresses.**

Operations

Mobilization of *Vidar Viking*, Aberdeen, Scotland

The *Vidar Viking* came under contract on 22 July 2004, when mobilization began in Aberdeen, Scotland. Mobilization in Aberdeen included two major installations: a moonpool and a full coring/drilling spread. By 26 July, all equipment for the *Vidar Viking* had arrived, including information technology equipment bound for the *Oden*. The derrick was load-tested and certified. The *Vidar Viking* took on a full complement of fuel at Aberdeen.

Test Coring Site: Witch Ground, North Sea

The *Vidar Viking* set sail for Landskrona, Sweden, on 28 July 2004. While the ship was en route, a first test of the drilling equipment was conducted in the Witch Ground area of the North Sea, ~8 h steam from Aberdeen. A test borehole was drilled in 152 m water depth to a depth of 37 meters below seafloor (mbsf) using the British Geological Survey's (BGS's) advanced piston corer (APC) and extended core barrel. Cores were obtained with both systems. The APC recovered >4 m in all runs (maximum = 4.5 m). The *Vidar Viking* left the test coring site at 1900 h on 30 July and proceeded to Landskrona.

Meanwhile, mobilization of the *Oden* proceeded at Gothenburg, Sweden, which included loading the laboratory equipment. On the evening of 31 July, the *Oden* set sail for Tromsø, Norway.

Mobilization of *Vidar Viking*, Landskrona, Sweden

The *Vidar Viking* reached Landskrona on the morning of 1 August 2004. The stern notch, a 100 ton section required by the *Vidar Viking* when working in ice, and the helideck were installed. The remaining containers were loaded onto the deck, including the core and European Consortium for Ocean Research Drilling Science Operator curation containers sent from Bremen, Germany. Other mobilization work continued until the morning of 3 August, when the *Vidar Viking* departed for Tromsø.

Mobilization of *Vidar Viking* and *Oden*, Tromsø, Norway

The *Oden* arrived in Tromsø on the evening of 5 August 2004. The *Vidar Viking* arrived on the morning of 7 August. Two helicopters,

doi:10.2204/iodp.proc.302.104.2006

required for ice reconnaissance missions, landed on the *Oden* and were secured.

Rendezvous of three Expedition 302 ships

Expedition 302 officially began when the *Oden* left Tromsø, Norway, at 2350 h on 7 August 2004. The *Vidar Viking* remained in Tromsø for the next 12 h to wait for dynamic positioning spare parts to arrive.

The *Oden* transited to 81°56′N, 44°59′E to meet the other two ships in the Arctic Coring Expedition fleet for Expedition 302, the *Sovetskiy Soyuz* and the *Vidar Viking*, at the edge of the polar ice pack on 10 August. The fleet entered the ice together with the *Sovetskiy Soyuz* leading, the *Oden* following, and the *Vidar Viking* bringing up the rear.

Transit to first site

During the transit to the operational area, ice reconnaissance and personnel transfer flights began on 12 August 2004. The fleet made unprecedented headway of 8–10 kt in sea ice.

The fleet arrived on site at 2350 h on 13 August and began preparations for drilling and operations for maintaining position in sea ice.

Preparations for drilling began with clearing ice from the moonpool. Once this was done, a steel skirt was deployed through and below the moonpool to protect the drill string from ice impact below the hull. Once the ice protection skirt was in place, the drill floor and iron roughneck were installed. The drill floor was ready for operations by 0900 h on 15 August.

During this time, the fleet's ability to maintain station was tested by positioning the *Sovetskiy Soyuz* and the *Oden* upstream of the *Vidar Viking*. The initial stationkeeping tests were successful, and the Fleet Manager gave approval to start drilling operations at 1100 h on 15 August.

Site operations

Cores were recovered in five holes (Holes M0002A, M0003A, M0004A, M0004B, and M0004C) (Table **T1**). Hole M0001A was abandoned after the bottomhole assembly (BHA) was lost. Logging was attempted in two holes and data were collected in Hole M0004B.

Table **T2** documents the allocation of time, broken down into (1) waiting for better ice conditions, (2) operational breakdown, and (3) drilling operations.

Waiting for better ice conditions was labeled "W." If waiting on ice conditions required pulling pipe and subsequent preparations to begin drilling operations, these times were included in the W category because that time delay was caused by the "waiting for ice" situation. "Breakdown time" is defined as operational time consumed as a result of equipment or mechanical failure. The loss of a BHA, for example, regardless if caused by human error or mechanical failure, necessitated a drill string trip. If the trip time was caused by equipment failure, it was considered as breakdown time "B."

Site M0001 (SP 2720 on Line AWI 91090)

Site M0001 (shotpoint [SP] 2720 on Line AWI 91090) was reached at 1100 h on 15 August 2004. Later that day during drill string deployment, the high-pressure mud valve on the top drive was damaged. The valve was removed, the rest of the drill string was run, and then the broken valve was replaced. Pipe trips were slowed or stopped intermittently to allow overheated hydraulic fluid in the new drill rig to cool.

By 16 August, the drill string was deployed to the seafloor and the first piston corer was deployed at 0600 h. After pumping for 30 min, pressure was not obtained and the piston corer was retrieved without having fired. Damaged seals on the piston corer were replaced. Ice conditions were marginal, and at 0900 h operations were stopped and the drill string was lifted from the seabed. Ice conditions improved by 1400 h, and operations continued. The piston corer was deployed again, and no pressure developed in the drill string. Upon retrieval, the piston corer had not fired. It was suspected that the piston corer had not latched into the BHA. The extended core barrel was then deployed but was not recovered, which indicated that the BHA was lost. At 2000 h, the drill string was tripped to the surface and the BHA and extended core barrel losses were confirmed.

Beginning early on 17 August, a new BHA was assembled and lowering of the drill string began. When >800 m was deployed, the high-pressure mud valve on the swivel was damaged during pipe handling. The drill string was tripped to the surface because the operator did not want to risk leaving the drill string hanging in the water column for an unspecified period of time. After completing the pipe trip, the damage was assessed and the *Oden's* chief engineer was tasked with manufacturing a new valve using materials from a spare pup joint. As an interim solution, a conventional valve assembly was installed, which restricted operations so that no piston core could be deployed.

Ice conditions deteriorated between 0900 and 2200 h, and the time was utilized to move the *Vidar Viking* to a new position (Hole M0002A). Because there were no mud valve spares, the Swedish Polar Research Secretariat began making arrangements for a

Swedish Air Force C-130 airdrop of two new valve parts and one conventional valve assembly.

Site M0002 (SP 2560 on Line AWI-91090)

Based on a strategy developed by the ice management team, the drill string was lowered while drifting onto the location of Site M0002. By 2200 h on 18 August 2004, this strategy put the *Vidar Viking* within 190 m of the proposed site. The final positioning was done by icebreaking this short distance to Hole M0002A. Once on location at 0820 h, three more drill pipes were added and coring started. Because the mud valve was not yet repaired, the extended core barrel was deployed instead of the APC. A first attempt at coring was unsuccessful, but after adding more pipe and drilling another core run, some core was retrieved. The first core on deck arrived at 1335 h at a water depth of 1209 m. Drilling operations continued throughout the afternoon. The newly fabricated mud valve from the *Oden* arrived late in the afternoon, and preparations were made for its installation during a wireline trip. The temporary valve was replaced before more drill pipe was added for the next core run. By midnight on 19 August, a depth of 31 mbsf had been reached.

Drilling and extended core barrel coring continued until 23 August (Table **T1**) when the Fleet Manager ordered the drill pipe to be pulled to 40 mbsf because ice conditions had deteriorated. Permission to continue drilling operations was given midday, and operations continued until 2100 h when the ice conditions forced the termination of Hole M0002A at a depth of 271.69 m.

The drill string was tripped to the drill deck during the morning of 24 August. After waiting for ice conditions to change in the afternoon, a transit began at 1930 h to a position from which the *Vidar Viking* could drift onto location while tripping in the drill string.

While we waited for improved ice conditions and operations set up for the next site continued, an air gun seismic survey was run from the *Oden* to tie Site M0002 to the next site (Site M0003).

Site M0003 (SP 2521 on Line AWI-91090)

The *Vidar Viking* reached the ice-drift position at 2100 h and awaited ice reconnaissance results. The iron roughneck, which had been removed to repair oil leaks, was installed after repairs; the ice protector skirt was lowered; and the drill floor was prepared. At 2300 h, the BHA and drill collars were run. At 0240 h on 25 August 2004, after 400 m of pipe had been deployed, the housing of the iron roughneck cracked and had to be removed for major repairs. Operations resumed at 1400 h using power tongs. The seafloor was reached at ~2300 h, and at 0110 h on 26 August, the first APC core was recovered from Hole M0003A (Table **T1**).

A second APC core with a shattered liner was recovered. The third APC core became stuck in the BHA. While trying to release the corer, the wireline parted at the mechanical termination, and it was necessary to pull the string. Hole M0003A was terminated at 0440 h.

The ice management team conducted ice reconnaissance surveys, reviewed options, and recommended that the fleet move to a location farther west, where a longer-term prediction of relatively good ice could be made. Once the site was selected, the ice team predicted an upstream ice position for the *Vidar Viking* to start to drift onto the new location. The fleet steamed to the updrift ice position, arriving at 0630 h on 27 August. During this time, wireline termination repair, APC service, and iron roughneck testing and refitting took place.

Site M0004 (SP 3006 [Holes M0004A and M0004B] and 3004 [Hole M0004C] on Line AWI-91090)

At 0755 h on 27 August 2004 during the pipe trip to the seafloor, the high-pressure mud valve was damaged again. The valve was removed, and the remaining string was run to 1150 m depth while the valve was repaired. At 1800 h, the *Vidar Viking* was on location (Hole M0004A). Once on station, the repaired mud valve was installed and the drill string was run to the seabed. At 2230 h, drilling operations in Hole M0004A commenced and the hole was advanced by washing ahead to 17 mbsf (Table **T1**) before a piston corer was deployed.

Shortly after midnight on 28 August 2004, the APC became stuck in the BHA but was freed after ~1 h. Once on deck, the plastic liner in the core barrel was found to be shattered and 3.5 m of the core was stuck in the barrel. In light of these problems with the APC—in particular, the risk of junking the hole again—it was decided to switch to extended core barrel coring. Two extended core barrel cores were recovered to a depth of 30.5 mbsf followed by washing to 265 mbsf using the insert bit. This decision to wash ahead was made in order to recover sediment deeper than that recovered in Hole M0002A. By 2240 h, a depth of 265 mbsf was reached.

Extended core barrel coring operations continued for the next 3 days (29–31 August), where the hole was advanced at varying rates with good to poor recovery. During this time, the drilling was very slow (e.g., 1 m/h) and recovery in many cores was zero (Cores 302-M0004A-13X through 18X). Different strategies

were tried to improve the advance rate. At times, the hole was advanced by washing ahead in an attempt to make faster progress but this strategy was ultimately abandoned after it was found that the washing rate was almost the same as the coring rate. On 31 August from 0200 to 0500 h, for two coring runs in a row no core was recovered. The extended core barrel shoe was switched to a coring shoe for a third attempt at recovery. This coring run cleared a blockage in the bit as evidenced by a large drop in pump pressure. Following this core (with good recovery) and after clearing the blocked bit, core recovery and advancement improved over the next 12 h until basement was reached in Core 302-M0004A-35X. Basement penetration was difficult (8 m penetration in 12 h with low core recovery), and a decision was made at 0900 on 1 September to stop coring at a total depth of 428 mbsf and conduct logging in Hole M0004A.

The logging tools were moved to the rig floor, and the tool string (Formation MicroScanner–Accelerator Porosity Sonde–Natural Gamma Ray Spectroscopy Tool–Scintillation Gamma Ray Tool [FMS-APS-NGT-SGT]) and wireline rig-up proceeded simultaneously. The run into hole commenced at 2130 h. This was done at low speed in order to allow the tools to warm up. Communication with the tool was initially established, and it was lowered to the end of the drill pipe. A computer malfunction caused a communication loss to the tools. The problem was corrected by 0200 h. The tool was powered up, and attempts were made to get the tool to pass through the BHA into the open hole. All efforts failed at the same depth (~1366 meters below rig floor [mbrf]); so, while at rest at this depth, the calipers were opened on the FMS to check whether it was free or lodged. The calipers had some movement, which indicated that the tool string was free.

The landing ring for the core barrel is the narrowest section of the whole pipe string (95 mm) and lies ~6 m above the bit. All the logging tools had been checked through a landing ring dockside in Aberdeen, but there was no hole calibration ring on board that could be used as a second check. Sequentially, four more logging attempts were made. Each time, it was assumed that the logging tools were too large in diameter and the string diameter was further reduced by removing the larger diameter components. The APS bowspring was removed first, followed by the knuckle joint. Finally, only the narrowest velocity-density string was deployed, which failed to clear the bit at the same depth as the previous runs. After the fifth attempt failed, the logging time allocated had been consumed and attempts to log Hole M0004A ended at 1045 h on 2 September.

After the logging gear was cleared away and the drill string was lifted out of the seabed, preparations were made to start a second hole (Hole M0004B) at the site. During preparations, the inner barrel was deployed but did not latch. After an improvised downhole hammer was deployed and worked for 2 h, a short length of core (~10 cm of mudstone), which had been partially blocking the BHA, was recovered.

By 2030 h on 2 September, the *Vidar Viking* was at the new position for the next hole (Hole M0004B). Coring in Hole M0004B started at a depth of 10 mbsf using the extended core barrel because the APC was deemed too risky. After retrieving the first sample, the hole was washed to 20 mbsf for an in situ temperature measurement. The BGS temperature probe was lowered to the base of the hole, pushed into the sediment, and programmed to record the temperature every 5 s. The probe was left to record temperature for 40 min, after which it was retrieved. Plans to wash to a depth of 215 mbsf, core to 230 mbsf, and then wash to 250 mbsf and log were stymied by problems with drilling pressure lines/gauges freezing at –10°C. Because of these problems and the limited time left, the hole was only advanced to a depth of 220 mbsf. Temperature measurements were made at 60 and 100 mbsf.

At 0000 h on 4 September, the pipe was pulled to 65 mbsf to prepare for logging. Rigging of the wireline and tool string occurred concurrently, and rig-up of both was completed by 0415 h. The tool string comprised the FMS-Borehole Compensated Sonic (BHC)-NGT-SGT; the choice of tools was such that it could be run as a straight-through tool string without the need for articulation and eccentralization subs. The logging string was run slowly to the bit to warm the tools before powering them up. The logging string passed through the bit at 0530 h, and the first pass was completed at 0610 h. Logging operations were completed at 0710 h. Rig-down of the logging tool and wireline was completed by 0905 h, and preparations began for a third hole (Hole M0004C).

Hole M0004C was spudded at 1200 h on 4 September, and the first APC core was recovered at 1420 h. Two more APC cores were recovered during the next 10 h. An attempt to make a temperature measurement at 9 mbsf using the Adara tool on the APC failed because of a dead battery. At a depth of 14 mbsf, the APC core barrel became stuck after being fired. The period from midnight to 0530 h on 5 September was spent trying to retrieve the piston tool. Various attempts to recover the tool included flush only, hoist only, mixture of flush and hoist, and hoist and leave at top of hoist for some time. The APC was freed and recovered by 0530 h, and the barrel was slightly bent (the liner was easily removed).

Because of the risk of getting stuck again, coring continued using the extended core barrel with a modified Adara shoe to complete two more temperature measurements to a depth of 37 mbsf. Drilling operations ended at 1500 h. The drill string was retrieved by 0500 h on 6 September.

The *Oden* came alongside the *Vidar Viking* to transfer 400 tons of fuel, and all three ships carried out required maintenance before the return transit. A seismic survey was attempted from the *Oden* but was abandoned because of difficult ice conditions. The operational phase of the expedition ended, and the return transit began.

Transit from Expedition 302 coring sites to Tromsø, Norway

The convoy left the study area at 1930 h on 6 September 2004 and headed toward the North Pole. Progress was slow in the first half of the day but improved later, and the fleet arrived at the Pole at ~2230 h. The convoy departed at 0100 h on 7 September and made good progress toward Tromsø in almost continuous open water. The *Oden* arrived in Tromsø at 2300 h on Tuesday 13 September.

The *Vidar Viking* parted company with the *Oden* at the ice edge in the early hours of 11 September and headed due south. A crew change and demobilization were effected in Tanager, Norway, on 16 and 17 September. The *Vidar Viking* then sailed for Landskrona in Sweden, where the helideck was removed, together with the core and curation containers and the deep freeze samples. BGS/Seacore personnel continued the reconstruction of the deck, while vessel and shipyard personnel removed the moonpool and other expedition-linked items.

On 22 September, the *Vidar Viking* sailed for Aberdeen, Scotland, to complete the demobilization. Upon arrival in Aberdeen at 0800 h on 24 September, the remainder of the expedition equipment was demobilized and the vessel was cleared for her next charter by 2200 h that day. Formal end of charter, following tank cleaning and reinstatement and offhire recertification, was completed on 25 September.

Lithostratigraphy

Sediments recovered from Expedition 302 Sites M0002, M0003, and M0004 span 0 to 427.6 mbsf and range in age from Holocene to Late Cretaceous. There is no lithologic description for Site M0001, as this site was abandoned after recovering a single core catcher. The suite of sites are treated as a single stratigraphic section based on correlative seismic signatures, logging and physical properties, chemostratigraphies, lithostratigraphies, and biostratigraphies of these closely spaced sites.

Four lithologic units (Table **T3**) are defined on the basis of color, texture, and compositional variations identified from visual core description and smear slide analysis (Figs. **F1, F2**), as well as X-ray diffraction (XRD) (Fig. **F3**) and total organic carbon (TOC) content analyses (Fig. **F40**). A first-order observation of downcore compositional variations, which helped define the lithostratigraphic units, is a shift from siliciclastic-dominated (Unit 1) to biogenic-dominated (Unit 2) and back to siliciclastic-dominated (Unit 3) lithologies. Unit 4 was distinguished from Unit 3 based on an abrupt coarsening of the sediment texture following an interval of poor core recovery. Second-order observations of a textural and compositional nature, including variation in the amount of sand, biogenic carbonate and silica, pyrite, TOC, and a downcore shift in sediment color from generally brown to olive, back to brown, and then to gray and black, enabled further differentiation of subunits within Unit 1.

Lithostratigraphic Unit 1

Intervals: Sections 302-M0002A-1X-1, 0 cm, through 51X-1, 150 cm; 302-M0003A-1H-1, 0 cm, through 3H-CC, 5 cm; 302-M0004A-1H-1, 0 cm, through 3X-2, 128 cm; 302-M0004B-1X-1, 0 cm, through 1X-2, 85 cm; 302-M0004B-3X-1, 0 cm, through 3X-CC, 25 cm; and 302-M0004C-1H-1, 0 cm, through 9X-CC, 25 cm

Depths: Hole M0002A: 0–220.24 mbsf, Hole M0003A: 0–15 mbsf, Hole M0004A: 17.0–28.28 mbsf, Hole M0004B: 10.0–12.29 and 215.0–219.0 mbsf, and Hole M0004C: 0–36.66 mbsf

Age: Holocene to middle Eocene

Lithology: silty clay, silty mud, and clayey silt

Unit 1 (0.01–220.24 mbsf; Hole M0002A) is characterized by siliciclastic sediments, color banding, sandy lenses, and isolated pebbles. The dominant lithology of Unit 1 is silty clay. The top of Unit 1 contains small amounts of biogenic carbonate, whereas the base of Unit 1 contains small amounts of biogenic silica (Table **T3**). Smear slide analyses indicate that clay minerals, quartz, and feldspar constitute the major siliciclastic components. Other mineral components include pyrite, accessory minerals, mica, opaque minerals, and siderite. Volcanic glass is also present in trace amounts. TOC content generally increases downcore in Unit 1, ranging from <0.5 wt% near the top of Unit 1 to 2–3 wt% at the base (see **"Geochemistry"**). Isolated pebbles occur throughout Unit 1 (Table **T4**).

Unit 1 ranges in color primarily from brown to olive and back to brown above 192.94 mbsf (Section 302-M0002A-44X-1, 95 cm) and is gray to very dark gray or black below this level. Color banding of variable thicknesses (centimeters to meters) is common throughout the upper 196.2 mbsf (Section 302-M0002A-45X-1, 24 cm). These color bands generally have horizontal sharp to gradational (mottled) contacts. From 196.2 to 198.13 mbsf (Section 302-M0002A-46X-1, 113 cm), color banding is quite different from the overlying sediments. This interval is characterized by variably tilted, black to gray couplets, often with sharp basal contacts, which truncate underlying couplets. From 198.13 mbsf to the base of Unit 1, color banding is absent.

The abrupt downcore color shift to darker (grayer) lithologies at 192.94 mbsf is associated with a gradual increase in microconcretions and pyrite content and decrease in millimeter- to centimeter-scale sandy lenses (absent below Section 302-M0002A-46X-1, 58.5 cm; 197.59 mbsf). Dark gray to black millimeter- to gravel-size concretions first occur at 131.09 mbsf (Section 302-M0002A-29X-2, 141 cm). Distinct millimeter- and centimeter-size metallic yellow pyrite concretions and burrow infillings then appear from Section 302-M0002A-44X-2, 27 cm, through 44X-4, 12 cm (195.93 mbsf). Concretions are absent in Unit 1 below this depth. However, disseminated pyrite is a significant bulk mineral component of Unit 1 downcore from 198.13 mbsf (Section 302-M0002A-46X-1, 113 cm) according to smear slide and XRD data (Figs. **F2A, F3**). Unit 1 is divided into six subunits reflecting these changes in texture, composition, and color.

Subunit 1/1

Intervals: Sections 302-M0002A-1X-1, 0 cm, through 2X-1, 108 cm; 302-M0003A-1H-1, 0 cm, through 1H-1, 110 cm; and 302-M0004C-1H-1, 0 cm, through 2H-1, 129 cm

Depths: Hole M0002A: 0–2.58 mbsf, Hole M0003A: 0–1.1 mbsf, and Hole M0004C: 0–2.59 mbsf

Age: Holocene to late Pleistocene

Lithology: silty clay, silty mud, and sandy mud

Subunit 1/1 comprises silty clay, silty mud, and sandy mud with strong color banding including brown (10YR 4/3), yellowish brown (10YR 5/4), light olive-brown (2.5Y 5/4), light reddish brown (5YR 6/4), gray (2.5Y 6N 6/0), pale brown (10YR 6/3), light yellowish brown (2.5Y 6/4), dark brown (10YR 4/3), olive-gray (5Y 4/7), olive (5Y 5/4), dark yellowish brown (10YR 4/6), and dark gray (10YR 4/1). Color bands range in thickness from 2 to 50 cm, generally with sharp contacts between them. Bioturbation is slight throughout the unit. Smear slide analyses indicate minor amounts of biogenic carbonate. Isolated pebbles (0.5–1.0 cm in diameter) occur throughout the subunit. TOC content is <0.5 wt%.

Subunit 1/2

Intervals: Sections 302-M0002A-2X-1, 108 cm, through 5X-1, 88 cm; 302-M0003A-1H-1, 110 cm, through 3H-CC, 15 cm; 302-M0004A-1H-1, 0 cm, through 2X-1, 118 cm; 302-M0004B-1X-1, 0 cm, through 1X-2, 85 cm; and 302-M0004C-2H-1, 129 cm, through 6X-1, 2 cm

Depths: Hole M0002A: 2.58–17.38 mbsf, Hole M0003A: 1.1–15.0 mbsf, Hole M0004A: 17.0–21.68 mbsf, Hole M0004B: 10.0–12.29 mbsf, and Hole M0004C: 5.29–23.59 mbsf

Age: late Pleistocene

Lithology: silty clay

The main lithologic distinction between Subunits 1/1 and 1/2 is textural. The major lithology of Subunit 1/2 is silty clay and therefore contains less sand than Subunit 1/1, which includes lithologies of silty clay, silty mud, and sandy mud. Light olive-brown (2.5Y 5/4) silty clay with olive-brown (2.5Y 4/4) thin to medium banding is present in the upper part of Subunit 1/2, and dark brown (10YR 4/3) and yellowish brown (10YR 5/4) silty clay with centimeter-scale, very dark gray mottling is present in the lower part of Subunit 1/2. Isolated pebbles and millimeter- to centimeter-scale sand lenses are present throughout. A 7 cm interval of yellow (10YR 7/6) clay with a sharp upper and gradational basal contact is present in interval 302-M0003A-1H-3, 107–114 cm. Light olive-brown (2.5Y 5/4) silty mud is present in minor amounts in interval 302-M0004C-4H-1, 74–68 cm.

This subunit is slightly to moderately bioturbated throughout. A *Thalassinoides* burrow is present in interval 302-M0003A-1H-3, 10–20 cm, and several *Chondrites* burrows are present in Core 302-M0004C-3H. Minor amounts of biogenic carbonate are present in Subunit 1/2. TOC content of Subunit 1/2 is <0.5 wt%. Drilling disturbance is common, with slurry and flow-in in Sections 302-M0002A-3X-1 through 3X-4 and 4X1-1 through 4X-4.

Subunit 1/3

Intervals: Sections 302-M0002A-5X-1, 88 cm, through 38X-3, 45 cm; 302-M0004A-2X-1, 118 cm, through 3X-2, 128 cm; and 302-M0004C-6X-1, 2 cm, through 9X-CC, 25 cm

Depths: Hole M0002A: 17.38–168.53 mbsf, Hole M0004A: 21.38–28.28 mbsf, and Hole M0004C: 23.59– 36.66 mbsf

Age: Pleistocene to middle Miocene

Lithology: silty clay and silty mud

The lithostratigraphic distinction between Subunit 1/3 and overlying Subunit 1/2 is primarily based on downcore sediment coarsening, a brown to olive color transition, and an absence of biogenic carbonate.

Silty clay and silty mud with alternating olive (5Y 5/3, 5Y 4/3, and 5Y 5/6), gray (5Y 5/1), olive-gray (5Y 5/2 and 5Y 4/2), olive-brown (2.5Y 4/4), dark gray (2.5Y N4/1, 2.5Y N4/0, and 5Y 4/1) and light olive-brown (2.5Y 5/4) color bands are found at scales ranging from decimeters to meters, sometimes with mottled contacts between them. Some intervals are characterized by thin centimeter-scale color banding. Short intervals of gray (5Y 5/1) to olive-brown (2.5Y 4/4) sandy mud occur in intervals 302-M0002A-32X-2, 11–18 cm, 32X-3, 26–32 cm, and 302-M0004C-6X-2, 46–47 cm. Millimeter- to centimeter-scale sand lenses and isolated pebbles occur throughout. Millimeter-scale dark gray to black microconcretions are occasionally present from Section 302-M0002A-29X-2, 141 cm, through the base of the subunit. An interval of firm sediment occurs from Section 302-M0002A-30X-1, 0 cm, through 31X-CC. Bioturbation is slight to moderate with well-defined *Chondrites* burrows in Cores 302-M0002A-17X, 20X, 21X, 32X, and 35X. TOC content is <0.5 wt%. Drilling disturbance in recovered cores is generally minor, although moderate disturbance (biscuiting), slurry, and flow-in occur in discontinuous intervals in Cores 302-M0002A-6X through 12X, within parts of Cores 302-M0002A-16X, 27X, and 32X, and within parts of Cores 302-M0004C-8X through 9X.

Subunit 1/4

Interval: Sections 302-M0002A-38X-3, 45 cm, through 44X-1, 95 cm
Depth: 168.53–192.94 mbsf
Age: middle Miocene
Lithology: silty clay

The lithostratigraphic distinction between Subunit 1/4 and overlying Subunit 1/3 is based on a downcore color change from olive back to brown (Fig. **F4;** somewhat similar to Subunit 1/2), in addition to a slight downcore sediment coarsening, increase in the presence of gray and black microconcretions, and decrease in TOC content.

Subunit 1/4 lithology comprises silty clay, which alternates between dark brown (10YR 4/3 and 10YR 3/3), very dark grayish brown (10YR 3/2), very pale brown (10YR 7/3), and pale yellow (2.5Y 7/4) intervals at scales of decimeters to meters. Millimeter- to centimeter-scale sand lenses (e.g., interval 302-M0002A-38X-4, 100–101 cm) and isolated pebbles are present throughout this subunit. Millimeter-scale dark gray to black microconcretions are common in Core 302-M0002A-39X and below. Bioturbation is slight throughout Subunit 1/4 and includes a *Chondrites* burrow in Section 302-M0002A-42X-3. The brown sediments of Subunit 1/4 between ~170 and ~193 mbsf are barren of all palynomorphs. TOC content is <0.2 wt%.

Subunit 1/5

Interval: Sections 302-M0002A-44X-1, 95 cm, through 46X-1, 113 cm
Depth: 192.94–198.13 mbsf
Age: middle to early Miocene
Lithology: silty clay

The lithostratigraphy of Subunit 1/5 is distinguished from overlying Subunit 1/4 in several ways, including a downcore shift in general sediment color from brown to gray and black, a change to an unusual cyclic color banding pattern that resembles "zebra stripes," a downcore shift from gray/black microconcretions to metallic yellow pyrite microconcretions, and an increase in TOC content. The contact between Subunits 1/4 and 1/5 at 192.94 cm is sharp (Fig. **F5**).

The top of Subunit 1/5 is characterized by light gray (2.5Y N7/0), gray (2.5Y N5/0), and olive-gray (5Y 5/2) silty clay. This interval is slightly bioturbated and contains metallic yellow millimeter- to centimeter-scale pyrite microconcretions. The majority of this subunit is dominated by tilted color bands, or couplets, 0.5 to 3 cm thick, of very dark gray (5Y 3/1) and black (5Y 2.5/1) firm silty clay. The top of this zebra-stripe interval begins at Section 302-M0002A-45X-1, 24 cm, and continues to the base of the subunit. A 0.5 cm thick layer of dark brown (10YR 4/3), hard silty clay (interval 302-M0002A-45X-1, 27.5–28 cm) is present close to the top of the zebra-stripe interval. Packages of couplets within the zebra-stripe interval are tilted, and bases of many of these sediment packages are sharp and truncate (crosscut) the underlying layers as the tilting direction changes (Fig. **F6**). Within individual tilted packages, upper layers also appear to crosscut underlying layers, but some gradational contacts exist as well. The thickness of the couplets and the angle of tilt increases upsection. Bioturbation is absent in the zebra-stripe interval. Millimeter- to centimeter-scale sand lenses and isolated pebbles occur throughout Subunit 1/5. TOC content of Subunit 1/5 is 0.75–1.0 wt%.

Subunit 1/6

Intervals: Sections 302-M0002A-46X-1, 113 cm, through 51X-1, 150 cm; and 302-M0004B-3X-1, 0 cm, through 3X-CC, 25 cm

Depths: Hole M0002A: 198.13–220.24 mbsf and Hole M0004B: 215.0–219 mbsf
Age: middle Miocene to middle Eocene
Lithology: silty clay and clayey silt

The lithostratigraphy of Subunit 1/6 is distinguished from overlying Subunit 1/5 by a downcore change to very dark gray (5Y 3/1), firm to very firm, homogeneous silty clay to clayey silt. Smear slide and XRD data indicate that an abrupt increase in pyrite defines the boundary between Subunits 1/5 and 1/6. XRD data further indicate that a downcore increase in the ratio of kaolinite to chlorite and a decrease in quartz also mark this subunit boundary (Fig. F3). Black millimeter-scale mottling is present in Sections 302-M0002A-46X-3, 36 cm, and 48X-2, 34 cm. A piece of hard very dark grayish brown (10YR 3/2) material, possibly coal, is present in interval 302-M0002A-46X-2, 51–53 cm. Isolated pebbles are present throughout this subunit. Smear slide analyses indicate that siliceous microfossils (diatoms, ebridians, and silicoflagellates) are present in minor amounts toward the base of this Subunit. TOC content of Subunit 1/6 is 2–3 wt%. Moderate drilling disturbance (biscuiting) is common in Core 302-M0002A-48X through Section 50X-1, 29 cm. Slurry occurs below this level to the base of the unit.

Lithostratigraphic Unit 2

Intervals: Sections 302-M0002A-51X-1, 150 cm, through 62X-CC, 11 cm; and 302-M0004A-4X-1, 0 cm, through 15X-1, 26 cm
Depths: Hole M0002A: 220.24–267.71 mbsf and Hole M0004A: 265.0–313.61 mbsf
Age: middle Eocene
Lithology: mud-bearing biosiliceous ooze

Unit 2 (220.24–313.61 mbsf) is dominated by very dark gray (5Y 3/1) mud-bearing biosiliceous ooze. Submillimeter-scale light and dark laminations occur throughout Unit 2, occasionally exhibiting cross bedding that is visible in both undisturbed intervals and within coherent biscuits (e.g., intervals 302-M0002A-60X-3, 60–98 cm, and 302-M0004A-6X-4, 34–38 cm). No bioturbation is visible throughout the unit. Isolated pebbles are observed as deep as Section 302-M0002A-55X-4, 122 cm (239.34 mbsf). Smear slide analyses indicate that dominant components include biosiliceous matrix and microfossils (abundant diatoms, common to rare ebridians, and silicoflagellates). Siliciclastic components are minor. Unlike Units 1, 3, and 4, XRD data indicate that Unit 2 is characterized by the dominance of K-feldspar over plagioclase (Fig. F3). Millimeter-scale pyritized lenses occur in Sections 302-M0002A-52X-2, 5 and 10 cm. TOC content in Unit 2 is generally between 2 and 3 wt%. Within recovered sections, drilling disturbance is highly variable, ranging from undisturbed to slightly rotated drilling biscuits to drilling slurry.

Lithostratigraphic Unit 3

Interval: Sections 302-M0004A-15X-1, 26 cm, through 35X-CC, 18 cm
Depth: 313.61–404.79 mbsf
Age: early Eocene to late Paleocene
Lithology: clay and silty clay

The primary distinction between Units 2 and 3 is the major lithology of mud-bearing biosiliceous ooze (Unit 2) in contrast to clay (Unit 3). In several ways, Unit 3 resembles Subunit 1/6; both are dark gray fine-grained siliciclastic-dominated transitional lithologies that contain pyrite and minor amounts of biogenic silica toward their contacts with Unit 2. Smear slide analyses indicate that siliceous microfossils are present in rare amounts in Sections 302-M0004A-15X-CC, 18X-CC, and 19X-CC. XRD analysis suggests that biogenic opal may be present down to Section 302-M0004A-26X-CC. Geochemical analyses indicate that the fine-grained sediment in the upper part of Unit 3 (to ~350 mbsf) is largely authigenic (silica altered to crystoballite), with only minor terrigenous input. These distinct geochemical changes in Unit 3 are described further in "Geochemistry."

The top of Unit 3 comprises gray (5Y 3/1) to very dark gray (5Y 4/1) firm to very firm clay. From Core 302-M0004A-31X through Core 34X, the sediment coarsens slightly and is dominated by a gray (5Y 3/1) to dark olive-gray (5Y 3/2) silty clay. A 3 cm interval of yellowish brown (10YR 5/4) sandy mud is present in interval 302-M0004A-32X-CC, 6–9 cm, and Section 33X-1 is a very disturbed, dark olive-gray (5Y 3/2) silty mud. Dark olive-gray (5Y 3/2) clay is again present from Core 302-M0004A-35X to the base of the unit. Smear slide analyses indicate that the dominant components in the terrigenous clay and silty clay are, in increasing order, feldspar, pyrite, quartz, and clay minerals. Accessory minerals include minor amounts of zircon.

Submillimeter-scale laminations are present in Cores 302-M0004A-19X through 32X. Millimeter to centimeter-scale pyrite concretions occur in Cores 302-M0004A-27X, 28X, 30X, 32X, 34X, and 35X. A concretion is present near the base of the unit (302-M0004A-31X-CC, 48–50 cm), but this may be a product of core disturbance and could represent part of a harder underlying interval that was not well recovered. Slight bioturbation occurs in parts of Cores 302-M0004A-27X, 28X, 29X, 30X, 34X, and 35X. TOC content in Unit 3 is generally between 1 and 2.5 wt%. Drilling disturbance (biscuiting) is moderate in Cores 302-M0004A-19X to 34X.

Lithostratigraphic Unit 4

Interval: Sections 302-M0004A-41X-1, 0 cm, through 42X-CC, 17 cm

Depth: 424.50–427.63 mbsf

Age: Late Cretaceous

Lithology: clayey mud, silty clay, and silty sand

Loose coarse sand was recovered in Section 302-M0004A-39X-CC and was bagged at sea. Because the stratigraphic position of this sand cannot be constrained, Unit 4 begins at the top of Core 302-M0004A-41X, where a 4 cm sandstone fragment was recovered. Dark olive-gray (5Y 3/2) clayey mud and very dark gray (5Y 3/1) silty clay to clayey mud are the dominant lithologies in Unit 4, occurring from Sections 302-M0004A-41X through 42X-CC, 10 cm. Very dark gray (5Y 3/1) homogeneous silty sand occurs in the deepest 7 cm of the unit. Smear slide analysis indicates that Unit 4 is dominated by quartz, feldspar, and clay minerals. Submillimeter to centimeter-size pyrite concretions are present in Sections 302-M0004A-41X-1 and 42X-1. Centimeter-size gravel is present at the base of 42X-1, but this may be a product of core disturbance. The TOC content of Unit 4 is 1 wt%. The entire unit is highly disturbed by drilling.

Summary

Fine-grained siliciclastic sediments (clays to silty muds), ranging in age from Holocene to Late Cretaceous (0–428 mbsf), are the dominant lithogenic material recovered in the suite of Expedition 302 sites. This is interrupted in the middle Eocene by dark gray laminated mud-bearing biosiliceous ooze (~220 to ~313 mbsf; Unit 2). This ooze is also characterized by elevated amounts of TOC and algal-derived organic carbon (see **"Organic geochemistry"**). Dark, organic-rich and biosiliceous laminated units are indicative of high productivity but relatively low oxygen bottom waters.

The largely fine grained texture of the siliclastic sediments is indicative of predominantly low energy marine environments throughout most of the Cenozoic. However, the fine-grained zebra-stripe interval within Subunit 1/5 is an exception. Cores within Subunit 1/5 (302-M0002A-44X, 45X, and 46X) give ample evidence of rapid changes in depositional environment with distinct breaks in layering, crosscutting, and cyclic changes in color. Seismic reflection data taken near the sites (Fig. **F7B**) indicate an interval of high-frequency, anastomosing reflections (see **Jakobsson et al.,** this volume), equivalent to this zebra-stripe interval. Both the character of the bed forms and their apparent seismic signature suggest a dynamic sedimentary environment during part of the middle Miocene(?). This "cut and fill" character may indicate migrating sediment waves (Hall, 1979). Currents that could create such an energetic environment include strong baroclinic or boundary currents (Aagard and Carmack, 1994), tidal-driven turbulence on top of and around the ridge, and the oscillation of internal waves on a surface with a high density gradient.

Sand lenses are observed as deep as 198 mbsf (bottom of Subunit 1/5, early Miocene). Isolated pebbles are present throughout Unit 1, with the deepest one observed, visually, in Unit 2 (302-M0002A-55X-4, 122 cm; 239.34 mbsf; middle Eocene). The sand lenses and isolated pebbles are interpreted as ice-rafted debris, suggesting that at least seasonal ice has been present in the central Arctic since the middle Miocene and perhaps as early as the middle Eocene.

Lithologic unit changes do not necessarily coincide with hiatuses interpreted on the basis of biostratigraphy. However, a major hiatus is likely within Core 302-M0002A-46X near the Subunit 1/5 and 1/6 boundary. Although color is used as a factor in defining lithologic units, color changes do not always coincide with mineralogical and textural changes, suggesting a strong diagenetic influence on color banding in these sediments.

Micropaleontology

During Integrated Ocean Drilling Program (IODP) Expedition 302, four closely spaced sites (Sites M0001–M0004) were drilled along a single seismic profile, and cores from the various holes could be confidently spliced and correlated. The different sequences are treated as a single succession. Among the holes, only Holes M0002A and M0004A reached significant depths; the others captured parts of the Pleistocene. Hole M0002A penetrated into the middle Miocene and upper middle Eocene, with a marked hiatus separating these units. Hole M0004A continued from where Hole M0002A ended, recovered portions of the underlying middle and lower Eocene and the Paleocene/Eocene transition, and bottomed in lower Campanian basement at ~410 mbsf.

Onboard micropaleontology included the analysis of calcareous nannofossils, diatoms, silicoflagellates, ebridians, radiolarians, calcareous and agglutinated benthic foraminifers, planktonic foraminifers, ostracodes, organic-walled dinoflagellate cysts (dinocysts), other palynomorphs, and fish remains. Only core catcher samples were analyzed during the offshore phase.

All but one of the studied samples were barren of calcareous nannofossils. A single productive sample is

reported from the Holocene in Hole M0001A. Siliceous microfossils, notably diatoms, silicoflagellates, and ebridians, are most abundant and well preserved in the middle Eocene interval. Calcareous planktonic and benthic foraminifers and ostracodes are rare in the Pleistocene and absent in older parts. Agglutinated benthic foraminifers are generally scarce but are locally abundant and well preserved in the Campanian and the Paleocene to lower Eocene intervals. Organic-walled dinoflagellate cysts (dinocysts) are patchy in the Quaternary–Neogene but are abundant and well preserved in the Paleogene and Cretaceous intervals. Other palynomorphs, notably pollen and spores, and remains of aquatic algae (chlorophytes) are common in most intervals. An acme of the remains of the hydropterid fern *Azolla* marks the basal middle Eocene.

Preliminary age-depth relationships are based on dinocyst, ebridian, and silicoflagellate datums and the *Azolla* event. Dinocysts represent the only group that by and large is present throughout the entire Cenozoic section. Paleogene dinocyst events have been calibrated to magnetostratigraphy by Eldrett et al. (2004) from Hole 913B in the Norwegian-Greenland Sea. Additional age information is derived from silicoflagellates and ebridians in the middle Eocene and a few benthic foraminifer events in the older Paleogene.

During Expedition 302, cores ranging in age from the Campanian (basement) to the Holocene were recovered. Major hiatuses occur between the Campanian and the Paleocene, the middle Eocene and early Miocene, and within the Pliocene.

Paleoenvironments ranged between marginal marine neritic settings in the Campanian through earliest Eocene to an enclosed marginal basin setting marked by episodic brackish to possible freshwater conditions in the middle Eocene, as indicated by the *Azolla* event. The upper part of the Miocene through the Pleistocene is characterized by deep marine conditions. The palynological assemblage in Samples 302-M0002A-44X-CC and 45X-CC resembles that of a coastal, restricted marine, brackish setting. Reworking of Cretaceous through late Eocene elements is common in this interval. The Oligocene elements may be reworked as well, tentatively placing this succession in the Miocene. Non-fossil-bearing strata, provisionally assigned to the Miocene, overlie this interval. Paleoenvironmental information is not available for this interval (Samples 302-M0002A-38X-CC through 43X-CC).

Calcareous nannofossils

During the offshore phase of IODP Expedition 302, 124 smear slides made with the core catcher sediments from each of the four sites were studied for calcareous nannofossils. All of the studied samples were barren, except for one sample from Hole M0001A. Although calcareous nannofossils are poorly represented in high-latitude sediments (Perch-Nielsen, 1985a), this result was striking. Studies carried out in recent years on several piston cores from the Arctic Ocean (e.g., Gard, 1993; Jakobsson et al., 2000, 2001) have shown that calcareous nannofossils are present in low abundances only in short intervals during the present and the last interglacial periods. Expedition 302 recovered a long Cretaceous to Cenozoic stratigraphic record, and so it was a surprise not to find calcareous nannofossils, a fossil group that normally is well represented in marine sediments.

After the cores were split at the IODP Bremen Core Repository (BCR), the upper 19 m of Hole M0004C and the top 3 m of Hole M0002A were sampled at varying intervals downcore, using a strategy based largely on visual observations of core coloration. Although many of the samples subsequently proved to be barren, a surprising large number did contain poor–moderate–well-preserved calcareous nannofossil assemblages. Moreover, a few of the samples from Hole M0004C equate to 18 mbsf. Although some of these nannofossils are undoubtedly reworked from Mesozoic–Cenozoic sediments and transported over long distances to the core sites (Gard and Crux, 1994), others may have been produced in situ.

Hole M0001A

Four samples from Section 302-M0001A-1H-CC (collected at depths of 10, 12, 14, and 26 cm) were analyzed for calcareous nannofossils. Only the sample collected in a brown interval at 14 cm contains an impoverished assemblage of calcareous nannofossils. The following forms have been determined: *Coccolithus pelagicus* (small form), *Calcidiscus leptoporus*, and a species of *Gephyrocapsa*. All of them are rare. This assemblage has been previously recorded in Holocene sediments from the Arctic Ocean (Gard, 1993).

Hole M0002A

Seventy-nine samples from the core catchers were analyzed on board for calcareous nannofossils, but all of them were barren (Table **T5**). Samples taken from the first core opened proved to be more fruitful. The coccoliths in the top 10 cm were moderately preserved and largely comprised *Emiliania huxleyi* and small–medium *Gephyrocapsa* species, the latter being absent in the top two samples (Sections 1X-1, 2.0 cm, and 1X-1, 3.5 cm). The samples in the top 10 cm also included a number of unidentified cocco-

liths, and a few specimens of *C. pelagicus*, *C. leptoporus*, and thoracospheres were found. Some coccoliths were found in deeper samples from Cores 1X and 2X but were poorly preserved and very rare.

Hole M0003A

Three core catcher samples (1H-CC, 3 cm, 2H-CC, 16 cm, and 3H-CC, 24 cm) were analyzed on board for calcareous nannofossils, but all were barren. Fifteen samples were analyzed onshore, most of which were barren, but with a gephyrocapsid specimen in Section 1H-1, 11 cm, two reworked coccoliths in Section 1H-1, 12 cm, and a coccolith of *C. pelagicus* in section 1H-2, 59 cm.

Holes M0004A, M0004B, and M0004C

Thirty-two core catcher samples from Hole M0004A (Table T6), two from Hole M0004B (302-M0004B-3X-CC, 2 cm, and 13 cm), and four samples from Hole M0004C (302-M0004C-1H-CC through 4H-CC and 6X-2, 149 cm) were analyzed on board for calcareous nannofossils, but all samples were barren.

Samples taken from the opened cores of Hole M0004C yielded significant numbers of coccoliths. The top 35 cm of Section 302-M0004C-1H-1 contained good to moderately preserved specimens of *E. huxleyi*, small to medium *Gephyrocapsa* spp., and *C. pelagicus*, as well as a few *C. leptoporus* and *Syracosphaera* species. Unidentified coccoliths were also present. Below this, most of the samples were either barren or contained rare and poorly preserved coccoliths of small to medium *Gephyrocapsa* spp., *C. pelagicus,* and *C. leptoporus*. In Section 302-M0004C-1H-2, 2 cm, there were many small and medium *Gephyrocapsa* spp. as well as a few *E. huxleyi*, whereas another sample at 4H-3, 3 cm, comprised a few specimens of moderately preserved small to medium *Gephyrocapsa* species. It should be pointed out that samples from the same core depth but from different horizontal locations often yielded dissimilar results.

Nannofossil stratigraphy

The findings in Hole M0004C suggest that coccolithophorids were living in the Arctic prior to the last interglacial. However, their rare presence in the lower core sections does not allow us at this time to assign an age or zone with any confidence. On the other hand, the "dominance" of *E. huxleyi* in the uppermost part of the first section indicates that the sediments represent the Holocene, prior to which (i.e., before the beginning of the *E. huxleyi* acme) there is a "dominance" of small to medium *Gephyrocapsa* species. The presence of large specimens (>4 µm) of *E. huxleyi*, reportedly indicative of the last glacial period at lower latitudes (Colmenero-Hidalgo et al., 2002), occur in the Arctic sediments presumably during the warmer Holocene. The presence of large specimens (9–15 µm) of *C. pelagicus* indicates that temperate waters infiltrated the Arctic region during the Holocene (Young et al., 2003).

Diatoms

Hole M0001A

Samples 1H-CC, 18 and 25 cm, were studied, but diatoms were not observed in these samples.

Hole M0002A

A total of 87 samples (about one sample per section) in interval 1X-1, 3 cm, through 47X-2, 37 cm, were prepared, but these were barren of diatoms and other siliceous microfossils (silicoflagellates, ebridians, and archaeomonads), apart from Sample 46X-CC, 6 cm, which yielded rare diatoms (Table T7). Samples 47X-2, 50 cm, to 49X-3, 31 cm, contained few diatoms but generally abundant ebridians. Samples 51X-1, 25 cm, to 62X-3, 50 cm, contained a diverse siliceous assemblage with abundant diatoms, common to abundant ebridians, and few to common silicoflagellates. Sediments of this interval are dominated by diatoms.

Based on qualitative analysis of smear slides and some quantitative counts, the diatoms in the biosiliceous interval can be divided into different assemblages. Given the sparsity of published information on middle Eocene diatoms in northern high latitudes, most of the species recorded in these samples have been identified only to generic level. Diatoms in the ebridian-dominated interval 47X-2, 50 cm, to 49X-3, 31 cm, are dominated by *Pyxilla* spp. The diatom assemblage in interval 51X-1, 25 cm, to 53X-3, 100 cm, is mainly composed of species of *Hemiaulus* and *Huttonia*. In interval 53X-4, 38 cm, to 57X-3, 60 cm, the assemblage is composed of species of *Goniothecium*, *Eunotogramma*, *Hemiaulus,* and *Huttonia*. We have specifically sampled some of the white layers of the laminated interval. One of these samples (57X-4, 50 cm) is a pure diatomite composed mainly of species of *Eunotogramma*. The other three samples (58X-2, 69 cm, 58X-3, 5 cm, and 59X-3, 79 cm) are composed mainly of species of *Hemiaulus*. The diatom assemblage in interval 60X-1, 39 cm, to 62X-3, 50 cm, is composed of species of *Eunotogramma*, *Trinacria,* and *Odontotropis*. Within this diatom-dominated interval there is one sample (61X-2, 20 cm) that is dominated by ebridians.

The diatom species assemblages in Hole M0002A show some similarities to those reported from Deep Sea Drilling Project (DSDP) Leg 38, Sites 338–340 (e.g., Schrader and Fenner, 1976; Dzinoridze et al.,

1978; Fenner, 1985), Ocean Drilling Program (ODP) Leg 151 from the middle Eocene to the late Oligocene in the Norwegian-Greenland Sea (Scherer and Koç, 1996), Core Fl-422 from the Alpha Ridge of the central Arctic Ocean assigned to early to middle Eocene by Dell´Agnese and Clark (1994), the Eocene of the Urals (Strelnikova, 1974), and to the early Eocene Moler/Für Formation of Denmark (Homann, 1991). Because of the sparsity of sediments of this age and consequently a poorly established high-latitude northern hemisphere Eocene diatom biostratigraphy, it is not possible to provide a more detailed age assessment to the interval 47X-2 to 62X-3 in Hole M0002A other than middle Eocene. However, the present material yielded significant changes in the presence and abundance of species that may potentially be useful for the establishment of a diatom biostratigraphy for the Arctic Ocean. Counts of species in Samples 51X-2, 117–118 cm, through 62X-CC show some significant changes in the species composition of this interval (Table **T7;** Fig. **F8**).

There are three peaks in the abundance of *Hemiaulus* sp. 1 between interval 51X-2, 117–118 cm, and 62X-CC, namely in Samples 62X-CC through 61X-CC, 59X-CC, and the interval from 57X-CC through 55X-CC. Similar changes are also recognized in the patterns of *Hemiaulus danicus, Hemiaulus incisus, Hemiaulus kittonii*, and *Hemiaulus* spp. indet., which have abundance maxima in Samples 54X-CC and 51X-2, 117–118 cm. *Pseudopyxilla* spp. are abundant from Sample 62X-CC through 59X-CC, whereas *Cymatosira* spp. show a maximum abundance in the upper part of Sample 59X-CC. *Goniothecium* is abundantly present in all samples that yielded diatoms. Among representatives of this genus, *Goniothecium loricatum* has two peaks (i.e., from Samples 60X-CC through 57X-CC and from 54X-CC through 52X-CC). *Goniothecium odontella* var. *danica* also has two peaks, in Samples 60X-CC and 52X-CC. Abundant occurrences of *Costopyxis trochlea* were also recognized. This species was formerly known as "*Trochosira trochlea*" from middle Eocene sediments in high and low latitudes (Dzinoridze et al., 1978; Fenner, 1985; Scherer and Koç, 1996).

The Eocene *Chaetoceros* resting spore assemblages are of low diversity, represented only by two species, resting spore sp. 1 and *Syndendrium diadema*? Resting spore sp. 1 is common only in Sample 52X-CC.

Paleoenvironment

The diatom species of Hole M0002A are all marine. The presence of abundant diatoms (and other biosiliceous organisms) indicates extremely productive surface ocean conditions in the interval 51X-1 through 62X-CC. Presence of laminations with pure diatom assemblages in the light layers throughout the interval is a further confirmation of the extremely productive nature of the surface waters. A large number of the observed species, such as *Pseudotriceratium radiosoreticulatum*, which occurs from Samples 48X-CC through 57X-CC, is especially common in neritic environments (Fenner, 1985).

Diatom resting spore assemblages, including *Pterotheca aculeifera*, resting spore sp. 1, and *S. diadema*?, are common in Sample 52X-CC. Their presence may indicate proximity to the shelf edge, as only neritic planktonic diatoms form resting spores in the modern oceans. The abundance of resting spores also suggests a highly productive environment.

Hole M0003A

Three core catcher samples (1H-CC, 22 cm, 2H-CC, 14 cm, and 3H-CC, 1 cm), in addition to Samples 1H-1, 12 cm, 1H-2, 59 cm, 3H-3, 12 cm, 3H-3, 70 cm, and 3H-3, 85 cm, were investigated for diatoms. All of these samples were barren.

Hole M0004A

Fifty-seven core samples from Hole M0004A (i.e., between Sections 4X-1, 10 cm, and 42X-CC) were investigated for biosiliceous components (diatoms, ebridians, silicoflagellates, and archaeomonads). Well-preserved and abundant diatoms are recognized in Samples 4X-1 through 12X-CC, whereas rare, poorly preserved specimens occur in Sections 15X-CC through 19X-CC. Samples between 20X-CC, 5 cm, and 42X-CC were barren (Table **T8;** Fig. **F9**).

Biosiliceous sediments in the interval 4X-1, 10 cm, through 7X-1, 60 cm, are mostly dominated by diatoms. Only in Samples 5X-1, 15 cm, and 5X-2, 30 cm, are the sediments dominated by ebridians. The rest of the biosiliceous interval between 7X-2, 80 cm, and 15X-1, 10 cm, is mainly dominated by ebridians.

Based on the qualitative analysis of smear slides, the diatom record can be grouped into different assemblages. In the interval 4X-1, 10 cm, through 6X-3, 70 cm, the assemblage is mostly composed of species of *Eunotogramma*, *Trinacria,* and *Odontotropis*. Species of *Pterotheca* and *Trinacria* are the most common elements of the diatom assemblage in the interval 6X-4, 30 cm, through 10X-CC. In the interval 11X-1, 40 cm, through 11X-3, 100 cm, the assemblage is mainly composed of *Pseudostictodiscus picus* and species of *Trinacria*. In Sample 11X-3, 20 cm, an especially common occurrence of *Odontotropis* ex gr. *carinata/hyalina* is observed. *Pyxilla oligocaenica* var. *oligocaenica* and species of *Trinacria* make up most of the assemblage in the interval 11X-4, 5 cm, through 15X-1, 10 cm.

Counting of species in nine samples between Sections 4X-1 and 12X-CC showed the presence of abundant well-preserved resting spores in this interval (Table T8). In these samples, representatives of 24 genera, comprising 26 species and 12 unidentified species, including two unknown resting spore species, were observed. Samples 15X-CC and 18X-CC included rare and poorly preserved small-sized diatom valves of *Goniothecium* spp., *Hemiaulus* spp., *P. picus,* and *P. aculeifera*. In addition, a few well-preserved large-size diatom valves in the >45 µm fraction, including *Odontotropis carinata, Stephanopyxis* spp., and *Trinacria cornuta*, were recognized. The abundance of *Hemiaulus* sp. 1 (>70%) and *Pseudopyxilla* spp. (>20%) and absence of *Anaulus* spp. and *Cymatosira* spp. resemble diatom assemblages in the lower part of the diatomaceous sediments in Hole M0002A.

Few age-diagnostic taxa are recorded in Hole M0004A. Sample 6X-CC contained rare but well-preserved *Brightwellia hyperborea*, which is an age-diagnostic taxon from the middle Eocene of the North Atlantic Ocean (Fenner, 1985). Samples 11X-4, 5 cm, and 11X-4, 40 cm, contained few *P. oligocaenica* var. *oligocaenica* indicating an early Eocene age for these samples (Fenner, 1985). Species recorded in Hole M0004A show some similarities to those reported from DSDP Leg 38, Site 338 (Schrader and Fenner, 1976; Dzinoridze et al., 1978), and from ODP Leg 151, from the middle Eocene to the late Oligocene in the Norwegian-Greenland Sea (Scherer and Koç, 1996), Core Fl-422 from the Alpha Ridge of the central Arctic Ocean assigned to early to middle Eocene by Dell´Agnese and Clark (1994), Eocene of the Urals (Strelnikova, 1974), and early Eocene Moler/Für Formation of Denmark (Homann, 1991).

Paleoenvironment

All diatoms observed in Hole M0004A are marine species. Most species occurring abundantly at this site, like *Hemiaulus* spp., *Goniothecium* spp., and *Stephanopyxis* spp., indicate a neritic environment (Fig. F10). Resting spore assemblages (notably *P. aculeifera* and *Pseudopyxilla* sp.) are abundant and also indicate a nearshore, coastal setting. The abundance of biosiliceous organisms together with diatom resting spores may suggest a highly productive environment, possibly associated with active upwelling in the interval 4X-1, 10 cm, through 15X-1, 10 cm.

Correlation of Holes M0002A and M0004A

Diatom assemblages of Hole M0002A in interval 60X-1, 39 cm, through 62X-3, 50 cm, and Hole M0004A in interval 4X-1, 10 cm, through 6X-3, 70 cm, are very similar. Both are composed of species of *Eunotogramma*, *Trinacria,* and *Odontotropis*. Furthermore, even though both intervals are primarily dominated by diatoms, there is a short interval in both holes where ebridians dominate over diatoms and where the two holes overlap. These are Sample 302-M0002A-61X-2, 60 cm, and interval 302-M0004A-5X-1, 15 cm, through 5X-2, 30 cm.

Hole M0004B

Two core catcher samples, 1H-CC, 2 cm, and 3X-CC were investigated. The former sample was barren. The latter contained poorly preserved, small-size diatom valves, including *Pyxilla* spp. and some fragments, and few but well-preserved large-size diatom valves in the >45 µm fraction, including *Pseudotriceratium radiosoreticulatum, Paralia crenulata, Actinoptychus* spp., *Stephanopyxis* spp., *Hemiaulus* spp., and *Pseudopyxilla* spp. This assemblage is not age diagnostic. The occurrence of *Pseudotriceratium radiosoreticulatum* indicates neritic conditions (Fenner, 1985).

Hole M0004C

A total of 24 samples including the seven core catcher samples, 1H-CC, 2H-CC, 3H-CC, 4H-CC, 6X-2, bottom, 8X-CC, and 9X-CC were studied but did not contain diatoms.

Diatom and paleoenvironment summary, Holes M0002A and M0004A

The biosiliceous sediments in Cores 302-M0002A-47X through 62X as well as 302-M0004A-4X through 15X indicate productive surface ocean conditions in the Arctic during the early Eocene through the middle Eocene. The start and end of this biosiliceous interval is dominated by ebridians, possibly indicating a nearshore environment with moderate productivity, whereas the middle part of the interval, which is dominated by diatoms, indicates highly productive surface waters with neritic to pelagic conditions (Figs. F10, F11). The recovered diverse diatom assemblages show high temporal variability in their composition, indicating significant climate variability within the recovered time interval.

Silicoflagellates and ebridians

Seventeen samples above 33.9 mbsf from all holes were processed, and all were barren of silicoflagellates and ebridians. These include samples from Holes M0001A (Core 302-M0001A-1H), M0002A (Cores 302-M0002A-1X-CC and 3X-CC), M0003A (Cores 302-M0003A-1H, 2H, and 3H), M0004A (Samples 302-M0004A-2X-1, 149–151 cm, 2X-2, 0–2 cm, and 3X-1, 149–151 cm), and M0004C (Cores 302-M0004C-1H through 4H, 6X, 8X, and 9X).

Below 33.9 mbsf, a total of 104 cores were recovered from Holes M0002A (59 cores), M0004A (42 cores), and M0004B (3 cores). Here, we briefly discuss the silicoflagellate and ebridian biostratigraphy, after splicing Holes M0002A and M0004A and inserting data from Hole M0004B (Core 302-M0004B-3X).

Holes M0002A and M0004B

In Hole M0002A, silicoflagellates and ebridians were absent in all samples between Samples 302-M0002A-1X-CC and 46X-CC. Samples 302-M0002A-47X-CC through 62X-CC, 9–11 cm, yielded well-preserved, abundant, and highly diversified (~40 taxa) silicoflagellate and ebridian assemblages, permitting preliminary age assignments (Table **T9**).

Both the silicoflagellate and ebridian assemblages are similar to those reported in Core Fl-422 from the Alpha Ridge in the Arctic Ocean (Ling, 1985), a core whose age was considered to be early Paleogene. All 18 taxa illustrated by Ling (1985) are present in Samples 302-M0002A-47X-CC through 62X-CC, 9–11 cm, in addition to at least a dozen more taxa in Hole M0002A. The two most critical taxa for biostratigraphy (*Corbisema hexacantha* and *Dictyocha frenguellii*, see below) were not reported by Ling (1985).

Using samples from the same Alpha Ridge core, Bukry (1984) gave an age range of late middle Eocene to late Eocene. Based on his photomicrographs, six taxa occur in the present cores (Samples 302-M0002A-47X-CC through 62X-CC, 9–11 cm) from the Lomonosov Ridge, although the taxonomic nomenclature of a few taxa differs from ours. More recently, Dell'Agnese and Clark (1994) provided an age estimate of early to middle Eocene for Alpha Ridge Core Fl-422. There are thus three possible ages for Core Fl-422: early Paleogene, early to middle Eocene, and late middle to late Eocene.

Samples 302-M0002A-47X-CC (207.35 mbsf) and 48X-CC (210.64 mbsf) belong to the silicoflagellate *C. hexacantha* Zone, which ranges from the middle Eocene to the late Eocene. In terms of calcareous nannofossil zonation, this represents the upper part of Zone NP15 to Zones NP19/NP20. An age of ~44.1 Ma is estimated between Samples 302-M0002A-48X-CC and 49X-CC, where the first occurrence (FO) datum of *C. hexacantha* occurs. Note that abundant *C. hexacantha* occurred in Sample 302-M0002A-48X-CC (362 specimens) followed by rare occurrences of this taxon in Sample 48X-2, 139–151 cm, and Core 47X-CC.

Samples 302-M0002A-49X-CC through 62X-CC, 9–11 cm, belong to the silicoflagellate *Corbisema spinosa* and *Naviculopsis robusta* Zones. The zonal ranges of these species correspond to the middle part of nannofossil Zones NP15 (middle Eocene) to NP12 (lower Eocene). Age information from dinoflagellate cysts (see **"Palynology, organic-walled dinoflagellate cysts"**) combined with silicoflagellate data constrains the age of Cores 302-M0002A-49X through 62X to the middle Eocene. The following is a preliminary discussion of silicoflagellate age determinations for Hole M0002A.

Sample 302-M0002A-47X-CC contains moderately preserved and abundant *C. hexacantha* and *D. frenguellii*, which are the most age-diagnostic taxa. Less diagnostic taxa with long stratigraphic ranges include *Dictyocha crux parvus, Dictyocha lockerii, Dictyocha deflandrei, Corbisema hastata hastata, Corbisema hastata globulata, Corbisema apiculata, Distephanus quinquengellus, Distephanus quinarius, Ammodichium rectangulare*, and *Pseudoammodochium dictyoides*. Sample 302-M0002A-48X-CC contains the key species *C. hexacantha, C. hastata globulata, C. hastata hastata, Corbisema* sp. aff. *toxeuma*, and *P. dictyoides*.

Based on the material from Leg 151 Site 913 from the Greenland Basin, Locker (1996) provided the FO and last occurrence (LO) of *C. hexacantha* as 44.1 and 37.4 Ma, respectively. The range of *D. frenguellii* in the *C. hexacantha* Zone was discussed by Perch-Nielsen (1985b). Thus, Samples 302-M0002A-47X-CC and 48X-CC are assigned to the *C. hexacantha* Zone of the middle to upper Eocene.

About two samples per core were investigated between Cores 302-M0002A-49X and 62X (Table **T9**). Samples 302-M0002A-49X-CC through 62X-CC, 9–11 cm, contained well-preserved and abundant silicoflagellate and ebridian assemblages, except for Samples 302-M0002A-49X-CC and 50X-CC, which contained few specimens. Samples 302-M0002A-49X-CC through 62X-CC, 9–11 cm, may belong to the *C. spinosa* and *N. robusta* Zones, which correlate to nannoplankton Zone NP15 (middle Eocene). Several taxa such as *Distephanus crux* and *Dictyocha quinquengellus* may have biostratigraphic value pending further study. Broadly age diagnostic (early to middle Eocene) taxa include *D. frenguellii, D. deflandrei, Corbisema glezerae, Corbisema toxeuma, Corbisema ovalis, C. apiculata, C. hastata hastata*, and *C. hastata globulata*. As Samples 302-M0002A-49X-CC through 50X contained few silicoflagellates, an effort was made to count as many specimens as possible using more than the standard eight traverses at 400×. This resulted in the recognition of >70 specimens in each sample and confirmed that the index taxon *C. hexacantha* was absent in Samples 302-M0002A-48X-CC and 49X-CC. Single specimens of *C. spinosa*, an important age-diagnostic taxon, which ranges from the upper part of the *Naviculopsis foliacea* Zone to the *C. hexacantha* Zone (Perch-Nielsen, 1985b), was

present in Samples 302-M0002A-49X-CC, 2–4 cm, and 52X-CC. This concurs with an age assignment of Cores 302-M0002A-49X through 62X that correlates to Zone NP15. A single specimen of *Corbisema lamellifera*, which occurs in the *C. hexacantha* Zone, was found in Sample 302-M0002A-62X-CC, 9–11 cm. Single specimens of *Naviculopsis foliacea tumida, Naviculopsis constricta*, and *Naviculopsis punctilia* were present in Sample 302-M0002A-50X-CC, 8–10 cm. A single specimen of *N. robusta*, which is characteristic of the *N. foliacea* Zone, was present in Sample 302-M0002A-62X-CC, 9–11 cm, in the >45 µm fraction.

Small (14–20 µm equatorial diameter) silicoflagellate taxa reported by Ling (1985) from the Alpha Ridge were observed in several samples below Core 302-M0002A-52X-CC to the bottom of the hole (Table **T9**). These taxa include *Dictyocha curta* and *Dictyocha* sp. cf. *rotundata*. The silicoflagellate *Dictyocha* sp. cf. *carentis incerta* (diameter of basal ring = 17–24 µm) illustrated by Ling (1985) also was continuously present between Samples 302-M0002A-52X-1, 0–2 cm, and 62X-CC, 9–11 cm, except in Samples 52X-CC and 53X-CC. Samples 302-M0002A-61X-CC, 0–1 cm, and 62X-CC, 9–11 cm, yielded eight and six specimens, respectively. These small, rare taxa suggest a similarity between Alpha Ridge Core Fl-422 and Samples 302-M0002A-52X-1, 0–2 cm, through 62X-CC, 9–11 cm, and an age of early to middle Eocene for both cores.

Distephanus speculum speculum was present sporadically between Cores 302-M0002A-49X and 57X. Today, this taxon is a typical temperate to cold-water form. *Distephanus antiqua* was present continuously from Cores 302-M0002A-49X through 57X, except in Section 56X-CC.

A single specimen of *Mesocena apiculata inflata* was present at the top of Sample 302-M0002A-57X-CC (<45 µm fraction), which ranges from the *N. foliacea* Zone of the lower to the middle Eocene to the *C. apiculata* Zone of the Oligocene. Abundant and well-preserved specimens of the undescribed species *Dictyocha* sp. A and *Dictyocha* sp. B were found throughout Samples 302-M0002A-49X-CC through 59X-CC and 60X-1, 0–2 cm. In particular, high numbers of *Dictyocha* sp. B were recorded from Samples 302-M0002A-54X-CC through 55X-CC and *Dictyocha* sp. A in Samples 53X-CC through 51X-CC.

Paleoenvironment

Abundant *Corbisema* in the >45 µm fraction and ebridians in the <45 µm fraction of Sample 302-M0002A-62X-CC suggest the following paleoenvironmental conditions favorable to these groups: warm waters, nearshore habitats, and high productivity.

Hole M0004A

Cores 4X (265.03 mbsf) through 18X (318.96 mbsf) yielded silicoflagellates and ebridians with variable abundance and states of preservation. No silicoflagellates and ebridians were found below Core 18X. The silicoflagellate assemblages from this site are similar to those at Site M0002 but differ lower in the section. These cores are assigned to the *C. spinosa* and *N. robusta* Zones, analogous to cores from Hole M0002A (Cores 302-M0002A-49X through 62X).

C. glezerae was consistently present in the lower section of this hole except in Cores 302-M0004A-6X, 9X, and 10X. According to Perch-Nielsen (1985b), this taxon ranges from the *Corbisema hastata* Zone to the *N. constricta* Zone. However, observations from this site and Site M0002 suggest that the range of *C. glezerae* extends to the top of the *C. spinosa* Zone in the Arctic Ocean.

Well-preserved specimens of *C. ovalis* were found in Samples 4X-CC, 15X-CC, and 18X-CC. In contrast to *C. glezerae*, *C. ovalis* was known to be present only in the *C. hexacantha* Zone (Perch-Nielsen 1985b), but this taxon was found in Cores 56X, 61X, and 62X; therefore, the range of *C. ovalis* can be extended into the *C. spinosa* Zone in the Arctic Ocean.

About two dozen specimens of *Mesocena* were found in Section 7X-CC and Cores 10X through 12X (Table **T10**). As the size of *Mesocena* is large (~90–110 µm), scanning the >45 µm size fraction at 100× magnification readily provides common specimens in addition to those observed in the standard census at 400× magnification. The following taxa also were encountered: *M. apiculata inflata* (with and without spines), *Mesocena apiculata apiculata*, and *Mesocena occidentalis*. Their ranges suggest a middle Eocene age. One exception is the presence (two specimens) of *M. apiculata apiculata*, which ranges from the upper Eocene to the middle Miocene (Perch-Nielsen, 1985b). The Arctic range of this taxon is hereby extended into the *C. spinosa* Zone of the lower to middle Eocene. The genus *Mesocena* is present approximately at the maximum abundance of the spores of the freshwater fern *Azolla*, which has an age of 49.2 Ma (see **"Palynology, organic-walled dinoflagellate cysts"**).

Paleoenvironment

Fluctuations in the abundances of *Corbisema* and ebridians are present in Hole M0004A and are similar to those present in Sample 302-M0002A-62X-CC. These two groups tended to occur in high numbers in Cores 302-M0004A-8X through 12X. Variable abundances of these taxa may be related to paleoenvironmental changes in the Arctic Ocean.

Silicoflagellate and paleoenvironment summary, Holes M0002A, M0004A, and M0004B

Based on the assemblages in Cores 302-M0002A-47X through 62X as well as 302-M0004A-4X through 18X, paleoclimatic conditions for the early Eocene through the middle Eocene were warm relative to those in the Arctic today. The presence of sporadic and rare (<1% of population) presences of *Distephanus* (cold-water hexagonal forms) and quadrate forms of the genus *Dictyocha* (e.g., *Dictyocha crux crux*; temperate water) may also have paleoclimatic significance.

The relatively high diversity of well-preserved distinctive silicoflagellate and ebridian assemblages appears to indicate that the Eocene environment in the central Arctic ranged from coastal neritic to hemipelagic (Fig. **F12**). It is possible that brackish water conditions existed with intrusions of pelagic waters indicated by the sporadic presence of radiolarians.

Radiolarians

Samples taken at Sites M0001–M0004 were barren of radiolarians except Samples 302-M0002A-49X-CC, 50X-CC, and 52X-CC. By treating samples for 20 s in an ultrasonic bath and resieving at 45 µm, the coarse residue was sufficiently concentrated to identify approximately a dozen specimens in four slides made from Sample 302-M0002A-49X-CC and fewer than six specimens in two slides from Sample 302-M0002A-50X-CC. A single unidentifiable specimen was seen in the fine fraction (<45 µm) in Sample 302-M0002A-52X-CC during the silicoflagellate census. The presence of *Calocyclas talwanii* and *Botryostrobis joides* indicates an age of middle to late Eocene (*C. talwanii* to *Artostrobus quadriporus* Zones) (Table **T11**), based on the work of Bjørklund (1976).

Work on modern radiolarians indicates that many of the species can live at depths below the pycnocline, but they do not generally tolerate salinities less than ~20 ppt (Bjørklund and Swanberg, 1987; Boltovskoy et al., 2003). Thus, the trace amount of radiolarians in Eocene samples, combined with the results from the dinocysts, silicoflagellates, ebridians, and diatoms, suggests a relatively brief incursion of pelagic waters may have occurred, perhaps at depths below the upper brackish waters of the Arctic Ocean.

Planktonic and benthic foraminifers and ostracodes

Hole M0001A

Shipboard analyses of foraminifers at Site M0001 were conducted using five core catcher samples from Section 1H-CC. Foraminifers from Samples 1H-CC, 0–2 cm, and 1H-CC, 14–16 cm, contained the planktonic species *Neogloboquadrina pachyderma* (sinistral) and several ostracode species. Sample 1H-CC, 26–28 cm, contained the agglutinated species *Cyclammina pusilla* and unidentified fragments of other species. Two additional Samples (1H-CC, 10–12 cm, and 1H-CC, 20–22 cm) contained *C. pusilla* and other agglutinated species.

Hole M0002A

Shipboard analyses of benthic foraminifers at Site M0002 were conducted using core catcher samples. Benthic foraminifers from Hole M0002A range in age from Miocene to Holocene and consist of both calcareous and agglutinated taxa. Calcareous benthic foraminifers were found only in Sample 1X-CC, where they were rare. The agglutinated benthic foraminiferal record recovered from Hole M0002A can be subdivided into the following four informal stratigraphic assemblage zones:

- Zone 1: Samples 1X-CC through 10X-CC contained rare to common abundances of agglutinated foraminifers dominated by *C. pusilla*, with lesser numbers of *Recurvoides, Alveolophragmum,* and *Trochammina* spp. intermittently present. The preservation state varies from fair to excellent. A reworked specimen of *Haplophragmoides* from either the Paleocene or Eocene was found in Sample 4X-CC.
- Zone 2: Samples 12X-CC through 34-X-CC contained no agglutinated foraminifers except very occasional fragments of unidentified genera.
- Zone 3: Samples 35X-CC through 42X-CC contained few to common agglutinated foraminifers including *C. pusilla, Cyclammina* aff. *cancellata, Recurvoides*, and *Trochammina*.
- Zone 4: Samples 44X-CC through 62X-CC were barren of benthic foraminifers.

The assemblages in the upper part of Zone 1 represent the agglutinated foraminiferal assemblages observed in numerous short cores from various ridges in the Arctic at ~2–7 mbsf (Ishman et al., 1996; Jakobsson et al., 2001; Backman et al., 2004). The agglutinated foraminiferal facies underlies sediments rich in calcareous microfossils deposited during and since about marine isotope Stage 5 (~127 ka). These agglutinated assemblages usually have been assigned ages of Pliocene to early Pleistocene. However, rigorous confirmation of their ages is usually lacking. Site M0002 is therefore important in extending the available record of agglutinated foraminifers from short cores down to at least 45 mbsf (Core 10X), which includes the Pleistocene and perhaps part of the Pliocene.

The analysis of assemblages in Zone 2 requires additional sampling to obtain more abundant foraminifers.

The assemblages in Zone 3 (Table **T12**) represent middle Miocene material. At present, the agglutinated assemblages cannot be correlated with other Miocene faunas from the region (in particular Leg 151 Site 909).

In summary, the material from Site M0002, when combined with that of Site M0004, offers an opportunity to develop a Cenozoic agglutinated foraminiferal biozonation for the Lomonosov Ridge region of the central Arctic Ocean.

Hole M0003A

Shipboard analyses of benthic and planktonic foraminifers at Site M0003 were conducted using core catcher samples. Benthic foraminifers from Sample 2H-CC, 14–19 cm, included the agglutinated taxa *C. pusilla*, *Haplophragmoides* sp., *Trochammina* sp., and *Saccammina* sp., which are typical of Pleistocene sediments containing common agglutinated foraminifers, which usually underlie the uppermost 1–2 m containing calcareous foraminifers.

Four samples from Section 3H-CC were examined, yielding the following results from different lithofacies:

- 3H-CC, 0–1 cm = olive layer, containing unidentified agglutinated foraminiferal fragments.
- 3H-CC, 2–3 cm = olive layer, containing rare *Trochammina* sp.
- 3H-CC, 2–5 cm = olive layer, with darker streaks of manganese, agglutinated foraminifers *C. pusilla* and *Alveolophragmium polarensis*, planktonic foraminifer *N. pachyderma* (sinistral), and fragments of ostracodes *Polycope* and *Cytheropteron*.
- 3H-CC, 4–5 cm = dark manganese layer containing agglutinated foraminifers *C. pusilla, Haplophragmoides* sp., and *Recurvoides* sp.; planktonic foraminifers *N. pachyderma* (sinistral) and *Turborotalia quinqueloba*; and calcareous benthic foraminifer *Cassidulina*.

These results suggest that well-preserved foraminifers are present in some lithofacies of Pleistocene sediments of the Lomonosov Ridge as deep as 19.3 meters composite depth (mcd) (see below).

Hole M0004A

Shipboard analyses of benthic foraminifers at Site M0004 were conducted using core catcher samples. Benthic foraminifers from Hole M0004A range in age from Campanian to early Eocene and consist entirely of agglutinated taxa. No calcareous microfossils were found in the samples, probably owing to dissolution (Table **T13**).

The agglutinated benthic foraminiferal record recovered from Hole M004A can be subdivided into three stratigraphically significant assemblages, discussed below from top to bottom:

1. Samples 4X-CC through 24X-CC were barren of any foraminifers. The uppermost sample containing foraminifers is Sample 27X-CC. This sample, along with the next deeper core catcher (28X-CC), contained a moderately diverse assemblage of agglutinated foraminifers containing the species *Ammodiscus planus, Convallina* spp., *Haplophragmoides excavatus, Haplophragmoides perexilis, Psammosphaera eocenica,* and *Trochammina* spp. and common *Verneuilinoides subtilis* and *Verneuilinoides macintyrei*. The assemblage is assigned an early Eocene age based on superposition and the presence of *V. subtilis*, which was described from the Paleocene–lower Eocene Aklak Formation of the Beaufort Sea (McNeil, 1997). The genus *Verneuilinoides* is also a frequent component of early Eocene assemblages in the Barents Sea described by Nagy et al. (2000). The genus is characteristic of neritic environments.

   Sample 29X-CC contains an unusual type of agglutinated foraminiferal assemblage in sediment with a large amount of quartz sand. The dominant taxa are coarsely agglutinated species of *Lagenammina, Reophax*, and *Psammosphaera*. The tubular form of *Jaculella* and a finely agglutinated species of *Trochammina* are also present. The taxa recorded in this sample are not age diagnostic but are characteristic of a shallow-marine environment. Assemblages with common *Psammosphaera* are known from the Paleogene of Spitsbergen, and *Reophax*-dominated assemblages are known from the Eocene of western Siberia (Podobina, 1998). Based on these comparisons, the environment is interpreted as inner neritic. Samples 30X-CC and 31X-CC are barren of foraminifers.
2. Beneath a barren interval containing only pyrite and fish remains, a diverse assemblage of agglutinated foraminifers is present in Sample 32X-CC. This assemblage is distinctive, containing three species of primitive *Reticulophragmium* that dominate the assemblage. The species *Reticulophragmium ministicoogense, Reticulophragmium arcticum,* and *Reticulophragmium boreale* are known from the upper Paleocene in the Beaufort Sea (McNeil, 1997). *R. arcticum* is known from Paleocene strata in Alaska and Spitsbergen. Primitive species of *Reticulophragmium* are also known from the Paleocene of the North Sea and Western Siberia. The genus may have evolved in the northern hemi-

sphere during the middle Paleocene and is not known from Cretaceous strata. This "*Reticulophragmium* assemblage" also contains tubular forms such as *Nothia* and *Rhabdammina*, as well as *A. planus, Haplophragmoides raindeerensis, Recurvoides* sp., and *Trochammina* spp. The assemblage is present downhole to Sample 35X-CC. The age of the interval from Samples 32X-CC through 35X-CC is regarded as late Paleocene based on the FO of *Reticulophragmium* in Sample 35X-CC.

3. A completely different assemblage of agglutinated foraminifers was found in Samples 39X-CC through 42X-CC beneath an interval with no recovery. Agglutinated foraminifers in this assemblage are stained a medium yellowish brown color, perhaps indicating a higher level of thermal maturation of the enclosing sediment. The assemblage displays a high dominance of one *Trochamminoides* species. The assemblage is accompanied by rare specimens of *Glaphyrammina spirocompressa*, a species known from the Santonian to Campanian Smoking Hills sequence of the Beaufort-MacKenzie Basin. Another species present in Sample 41X-CC is *Recurvoides* cf. *obskiensis*, a taxon known from mid–Upper Cretaceous strata in the Norwegian offshore. Based on the low diversity, high dominance, and lack of any tubular forms, the environment is interpreted as inner neritic.

Hole M0004B

Shipboard analyses of benthic and planktonic foraminifers in Hole M0004B were conducted using two core catcher samples. Benthic foraminifers from Sample 1X-CC, 0–2 cm, contained rare *C. pusilla* and a single specimen of the planktonic foraminifer *N. pachyderma* (sinistral). Sample 3X-CC, 2–5 cm (~219 mbsf), was barren of foraminifers but contained many pyritized diatoms and other pyritized material, fish parts, and large unidentified spores.

Hole M0004C

Shipboard analyses of benthic and planktonic foraminifers in Hole M0004C were conducted using two core catcher samples. Benthic foraminifers from Sample 1X-CC, 0–2 cm, contained no foraminifers. Samples 2X-CC and 3X-CC, 0–2 cm, contained the agglutinated foraminifers *C. pusilla, Reophax, Rhizammina, Ammodiscus*, and *Recurvoides*. Sample 4X-CC contained a single specimen of the planktonic foraminifer *N. pachyderma* (sinistral); Sample 6X-CC was barren of foraminifers. Samples 8X-CC and 9X-CC contained the agglutinated taxon *C. pusilla* and unidentified fragments of agglutinated species. The sequence of foraminifers at this site is generally similar to those recovered from Holes M0002A and M0003A.

Pliocene and Pleistocene results summary

Previous studies have found that calcareous microfossils (benthic, planktonic foraminifers, and ostracodes) characterize the uppermost 1–2 m of sediments on ridges in various locations in the Arctic Ocean including the Lomonosov Ridge (Scott et al., 1989; Stein et al., 1994; Cronin et al., 1994, 1995; Evans and Kaminski, 1998).

The calcareous facies is underlain by predominantly agglutinated foraminiferal assemblages in many regions of the Arctic. The calcareous–agglutinated transition has been dated within marine isotope Stage 7 (Backman et al., 2004).

The calcareous–agglutinated transition was present at several sites and extended the depth of the predominantly agglutinated fauna to ~12–45 mbsf in Hole M0002A, >15 mbsf in Hole M0003A, and >14 mbsf in Hole M0004C (Table **T14**). However, sparse planktonic foraminifers are present in thin layers to 15 mbsf (= 19.3 mcd). By sampling a 1 cm dark layer in Sample 302-M0003A-3X-CC, 4–5 cm, we found *N. pachyderma* (sinistral) and *T. quinqueloba*. A single specimen of *N. pachyderma* was observed in Sample 302-M0004C-4H-CC (~18.4 mbsf = 17.1 mcd). Based on recent studies of *N. pachyderma* (sinistral) morphology, genetics, and stratigraphy, it is possible that the recent forms of this species had their first appearance at ~1.1 Ma and those from the earlier Pleistocene represent a different species (Kucera and Kennett, 2002).

Carbonate fossil preservation is intermittent at best down to 15 mbsf, and, as is the case with the uppermost few meters of Arctic sediments, fine-scale sampling is required to obtain calcareous material. The downcore appearance of what appear to be spherical (carbonate?) concretions begins near 20–30 mbsf. These first appear as small (~0.5 mm) rare barbell-shaped objects that increase in abundance and size downcore, often forming cemented accumulations of spheres. Peak abundances in these concretions occur in Hole M0002A at ~20–30, 50–63, and 117–123 mbsf before disappearing at ~155–170 mbsf, where major lithologic changes occur.

Cretaceous–Paleocene–Eocene results summary

The sequence of agglutinated foraminiferal assemblages found in Hole M0004A includes several distinct biofacies that have been recognized in circum-Arctic exposures and deep onshore and offshore wells. They can be used to reconstruct shallow-water marine depositional environments from prodeltaic–

inner neritic to outer neritic–uppermost bathyal environments.

Palynology, organic-walled dinoflagellate cysts

In total, 98 samples were processed for organic-walled microfossils. Palynomorphs were distinguished in different categories, but only dinoflagellate cysts (dinocysts) were identified to genus and species level. Assignment of some species must be considered provisional because of poor preservation and strong morphological variability and because safety considerations precluded the use of hydrofluoric acid. The abundance of dinocysts from Neogene and Pleistocene sediments is particularly low because of dilution by siliciclastic components. Despite the variable abundances, a tentative biostratigraphy could be established based on the presence of a few age-diagnostic species.

Hole M0001A

Two samples from Hole M0001A were analyzed for palynomorphs. Sample 1H-CC, 0 cm, contained pollen (*Pinus* and *Picea*) and a few dinocysts assignable to the genus *Brigantedinium*. This assemblage may be indicative of the modern conditions in the area. Sample 1H-CC, 24 cm, was barren (see Table **T15**).

Hole M0002A

Core catcher samples and a few additional samples were processed for palynological studies, allowing the recognition of four intervals in Hole M0002A. The upper ~160 m has a rather patchy record, as almost half of the samples were barren of palynomorphs. Following a barren interval (~23 m), an interval spanning ~1 m (Samples 44X-CC through 45X-CC) contained a dominant organic-walled dinoflagellate cyst (dinocyst) with some reworking of older dinocysts and massively abundant terrestrial pollen and spores, in addition to probably freshwater to brackish water algal cysts. Below that unit, the remainder of the drilled succession (down to Sample 62X-CC) contained both marine and terrestrial palynomorphs in high abundances. Preservation was moderate to fair in most samples containing dinocysts. Reworked dinocysts, pollen, and spores were present in almost all samples. Some of these may be as old as Carboniferous.

The uppermost 50 m of Hole M0002A lacks true age-diagnostic taxa. The presence of abundant *Filisphaera microornata* in Sample 12X-CC (51.26 mbsf) indicates a late Miocene to early Pleistocene age for this interval (cf. Head, 1993). The specimens recorded on the Lomonosov Ridge are morphologically different from *Filisphaera filifera* s.s. but may contain specimens of the subspecies *Filisphaera filifera pilosa*. Relatively high abundances of *Filisphaera filifera* s.l. are reported from the Middle to Upper Pliocene sediments of Yermak Plateau, Fram Strait, and East Greenland (e.g., Matthiessen and Brenner, 1996; Smelror, 1999; Bennike et al., 2002), indicating a Pliocene age for Sample 12X-CC. The age of the uppermost 50 m (Core 1X through Section 12X-3) cannot be resolved further (see Table **T16**).

Evittosphaerula sp. 2 of Manum et al. (1989) was recorded in Samples 17X-CC, 18X-CC, and 23X-CC (76.08–101.32 mbsf). It has a widespread distribution in Miocene sediments from the Norwegian-Greenland Seas and the Labrador Sea (Manum et al., 1989; Head et al., 1989; Poulsen et al., 1996). The total stratigraphic range in the high northern latitudes appears to be from the uppermost Serravallian to the lower Messinian, but higher abundances seem to be restricted to the Tortonian. Poulsen et al. (1996) recorded its first occurrence and subsequent acme interval in Core 151-908A-20X. That interval may correlate to the base of Chron C3Bn (Hull et al., 1996). This species has its last occurrence at the base of Core 151-908A-19X, approximating the top of Chron C3An (see Hull et al., 1996), giving a total age range of its acme from 5.9 to 7.1 Ma. It is here assumed that *Evittosphaerula* sp. 2 of Manum et al. (1989) migrated northward into the Arctic Ocean at the time of the acme in the Fram Strait, suggesting a similar age for its occurrence in Hole M0002A. The presence of *Bitectatodinium*? *serratum* confirms a late Miocene age for Sample 23X-1, 11–13 cm. It has previously been described from the Labrador Sea only (Leg 105 Hole 646B), from an interval assigned to nannoplankton Zones NN10 to mid-NN11 (Head et al., 1989a), which is consistent with our results based on dinocyst biostratigraphy.

As Samples 13X-CC, 14X-CC, and 15X-CC were barren of dinocysts, except for a single specimen of *Filisphaera* sp., the upper Miocene/Pliocene boundary must be placed between Cores 12X-CC and 17X-CC.

Habibacysta tectata is present from Sections 23X-1 through 35X-1, between 101.32 and 154.06 mbsf. This species has its first occurrence in the northern mid-latitudes during the middle Miocene at 14 Ma (Williams et al., 2004), suggesting an age not older than Serravallian for Section 35X-1. The presence of a single specimen of *Operculodinium janduchenei* in Sample 35X-1 is consistent with this assignment because it has a recorded range from lower Miocene to Upper Pliocene (e.g., Head et al., 1989a). The LO of *H. tectata* is not well defined, but it had its last appearance on the Yermak Plateau in Leg 151 Hole 911A in the lower Pleistocene (Matthiessen and

Brenner, 1996). Its co-occurrence with *Evittosphaerula* sp. 2 of Manum et al. (1989) in Sample 23X-CC indicates that its range may be restricted in the central Arctic Ocean to the middle and upper Miocene (see Table **T16**).

The presence of a single specimen of *B.? serratum* in Sample 35X-1 may extend its range into the middle Miocene. Species of *Impagidinium (Impagidinium japonicum, Impagidinium major, Impagidinium pallidum,* and *Impagidinium velorum*) that occur in the same interval as *H. tectata* are not age diagnostic, but *I. major* has previously been recorded (only once) from nannoplankton Zone NN10 (Tortonian) in the Labrador Sea (Head et al., 1989a). Samples 302-M0002A-38X-CC through 44X-1 are palynologically barren.

The age assessment of the interval represented by Samples 44X-CC and 45X-CC is problematic. Although some taxa present in Sample 44X-CC suggest a Rupelian (early Oligocene) or, more likely, Chattian (late Oligocene) age, others indicate older intervals. Moreover, Sample 45X-CC yielded a monotypic assemblage of a new peridinioid taxon (genus et sp. indet. B) of which no age indication is available. The same sample thus has apparently reworked elements ranging in age from Cretaceous, earliest Eocene, middle Eocene, late Eocene, to early Oligocene (e.g., isolated specimens of *Cribroperidinium muderongense, Apectodinium augustum, Glaphyrocysta semitecta, Phthanoperidinium amoenum, Svalbardella cooksoniae*, and *Wetzeliella gochtii*). Thus, the age of the interval 44X-CC to 45X-CC may not be older than (early) Oligocene but is more likely to be much younger (late early Miocene?). Significantly, the reworked taxa suggest that sediments of late middle Eocene to Oligocene age were once present in the area (see Table **T16**).

Interval 46X-CC through 62X-CC has a similar palynological composition throughout, including massive abundances of the *Phthanoperidinium echinatum* group and *Senegalinium* spp., with isolated *Thalassiphora delicata, Cerodinium depressum,* and *Phthanoperidinium clithridium* (with the exception of Sample 47X-CC, which is dominated by *Impagidinium* spp.). In addition, there are consistent occurrences of an intermediate form between *Lentinia wetzelii* and *Lentinia serrata*. Combined provisional evidence thus suggests an age of ~45.5 Ma (Chron C20r) and older for this interval, applying the scheme of Eldrett et al. (2004) from Leg 151 Hole 913B. Alternatively, if the form described above can be attributed to *L. serrata* and the specimens of *P. clithridium* and *C. depressum* are reworked, then the age may be as young as mid-Bartonian (middle Eocene, ~40 Ma). However, many typical Bartonian species, also known from an interval of that age from Leg 151 Hole 913B (e.g., Firth, 1996), are conspicuously missing in Hole M0002A.

The interval between Samples 46X-CC and 62X-CC is also characterized by high abundances of terrestrial palynomorphs in addition to abundant, remarkably large (>500 µm) spherical phycomata(?) of *Tasmanites* spp. (= gen. et sp. indet. A in Table **T17**). From Sample 60X-CC downhole, the moderately diversified dinocyst assemblage is joined by a new distinctly elongated and large species of *Operculodinium—Operculodinium* cf. *microtriainum*. The biostratigraphic significance of this taxon is unknown.

The bottom age of Hole M0002A (Sample 62X-CC) is, in view of only minor compositional changes from the interval between Samples 46X-CC and 62X-CC, thought to be comparable (i.e., on the order of ~45–46 Ma). The FO of *P. clithridium* is reported to be at 46.2 Ma (Eldrett et al., 2004) (see Table **T16**).

Preliminary paleoenvironmental interpretation

Most dinocyst taxa recorded in the Neogene sediments of Hole M0002A have a restricted geographic distribution in the northern high latitudes. *Filisphaera* spp., *Evittosphaerula* sp. 2 of Manum et al. (1989), *I. japonicum, I. major,* and *I. pallidum* prefer cool–temperate to cold (ice margin) waters. *H. tectata* lived in cool–temperate to subtropical conditions but apparently preferred cooler conditions (e.g., Head, 1994). *I. velorum* and *O. janduchenei* are more widely distributed in northern hemisphere Paleogene, Neogene, and Quaternary sediments but are mainly associated with cooler intervals (e.g., Brinkhuis and Biffi, 1993; Versteegh et al., 1996).

Nematosphaeropsis labyrinthus and *Spiniferites ramosus* are cosmopolitan species (e.g., Marret and Zonneveld, 2003). Thus, the ecological preferences of the taxa suggest that cold to cool-water but seasonally ice-free conditions occurred during the Neogene at the Lomonosov Ridge or were influenced by such settings. Barren samples might be indicative of perennial sea ice cover, postmortem degradation, or absence of cyst-forming species.

The presence of freshwater algae of the genera *Botryococcus* and *Pediastrum* is a distinct signal in some Neogene and Quaternary sediments. In particular, Sample 1X-CC contains abundant freshwater algae. Comparable acmes of *Pediastrum* have been found in a sediment core from the Alpha Ridge (Mudie, 1985). The occurrence of freshwater algae is clearly related to river run-off from large rivers draining into the Arctic Ocean (Matthiessen et al., 2000). These algae are incorporated into sea ice during formation in au-

tumn and winter and are further transported via the Transpolar Drift or the Beaufort Gyre.

The monotypic assemblages of gen. et sp. indet. B in Samples 44X and 45X, together with the pronounced terrestrial and freshwater and/or brackish water algal components, strongly indicate restricted marine, brackish water (estuarine?) conditions for this interval.

In general, the only moderately diversified assemblages below Sample 45X-CC (down to the bottom of the hole) are mainly composed of typical high-latitude Eocene taxa and mainly represent heterotrophic dinoflagellates (Brinkhuis et al., 2004a, 2004b). The concomitant abundance of siliceous microfossils throughout indicates a highly eutrophic setting (Reichart and Brinkhuis, 2003). Meanwhile, runoff-related low salinity might be indicated by the abundance of terrestrial palynomorphs and the phycomata of chlorophytes such as *Tasmanites*. The absence of benthic biota (see **"Planktonic and benthic foraminifers and ostracodes"**) and the high organic matter content indicate suboxic to anoxic bottom conditions at this time, such as the highly stratified, restricted marine, poorly ventilated waters of the modern Black Sea.

The exception to this is Sample 47X-CC, which is dominated by *Impagidinium* spp., roughly assignable to the cosmopolitan Eocene taxon *Impagidinium dispertitum*. In modern oceans, most *Impagidinium* consistently occur in tropical to subtropical, oligotrophic oceanic environments (e.g., Wall et al., 1977; Rochon et al., 1999; Marret and Zonneveld, 2003). Only *I. pallidum* characterizes polar environments today. The composition of the dinocyst assemblage of Sample 47X-CC is thus indicative of warm and oligotrophic surface water conditions. Yet, terrestrial palynomorphs and the phycomata remain prominent in this sample, suggesting the continual influence of runoff.

The anomalous Sample 47X-CC may thus reflect a short-lived phase of warm conditions at the end of the middle Eocene. Bohaty and Zachos (2003) have recently documented such a phase, occurring at ~41.5 Ma in the Southern Ocean, coined the Middle Eocene Climatic Optimum.

Hole M0003A

Three core catcher samples (1H-CC, 22–27 cm, 2H-CC, 14–19 cm, and 3H-CC, 3–5 cm) were analyzed for palynomorphs. All samples were barren except for a single specimen of bisaccate pollen (*Pinus*) in the uppermost and lowermost samples (see Table **T18**).

Hole M0004A

Samples from core catchers (4X-CC through 42X-CC) and a few additional samples yielded well-preserved and generally rich palynological associations. A number of dinocyst and other events have reasonably well constrained age calibrations (Table **T19**), providing an age model for the cored succession (Table **T20**). Hole M0002A was abandoned after reaching levels assignable to the mid-Lutetian. Despite overall poor recovery, Hole M0004A represents its continuation and penetrated the older Arctic Paleogene and even the Upper Cretaceous record.

The middle/lower Eocene (Lutetian/Ypresian) and Paleocene/Eocene (Thanetian/Ypresian) boundaries may be recognized using abundance peaks of the freshwater fern *Azolla* spp. and dinocysts assignable to the (sub)tropical genus *Apectodinium* (particularly *A. augustum*), respectively. Note that here we follow the recently revised concept of the position of the Paleocene/Eocene boundary (i.e., the base of the carbon isotope event [CIE] at the Global Stratotype Section and Point [GSSP] in Egypt). This means that the oldest *Apectodinium* acme, and the range of *A. augustum*, is now placed in the lowermost Eocene.

The FO and LO of the acme of *Azolla* spp. have been calibrated against magnetostratigraphy in ODP Leg 151 Hole 913B (Eldrett, 2003; Eldrett et al., 2004), indicating that the base of the middle Eocene must be placed between Sections 10X-CC and 11X-CC. The entire (short) range of *A. augustum* marks the lowermost Eocene interval and its well-known "thermal maximum," called the Paleocene/Eocene Thermal Maximum (PETM) (cf. Zachos et al., 2001) throughout the northern hemisphere (i.e., sensu the new GSSP). The base of the Eocene thus occurs in Core 32X. An overlying continuous and expanded lower Eocene record is demonstrated by the subsequent *Cerodinium wardenense* and *Deflandrea oebisfeldensis* acme intervals, which, in turn, are overlain by the FO of the *Wetzeliella articulata-hampdenensis* complex (Table **T20**). This succession is well known from among other places (e.g. the entire North Sea Basin) and the entire North Atlantic region, including the Norwegian, Greenland, Beaufort, and Barents Basins, albeit mostly from industry wells (H. Brinkhuis, unpubl. data; J.P. Bujak, pers. comm., 2004). The PETM is calibrated against the lower part of Chron C24r. Its onset has an age of 54.98 Ma, and the PETM spans ~200 k.y. (Röhl et al., 2000). The underlying succession does not truly yield age-diagnostic dinocysts. Yet, because no sedimentological break is apparent downhole until Sample 35X-CC, it appears that the interval underlying the PETM may tentatively be regarded as representing the uppermost Paleocene (see Tables **T19, T20**).

Stratigraphically below the PETM, the assemblage from Sample 34X-CC has a Paleocene character, with the occurrence of *Deflandrea denticulata* and *Membranosphaera* spp. (e.g., Heilmann-Clausen, 1985). This contrasts with assemblages from the underlying Sample 35X-CC, where isolated specimens of the late Cretaceous dinocysts *Chatangiella verrucosa* and *Palaeohystrichophora infusorioides* and the lack of typical Paleocene dinocysts in the midst of rich but non-age-diagnostic sporomorphs may well indicate a (early) Campanian age. Alternatively, these specimens may represent late Paleocene reworking of the underlying sedimentary bedrock.

Samples also rich in sporomorphs but totally dominated by typical mid–Late Cretaceous species of *Chatangiella* have been recorded from Sample 39X-CC and further downhole. Despite a few co-occurring Paleogene dinocysts, this aspect, including major changes in palynofacies and organic maturity, strongly suggests that Sample 39X-CC is early Campanian or older in age and that a major unconformity sits above it (see Tables **T19, T20**).

Conspicuously, there was no core recovery between Samples 35X and 39X. The agglutinated benthic foraminifer assemblage (see **"Planktonic and benthic foraminifers and ostracodes"**) of Sample 35X-CC is apparently of Paleocene aspect and indicative of shallow-marine environments. This agrees with a palynological assemblage dominated by sporomorphs, although it is remarkable that no Paleocene dinocysts were found. The few Cretaceous dinocysts found in Sample 35X-CC may thus indeed represent reworking from the directly underlying sedimentary bedrock during the late Paleocene. It therefore appears that the latter sample marks the base of the Paleocene succession overlying the unconformity because cores could not be retrieved from the underlying 20 m (see Tables **T19, T20**).

Preliminary paleoenvironmental interpretation

The rather mature Campanian assemblages are dominated by sporomorphs, notably spores, and comprise many representatives of the probable heterotrophic dinocyst *Chatangiella*. This aspect suggests nearshore conditions at this time, in agreement with the interpretation of the co-occurring agglutinated benthic foraminifer assemblages (see **"Planktonic and benthic foraminifers and ostracodes"**). Both the lithology and the palynomorph assemblages are distinctly different from those in the organic-rich black muds of Core Fl-533 and the laminated biosiliceous ooze of Cores Fl-437 and the Canadian Expedition to Study the Alpha Ridge (CESAR) 6 that were deposited at the Alpha Ridge in high-productivity environments (perhaps due to upwelling) in the Campanian to Maastrichtian (e.g., Firth and Clark, 1998).

The upper Paleocene–lower Eocene palynological associations are generally dominated by sporomorphs and only occasionally by dinocysts. The dinocyst assemblages are usually dominated by *Senegalinium* spp., except for the *Apectodinium*-dominated PETM interval (Samples 30X-CC and 31X-CC). Additional elements in the lower Eocene are *D. oebisfeldensis, C. wardenense*, and, in younger strata, the *Cerodinium striatum–D. denticulata* complex. Environmental conditions apparently did not vary significantly during the later Paleocene to the early middle Eocene.

Sporomorphs disappear completely at about the end of the early Eocene (Ypresian) only to return by early middle Eocene (Lutetian) times. The dominance of cysts of probable heterotrophic dinoflagellates (mainly *Senegalinium* spp. and *Cerodinium/Deflandrea* spp.), some of them possibly being tolerant of freshwater conditions, and the concomitant abundance of diatoms and silicoflagellates from Samples 4X-CC through 18X-CC overall indicate eutrophic conditions. The low diversity of the dinocyst assemblages may indicate reduced sea-surface salinities. In the middle of this succession (Cores 11X and 12X), there is an extremely dense concentration of remains of the hydropterid (freshwater) fern *Azolla*—unprecedented in other Eocene sections yielding *Azolla*. The event testifies to an extreme change in environmental conditions at the base of the lower middle Eocene (Lutetian). A distinct acme of *Azolla* spp. has previously been recognized across northern high and mid-latitudes from many marine and even deep marine settings (as transported elements) (e.g., Boulter and Manum, 1989; Eldrett, 2003; Eldrett et al., 2004; J.P. Bujak and H. Brinkhuis, unpubl. data). In an unpublished Ph.D. thesis concerning Leg 151 Site 913, J.S. Eldrett showed that the *Azolla* maximum can be calibrated to mid-Chron C22n (~49.2 Ma). Note that the concentrations of *Azolla* remains recovered during Expedition 302 are several orders of magnitude higher than those recorded elsewhere. Yet, apparently microfossils indicative of marine environments (dinocysts, silicoflagellates, and diatoms) continue to occur in the assemblages in samples studied to date.

The acme of (sub)tropical *Apectodinium* spp. is of global paleoenvironmental significance because it reflects a pronounced short-term warming at the onset of the Eocene (i.e., the PETM) (e.g., Bujak and Brinkhuis 1998; Crouch et al., 2001, 2003a, 2003b; Röhl et al., in press). It has been shown to occur synchronously across hemispheres and to precisely coincide with the onset of the so-called PETM CIE and benthic extinction event. Dinocyst assemblages con-

taining common *Apectodinium* were also recovered from intrabasaltic sediments of the lower basalt series at ODP Leg 104 Site 642 (Boulter and Manum, 1989) that were dated by a single radiometric age at 57.8 ± 1.0 Ma. This suggests a similar age range in the arctic regions. Multiple acmes of *Apectodinium* have been reported from the late Paleocene and early Eocene in the literature (e.g., Iakovleva et al., 2001; Crouch et al., 2003a, 2003b), but a large number of published and unpublished (oil exploration) studies have shown that *A. augustum* is strictly confined to the PETM itself (see summary in Bujak and Brinkhuis, 1998).

Hole M0004B

Samples 1X-CC and 3X-CC were analyzed for palynomorphs. Sample 1X-CC was barren. Sample 3X-CC contains an assemblage comparable to that found in cores of Hole M0002A (see Table **T21**).

Hole M0004C

Six core catcher samples and one additional sample were analyzed for palynomorphs. All samples were barren of dinocysts except for Sample 6X-2, which contained rare *H. tectata*. The last occurrence of *H. tectata* is not well defined, but it has its last appearance on the Yermak Plateau in Leg 151 Hole 911A in the lower Pleistocene, approximately at the base of the Jaramillo Subchron (Matthiessen and Brenner, 1996). Based on lithologic correlation to Hole M0002A, the base of Hole M0004C is not older than Pliocene. Therefore, Samples 1H-CC through 4H-CC are probably younger than 1 Ma (see Tables **T22, T23**).

Stratigraphic correlation

During the coring operations of Expedition 302, it became clear that the aim of recovering multiple core copies across the same stratigraphic intervals for hole-to-hole correlation could not be achieved to the extent planned. However, material recovered from separate but closely spaced sites allowed a limited amount of site-to-site correlation, based primarily on physical property data (gamma ray attenuation [GRA] bulk density, magnetic susceptibility [MS], *P*-wave velocity, and electrical resistivity [RES]), generated with the multisensor core logger (MSCL) (see **"Petrophysics"**) but also aided by high-resolution geochemical pore water measurements of ammonia concentrations, alkalinity, and other pore water measurements (see **"Geochemistry"**). Additional shore-based measurements of color reflectance values and natural gamma radiation (NGR) counts proved useful to refine stratigraphic correlations during the shore-based part of the expedition. For the final shore-based splice, inclination data provided by postcruise paleomagnetic studies proved important. When the cores were split, many of them showed signs of disturbance and/or "flow-in," which could not be identified aboard the ship. These intervals were systematically tabulated and are given in Table **T24.** Additional data acquired from the onshore phase led to revisions in the original splice. In terms of recovered stratigraphy, the bulk of the material was recovered from Hole M0002A in the upper half of the stratigraphic record and from Hole M0004A in the lower half. Apart from the deeper Core 302-M0004B-3X, which provided overlap with Cores 302-M0002A-49X and 50X at ~216 mbsf, only in the upper ~30 m were multiple copies of cored intervals recovered, allowing for construction of a composite depth scale and spliced record for this short interval.

Depth offset determination data

Three main sources of information were used to determine the vertical stratigraphic offset between cores. The first information was the drillers depths in relation to the mudline. Because of problems with the piston coring device, which was only used for Cores 302-M0001A-1H and 2H, 302-M0003A-1H through 3H, and 302-M0004C-1H through 4H, the mudline was identified confidently only for Core 302-M0004C-1H, which represents the shallowest stratigraphic interval recovered from all holes. Those cores recovered with the extended corer system showed variable recovery rates. In cases where core recovery was low, the absolute depth of the core material could be from anywhere within the cored interval, which occasionally included material from the previous, shallower core and resulted in >100% recovery. Thus, the real stratigraphic depth was adjusted by using the closely spaced physical property measurements from the MSCL (see **"Petrophysics"**). Because the core flow was slower than expected, it was possible to measure all four physical properties at a resolution of 2 cm, with repeat measurements for MS, allowing data quality control. GRA bulk density and MS data were determined shipboard for all cores except Core 302-M0004C-6X, which did not fit through the MS loops. This core was remeasured during the onshore phase of the expedition. For this core, the absolute magnitude of *P*-wave velocity, GRA bulk density, and NGR data need to be corrected for sediment volume effects, whereas MS measurements require correction for sensor-type effects (see **"Petrophysics"**).

Finally, after the high-resolution pore water squeeze and Rhizone samples were analyzed (see **"Geochemistry"**), the ammonia, alkalinity, and manganese

profiles were found to exhibit a characteristic linear change below the top few meters and allowed determination of stratigraphic offsets for cores where MSCL data alone gave ambiguous results. Shore-based paleomagnetic measurements allowed further refinement of stratigraphic offsets.

Data pruning

Raw data, comprising all MSCL measurements, are available in electronic form. According to routinely performed standard calibrations, these data were processed with the Geotek software (see **"Petrophysics"** in the "Methods" chapter). All sensor values clearly showed the influence of section as well as core breaks. To avoid correlation of section breaks, the Geotek measurements of *P*-wave signal amplitude and liner thickness were used to programmatically remove data points from near core breaks and across section end caps, resulting in the removal of 4–6 cm at the top and bottom from each section.

MSCL, color, and NGR data, plotted against composite depth, are shown in Figure **F13A, 13B, 13C,** and **13D** for Site M0002; Figure **14A, 14B, 14C,** and **14D** for Site M0003; and Figure **15A, 15B, 15C,** and **15D** for Site M0004.

Composite depths and splice

With limited core recovery, an almost complete composite depth section could only be established for the upper ~30 m using a site-to-site integration. Data for the top 50 mcd are shown in Figure **F16A** (GRA bulk density), **F16B** (MS), **F16C** (*P*-wave velocity), **F16D** (RES), **F16E** (L*), **F16F** (chromaticity a*), **F16G** (chromaticity b*), **F16H** (NGR), and **F16I** (top 30 mcd, magnetic inclination). The stratigraphic ties, described in the following section, result in depth offsets for each core as summarized in Table **T25** and allow the definition of a stratigraphic splice as given in Table **T26**. Composite splice data are shown in Figure **F17A** and **F17B.**

A mudline was established for Core 302-M0004C-1H. There was no multiple core recovery to verify the interval between this core and Core 302-M0004C-2H, although the sediment from the top of Core 302-M0004C-2H appears to be identical to the lithology at the base of Core 302-M0004C-1H. Core 302-M0002-1X was matched to an interval covered by Core 302-M0004C-1H, based on NGR and color data. The top core from Hole M0002A also shows very low ammonia pore water concentrations, suggesting that it lies within the stratigraphic interval covered by Core 302-M0004C-1H. Cores 302-M0003A-1H and 302-M0004C-2H both show a characteristic dark layer overlying an olive-green clay, with distinct signals in the chromaticity parameter a*, GRA bulk density, *P*-wave velocity, and NGR data and supported by magnetic inclination data. Chemical pore water profiles strongly support a continuous stratigraphic succession from Cores 302-M0004C-1H and 2H, and Core 1H also shows higher *P*-wave velocities than Core 2H.

A strong tie can be made between Cores 302-M0003A-2H through 302-M0004C-3H and 4H, bridging the gap between these two cores. Core 302-M0004A-1H can be tied to Core 302-M0003A-3H. Core 302-M0003A-3H can be linked to Core 302-M0004C-4H and extends the semicontinuous splice to ~19 mcd. Starting from the dark layer found in Cores 302-M0004C-2H and 302-M0003A-1H, chromaticity a* data, which reflect red-green variations, show a distinct sinuisoidal succession from red values across Cores 302-M0004C-2H and 3H and 302-M0003A-1H and 2H to more green values at the base of Cores 302-M0004C-3H and 302-M0003A-2H, followed by more red values in Cores 302-M0004C-4H and 302-M0003A-3H. This succession culminates in a distinct shift to more green sediments downcore, recorded in Cores 302-M0004A-2X, 302-M0004C-6X, and 302-M0002A-5X. This distinct marker is found at ~21 mcd. Below this marker, Core 302-M0004A-3X ties to Core 302-M0002A-6X. Core 302-M0002A-6X can be tied to Core 302-M0004A-3X based on magnetic inclination data, extending the splice to ~28 mcd.

At ~215 mcd, a single Core 302-M0004B-3X can be tentatively tied to Core 302-M0002A-49X and 50X and partially fills a stratigraphic interval not recovered otherwise.

Drillers depths suggest overlap between Holes M0004A and M0002A at ~268 mcd, but this overlap cannot unequivocally be confirmed with MSCL data. For the cores below the top ~40 mcd, most depths were determined such that mcd = mbsf for simplicity. The only departure from this strategy was necessary when subsequent cores overlapped because of >100% recovery. In those cases, one or both of the overlapping cores was slightly depth adjusted to avoid overlap where MSCL measurements would clearly indicate that no such overlap existed.

Postcruise work will involve a more detailed correlation of individual features from the top 40 m, allowing stretching and squeezing in cores, helped by high-resolution image line-scan data. It must be noted that the offshore interpretation was achieved with no knowledge of the actual core quality and was revised during the onshore phase after cores were split and additional measurements were taken. The variable core quality meant that several cores had to be excluded from composite depth develop-

ment. Downhole logging data collected from Hole M0004B between ~218 and 65 mbsf might allow the placement of cores that fall within this interval to be constrained more tightly.

Timescale and sedimentation rates

Although the Arctic Basin is virtually landlocked and receives an abundant input of freshwaters from the surrounding continents (Aagard and Carmack, 1989), it has long been believed that the sedimentation rates in the Arctic Basin during the Quaternary and late Tertiary were ~1 mm/k.y. (Clark, 1970, 1971, 1974, 1990, 1996; Clark et al., 1980; Witte and Kent, 1988). These early estimates were based primarily on the paleomagnetic stratigraphy of relatively short gravity and piston cores. More recently, a review of these and other data (Backman et al., 2004), along with an evaluation of sedimentation rates based on a consideration of bedrock ages and total sediment thickness, gave estimates of long-term sedimentation rates that are ~10 times higher than previously thought (i.e., ~1 cm/k.y.). This estimate is borne out by inspection of Figure **F7A,** which shows ~410 m of sediment overlying what is believed to be the ~57 Ma rifting unconformity.

Here we consider all biostratigraphic, lithostratigraphic, and paleomagnetic data that provide time control in the sedimentary sections recovered during Expedition 302. All sites are located within 16 km of each other (Fig. **F18A, F18B**). Because of the very flat-lying section of relatively uniform thickness on the Lomonosov Ridge, all sites cored are correlated based on lithostratigraphy, chemostratigraphy, and the MSCL core logs. We treat all the material recovered as increments of a single section and calculate sedimentation rates for this integrated section as a whole.

Biostratigraphy

One reason that it has been difficult to establish sedimentation rates for the Arctic Ocean sediments is that there are very few microfossils preserved in the upper part of the sedimentary section (Backman et al., 2004). Carbonate microfossils are extremely sparse below the Holocene and disappear altogether within the Pleistocene. Siliceous microfossils are also absent below the uppermost thin layer of Holocene sediments, in which they are rare. Thus, it has been difficult to use biostratigraphy as a guide to aid interpretations of paleomagnetic stratigraphies. In the sections recovered during Expedition 302, we depend almost exclusively on organic microfossils (dinoflagellate cysts) for biostratigraphic control. This is especially true for the Neogene, where siliceous microfossils are absent and where carbonate microfossils are poorly preserved and largely absent.

In the Paleogene, dark organic-rich sediments were recovered that contained abundant siliceous microfossils (diatoms, silicoflagellates, and ebridians) in addition to rich dinoflagellate assemblages. In one short middle Eocene interval, a few specimens of radiolarians were also found; however, all the other assemblages indicate a predominantly brackish water environment in which radiolarians are not commonly present. The brackish water, high-latitude diatom, silicoflagellate, and ebridian assemblages are not well calibrated to the paleomagnetic timescale. Dinoflagellate stratigraphy, however, is well suited for more brackish water environments and has recently been tied to paleomagnetic records and to well-dated calcareous nannofossil stratigraphies in the Norwegian Sea and other high- to mid-latitude areas (Eldrett et al., 2004; Firth, 1996; Mudge and Bujak, 1996; Bujack and Mudge, 1994; Brinkhuis, 1994).

First and last occurrences of important organic microfossils are given in Table **T27.** The silicoflagellate biostratigraphic datums are given in Table **T28.** The diatom biostratigraphic datums are listed in Table **T29,** and the foraminifer and the calcareous nannofossil datums are given in Table **T30.**

Paleomagnetic stratigraphy

Paleomagnetic stratigraphy provides the chronostratigraphic context into which biostratigraphic datums are placed. However, biostratigraphy provides an important guide to the interpretation of paleomagnetic reversal patterns. This is especially true for sections in which sediment recovery is incomplete or where the paleomagnetic record is discontinuous. The paleomagnetic record for Expedition 302 is discontinuous because of incomplete core recovery and because some parts of the section (particularly the middle Eocene) do not retain a strong paleomagnetic signal. Although the inclination record is complicated, it has a characteristic pattern than can be correlated from core to core and site to site (see Fig. **F3** in the "Expedition 302 summary" chapter). Thus, the complicated nature of the record does not appear to be caused by simple disturbance of the core or of the local sedimentary section. With less than complete recovery and sparse biostratigraphic control, establishing a paleomagnetic stratigraphy from inclination data is open to multiple interpretations (see **"Paleomagnetism"**). Here we use our "preferred" model of paleomagnetic reversal boundaries (Table

T31). This model is used in the Neogene for estimating sedimentation rates (Fig. F19).

Sedimentation rates

All the paleomagnetic and biostratigraphic datums are plotted in Figure F19. In developing the models for average sedimentation rates in the combined Lomonosov Ridge section, we rely primarily on paleomagnetic data and dinoflagellate biostratigraphic datums. Linear sedimentation rates are calculated based on the most reliable data points. (Fig. F19).

The sediment surface is assumed to have "zero" age. This assumption is supported by the presence of modern nannofossils species in the near-surface sediments. The first million years of the section contain a few calcareous nannofossils and dinocyst datums (Tables T27, T30) and three paleomagnetic chron boundaries (Tables T31, T32). They lie on a nearly straight line when plotted versus depth (Fig. F19), with a sedimentation rate of 19.9 m/m.y. (Table T33).

There is a very low sedimentation rate estimated between the base of the Jaramillo and the top of the Olduvai Subchrons (2.1 m/m.y.) (Table T33); however, both the *N. pachyderma* datum (noted at ~21 mcd) (Table T30) and the *Habibacysta tectata* datum appear to fit well with the paleomagnetic interpretation.

Below this point, sedimentation rates vary from ~11 m/m.y. to >20 m/m.y. to the base of Chron C5AAn. Given the occasional poor preservation and rare occurrence of the organic microfossils, the paleomagnetic stratigraphy is in good general agreement with the biostratigraphy (Fig. F19). Below Chron C5AAn, sedimentation rates drop markedly from 7 m/m.y. to slightly more than 1 m/m.y. in lithostratigraphic Subunit 1/5.

Immediately below lithostratigraphic Subunit 1/5, the color abruptly turns to gray and the magnetic signal becomes weak and uninterpretable. The next older dinoflagellate datum identified (between Cores 302-M0002A-44X and 5X) is the LO of *W. gochtii* (Table T27) with an age of 27 Ma (late Oligocene); however, there are other unidentified species of dinoflagellates and pollen in this interval that suggest a Miocene age for this sample. In and below this level there are also reworked specimens of dinoflagellates that are clearly of late Eocene and even older ages.

Cores 302-M0002A-44X, 45X, and 46X give ample evidence of rapid changes in depositional environment with distinct breaks in layering and marked changes in color. Between Core 302-M0002A-44X (~195 mcd) and Core 48X (~212 mcd), biostratigraphic datums range in age from 27 to 45.5 Ma. This, together with the clear breaks in color and layering in the sediments, suggests that much of the section in this interval has been removed by erosion. Just below what appears to be an erosional unconformity in the base of Core 302-M0002A-46X, there are several last occurrence datums for dinoflagellate species and one well-constrained first occurrence datum for a silicoflagellate species (FO of *C. hexacantha*) (Locker, 1996). The oldest last occurrence datum in the group of dinoflagellate events is the LO of *T. delicata* (45.5 Ma) at ~212 mcd. The FO of *C. hexacantha* (44.1 Ma) is at ~215 mcd. In this case, where erosion and reworking may have affected the position of a last occurrence datum, we take the FO of *C. hexacantha* as the more reliable age marker. Using this datum and the next older dinoflagellate datum (the FO of *Phthanoperidinium clithridium*) at 46.2 Ma, we estimate a sedimentation rate of 28.6 m/m.y. for this middle Eocene part of the section. The latter dinoflagellate datum is found in both Holes M0002A and M0004A and is used along with other data to correlate the two sections.

The next older, well-dated biostratigraphic datums are the top and bottom of the *Azolla* spp. event (48.6 and 49.2 Ma, respectively) (Eldrett et al., 2004). Combined with the FO of *P. clithridium* datum, these closely spaced events give an average sedimentation rate of 10.5 m/m.y. (Fig. F19). Between the FO of *Azolla spp*. (49.2 Ma) and the LO of *D. oebisfeldensis* (52.9 Ma), the sedimentation rate falls to 7.9 m/m.y. (Fig. F19).

The next older well-dated events are the closely spaced FO and LO of *A. augustum*. These events span the PETM and are dated at 55 and 55.6 Ma, respectively. The PETM lies close to the oldest identified paleomagnetic chron datum (top of Magnetochron C25n) (Table T30) found in the section. A straight line connecting the LO of *D. oebisfeldensis* datum and the paleomagnetic datum passes very close to the *A. augustum* datums (especially the LO of *A. augustum*) and gives an average sedimentation rate of 20.3 m/m.y. (Fig. F19).

The top of Chron 25n lies within 3 m of dinoflagellate datums LO of *Palaeohystrichophora infusorioides* and LO of *Chatangiella verrucosa* complex (dated at 69.42 and 72.5 Ma, respectively) (Table T27), and thus marks a sharp break in the record. This hiatus is probably associated with the rifting unconformity estimated to be ~57 Ma and lies near Core 302-M0004A-35X at 405 mcd. At and below this depth, the identified dinoflagellate datums grow rapidly older, stretching well into the Cretaceous, and have an average sedimentation rate of ~1.6 m/m.y. (Fig.

F19). This average rate is consistent with a very slowly subsiding or episodically uplifted continental margin on which the lack of accommodation space for sediment leads to frequent erosional episodes and very slow average sedimentation rates.

Conclusion

The debate about the true average sedimentation rate in the Arctic Basin has been resolved. Average sedimentation rates on the Lomonosov Ridge are on the order of 10–20 m/m.y. In the Pleistocene section (that part of the record most frequently studied prior to Expedition 302), sedimentation rates are close to 20 m/m.y. This is >20 times the rate commonly applied to the gravity and piston cores studied by Clark and his colleagues (Clark, 1970, 1971, 1974, 1990, 1996; Clark et al., 1980), and it is ~2.5 times the long-term average rate proposed by Backman et al. (2004). The difference between the long-term average and the shorter-term averages presented here result from the presence of at least one substantial break in the sedimentary record. There may be as much as 30 m.y. missing between the middle part of the middle Eocene and the middle to lower Miocene. Given the limited age control, there may be other gaps in the record that we have not detected.

The major hiatus above the middle Eocene divides the cored section: the upper half is a siliciclastic section, with a few preserved biogenic remains. The lower half, below ~217 mcd, is relatively rich in biogenic debris and generally has finer-grained siliciclastic material. The preservation of the organic content of these sediments is likely to have resulted from relatively high productivity and a strong pycnocline controlled by salinity. Both the upper and lower parts of the section have average sedimentation rates ranging from ~10 to >20 m/m.y.

Petrophysics

Laboratory and in situ measurements were performed to characterize downhole variations in the physical properties of sediments on the Lomonosov Ridge. Petrophysical measurements included (1) downhole wireline logging, (2) nondestructive whole- and split-core measurements performed with the Geotek MSCL, and (3) discrete measurements carried out on both whole and split cores. Wireline logging provided in situ measurements of NGR, *P*-wave velocity, and resistivity (FMS). These data complement nondestructive whole-core determinations of bulk density, compressional *P*-wave velocity, electrical RES, MS, and NGR. In addition to whole-core measurements, split-core MSCL measurements of *P*-wave velocity, MS, and density were made on selected sections. Digital line scanning was performed on all split cores, as well as discrete color reflectance measurements. Other discrete measurements included needle point probe thermal conductivity, moisture and density (MAD) properties (bulk density, porosity, water content, and grain density) and shear strength (Torvane, pocket penetrometer, and fall cone). For a full description of petrophysical measurement methods, refer to **"Petrophysics"** in the "Methods" chapter.

Data quality and overview

Downhole logs were acquired in Hole M0004B from below the pipe at 65 mbsf to the bottom of the hole at 218 mbsf, providing data through lithostratigraphic Subunits 1/3 to 1/6. The tool string included the FMS, BHC tool, NGT, and the SGT (for a full description of the logging tools see **"Petrophysics"** in the "Methods" chapter). Two successful passes were made with the wireline depth to seafloor, determined using the step increase in the SGT and NGT data, set at 1291 mbrf. This compares favorably with the drillers depth of 1289.7 mbrf.

Caliper logs from the FMS provide a method for assessing borehole conditions. Caliper logs from both passes are presented in Figure **F20.** The outside diameter of the bit was 9½ inches; it can be seen that for much of the formation the hole diameter is under gauge. Narrowing of the hole occurs between 75 and 90 mbsf, at 155 mbsf, and again between 180 and 184 mbsf. The caliper logs indicate that borehole conditions are good, and given the narrow borehole diameter, the FMS pads should have made contact with the borehole wall for the entire length of the logged section. Nowhere is the borehole washed out to a degree where it would adversely affect tool response.

Because of the ice pack, wireline heave compensation was not required. The depth match between the logging passes is good, generally less than ±1 m. The largest offset is 2.6 m at ~155 mbsf. This offset has been removed by depth-matching the passes. It should be noted that the microresistivity images provided by the FMS have not yet been used to aid any interpretation. This is because they have been obscured in large part by the selected drill bit that marked the wall of the borehole (Fig. **F21**). Further reprocessing and detailed core-log integration could improve the quality of these images.

Offshore, all undisturbed cores >14 cm in length were run on the MSCL except for Core 302-M0004C-6X, which was cored without using a liner and subsequently was too thick to fit through the MS loops. This core was logged at the BCR using the split core configuration of the Geotek MSCL for measurements

of density, *P*-wave velocity, and point-source MS. The split core MSCL records sediment thickness during logging and uses this value to correct density and velocity measurements.

Even after the automated thickness correction was applied to Core 302-M0004C-6X, split-core density measurements remain positively correlated with sediment thickness (Fig. **F22**). Furthermore, the higher density values in Section 302-M0004C-6X-1 are not supported by MAD measurements. The positive correlation between density and core thickness and the divergence of logged values from those acquired through MAD measurements suggests that the displacement transducers on the split core system were not calibrated. Corrections to the logged values were obtained by detrending the density data using the slope of the density versus core thickness regression. Further refinement can be achieved by correcting the density for the offset between MAD-derived results and logged results, a procedure that should also be applied to whole-core measurements.

Split-core logging of *P*-wave velocity was also performed on Cores 302-M0002A-5X, 15X, 21X, 23X, 24X, 27X, 30X, 37X, 38X, 40X, 42X, and 44X. Similar corrections for *P*-wave velocity on split cores were attempted, and an integrated data set of split-core, whole-core, and logging velocity is planned. Finally, susceptibility values obtained using the Bartington MS2F point sensor on the split-core system are not corrected for volume effects. Bartington recommends multiplying the point sensor values by 2 to acquire susceptibility values comparable to those obtained using the loop sensor.

In general, core quality was good during APC operations in Holes M0003A and M0004C. However, the majority of the material recovered from the Lomonosov Ridge was cored with an APC or extended core barrel shoe on a traditional, rotating extended core barrel. The rotating barrel caused undercutting through many of the more lithified intervals and resulted in significant core disturbance through the softer sediments. These disturbance effects are especially pronounced in the shallower intervals (Subunits 1/2 and 1/3), where less consolidated material is found.

MAD data collected during both the offshore and onshore phases of Expedition 302 included bulk density, porosity, water content, and grain density. Comparison of the bulk density from MAD measurements with those calculated on the MSCL reveals close agreement through most of the section (Fig. **F23;** Tables **T34, T35**). Corrections to the MSCL-derived density can be made on a core-by-core basis using MAD measurements.

The most likely source for errors in offshore MAD measurements lies in the sample weighing process using the marine analytical balance. Intense shaking and vibration associated with icebreaking reduced the accuracy and precision of the balance. Further measurement errors in offshore data are likely due to the sampling procedure and sediment texture. For example, the four samples taken from the interval between 243 and 250 mbsf all show a lower bulk density than the MSCL data. These are from an interval that is categorized as a mud-bearing biosiliceous ooze and consists mainly of diatoms (see **"Lithostratigraphy"**). The dry ooze easily disintegrates into small particles of millimeter to centimeter size. For this reason, the constant-volume samples were difficult to fill properly, causing the anomalously low densities. Density values acquired using the MSCL may also be slightly biased through the biosiliceous interval, as the calibration technique of the MSCL GRA-derived bulk density assumes that the sediment measured is quartz-based.

Downhole variations in all petrophysical properties highlight a number of prominent changes that correlate well with observed seismic reflectors (see **Jakobsson et al.,** this volume). Composite profiles of MSCL data are described in **"Stratigraphic correlation."** In this section, results from all petrophysical measurements are presented for each hole in mbsf depths (Figs. **F24, F25, F26, F27**) and described by the main lithostratigraphic units (1–4). For more detailed sedimentological descriptions see **"Lithostratigraphy."**

Lithostratigraphic Unit 1: 0–219 mbsf

Broadly speaking, this unit is a silty clay becoming coarser toward the bottom of the section (see **"Lithostratigraphy"**). The increase in the *P*-wave velocity downhole log from the pipe (65 mbsf) to 195 mbsf occurs without any appreciable change in bulk density, reflecting this coarsening trend (Fig. **F28**).

Lithologically, the unit was divided into a number of subunits (see **"Lithostratigraphy"**) that correlate with changes in color reflectance data (Fig. **F29, F30, F31, F32**) but do not necessarily match distinct changes within the other petrophysics data sets. The continuous core and downhole logs reveal significant variation throughout the unit, occurring at decimeter and larger (depth) scales.

The upper ~20 mbsf cored in Holes M0002A, M0003A, and M0004C and MSCL data sets exhibit a first-order increase in both density and velocity that presumably results from normal consolidation processes. Well-defined, in-phase, decimeter-scale variations in density, velocity, susceptibility, and NGR are present. High values of a* and b* chromaticity repre-

sent dark brown color banding of silty clay layers in the upper ~20 mbsf.

A distinct color change occurs at the boundary between lithostratigraphic Subunits 1/2 and 1/3 (Fig. F29, F31, F32). The existence of this color change as a syndepositional feature at all sites remains uncertain, and it may prove to be a geochemical front found at different stratigraphic intervals (Fig. F32). Much of the variability below 20 mbsf in the MSCL data may be tied to drilling-induced disturbances and needs to be carefully edited prior to use by referring to the disturbance table constructed while the cores were being split at the BCR (see "Core Descriptions;" Table T24).

At 45 mbsf, there is a noticeable decrease in the MAD-derived porosity that is mirrored by a slight increase in bulk density and very little change in the grain density (Fig. F23). This shift is associated with an increase in the consolidation ratio (see discussion below). Between 70 and 100 mbsf, cored only in Hole M0002A, there appears to be a reduction in variability in MSCL data, but poor recovery through this interval makes it difficult to decipher the extent of this change. This is the first interval for which downhole logging data are available, and it is characterized by a small increase in the baseline gamma radiation measurements, reflecting a potential increase in clay content (potassium contribution) (Fig. F24). Downhole velocity shows a small increase from the pipe to ~75 mbsf where it fluctuates around a baseline value of 1550 m/s to ~95 mbsf (Fig. F28).

Below 100 mbsf, the downhole gamma radiation logging cyclicity shows a number of frequencies (meter and larger depth scale) varying across a relatively constant baseline of 80–85 gAPI (Fig. F33). A shift in wireline velocity from ~1550 to ~1650 m/s occurs between 99 and 101 mbsf. It appears in both passes of the BHC, with the caliper logs indicating that the hole is in good condition, and is interpreted to be a true high-velocity layer that may prove useful as a tie to the seismic stratigraphy. This feature was not recovered in Hole M0002A. Another distinct change in the character and magnitude of the *P*-wave velocity trace occurs at 136 mbsf and is not accompanied by any noticeable change in the gamma radiation log (Figs. F33, F28). This suggests that the change in velocity is not driven by a change in clay mineral composition. The velocity contrast at this depth is of sufficient magnitude to produce a seismic reflector and to provide a tie to the seismic stratigraphy.

At ~153 mbsf, the borehole rapidly becomes under gauge (Fig. F20) and this is closely associated with a peak in downhole gamma radiation and drop in velocity. The decrease in velocity suggests a more porous, perhaps less consolidated, layer. This interval is assumed to represent swelling clays closing the borehole. Changes in the clay composition should be addressed by more detailed postcruise analysis, but a change in color reflectance (b*) at this same depth seems to support this interpretation (Fig. F28).

A slight but noticeable drop in all MSCL logs occurs in Core 302-M0002A-38X (~166 mbsf) (Fig. F24) and accompanies the transition from predominantly olive-green sediments into those characterized by a more yellowish to brown hue (see "Lithostratigraphy"). A change in the character and baseline value of the gamma radiation log is also apparent at this depth (Fig. F33). The borehole is again under gauge between ~180 and 185 mbsf, and this correlates with increasing gamma radiation values. Spectral gamma ray data point toward an increase in thorium content at this depth (Fig. F33). This section is not recovered in Hole M0002A. Below 185 mbsf, there is a rapid drop in the downhole gamma radiation log that displays low-amplitude meter-scale cyclicity downhole. A distinct brownish layer between 168 and ~192 mbsf in Subunit 1/4 is clearly identified in high a* and b* chromaticity values (Fig. F29).

One of the most prominent changes in MSCL data starts in Core 302-M0002A-44X at ~192 mbsf (Fig. F24), where a drop in susceptibility marks a sharp transition from the brown to a light greenish gray matrix material marking the boundary into Subunit 1/5 (see "Lithostratigraphy"). Over the next few meters, black banding in the cores correlates with a zone of large susceptibility spikes. Sharp peaks of high L* and low a* correspond to particular light gray and dark brown zebra-stripe color banding in Subunit 1/5 between 192.94 and 198.13 mbsf (Fig. F29).

A large drop in the MSCL *P*-wave velocity at ~198 mbsf (Fig. F24) marks the transition into Subunit 1/6, a silty clay to clayey silt with minor amounts of siliceous microfossils and enriched in both organic carbon and pyrite (see "Lithostratigraphy" and "Geochemistry"). This is reflected in MSCL data as the low-velocity, high-density unit extending between Cores 302-M0002A-47X and 51X. The high density originates from the presence of pyrite, and low velocity is likely associated with the increased organic carbon content of the sediment. A unique meter-long interval where density decreases from ~1.9 to 1.3 g/cm^3 is captured in Section 302-M0002A-47X-2 and closely matches a darkening of the sediments. Below Core 302-M0002A-51X at ~220 mbsf, the density steps dramatically from 1.7 to 1.3 g/cm^3 without a noticeable change in the *P*-wave velocity. This change accompanies a reduction in the pyrite concentration, as documented in the core descriptions, and a transition into the mud-bearing

biosiliceous ooze of Unit 2. Core recovery through this interval (~195–205 mbsf) is such that the true nature of the boundary is not yet apparent. The downhole velocity log shows the boundary as a sharp increase in velocity at ~200 mbsf that drops in a series of cyclic fluctuations. Unfortunately, it is at this depth that downhole logging data terminate. Postcruise integration of core and logging data should aid in interpreting the exact nature of this critical transition.

Lithostratigraphic Unit 2: 220–318 mbsf

From the top of the unit to ~240 mbsf, all of the core physical properties vary around a constant baseline value. From 240 mbsf to the bottom of the unit, a gradual increase is apparent in the bulk density (Fig. F23). The increase in density through this unit may result from either normal consolidation processes or from a gradual downhole increase in the clay content. Discrete sample MAD grain density decreases sharply between 220 and 240 mbsf before increasing gradually to the bottom of the unit. The core NGR suggests a subtle increase in clay downhole, increasing more rapidly between ~285 mbsf and the bottom of the unit. MS shows little change through this unit.

Lithostratigraphic Unit 3: 318–404.75 mbsf

From the top of the unit to ~345 mbsf, there is little change apparent in any of the physical property data (Fig. F26). Below ~360 mbsf, the unit is characterized by higher bulk and grain density, which co-vary with porosity (bulk density fluctuates between 1.6 and 2.1 g/cm^3). Core velocity also increases below 360 mbsf and is >1600 m/s. Magnetic susceptibility becomes significantly elevated below 370 mbsf (>1.5 × 10^{-3} SI units). Throughout this interval, large amounts of pyrite are found in the cores. Very large peaks in susceptibility (>5 × 10^{-3} SI) and density (>3 g/cm^3) indicate the presence of clastic material that is probably of diagenetic origin.

Lithostratigraphic Unit 4: 404.75–427.63 mbsf

The cores recovered from this unit, documenting the transition through sandstone and mudstones and into the basement, were too short and disturbed to be run on the MSCL. NGR data were measured on a few short sections in the bottom of the hole but should be treated with caution.

Undrained shear strength

Measurements of the undrained shear strength (S_u) were performed offshore using either the pocket penetrometer or Torvane (Fig. F34; Table T36). Torvane measurements were restricted to the upper 40 mbsf, where sediments were soft enough to allow for the rotation of the shearing vane. For accurate strength measurements, the sample must be fairly cohesive and remain saturated during the test. Very stiff samples often crumble rather than shear, thereby underestimating the actual value. Torvane determinations of shear strength were made on cores from Holes M0003A, M0004A, and M0004C.

In Hole M0002A, the pocket penetrometer was used to measure the unconfined compressive strength of the sediments. Measurements made with the pocket penetrometer were converted from kilograms per square centimeter to kilopascals and then divided by 2, as the penetrometer measures unconfined compressive strength which is equal to twice the undrained shear strength in an ideal clay (Holtz and Kovacs, 1981). The maximum measurable strength was 245 kPa. Below 200 mbsf, clayey intervals were generally too stiff for this test method.

Onshore, the undrained shear strength was measured on split cores using a cone penetrometer (Fig. F34; Table T36) (for conversion formula see "Petrophysics" in the "Methods" chapter). The fall-cone device (Skempton and Bishop, 1950) provides a rapid and simple method for determination of undrained shear strength for undisturbed (as well as remolded) clays.

The consolidation ratio (CR), determined by dividing the undrained shear strength by the in situ effective stress (P'; assuming hydrostatic pressure), is an index for assessing the stress history of sediments. For normally consolidated clays, the consolidation index should be uniform with depth and fall between 0.2 and 0.3. The consolidation index (S_u/P'), calculated by assuming an average sediment bulk density of 1.85 g/cm^3, is illustrated for the upper 260 mbsf in Figure F34.

There is generally close agreement in the consolidation index derived from shipboard and shore-based measurements. Between the seafloor and 40 mbsf, there is a decrease in the CR, beginning at the seafloor at ~0.5 and decreasing to ~0.05. An abrupt shift from 0.05 to 0.2 occurs at this depth. This shift coincides with the transition from Torvane to pocket penetrometer measurements but has also been recorded in the fall-cone data collected onshore. Although the consolidation ratio changes significantly here, it still remains within the range for normally consolidated marine sediments. This shift in the CR does not occur across any lithologic boundary, but is mirrored by a shift in the MAD-derived porosity (Fig. F23).

Measurements made with the fall cone become increasingly scattered below 130 mbsf and tend to fluctuate between 0.1 and 0.6. This variability is not captured in the lower-resolution cone penetrometer tests, suggesting that the variability is a measurement artifact resulting from the sediment strength exceeding the limit for the cone used during testing. Results from incremental load consolidation tests on samples taken from below this transition interval will offer a more accurate means for assessing the stress history of sediments in this interval.

Thermal conductivity

Thermal conductivity measurements were collected throughout lithostratigraphic Units 1 and 2 and document a clear a downhole trend (Table **T37;** Fig. **F35**). Conductivity values have not yet been corrected for in situ temperature conditions. Uncorrected conductivity initially increases from 1.07 to 1.35 W/m·K at ~50 mbsf. A slight decrease in the conductivity occurs below 50 mbsf; however, a limited number of measurements over the subsequent 20 m makes it difficult to assess the significance of this drop. Between 90 and 160 mbsf, thermal conductivity values remain around 1.4 W/m·K before they begin to fall toward the base of the unit. The single low value at 197 mbsf is a good measurement and was obtained in Subunit 1/5. Only one thermal conductivity measurement (0.739 W/m·K) was obtained in the biosiliceous ooze of Unit 2 at 275 mbsf.

In situ temperature measurements

Five in situ temperature measurements were made during coring operations in Holes M0004B and M0004C (Fig. **F36**). Three measurements made in Hole M0004B were performed using the BGS temperature tool, whereas two taken in Hole M0004C were made using the Adara temperature tool (Fig. **F37**). Frictional heating of the sediments during probe insertion is much less likely with the BGS temperature tool as evidenced by the temperature decay curves, and frictional heating of the tool does not appear to have raised the tool temperature above the in situ temperature (see **"Petrophysics"** in the "Methods" chapter for a description of the tools). Data for the BGS and Adara tools have not been processed to acquire the equilibrated in situ temperature, a process that should be completed postcruise. Equilibrium temperatures are generally calculated using an automated curve-fitting approximation technique (Davis et al., 1997). However, both the material and geometry of the tool influence the temperature decay process after insertion into the sediments. Postcruise processing of the BGS temperature measurements will need to address the differences in the tool's temperature decay response.

The mudline temperature was recorded on all runs and varied between tools. A preliminary attempt to normalize the in situ measurements was made by using the average Adara-determined mudline temperature and adjusting all in situ measurements to this baseline value. The results from all the runs and the applied correction factors are shown in Table **T38.** The average gradient calculated using all available data points is 43.2°C/km (Fig. **F36**).

The two deepest measurements were taken in Hole M0004B at depths of 60 and 100 mbsf using the BGS temperature tool. The values from these two runs are quite similar, with the measured temperature at 100 mbsf actually being less than that at 60 mbsf. Errors associated with in situ temperature measurements can arise from frictional heating if the tool is moved during the measurement process by either ship heave or rotation of the core barrel, or when a cooler temperature is measured, it may indicate that the tool was exposed to drilling fluid while it was supposed to be embedded in the seafloor. The measurement taken at 100 mbsf may be an example of the latter case. Data quality and equilibrated in situ temperatures will be reviewed postcruise.

Geochemistry

Shipboard results

Chemical profiles constructed from the pore waters of deep marine sediment are typically characterized by smooth changes in concentration with respect to depth because of diffusion. Moreover, identical pore water profiles are usually found in adjacent deep-sea drill holes because of diffusion and similar sediment composition (e.g., D'Hondt, Jørgensen, Miller, et al., 2003). Because sediment properties are discussed in other chapters, all pore water samples from all holes have been placed on a common depth scale (Table **T39**) and they are discussed as if they came from a single hole. It is noted, though, that the common depth scale was partly revised using the pore water ammonium profile, given the above assumptions.

Across several shallow depth intervals, adjacent whole-round and Rhizone samples were taken to evaluate the merits of the latter technique. The precision for alkalinity and ammonium measurements is fairly high. For these two species, no significant difference was found between samples collected by the two techniques (Table **T39;** Fig. **F38**). Thus, samples collected by the two methods are discussed together. In sediment from above 15 mcd, Rhizone samplers almost always collected pore water faster

than 0.7 mL/h during a 5 h period. This rate dropped to <0.3 mL/h at 43 mcd, and Rhizone samplers were not used below this depth.

Salinity varies between 35 and 40 ppt (Table T39). In general, salinity decreases with depth, at least to 250 mcd. More subtle changes may occur downhole or in sediment deeper than 250 mcd, but this cannot be assessed with the shipboard data, which suffers from low resolution and low precision. Major changes in the laboratory temperature affected the precision of salinity measurements. When water was in short supply, salinity was not measured.

The pH varies between 6.9 and 7.7. In general, pH drops over the upper 100 mcd and then rises over the lower 300 mcd (Fig. F39A). Difficulties were encountered when accurately measuring pH at high pH because the meter would not stabilize (perhaps from the incessant shaking due to ice breaking or temperature fluctuations). Fortunately, this difficulty does not significantly affect the determination of alkalinity, which mostly depends on the amount of HCl added.

Alkalinity increases from nominally 2.5 mM at the sediment/water interface to 3.1 mM at ~5 mcd (Fig. F38). Alkalinity then decreases to 1.6 mM at 50 mcd and remains low until 100 mcd (Fig. F39A). This low in alkalinity broadly corresponds to the low in pH. Between 100 and 200 mcd, alkalinity rises to 6.5 mM. Akalinity then increases to 8.0 mM at the base of the Cenozoic sediment package (399 mcd).

The upper 5 mcd has no ammonium (Fig. F38). Beneath this depth, NH_4^+ steadily rises to ~500 µm at ~200 mcd and fluctuates irregularly between 500 and 1420 µM from 200 to 400 mcd (Fig. F39B). The sharp change in NH_4^+ gradient at 5 mcd corresponds to the shallow high in alkalinity.

Shipboard discussion

Rhizone sampling of shallow sediment was successful. Although Rhizone samplers consistently gave less water than squeezed whole rounds for given 5–10 cm long intervals, they provide an easy means to collect pore waters with limited impact on the whole core. Moreover, Rhizone sampling enables the construction of high-resolution pore water chemistry profiles (Fig. F38) in the shallow high-porosity zone.

Three features in the shipboard pore water chemistry profiles are worth highlighting because they pertain to the main paleoceanographic goals of the cruise. These are shallow carbonate dissolution, deep sulfate reduction, and shallow ammonium oxidation.

Lithological and micropaleontological descriptions of sediment note a general absence of primary carbonate below 19 mcd. In particular, no carbonate tests of ostracodes, foraminifers, or nannofossils were found in the core catcher samples. It is possible that calcareous tests were never deposited in sediment below 19 mcd. However, this is also where pH and alkalinity drop below 7.4 and 2.5 mM, respectively. This means that pore waters below 19 mcd (and to at least 100 mcd) are more corrosive to carbonate tests than the overlying sediment or water column. Carbonate tests may have dissolved when they were buried in these corrosive pore waters.

The inflection in alkalinity at ~200 mcd suggests that a chemical reaction is adding substantial amounts of HCO_3^- at this depth without accompanying H^+. The obvious candidate is sulfate reduction of organic carbon:

$$2CH_2O_{(s)} + SO_4^{2-}{}_{(aq)} \rightarrow 2HCO_3^-{}_{(aq)} + H_2S_{(aq)}.$$

Black firm clays were deposited during the Eocene below 200 mcd. The upper part of these firm clays may be driving sulfate reduction at present day. Interestingly, the firm clays host abundant pyrite and lie beneath dark bands in the sediment, which may be composed of other iron sulfide minerals. Organic matter in the black firm clays has probably reacted with dissolved SO_4^{2-} since they were buried, producing abundant H_2S and, ultimately, iron sulfide minerals.

A peak in alkalinity at ~200 mcd coincides with a change in gradient of NH_4^+ to one that is steeper than above. The peak in alkalinity again suggests that some chemical reaction is producing HCO_3^- without accompanying H^+. The NH_4^+ profile further suggests that upward diffusing NH_4^+ drives this reaction. This may be a zone where the two microbial reactions denitrification and anammox are coupled (e.g., Rysgaard et al., 2004). The ultimate source of NH_4^+ may be the diagenesis of N-bearing organic carbon in the Eocene black firm clays.

Methane

Headspace CH_4 concentrations are low, ranging from 10 to 140 ppmv (Table T40). The highest value was found at ~340 mcd.

Low CH_4 concentrations are expected for the organic-lean sediments above 200 mcd but are somewhat surprising for the organic-rich Eocene black firm clays below 200 mcd. Degradation of organic carbon generally proceeds through a sequence of microbial reactions. This sequence includes sulfate reduction followed by methanogenesis; the latter is thought to occur at high rates once sulfate reduction has resulted in very low SO_4^{2-} concentrations. The Eocene sediments have high organic carbon content (TOC often exceeding 2 wt%). This is a sufficient quantity to drive complete sulfate reduction and me-

thanogenesis, especially considering that the organic carbon is dominantly of marine origin and has a low thermal maturity (see below). However, surrounding pore waters have fairly high dissolved SO_4^{2-} concentrations (>7 mM) (Table T39) so that methanogenesis is not a dominant microbial pathway, at least at present day. The low CH_4 concentrations and high SO_4^{2-} concentrations below 200 mcd raise an intriguing question: why are microbes not readily consuming the abundant SO_4^{2-} and organic carbon?

Pore water chemistry

Calcium concentrations of pore waters show an unusual trend with respect to depth (Fig. F39A; Table T39). They are close to that of seawater (10 mM) in shallow sediment but then generally increase with depth to ~14 mM at ~200 mcd. Below this, pore water Ca varies between 13 and 15 mM. The inflection in the dissolved Ca profile at ~200 mcd suggests dissolution of Ca-bearing solids below this depth. The sediment chemistry results show anomalously high Ca/Al values from 200 to 400 mcd (Fig. F40), and the mineralogy results (Table T41) show anomalous amounts of calcite and gypsum from 200 to 400 mcd. Apparently, calcite, gypsum, or both are currently dissolving in the Eocene black firm clays.

Dissolved Fe concentrations are close to zero above 20 mcd and below 200 mcd (Fig. F39A). Between these depths, there is a broad peak centered at 80 mcd, where the Fe concentration exceeds 300 µM (Fig. F39A; Table T39). Before sulfate reduction, organic matter decomposition proceeds via iron oxide reduction. Presumably, small amounts of iron oxides are deposited on the seafloor and subsequently buried. Between ~20 and 200 mcd, microbes use these oxides to consume organic carbon, which releases Fe to pore waters. The dissolved Fe diffuses away from this zone, upward to where it reacts with oxygen to reprecipitate Fe oxides and downward to where it reacts with dissolved sulfide to precipitate pyrite. The color change of sediment at ~20 mcd may mark the loss of Fe oxides, and the high Fe, Fe/Al, and pyrite contents at ~200 mcd (Tables T41, T42) may indicate current precipitation of Fe sulfides.

Dissolved Mg concentrations are close to that of seawater (53 mM) in shallow sediment but steadily decrease with depth (Fig. F39A; Table T39). The lowest concentration (35 mM) is in the deepest pore water sample, taken at ~400 mcd. No obvious Mg-rich mineral (e.g., dolomite) preferentially occurs near the bottom of the Hole M0004A. A chemical gradient may extend across the hole, attesting to "basement" waters with low dissolved Mg.

The dissolved Mn profile shows two prominent peaks where concentrations exceed 200 µM (Fig. F39A; Table T39). The first peak is found between 1.5 and 80 mcd and is centered at 20 mcd; the second peak is found between 160 and 380 mcd and is centered between 200 and 300 mcd. Before iron oxide reduction, organic matter decomposition proceeds via manganese oxide reduction. Along with iron oxides, Mn oxides are probably deposited on the seafloor and subsequently buried. Certainly, the shallowest sediment examined (0.21 mcd) has a fairly high Mn content for marine sediment (2880 mg/kg) (Table T41). Between ~1.5 and 80 mcd, microbes use the Mn oxides to consume organic carbon, which releases Mn to pore waters. The dissolved Mn diffuses away from this zone, upward to where it reacts with dissolved oxygen to reprecipitate Mn oxides and downward to where it reacts with dissolved carbonate to precipitate rhodochrosite. The comparatively subtle peaks of solid-phase Mn content beginning at ~1.5 mcd may indicate precipitation of Mn oxides; the large peaks of solid-phase Mn content between ~28 and 105 mcd may indicate precipitation of rhodochrosite (Table T41). A rhodochrosite groundmass particle (~5 mm) was found at ~28 mcd (below). The deeper dissolved Mn peak is more difficult to explain in terms of the standard sequence of microbial reactions. It probably relates to the interval of high solid-phase Mn between 180 and 200 mcd, which may be composed of Mn oxides emplaced during a time of very low sedimentation.

Dissolved Na concentrations display an interesting profile with respect to depth (Fig. F39B; Table T39). In the shallowest samples, Na concentrations (~478 mM) are close to that of modern seawater (~470 mM). With depth, however, Na concentrations generally rise to a subsurface maximum of 489 mM centered at ~50 mcd and then decrease to 484 mM by 100 mcd. Sodium is often assumed to have a straight profile in shallow sediment because, with the exception of rare cases (e.g., near salt diapirs), there are no minerals that consume or release significant amounts of Na. It is possible that the profile reflects changes in bottom water salinity in the Arctic Ocean since the Last Glacial Maximum (e.g., McDuff, 1985; Adkins et al., 2002). This interpretation is not supported by the Cl^- measurements (Table T39), but we suspect that they have low precision.

Both S and SO_4^{2-} were measured on pore waters (Table T39). In general, the independent analyses give similar results, showing that S (as SO_4^{2-}) steadily drops from concentrations near that of seawater (28 mM) at the seafloor to 11 mM at 200 mcd (Fig. F39B). Below this depth, S (as SO_4^{2-}) slowly decreases to 8 mM. As expected from discussion of the shipboard alkalinity (above), dissolved SO_4^{2-} is being consumed below 200 mcd, presumably through sulfate reduction of organic carbon, a reaction that pro-

duces dissolved sulfide. Although we did not quantify dissolved sulfide, its presence is indicated in samples from 200 to 400 mcd. These samples produced a white precipitate when zinc acetate was added (Table T39).

Dissolved Si concentrations are fairly low (<300 µM) in the upper 180 m of sediment, fairly high (>1000 µM) from 200 to 300 mcd, and intermediate from 300 to 400 mcd. The overall profile suggests release of Si to pore waters between 200 and 300 mcd and its precipitation above and below these depths. We note the presence of abundant biogenic opal between 200 and 300 mcd, abundant zeolites at ~200 mcd, and abundant authigenic silica minerals below 300 mcd (Table T42). Presumably, biogenic opal in lithostratigraphic Unit 2 is slowly dissolving and releasing Si to surrounding lithostratigraphic units where it reprecipitates.

Dissolved Sr concentrations generally track those of dissolved Ca. Concentrations near the seafloor are close to that of seawater (90 µM). With depth, Sr concentrations steadily rise, reaching 160 µM by 260 mcd. After a drop, Sr concentrations rise again, reaching 187 µM at ~400 mcd. Possible explanations for this profile are the same as those for Ca.

Elemental composition of sediment

Background

Although all sediment samples were analyzed for 48 elements, useful results were obtained for only 25 elements. Fourteen elements (Al, Br, Ca, Cl, Fe, K, Mg, Mn, Rb, S, Si, Sr, Ti, and Zn) typically yielded analytical precision better than 5%. Results for most of these elements are presented as depth profiles (Fig. F40).

The remaining 11 elements (As, Ba, Co, Cr, Cu, Ga, Ni, P, Pb, Th, and V) often had low analytical precision (5%–30%). However, because the contents of these 11 elements varied significantly with depth, their downhole trends are meaningful. Depth profiles of Ba and Ni are presented as examples (Fig. F40). We discuss some of the profiles below.

Downcore profiles of "terrigenous elements"

Aluminosilicate minerals (e.g., clays and feldspars) typically host most of the Al, K, Rb, and Ti in marine sediment. With a few notable exceptions, these four elements show high contents over the upper 200 m, a major decrease between ~200 and 220 mcd, low contents between 220 and ~350 mcd, and high contents below ~350 mcd (Fig. F40). The overall profile is similar to the total peak area determined by XRD (Table T42), which appears to be dictated by the amount of silicate minerals. The exceptions to these trends are rocks, concretions, and nodules (Table T41).

The abundance of terrigenous material can be estimated by a normative calculation based on the concentration of Al in each sample and the concentration of Al in typical Post-Archean shale (PAAS), as follows:

$$\%\text{Terrigenous}_{\text{sample}} = (\text{Al}_{\text{sample}}/\text{Al}_{\text{PAAS}}) \times 100,$$

where the Al content of PAAS is ~100,000 ppm. Such normalization suggests that sediment between 0 and 200 mcd and below 350 mcd comprises between 80% and 100% terrigenous material (excepting concretions and nodules). Such high values agree with the predominance of silty clays in lithostratigraphic Subunits 1/1 through 1/5 and the lower part of Unit 3. Between ~220 and ~350 mcd, however, the terrigenous abundance decreases to as low as 7% and is usually not greater than 30%. These low values are consistent with abundant silica and organic matter in Units 2 and 3, which dilute the terrigenous component. Dilution of terrigenous material also occurs between 200 and 220 mcd. Here, however, the main dilutant is pyrite, evident from extreme Fe and S contents (below) and mineralogy (Table T42).

Changes in the type of terrigenous material are often reflected by variations in normalized abundances of terrigenous elements. As a preliminarily examination, we normalized K and Ti to Al. Profiles of Ti/Al and K/Al both show a prominent change with respect to depth (Fig. F41). Between 0 and ~220 mcd and below ~350 mcd, both elemental ratios are relatively low. By contrast, the intervening interval has relatively high Ti/Al and K/Al ratios. This suggests that the detrital material deposited in Unit 2 and the upper part of Unit 3 is distinctly different from overlying and underlying sediment. We note that this unit is characterized by a high abundance of K-feldspar, consistent with the elevated K content.

Downcore profile of silicon

The downcore profile of Si shows some similarities with those of terrigenous elements but also a major difference. Like the terrigenous elements, the contents are generally high (20–27 wt%) from 0 to 200 mcd and below 350 mcd. This is consistent with the high abundance of aluminosilicate minerals. There are also obvious drops in Si content between 200 and 220 mcd and in nodule samples, which are caused by dilution of authigenic minerals (e.g., pyrite). However, in contrast to the terrigenous elements, Si has its highest contents between 220 and 350 mcd. Here, Si typically exceeds 30 wt%. This reflects the high abundance of biogenic silica (~220 to ~313 mcd) or authigenic silica (~313 to ~350 mcd) in this interval.

Downcore profiles of iron and sulfur

For most of the sediment column, Fe contents are between 4 and 6 wt%. Somewhat analogous to Si, however, this downhole profile of Fe (Fig. **F40**) actually reflects major differences in sediment composition. Above 200 mcd and below 350 mcd (excluding pyrite nodules), most of the Fe probably resides in aluminosilicate minerals (e.g., clays). Between these depths, though, much of the Fe occurs in pyrite. This can be demonstrated using sediment chemistry results in two ways. First, S contents are close to zero above 200 mcd and below 350 mcd (excluding pyrite nodules); in the intervening interval, Fe and S are highly correlated, with S contents generally exceeding 4 wt%. Second, the Fe/Al ratio is low above 200 mcd and below 350 mcd; in the intervening interval, the Fe/Al ratio is high (Fig. **F41**). The confirmation comes from the mineralogy, which shows abundant pyrite between 200 and 350 mcd (Table **T42**) (see **"Lithostratigraphy"**).

As alluded to above, Subunit 1/6 (200–220 mcd) is greatly enriched in Fe, with contents exceeding 10 wt%. The S content of sediment and the mineralogy both indicate that this interval has an extremely high pyrite content. However, when Fe is normalized to Al, this depth interval does not stand out; in fact the Fe/Al ratio is lower in this interval than in Unit 2 below. This suggests that biogenic silica dilutes pyrite (and terrigenous components) in Unit 2. In other words, Subunit 1/6 and Unit 2 are distinct because Subunit 1/6 has a much lower amount of biogenic silica.

Downcore profiles of "evaporite elements"

Sediment contents of Cl and Br are strongly correlated (r^2 = 0.9) and exhibit clear downhole trends (Fig. **F40**). These elements generally have low contents (~5000 and 30 ppm, respectively) between 0 and 220 mcd and below ~310 mcd. Between these depth horizons and within lithostratigraphic Unit 2, sediment Cl and Br contents rise to >18,000 ppm and >100 ppm, respectively. The exceptions to these trends are the squeeze cake samples, which consistently have lower Cl and Br contents, usually by a factor of 2.

A simple explanation for the Cl and Br contents is that they are mostly added to sediment samples from evaporation of pore water during preparation for chemical analyses. In particular, if we assume a sediment porosity of 40% to 50% and normal seawater Cl concentrations, sediments should have nominally 5000–7000 ppm Cl when analyzed. The squeeze cake samples, therefore, would have lower Cl and Br contents because significant pore water has been extracted. At issue, however, are the high values in Unit 2. To explain these by evaporation from pore water, sediment porosity would have to exceed 70%.

We also note a slight increase in the Br/Cl ratio of sediment within Unit 2. Some of the Br in this interval may come from halogenated organic carbon.

Lithostratigraphic units

As discussed in **"Lithostratigraphy,"** the overall sediment column consists of several units defined on the basis of sediment composition and physical properties. For the most part, these units nicely coincide with major changes in sediment chemistry (and mineralogy, below).

However, there is an issue with the boundary between Unit 2 and Unit 3 at ~313 mcd. Except for the "evaporite elements," most profiles of sediment chemistry show limited change at this depth; instead, as noted above, major changes in sediment chemistry are found at ~350 mcd (Fig. **F40**). The discrepancy might be explained by a change in silica phases. Sediment between ~220 and ~313 mcd (Unit 2) contains abundant biogenic opal, whereas sediment between ~313 and ~350 mcd (top of Unit 3) contains abundant authigenic silica, tentatively labeled crystoballite and tridymite (Table **T41**). Much of the biogenic opal appears to have been altered between ~313 and ~350 mcd so that this interval has similar overall chemistry to Unit 2 but low amounts of biogenic silica (an obvious change in sediment composition). Because the conversion of opal to authigenic silica decreases the porosity, there is less water in this interval and, hence, lower contents of evaporite elements. Therefore, if biogenic opal had not been altered in the upper 47 m of Unit 3, it would have likely been described as part of Unit 2 (see **"Lithostratigraphy"**).

Mineralogy of sediment

A total of 214 samples were analyzed for their mineralogical composition by XRD. Across this sample suite, peaks for 23 minerals were identified and quantified on XRD traces. The sum of all peak areas was calculated as a "total peak area" (Table **T42**). The total peak area shows major changes downhole. Between 0 and ~200 mcd and below ~350 mcd, total peak area is generally high. The exceptions are analyses of pyrite-rich sediments and pyrite nodules found between 380 and 402 mcd. By contrast, between ~200 and ~313 mcd, total peak area is relatively low. A transition of increasing peak area occurs from ~313 to ~350 mcd. The overall profile of total peak area probably relates to changes in lithology and sediment chemistry. Sediments dominated by terrigenous siliclastic minerals have a high total peak

area, and sediments dominated by pyrite and biogenic silica have a low total peak area. The interval with abundant authigenic silica has moderate total peak area.

To account for major changes in lithology and bulk sediment mineralogy, peaks for each mineral were normalized to the total peak area (Table **T42**). There are several important downhole changes in these normalized mineral abundances, some which are discussed above and in **"Lithostratigraphy."**

Organic geochemistry

Total carbon (TC), total sulfur (TS), and TOC contents were determined on 52 samples of sediment at the BCR (Table **T43**). TOC and Rock-Eval parameters were determined on a second set of samples at Alfred Wegner Institute (Germany) (Table **T44**).

Total carbon, sulfur, and organic carbon

Based on TC, TS, and TOC content, the sedimentary sequence can be divided into several intervals that generally correlate with the lithostratigraphic units or subunits described elsewhere (Fig. **F42**).

Samples from lithostratigraphic Subunits 1/1, 1/2, and 1/3 (0 to ~165 mcd) are generally characterized by low TC (0.2–0.4 wt%), low TS (0.0–0.30 wt%), and low TOC (0.2–0.4 wt%). The exceptions are samples characterized by high Mn or high P, which have higher TC and TOC. These may correspond to intervals with rhodochrosite or carbonate fluorapatite.

Samples from lithostratigraphic Subunit 1/4 (~165 to ~198 mcd) have very low TC (~0.1 wt%) and TOC (~0.1 wt%). The TS is also relatively low (<0.3%).

Samples from lithostratigraphic Subunit 1/5 (~193 to ~198 mcd) have moderate TOC (0.7–1 wt%). (No samples from this interval were analyzed for TC and TS, although the elemental chemistry indicates the samples would have moderate S content.)

Samples from lithostratigraphic Subunit 1/6 and Unit 2 (~198 to ~313 mcd) have high TC (>2.5 wt%), high TS (>4.9 wt%), and high TOC (>2.2 wt%). However, Subunit 1/6 is distinct from Unit 2 because it is characterized by extreme TS contents (>10 wt%). In fact, the absolute values reported in Table **T43** may be inaccurate because the high S contents affect calibration of the instrument.

Samples from lithostratigraphic Unit 3 (~313 to ~424 mcd) have variable TC, TS, and TOC. Of the samples analyses, TC, TS, and TOC range between 1.8 and 3.5 wt%, 0.6 and 9.3 wt%, and 0.9 and 3.0 wt%, respectively.

Quality and maturity of organic matter

In immature sediments (TOC values >0.3 wt%), hydrogen index (HI) and oxygen index (OI) values of Rock-Eval pyrolysis are useful indicators for the characterization of the composition of the organic carbon fraction (i.e., to estimate the amount of terrigenous [higher plant] and aquatic [marine or freshwater] proportions) (e.g., Tissot and Welte, 1984; Stein, 1991). HI values <100 mg hydrocarbon (HC)/g C are typical of terrigenous organic matter (kerogen type III), whereas HI values of 300–800 mg HC/g C are typical of aquatic organic matter (kerogen types I and II).

HI values of organic matter show significant changes downcore (Figs. **F43, F44;** Table **T44**). Organic matter of lithostratigraphic Unit 1 is mainly characterized by HI values <100 mg HC/g C, indicating a terrigenous (higher plant) origin. In lithostratigraphic Unit 2 and the upper part of lithostratigraphic Unit 3 (~220 to ~350 mcd), however, HI values are generally between 150 and 350 mg HC/g C, suggesting significant amounts of aquatic (i.e., marine and/or freshwater algae type) organic matter. The lower part of Unit 3 (>350 mcd) is mostly characterized by low HI values of ~50 to 100 mg HC/g C, suggesting a dominance of terrigenous (higher plant) organic matter. The exceptions are Cores 302-M0004A-30X and 31X, from the middle part of lithostratigraphic Unit 3. These samples have HI values of ~350 mg HC/g C, again suggesting significant proportions of marine and/or freshwater algae-type organic matter.

T_{max} values also vary downhole (Table **T44**). T_{max} is >435°C in the upper part of the section (i.e., lithostratigraphic Subunits 1/2 and 1/3). This suggests the presence of refractive terrigenous organic matter. In Subunits 1/5 and 1/6 and Units 2 and 3, T_{max} values are <435°C and often <400°C, indicating immature, thermally unaltered organic matter.

Preliminary paleoenvironmental interpretation

The Pleistocene to Miocene interval (Subunits 1/1 to 1/4) is characterized by low TOC contents (<0.4 wt%) of terrigenous (higher plant) origin, as indicated by the low HI values. This is very similar to numerous late Quaternary organic carbon records from the central Arctic Ocean (e.g., Belicka et al., 2002; Stein et al., 1994, 2003, and further references therein). Low primary productivity due to sea ice coverage may have precluded the preservation and accumulation of significant amounts of marine organic matter.

The interval of Eocene sediment represented by Unit 2, on the other hand, has high TOC contents (1.5–

>3 wt%). For much of this interval, elevated HI values of 150 to 350 mg HC/g C suggest significant amounts of preserved marine and/or freshwater algae material. Along with other sediment parameters (e.g., laminations, high biogenic silica, and pyrite), the organic carbon suggests an unusual depositional environment.

The *Azolla* event and the PETM are also apparent in organic carbon data. The *Azolla* event (Sample 302-M0004A-11X-CC) is characterized by the maximum TOC content of 4.2 wt%. Samples from the PETM (Samples 302-M0004A-30X-CC and 31X-CC) are characterized by the maximum HI values. Both intervals seem to be times of increased accumulation and preservation of aquatic (marine and/or freshwater algae type) organic matter.

Scanning electron microscopy

Thirteen sediment samples were examined using scanning electron microscope (Table **T45**). The primary purpose of these analyses was to characterize samples of "special interest." Photomicrographs and descriptions of these samples are included in **"Supplementary Material."**

Microbiology

Sampling for microbiological analyses was conducted at fairly regular depth intervals from near surface (6.55 mbsf) to near basement (398.41 mbsf) with a notable gap between 169 and 241 mbsf. A total of 21 samples were preserved for enumeration of microorganisms to provide estimates of subsurface biomass. Nineteen samples were stored anaerobically for the purpose of shore-based cultivation studies. A subset of samples (18) was stored at –51°C for deoxyribonucleic acid extraction and subsequent microbial community characterization. Finally, 10 samples were stored at –51°C for lipid biomarker analysis. All microbiological samples and the depth of their recovery are listed in Table **T46.**

Paleomagnetism

General magnetic properties

The major features in the magnetic properties of the recovered sediments are a sharp decrease of natural remanent magnetization (NRM) and MS between 193 and 388 mbsf, in close correspondence with a sharp change in sediment color from olive-brown to light gray, followed by a large increase in these parameters between 388 and 405 mbsf (Fig. **F45**). Between 193 and 385 mbsf, NRM intensity values decrease by a factor of 200 and susceptibility values decrease by a factor of 10. In the interval with low NRM values (193–385 mbsf), some discrete intervals are strongly magnetic and may be associated with iron sulfide concretions. The strong and weak magnetic zones may be linked to the effects of depositional changes and diagenetic processes. The originally deposited iron oxides may have dissolved, leading to the formation of diagenetic iron sulfides (see **"Geochemistry"**). Further study of discrete samples should determine the magnetic mineralogy of both the strong and weak magnetic zones.

AF demagnetization behavior

Detailed stepwise alternating-field (AF) demagnetization was performed on U-channels taken from all cores recovered during Expedition 302. The AF demagnetization behavior is notably different in the intervals with high (>10^{-3} A/m) and low (<10^{-4} A/m) intensity of NRM. In the more magnetic intervals (0–193 mbsf and 388–405 mbsf), AF demagnetization allows the determination of a clear characteristic magnetization with steep inclination.

In the weak magnetic interval, the demagnetization plots are usually noisy and do not show evidence of a clear characteristic component of magnetization. The median destructive field is often as low as 10 mT. The low-coercivity components of NRM that can be identified for most levels are generally directed steeply downward and are likely to be either a viscous magnetization acquired in the present-day magnetic field or a magnetization acquired during drilling. After demagnetization of this low-coercivity component, the intensity is generally too low (<10^{-5} A/m) to identify a characteristic component. Postcruise thermal demagnetization of discrete samples may be able to erase the viscous overprint without affecting the characteristic magnetization. In some cases, shallow inclinations are found that may correspond to a magnetization acquired during core processing or U-channel sampling. For almost all samples in the weakly magnetic interval, there is a tendency for the NRM to behave erratically above demagnetization steps of ~40 mT. This suggests that parasitic anhysteretic remanent magnetizations have been acquired at high demagnetizing fields.

Magnetic polarity stratigraphy

The inclinations obtained in the weakly magnetized interval (193–385 mbsf) are frequently between –60° and 60°, too low for the latitude of the site. The overall distribution of inclination values after 30 mT demagnetization is clearly not satisfactory because there is no dominance of steep negative and positive inclinations. In fact, the inclination distribution is almost random, with a slight bias toward normal po-

larity directions, attributable to incomplete removal at 30 mT of a viscous component with normal polarity. Within this weakly magnetized interval, the largely indeterminate inclinations prevent any meaningful interpretation of the polarity.

The distribution of inclination values after 30 mT demagnetization in the strongly magnetic intervals is notably different, as steep positive and negative inclinations predominate. Between 0 and 193 mbsf, the inclination record can be interpreted in terms of normal and reversed polarity zones (Fig. **F46A, F46B**) (Ogg and Smith, 2004). A number of factors contribute to the difficulty in determining a unique and unambiguous magnetostratigrapy for Expedition 302 sediment. These include the tendency of Arctic sediments to record a large number of geomagnetic excursions during the Brunhes and Matuyama Chrons, sparse biostratigraphic data, incomplete core recovery, and core disturbance. Nevertheless, we have been able to narrow our interpretations to two models (Fig. **F46A, F46B**) and to identify a currently preferred age model within each interval. The age-depth curves that correspond to Figure **F46A** and **F46B** are shown in Figure **F19** (see **"Timescale and sedimentation rates"**).

Between 388 and 405 mbsf, the inclination record is also interpretable in terms of paleomagnetic polarity, except for Section 302-M0004A-33X-1, which is heavily disturbed (Fig. **F47**). Unfortunately, the recovery is poor and only a single reversal can be identified: the polarity shifts downward from reversed to normal within Section 302-M0004A-34X-3, at 399.63 mbsf. In view of the biostratigraphic data (see **"Biostratigraphy"**), this corresponds to the top of Chron C25n with an absolute age of 56.6 Ma (Luterbacher et al., 2005).

References

Aagaard, K., and Carmack, E.C., 1994. The Arctic Ocean and climate: a perspective. *In* Johannessen, O.M., Muensch, R.D., and Overland, J.E. (Eds.), *The Polar Oceans and Their Role in Shaping the Global Environment.* Maurice Ewing Ser., 85:5–20.

Adkins, J.F., McIntyre, K., and Schrag, D.P., 2002. The salinity, temperature and $\delta^{18}O$ of the glacial deep ocean. *Science,* 298:1769–1773. **doi:10.1126/science.1076252**

Backman, J., Jakobsson, M., Lovlie, R., Polyak, L., and Febo, L.A., 2004. Is the central Arctic Ocean a sediment starved basin? *Quat. Sci. Rev.,* 23:1435–1454. **doi:10.1016/j.quascirev.2003.12.005**

Bennike, O., Abrahamsen, N., Bak, M., Israelson, C., Konradi, P., Matthiessen, J., and Witkowski, A., 2002. A multi-proxy study of Pliocene sediments from Ile de France, northeast Greenland. *Palaeogeogr., Palaeoclimatol., Palaeoecol.,* 186:1–23. **doi:10.1016/S0031-0182(02)00439-X**

Bice, K.L., and Marotzke, J., 2002. Could changing ocean circulation have destabilized methane hydrate at the Palaeocene/Eocene boundary? *Paleoceanography,* 17(1018). **doi:10.1029/2001PA000678**

Bjørklund, K.R., 1976. Radiolaria from the Norwegian Sea, Leg 38 of the Deep Sea Drilling Project. *In* Talwani, M., Udintsev, G., et al., *Init. Repts. DSDP,* 38: Washington (U.S. Govt. Printing Office), 1101–1168.

Bjørklund, K.R., and Swanberg, N.R., 1987. The distribution of two morphotypes of the radiolarian *Amphimilissa setosa* Cleve (Nassellarida): a result of environmental variability? *Sarsia,* 72:245–254.

Bohaty, S.M., and Zachos, J.C., 2003. Significant Southern Ocean warming event in the late middle Eocene. *Geology,* 31:1017–1020. **doi:10.1130/G19800.1**

Boltovskoy, D., Kogan, M., Alder, V.A., and Mianzan, H., 2003. First record of a brackish radiolarian (*Polycystina*): *Lophophaena rioplatensis* n. sp. in the Rio de la Plata estuary. *J. Plankton Res.,* 25:1551–1559. **doi:10.1093/plankt/fbg107**

Boulter, M.C., and Manum, S.B., 1989. The Brito-Arctic igneous province flora around the Paleocene/Eocene boundary. *In* Eldholm, O., Thiede, J., Taylor, E., et al., *Proc. ODP, Sci. Results,* 104: College Station, TX (Ocean Drilling Program), 663–680.

Brinkhuis, H., 1994. Late Eocene to early Oligocene dinoflagellate cysts from the Priabonian type-area (Northeast Italy): biostratigraphy and paleoenvironmental interpretation. *Palaeogeogr., Palaeoclimatol., Palaeoecol.,* 107:121–163.

Brinkhuis, H., and Biffi, U., 1993. Dinoflagellate cyst stratigraphy of the Eocene/Oligocene transition in central Italy. *Mar. Micropaleontol.,* 22:131–183. **doi:10.1016/0377-8398(93)90007-K**

Brinkhuis, H., Munsterman, D.K., Sengers, S., Sluijs, A., Warnaar, J., and Williams, G.L., 2004a. Late Eocene–Quaternary dinoflagellate cysts from ODP Site 1168, off western Tasmania. *In* Exon, N.F., Kennett, J.P., and Malone, M.J., *Proc. ODP, Sci. Results,* 189, 1–36 [CD-ROM]. Available from: Ocean Drilling Program, Texas A&M University, College Station TX 77845-9547, USA. [**HTML**]

Brinkhuis, H., Sengers, S., Sluijs, A., Warnaar, J., and Williams, G.L., 2004b. Latest Cretaceous–earliest Oligocene and Quaternary dinoflagellate cysts, ODP Site 1172, East Tasman Plateau. *In* Exon, N.F., Kennett, J.P., and Malone, M.J., *Proc. ODP, Sci. Res.,* 189, 1–36 [CD-ROM]. Available from: Ocean Drilling Program, Texas A&M University, College Station TX 77845-9547, USA. [**HTML**]

Bujak, J.P., and Brinkhuis, H., 1998. Global warming and dinocyst changes across the Paleocene/Eocene boundary. *In* Aubry, M.-P., et al. (Eds.), *Late Paleocene–Early Eocene Climatic and Biotic Events in the Marine and Terrestrial Records:* New York (Columbia Univ. Press), 277–295.

Bujak, J.P., and Mudge, D.C., 1994. A high-resolution North Sea Eocene dinocyst zonation. *J. Geol. Soc. (London, U. K.),* 151:449–462.

Bukry, D., 1984. Paleogene paleoceanography of the Arctic Ocean is constrained by the middle or late Eocene age of USGS Core Fl-422: evidence from silicoflagellates. *Geology,* 12:199–201. **doi:10.1130/0091-7613(1984)12<199:PPOTAO>2.0.CO;2**

Clark, D.L., 1970. Magnetic reversals and sedimentation rates in the Arctic Basin. *Geol. Soc. Am. Bull.,* 81:3129–3134.

Clark, D.L., 1971. Arctic Ocean ice cover and its late Cenozoic history. *Geol. Soc. Am. Bull.,* 82:3313–3324.

Clark, D.L., 1974. Late Mesozoic and early Cenozoic sediment cores from the Arctic Ocean. *Geology,* 2:41–44. **doi:10.1130/0091-7613(1974)2<41:LMAECS>2.0.CO;2**

Clark, D.L., 1990. Arctic Ocean ice cover: geologic history and climatic significance. *In* Grantz, A., Johnson, L., and Sweeney, J.F. (Eds.), *The Geology of North America: The Arctic Ocean Region* (Vol. L): Boulder (Geol. Soc. Am.), 53–62.

Clark, D.L., 1996. The Pliocene record in the central Arctic Ocean. *Marine Micropaleontol.,* 27:157–164. **doi:10.1016/0377-8398(95)00057-7**

Clark, D.L., Whitman, R.R., Morgan, K.A., and Mackay, S.D., 1980. Stratigraphy and glacial-marine sediments of the basin, central Arctic Ocean. *Spec. Pap.—Geol. Soc. Am.,* 181:1–57.

Colmeno-Hidalgo, E., Flores, J.-A., Sierro, F.J., Schonfeld, J., and Lowemark, L., 2002. Abrupt short-term climatic events in the Gulf of Cadiz and Alboran Sea (Southern Spain) during MIS 2 and 3. *J. Nannoplankton Res.,* 24(2):84.

Cronin, T.M., Holtz, T.R., Jr., Stein, R., Spielhagen, R., Futterer, D., and Wollenberg, J., 1995. Late Quaternary paleoceanography of the Eurasian Basin, Arctic Ocean. *Paleoceanography,* 10:259–281. **doi:10.1029/94PA03149**

Cronin, T.M., Holtz, T.R., and Whatley, R.P., 1994. Quaternary paleoceanography of the deep Arctic Ocean based on quantitative analysis of Ostracoda. *Mar. Geol.,* 19:305–332. **doi:10.1016/0025-3227(94)90188-0**

Crouch, E.M., Brinkhuis, H., Visscher, H., Adatte, T., and Bolle, M.-P., 2003a. Late Paleocene–early Eocene dinoflagellate cyst records from the Tethys: further observations on the global distribution of *Apectodinium*. *In* Wing, S.L., Gingerich, P.R., Schmitz, B., and Thomas, E. (Eds.), *Causes and Consequences of Globally Warm Climates in the Early Paleocene.* Spec. Pap.—Geol. Soc. Am, 369:113–131.

Crouch, E.M., Dickens, G.R., Brinkhuis, H., Aubry, M.-P., Hollis, C.J., Rogers, K.M., and Visscher, H., 2003b. The *Apectodinium* acme and terrestrial discharge during the Paleocene–Eocene Thermal Maximum: new palynological, geochemical and calcareous nannoplankton observations at Tawanui, New Zealand. *Palaeogeogr., Palaeoclimatol., Palaeoecol.,* 194(4):387–403. **doi:10.1016/S0031-0182(03)00334-1**

Crouch, E.M., Heilmann-Clausen, C., Brinkhuis, H., Morgans, H.E.G., Rogers, K.M., Egger, H., and Schmitz, B., 2001. Global dinoflagellate event associated with the Late Paleocene Thermal Maximum. *Geology,* 29:315–318. **doi:10.1130/0091-7613(2001)029<0315:GDEAWT>2.0.CO;2**

Davis, E.E., Villinger, H., MacDonald, R.D., Meldrum, R.D., and Grigel, J., 1997. A robust rapid-response probe for measuring bottom-hole temperatures in deep-ocean boreholes. *Mar. Geophys. Res.,* 19:267–281. **doi:10.1023/A:1004292930361**

Dell'Agnese, D., and Clark, D.L., 1994. Siliceous microfossils from the warm Late Cretaceous and early Cenozoic Arctic Ocean. *J. Paleontol.,* 68:31–46.

D'Hondt, S.L., Jørgensen, B.B., Miller, D.J., et al., 2003. *Proc. ODP, Init. Repts.,* 201 [CD-ROM]. Available from: Ocean Drilling Program, Texas A&M University, College Station TX 77845-9547, USA. [**HTML**]

Dzinoridze, R.N., Jousé, A.P., Koroleva-Golikova, G.S., Kozlova, G.E., Nagaeva, G.S., Petrushevskaya, M.G., and Strelnikova, N.I., 1978. Diatom and radiolarian Cenozoic stratigraphy, Norwegian Basin; DSDP Leg 38. *In* Talwani, M., Udintsev, G., et al., *Init. Repts. DSDP,* 38, 39, 40, 41 (Suppl.): Washington (U.S. Govt. Printing Office), 289–427.

Eldrett, J.S., 2003. Magnetostratigraphic calibration of Eocene–Oligocene dinoflagellate cyst biostratigraphy from the Norwegian-Greenland Sea [Ph.D. dissert.]. Univ. Southampton.

Eldrett, J.S., Harding, I.C., Firth, J.V., and Roberts, A.P., 2004. Magnetostratigraphic calibration of Eocene–Oligocene dinoflagellate cyst biostratigraphy from the Norwegian-Greenland Sea. *Mar. Geol.,* 204:91–127. **doi:10.1016/S0025-3227(03)00357-8**

Evans, J.R., and Kaminski, M., 1998. Pliocene and Pleistocene chronostratigraphy and paleoenvironment of the central Arctic Ocean, using deep water agglutinated foraminifera. *Micropaleontology,* 44:109–130.

Fenner, J., 1985. Late Cretaceous to Oligocene planktic diatoms. *In* Bolli, H.M., Saunders, J.B., and Perch-Nielsen, K. (Eds.), *Plankton Stratigraphy:* Cambridge (Cambridge Univ. Press), 713–762.

Firth, J.V., 1996. Upper middle Eocene to Oligocene dinoflagellate biostratigraphy and assemblage variations in Hole 913B, Greenland Sea. *In* Thiede, J., Myhre, A.M., Firth, J.V., Johnson, G.L., and Ruddiman, W.F. (Eds.), *Proc. ODP, Sci. Results,* 151: College Station, TX (Ocean Drilling Program), 203–242.

Firth, J.V., and Clark, D.L., 1998. An early Maastrichtian organic-walled phytoplankton cyst assemblage from an organic-rich black mud in Core Fl-533, Alpha Ridge: evidence for upwelling conditions in the Cretaceous Arctic Ocean. *Mar. Micropaleontol.,* 34:1–27. **doi:10.1016/S0377-8398(97)00046-7**

Gard, G., and Crux, J.A., 1994. Reworked Jurassic–Neogene calcareous nannofossils in the central Arctic. *Mar. Geol.,* 119:287–300.

Gard, G. 1993. Late Quaternary coccoliths at the North Pole: evidence of ice-free conditions and rapid sedimentation in the central Arctic Ocean. *Geology,* 21:227–230. **doi:10.1130/0091-7613(1993)021<0227:LQCATN>2.3.CO;2**

Hall, J.K., 1979. Sediment waves and other evidence of paleo-bottom currents at two locations in the deep Arctic Ocean. *Mar. Geol.,* 23:269–299.

Head, M.J. (Ed.), 1993. A forum on Neogene and Quaternary dinoflagellate cysts: the edited transcript of a round table discussion held at the Third Workshop on Neogene and Quaternary dinoflagellates; with taxonomic appendix. *Palynology,* 17:201–239.

Head, M.J., 1994. Morphology and paleontological significance of the Cenozoic dinoflagellate genera *Tectatodinium* and *Habibacysta*. *Micropaleontology,* 40:289–321.

Head, M.J., and Norris, G., 1989. Palynology and dinocyst stratigraphy of the Eocene and Oligocene in ODP Leg 105, Hole 647A, Labrador Sea. *In* Srivastava, S.P., Arthur, M.A., Clement, B., et al., *Proc. ODP, Sci. Results,* 105: College Station, TX (Ocean Drilling Program), 515–550.

Head, M.J., Norris, G., and Mudie, P.J., 1989. New species of dinocysts and a new species of acritarch from the upper Miocene and lowermost Pliocene, ODP Leg 105, Site 646, Labrador Sea. *In* Srivastava, S.P., Arthur, M.A., Clement, B., et al., *Proc. ODP, Sci. Results,* 105: College Station, TX (Ocean Drilling Program), 453–466.

Heilmann-Clausen, C., 1985. Dinoflagellate stratigraphy of the uppermost Danian to Ypresian in the Viborg I borehole, central Jylland, Denmark. *Dan. Geol. Unders., Raekke A,* 7:1–69.

Hull, D.M., Osterman, L.E., and Thiede, H., 1996. Biostratigraphic synthesis of Leg 151, North Atlantic–Arctic Gateways. *In* Thiede, J., Myhre, A.M., Firth, J.V., Johnson, G.L., and Ruddiman, W.F. (Eds.), *Proc. ODP, Sci. Results,* 151: College Station, TX (Ocean Drilling Program), 627–644.

Holtz, R.D., and Kovacs, W.D., 1981. *An Introduction to Geotechnical Engineering:* Englewood Cliffs, NJ (Prentice-Hall).

Homann, M., 1991. Die diatomeen der Fur Formation (Alttertiär, Limfjord/Dänemark) *Geol. Jahrb. Reihe A,* 123:1–285.

Iakovleva, A.I., Brinkhuis, H., and Cavagnetto, C., 2001. Late Paleocene–early Eocene dinoflagellate cysts from the Turgay Strait, Kazakhstan: correlations across ancient seaways. *Palaeogeogr., Palaeoclimatol., Palaeoecol.,* 172:243–268. **doi:10.1016/S0031-0182(01)00300-5**

Ishman, S.E., Polyak, L., and Poore, R.Z., 1996. An expanded record of Pleistocene deep arctic change: Canada Basin, western Arctic Ocean. *Geology,* 24:139–142. **doi:10.1130/0091-7613(1996)024<0139:EROQOC>2.3.CO;2**

Jakobsson, M., Løvlie, R., Al-Hanbali, H., Arnold, E., Backman, J., and Mörth, M., 2000. Manganese and color cycles in Arctic Ocean sediments constrain Pleistocene chronology. *Geology,* 28:23–26. **doi:10.1130/0091-7613(2000)028<0023:MACCIA>2.3.CO;2**

Jakobsson, M., Løvlie, R., Arnold, E., Backman, J., Polyak, L., Knudsen, J.-O., and Musatov, E., 2001. Pleistocene stratigraphy and paleoenvironmental variation from Lomonosov Ridge sediments, central Arctic Ocean. *Global Planet. Change,* 31:1–22. **doi:10.1016/S0921-8181(01)00110-2**

Jokat, W., 2003. Seismic investigations along the western sector of Alpha Ridge, central Arctic Ocean. *Geophys. J. Int.,* 152:185–201. **doi:10.1046/j.1365-246X.2003.01839.x**

Kucera, M., and Kennett, J.P., 2002. Causes and consequences of a middle Pleistocene origin of the modern planktonic foraminifer *Neogloboquadrina pachyderma* sinistral. *Geology,* 30:539–542.

Ling, H.Y., 1985. Early Paleogene silicoflagellates and ebridians from the Arctic Ocean. *Trans. Proc. Paleontol. Soc. Jpn.,* 138:79–93.

Locker, S., 1996. Cenozoic siliceous flagellates from the Fram Strait and the East Greenland margin: biostratigraphic and paleoceanographic results. *In* Thiede, J., Myhre, A.M., Firth, J.V., Johnson, G.L., and Ruddiman, W.F. (Eds.), *Proc. ODP, Sci. Results,* 151: College Station, TX (Ocean Drilling Program), 101–124.

Luterbacher, H.P., Ali, J.R., Brinkhuis, H., Gradstein, F.M., Hooker, J.J., Monechi, S., Ogg, J.G., Powell, J., Röhl, U., Sanfilippo, A., and Schmitz, B., 2005. The Paleogene period. *In* Ogg, J.G., Gradstein, F.M., and Smith, A.G. (Eds.), *A Geological Time Scale 2004:* Cambridge (Cambridge Univ. Press), 384–408.

Manum, S.B., Boulter, M.C., Gunnarsdottir, H., Rangnes, K., and Scholze, A., 1989. Eocene to Miocene palynology of the Norwegian Sea (ODP Leg 104). *In* Eldholm, O., Thiede, J., et al., *Proc. ODP, Sci. Results,* 104: College Station, TX (Ocean Drilling Program), 611–662.

Marret, F., and Zonneveld, K.A.F., 2003. Atlas of modern organic-walled dinoflagellate cyst distribution. *Rev. Palaeobot. Palynol.,* 125:1–200.

Matthiessen, J., and Brenner, W., 1996. Dinoflagellate cyst ecostratigraphy of Pliocene–Pleistocene sediments from the Yermak Plateau (Arctic Ocean, Hole 911A). *In* Thiede, J., Myhre, A.M., Firth, J.V., Johnson, G.L., and Ruddiman, W.F. (Eds.), *Proc. ODP, Sci. Results,* 151: College Station, TX (Ocean Drilling Program), 243–253.

Matthiessen, J., Kunz-Pirrung, M., and Mudie, P.J., 2000. Freshwater chlorophycean algae from the Beaufort, Laptev, and Kara Seas (Arctic Ocean) as indicators of river runoff. *Int. J. Earth Sci.,* 89:470–485. **doi:10.1007/s005310000127**

McDuff, R.E., 1985. The chemistry of interstitial waters, Deep Sea Drilling Project Leg 86. *In* Heath, G.R., Burckle, L.H., et al., *Init. Repts. DSDP,* 86: Washington (U.S. Govt. Printing Office), 675–687.

McNeil, D.H., 1997. New foraminifera from the Upper Cretaceous and Cenozoic of the Beaufort-MacKenzie Basin of Arctic Canada. *Spec. Publ.—Cushman Found. Foraminiferal Res.,* 35:1–95.

Mudge, D.C., and Bujak, J.P., 1996. An integrated stratigraphy for the Paleocene and Eocene of the North Sea. *In* Knox, R.W.O.B., Corfield, R.M., and Dunay, R.E. (Eds.), *Correlation of the Early Paleogene in Northwest Europe.* Geol. Soc. Spec. Publ., 101:91–113.

Mudie, P.J., 1985. Palynology of the CESAR Cores, Alpha Ridge. *In* Jackson, H.R., Mudie, P.J., and Blasco, S.M. (Eds.), *Initial Geological Report on CESAR—the Canadian Expedition to Study the Alpha Ridge, Arctic Ocean.* Pap.—Geol. Surv. Can., 84–22:149–174.

Nagy, J., Kaminski, M.A., Kuhnt, W., and Bremer, M.A., 2000. Agglutinated foraminifera from neritic to bathyal facies in the Palaeogene of Spitsbergen and the Barents Sea. *In* Hart, M.B., Kaminski, M.A., and Smart, C.W. (Eds.), *Proceedings of the Fifth International Workshop on Agglutinated Foraminifera*. Grzybowski Found. Spec. Publ., 7:333–361.

Ogg, J.G., and Smith, A.G., 2004. The geomagnetic polarity time scale. *In* Gradstein, F., Ogg, J., and Smith, A. (Eds.), *A Geologic Time Scale:* Cambridge (Cambridge Univ. Press), 63–86.

Perch-Nielsen, K., 1985a. Cenozoic calcareous nannofossils. *In* Bolli, H.M., Saunders, J.B., and Perch-Nielsen, K. (Eds.), *Plankton Stratigraphy:* Cambridge (Cambridge Univ. Press), 427–554.

Perch-Nielsen, K., 1985b. Silicoflagellates. *In* Bolli, H.M., Saunders, J.B., and Perch-Nielsen, K. (Eds.), *Plankton Stratigraphy:* Cambridge (Cambridge Univ. Press), 811–846.

Podobina, V.M., 1998. *Paleogene Foraminifera and Biostratigraphy of Western Siberia:* Tomsk, Russia (Sci. Tech. Literature Publ.).

Poulsen, N.E., Manum, S.B., Williams, G.L., and Ellegaard, M., 1996. Tertiary dinoflagellate biostratigraphy of Sites 907, 908, and 909 in Norwegian-Greenland Sea. *In* Thiede, J., Myhre, A.M., Firth, J.V., Johnson, G.L., and Ruddiman, W.F. (Eds.), *Proc. ODP, Sci. Results,* 151: College Station, TX (Ocean Drilling Program), 255–287.

Radionova, E.P., Beniamovski, V.N., Iahovleva, H.I., Muzylor, W.G., Oreshkina, T.V., Shcherbinina, E.A., and Koylova, G.E., 2003. Early Paleogene transgressions: stratigraphical and sedimentological evidence from the northern Peri-Tethys. *In* Wing, S.L., Gingrich, P.D., Schmitz, B., and Thomas, E. (Eds.), *Causes and Consequences of Globally Warm Climates in the Early Paleogene*. Spec. Pap.—Geol. Soc. Am., 369:239–261.

Radionova, E.P., and Khokhlova, I.E., 2000. Was the North Atlantic connected with the Tethys via the Arctic in the early Eocene? Evidence from siliceous plankton. *In* Schmitz, B., Sundquist, B., and Andreasson, F.P. (Eds.), *Early Paleogene Warm Climates and Biosphere Dynamics: Short Papers and Extended Abstracts*. GFF, 122(1):133–134.

Reichart, G.J., and Brinkhuis, H., 2003. Late Quaternary *Protoperidinium* cysts as indicators of paleoproductivity in the northern Arabian Sea. *Mar. Micropaleontol.,* 49:303–315. **doi:10.1016/S0377-8398(03)00050-1**

Rochon, A., de Vernal, A., Turon, J.L., Mathiessen, J., and Head, M.J., 1999. Distribution of recent dinoflagellate cysts in surface sediments from the North Atlantic Ocean and adjacent seas in relation to sea-surface parameters. *Am. Assoc. Strat. Palynol. Found. Cont. Ser.,* 35:146.

Röhl, U., Bralower, T.J., Norris, R.D., and Wefer, G., 2000. New chronology for the Late Paleocene Thermal Maximum and its environmental implications. *Geology,* 28:927–930. **doi:10.1130/0091-7613(2000)028<0927:NCFTLP>2.3.CO;2**

Röhl, U., Brinkhuis, H., and Fuller, M., in press. On the search for the Paleocene/Eocene boundary in the Southern Ocean: exploring ODP Leg 189 Holes 1171D and 1172D, Tasman Sea. *In* Exon, N., Kennett, J.P., and Malone, M. (Eds.), *The Cenozoic Southern Ocean: Tectonics, Sedimentation and Climate Change between Australia and Antarctica*. Geophys. Monogr., 148.

Ryan, P.D., Harper, D.A.T., and Whalley, J.S. 1995. *PALSTAT: Statistics for Palaeontologists:* London (Chapman and Hall).

Rysgaard, S., Glud, R.N., Risgaard-Petersen, N., and Dalsgaard, T., 2004. Denitrification and anammox activity in Arctic marine sediments. *Limnol. Oceanogr.,* 49:1493–1502.

Scherer, R.P., and Koç, N., 1996. Late Paleogene diatom biostratigraphy and paleoenvironments of the northern Norwegian-Greenland Sea. *In* Thiede, J., Myhre, A.M., Firth, J.V., Johnson, G.L., and Ruddiman, W.F. (Eds.), *Proc. ODP, Sci. Results,* 151: College Station, TX (Ocean Drilling Program), 75–99.

Schrader, H.-J., and Fenner, J., 1976. Norwegian Sea Cenozoic diatom biostratigraphy and taxonomy. *In* Talwani, M., Udintsev, G., et al., *Init. Repts. DSDP,* 38: Washington (U.S. Govt. Printing Office), 921–1099.

Schröder-Adams, C.J., and McNeil, D.H., 1994. Oligocene to Miocene agglutinated foraminifera in deltaic and deep-water facies of the Beaufort-MacKenzie Basin. *Geol. Surv. Can. Bull.* 477:1–67.

Scott, D.B., Mudie, P.J., Baki, V., MacKinnon, K.D., and Cole, F.E., 1989. Biostratigraphy and late Cenozoic paleoceanography of the Arctic Ocean: foraminiferal, lithostratigraphic, and isotopic evidence. *Geol. Soc. Am. Bull.,* 101:260–277. **doi:10.1130/0016-7606(1989)101<0260:BALCPO>2.3.CO;2**

Shannon, C.E., and Weaver, W., 1949. *The Mathematical Theory of Communication:* Urbana (Univ. of Illinois Press).

Skempton, A.W., and Bishop, A.W., 1950. The measurement of shear strength of soils. *Geotechnique,* 2:90–108.

Smelror, M., 1999. Pliocene–Pleistocene and redeposited dinoflagellate cysts from the western Svalbard margin (Site 986): biostratigraphy, paleoenvironments, and sediment provenance. *In* Raymo, M.E., Jansen, E., Blum, P., and Herbert, T.D. (Eds.), 1999. *Proc. ODP, Sci. Results,* 162: College Station, TX (Ocean Drilling Program), 83–97. [**HTML**]

Stein, R., 1991. Accumulation of organic carbon in marine sediments: results from the Deep Sea Drilling Project/Ocean Drilling Program (DSDP/ODP). *In* Battacharji, S., Friedman, G.M., Neugebauer, H.J., and Seilacher, A. (Eds.), *Lecture Notes in Earth Sciences* (Vol. 34): Berlin (Springer-Verlag), 217.

Stein, R., Schubert, C., Vogt, C., and Fütterer, D., 1994. Stable isotope stratigraphy, sedimentation rates, and salinity changes in the latest Pleistocene to Holocene eastern central Arctic Ocean. *Mar. Geol.,* 119:333–355. **doi:10.1016/0025-3227(94)90189-9**

Stein R., Schubert, C.J., MacDonald, R.W., Fohl, K., Harvey, H.R., and Weiel D., 2003. The central Arctic Ocean: distribution, sources, variability, and burial of organic carbon. *In* Stein, R., and MacDonald, R.W. (Eds), *The Organic Carbon Cycle in the Arctic Ocean:* Berlin (Springer-Verlag), 295–314.

Strelnikova, N.I., 1974. *Diatoms of the Late Cretaceous*: Moscow (Nauka). (in Russian)

Tissot, B.P., and Welte, D.H., 1984. *Petroleum Formation and Occurrence:* Heidelberg (Springer-Verlag).

Versteegh, G.J.M., Brinkhuis, H., Visscher, H.,and Zonneveld, K.A.F., 1996. The relation between productivity and temperature in the Pliocene North Atlantic at the onset of Northern Hemisphere glaciation: a palynological study. *Global Planet.Change,* 11:155–166. **doi:10.1016/0921-8181(95)00054-2**

Wall, D., Dale, B., Lohmann, G.P., and Smith, W.K., 1977. The environmental and climatic distribution of dinoflagellate cysts in modern marine sediments from regions in the North and South Atlantic Oceans and adjacent seas. *Mar. Micropaleontol.,* 2:121–200. **doi:10.1016/0377-8398(77)90008-1**

Williams, G.L., Brinkhuis, H., Pearce, M.A., Fensome, R.A., and Weegink, J.W., 2004. Southern Ocean and global dinoflagellate cyst events compared: index events for the Late Cretaceous–Neogene. *In* Exon, N.F., Kennett, J.P., and Malone, M. (Eds.), *Proc. ODP, Sci. Results,* 189 [Online]. Available from World Wide Web: **http://www-odp.tamu.edu/publications/189_SR/107/107.htm**.

Witte, W.K., and Kent, D.V., 1988. Revised magnetostratigraphies confirm low sedimentation rates in Arctic ocean cores. *Quat. Res.,* 29:43–53. **doi:10.1016/0033-5894(88)90070-1**

Young, J.R., Geisen, M., Gros, L., Kleyne, A., Sprengel, C., Probert, I., and Ostergard, J., 2003. A guide to extant coccolithosphose taxonomy. *J. Nannoplankton Res.,* 1:1–125.

Zachos, J., Pagani, M., Sloan, L., Thomas, E., and Billups, K., 2001. Trends, rhythms, and aberrations in global climate 65 Ma to present. *Science,* 292:686–693. **doi:10.1126/science.1059412**

Publication: 7 March 2006
MS 302-104

Figure F1. Lithologic column for Holes M0002A and M0004A, including core recovery and results of visual core descriptions summarized at the subunit level. Within each unit and subunit, detailed downcore changes in lithology and/or structure cannot be shown. (Continued on next page.)

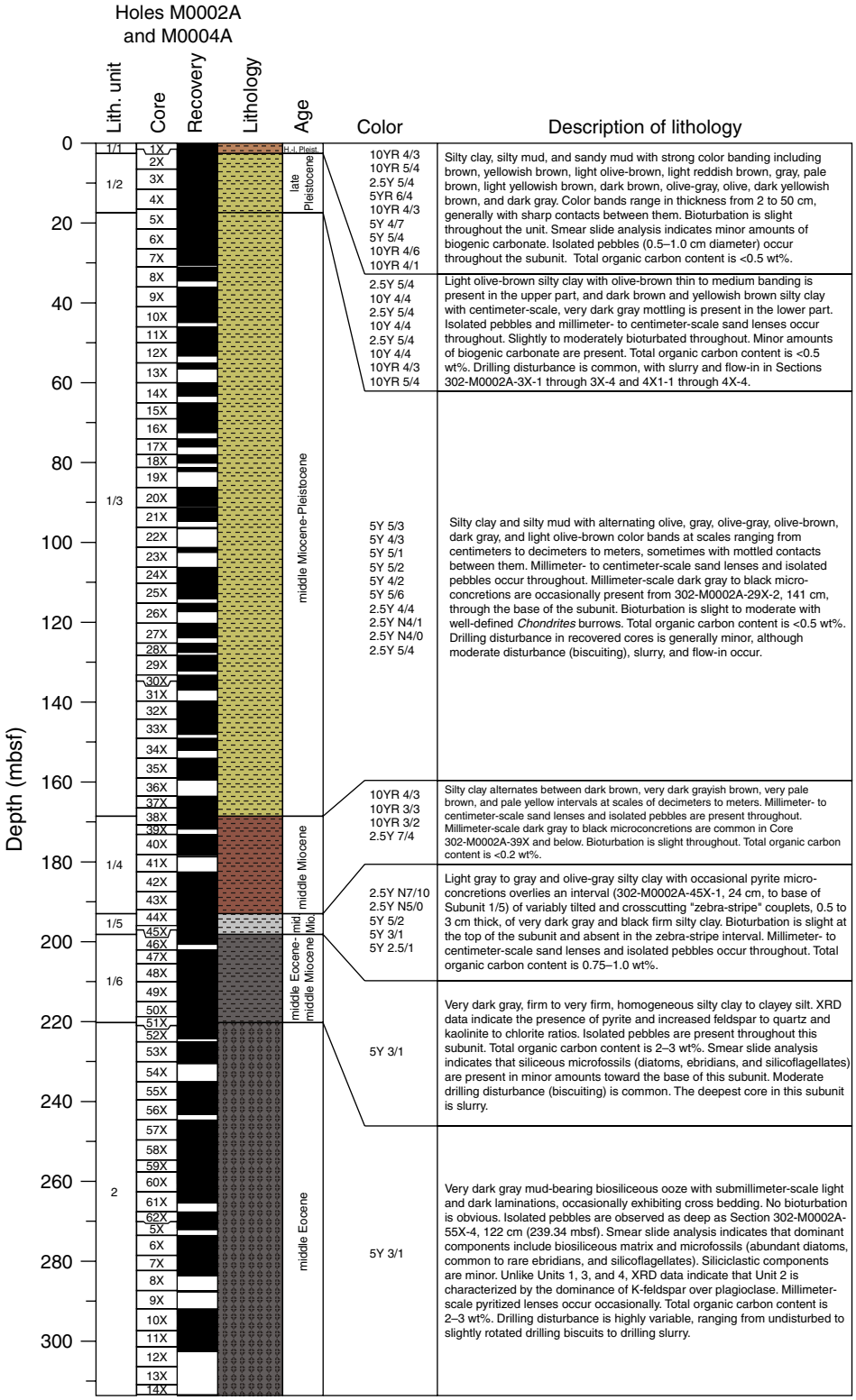

Figure F1 (continued).

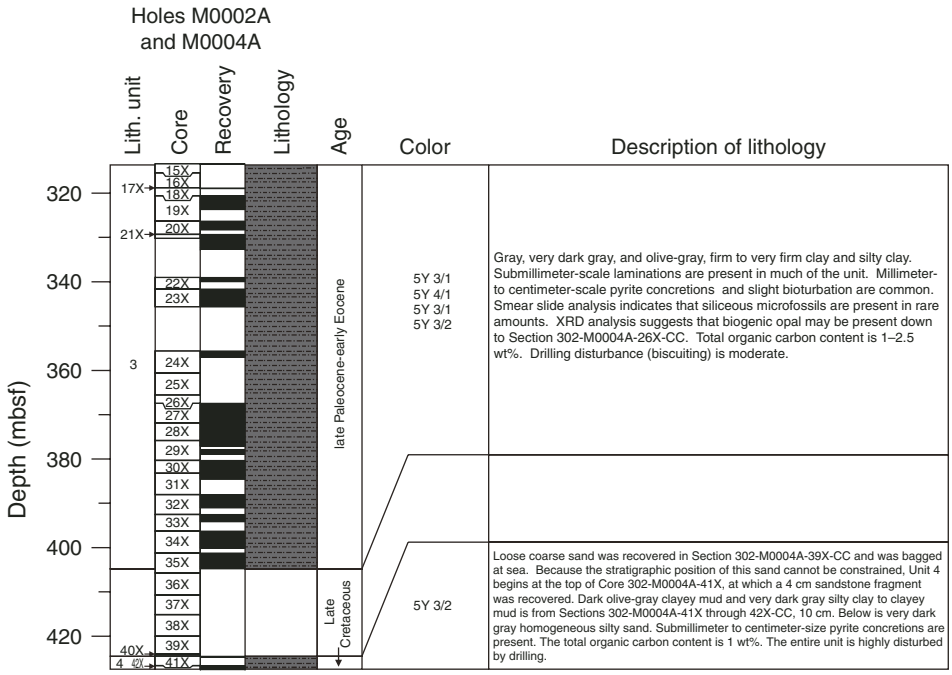

Figure F2. Lithostratigraphic subunits, core recovery, generalized lithology, and column plots of smear slide data, including textural and bulk mineral components from Holes M0002A (0–267.1 mbsf) and M0004A (265–427.63 mbsf), representing the entire recovered section. (Continued on next page.)

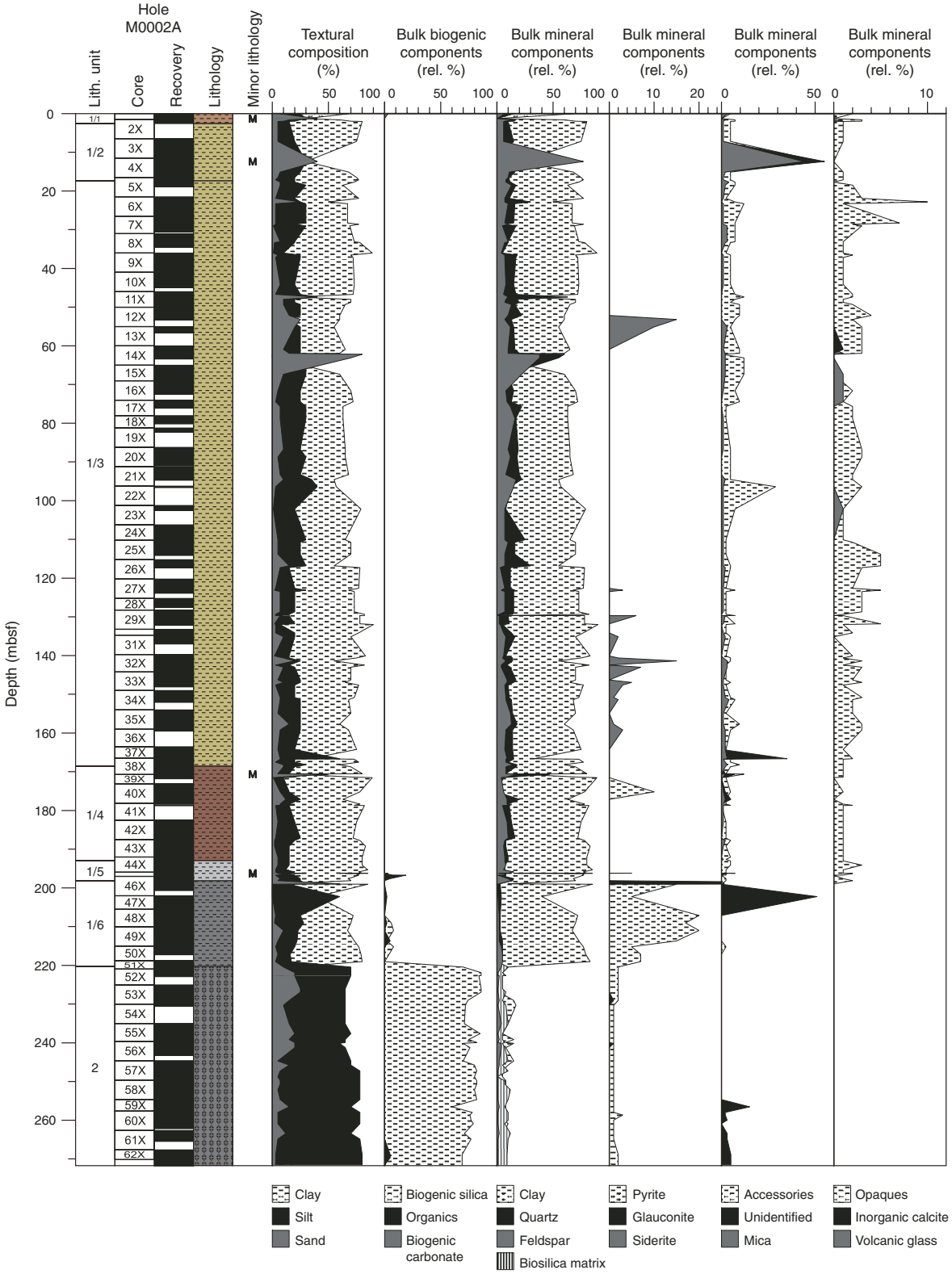

Figure F2 (continued).

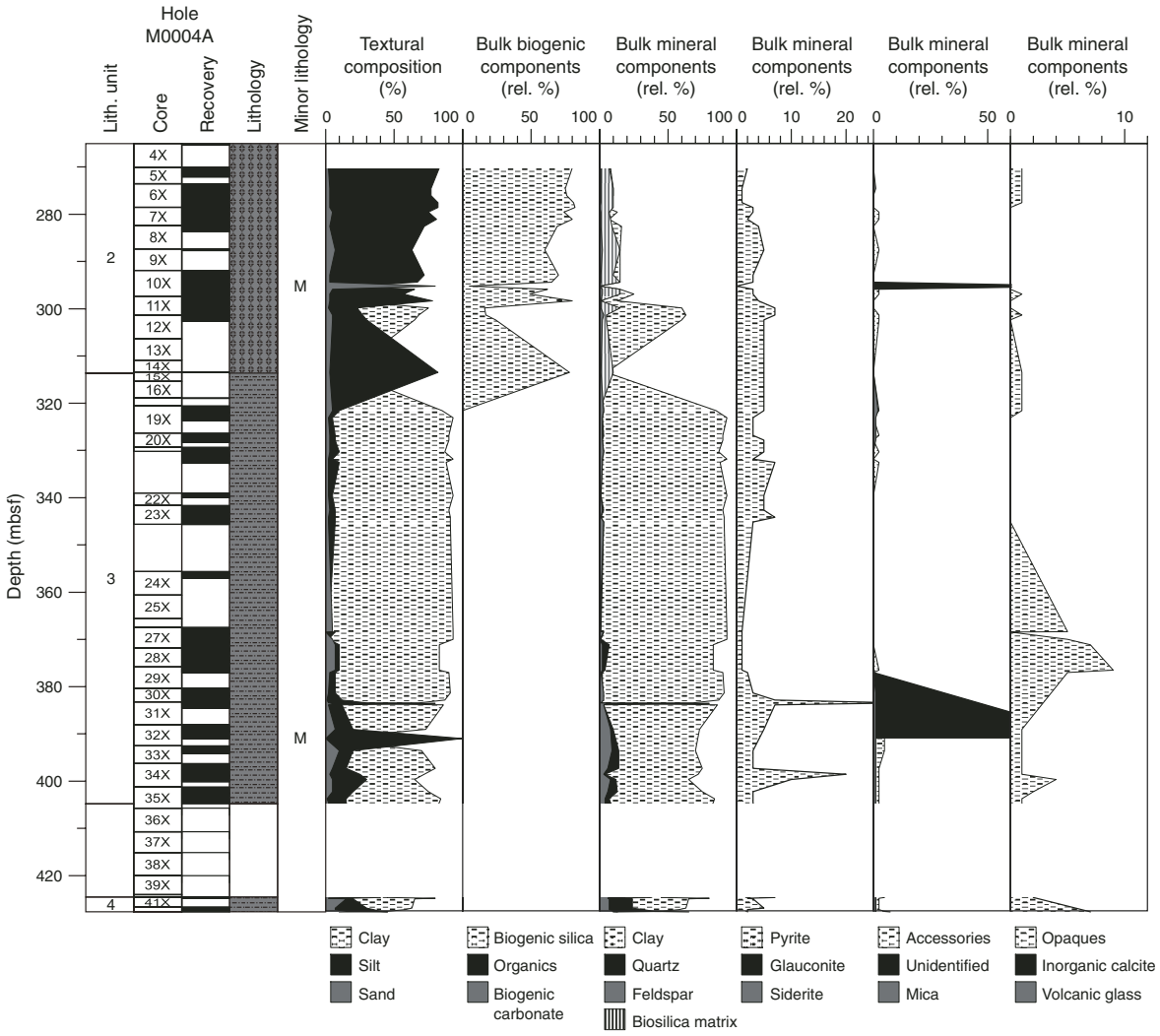

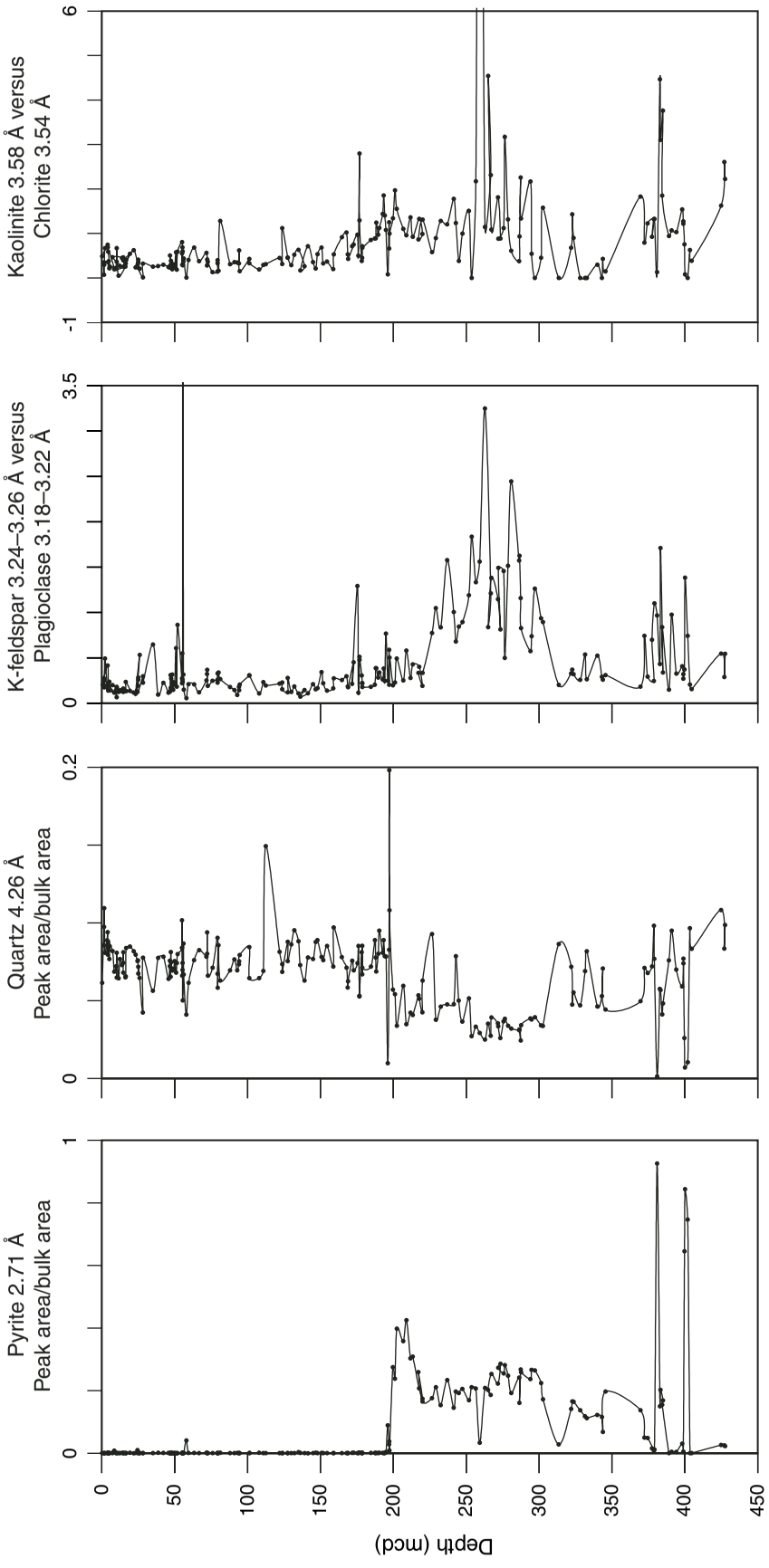

Figure F3. Downhole normalized abundances of minerals as determined by XRD (see Table T42).

Figure F4. Boundary between Subunits 1/3 and 1/4 at 45 cm (interval 302-M0002A-38X-3, 30–60 cm).

Figure F5. Boundary between Subunits 1/4 and 1/5 at 95 cm (interval 302-M0002A-44X-1, 80–100 cm).

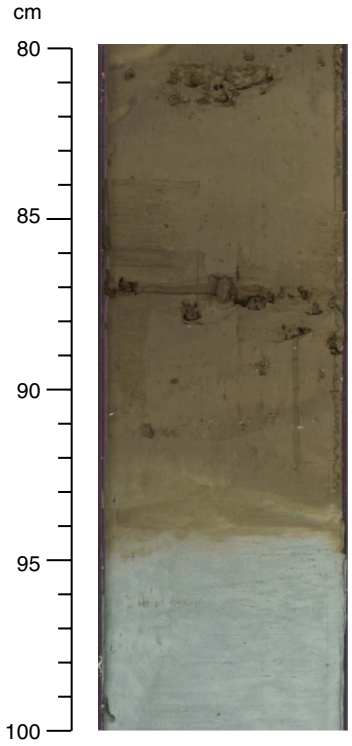

Figure F6. "Zebra-stripe" lithology (interval 302-M0002A-45X-1, 40–80 cm).

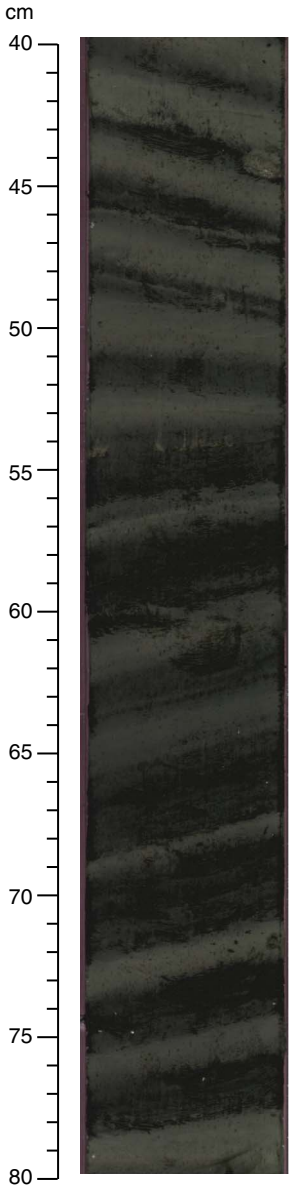

Figure F7. A. Seismic cross section taken near Expedition 302 sites (from Jokat et al., 1992). Note the flat-lying seismic reflections of the hemipelagic section overlying an angular unconformity formed at the time the Lomonosov Ridge rifted from the continental margin of Eurasia. Arrows at the edge of the ridge indicate a level at which erosion of the section is evident in the seismic record. **B.** Seismic reflection data taken during Expedition 302. The higher frequency of these data shows anastomosing reflectors just above the reflection, representing the top of the Eocene organic-rich sediments.

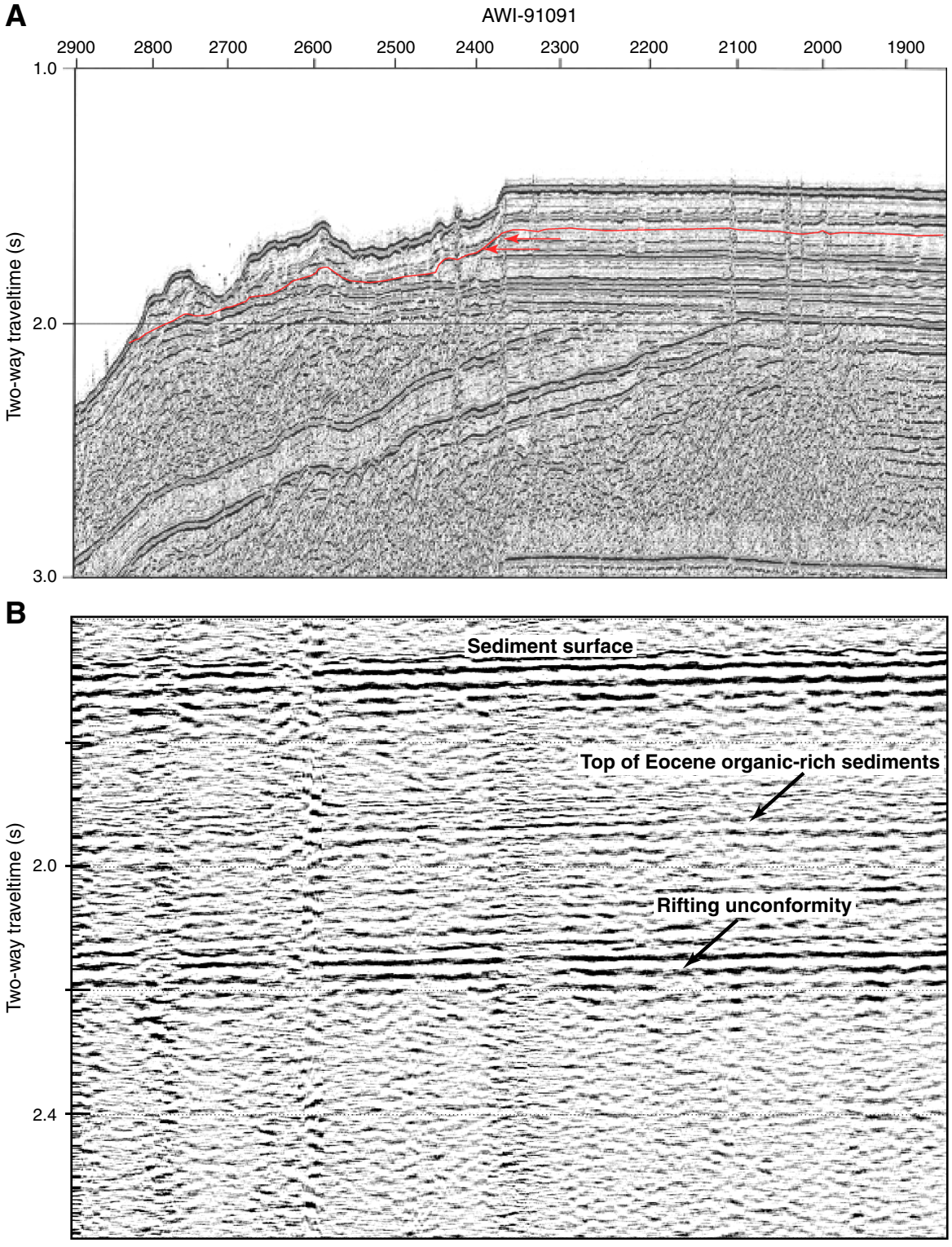

Figure F8. Quantitative distribution patterns of diatoms, Hole M0002A.

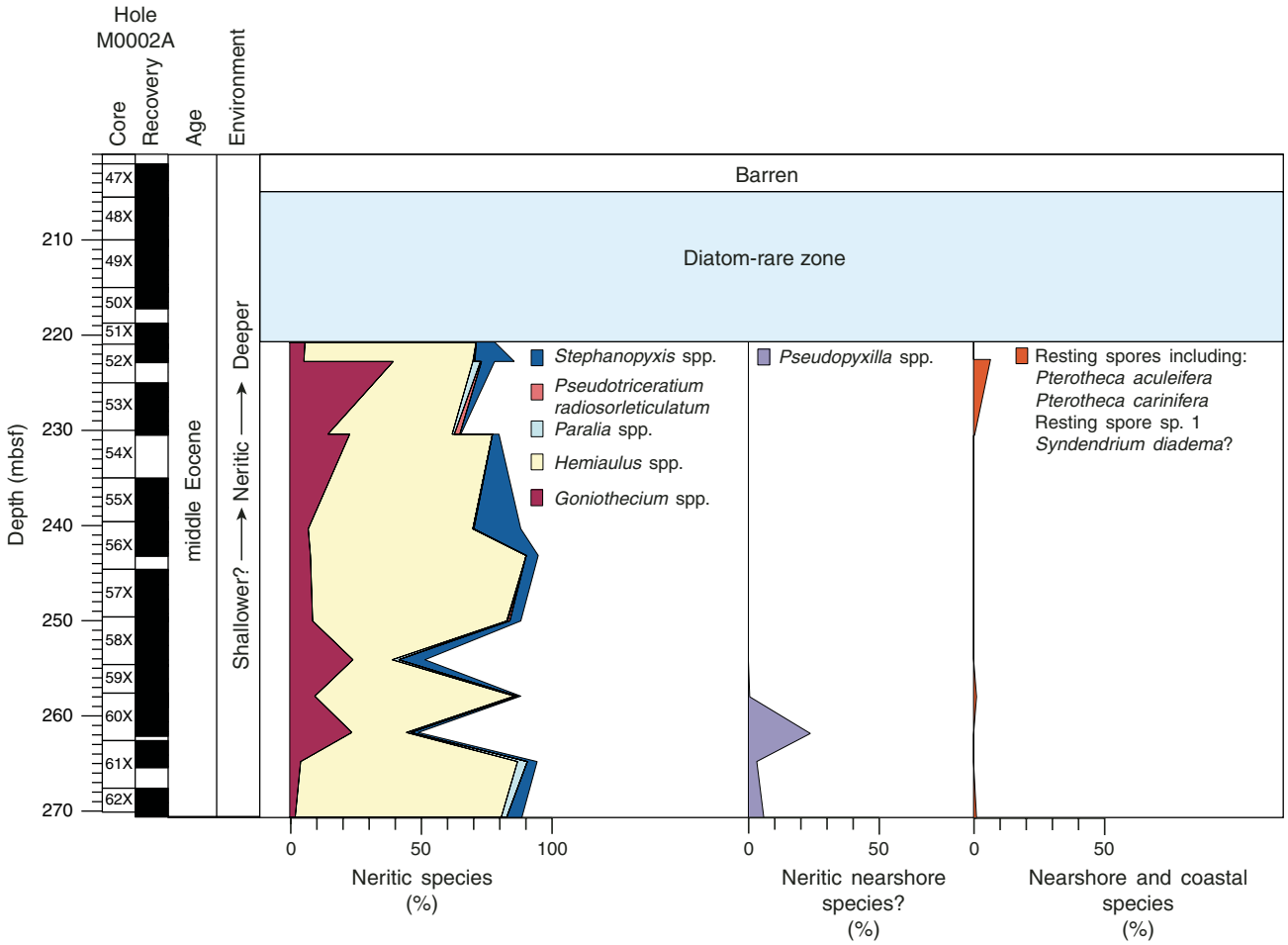

Figure F9. Quantitative distribution patterns of diatoms, Hole M0004A.

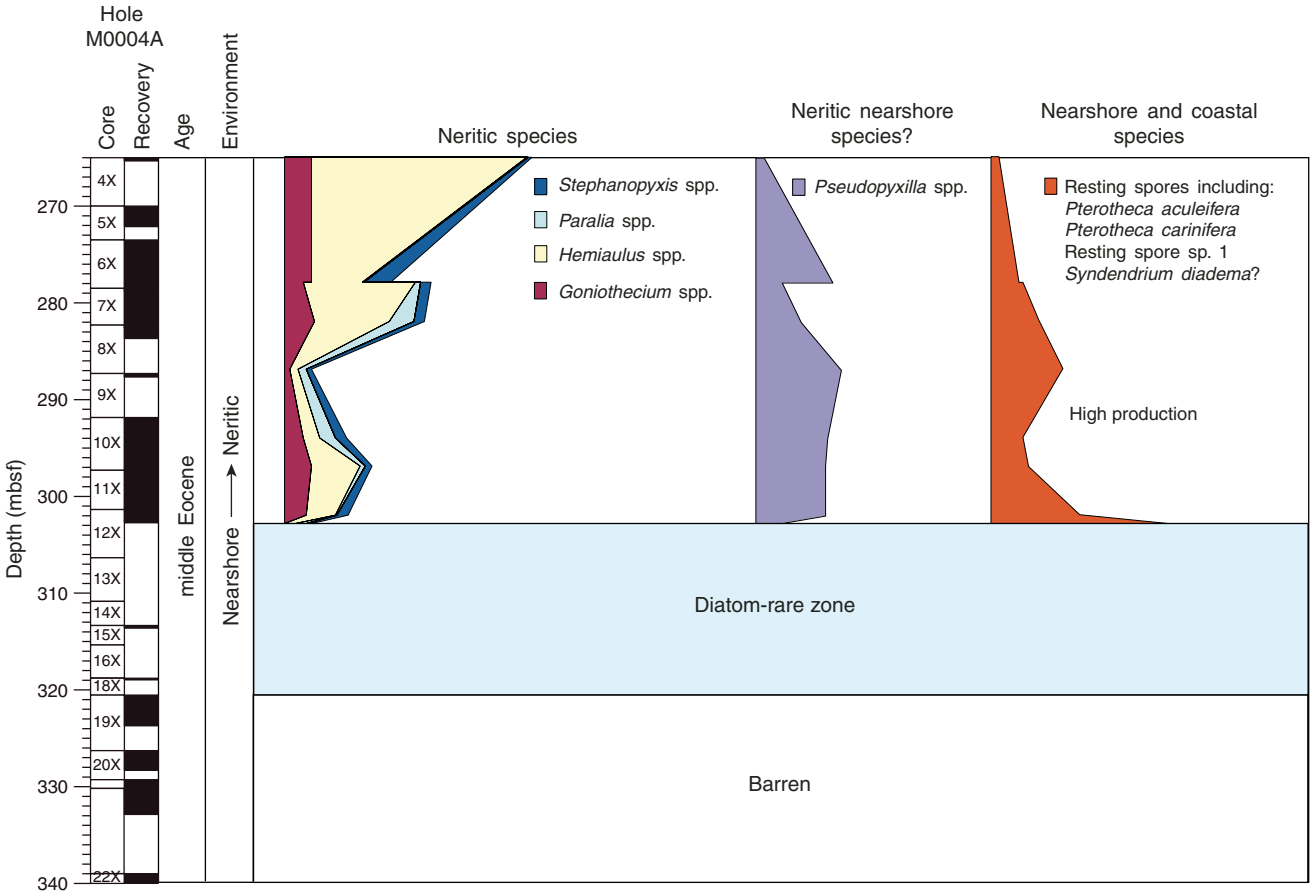

Figure F10. Relative abundance and shifting dominance between ebridians and diatoms, Hole M0004A. Dominant genera in the diatom assemblages are shown in the right column. A = abundant, C = common, F = few, R = rare.

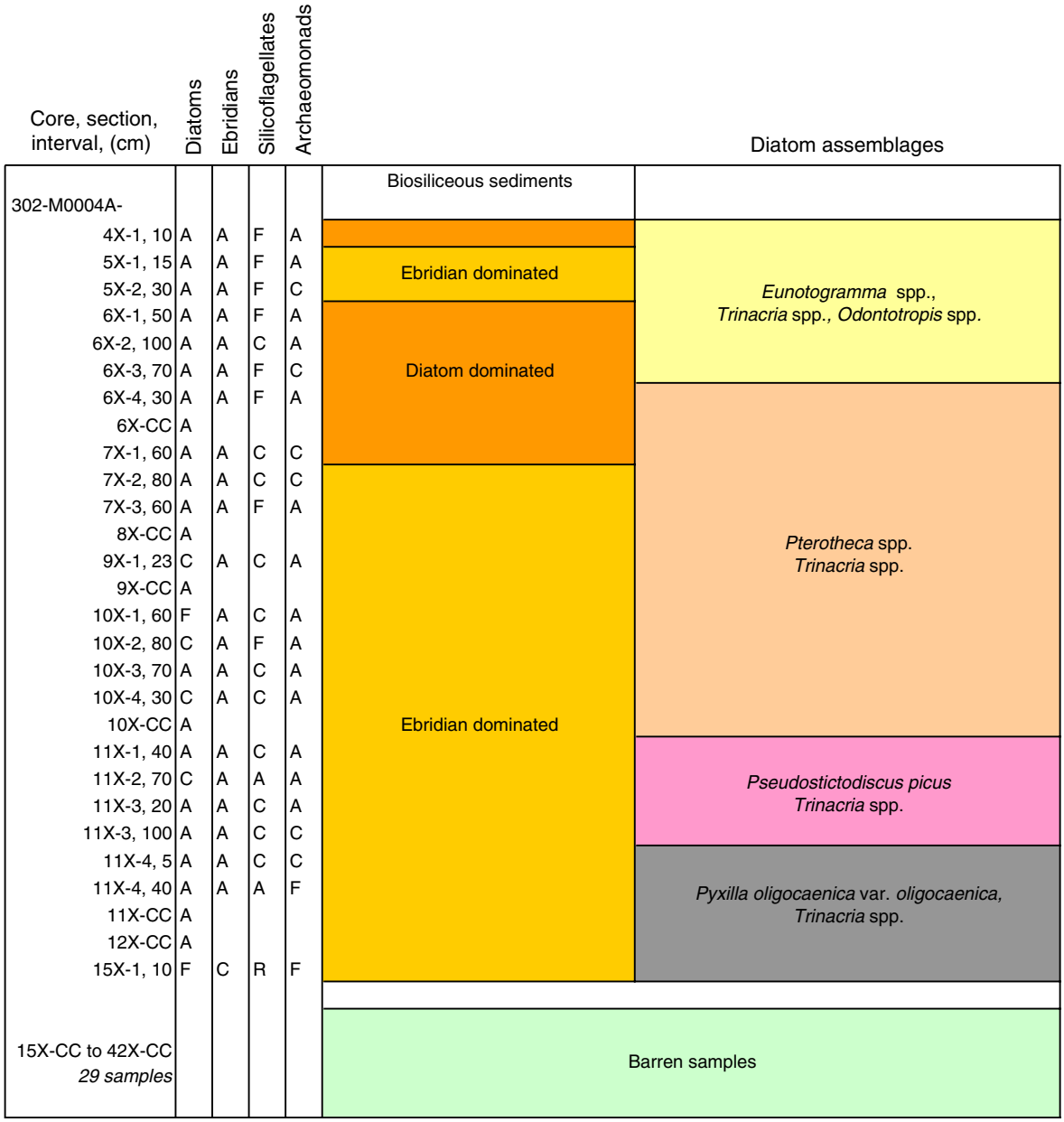

Figure F11. Relative abundance and shifting dominance between ebridians and diatoms, Hole M0002A. Dominant genera in the diatom assemblages are shown in the right column. A = abundant, C = common, F = few, R = rare.

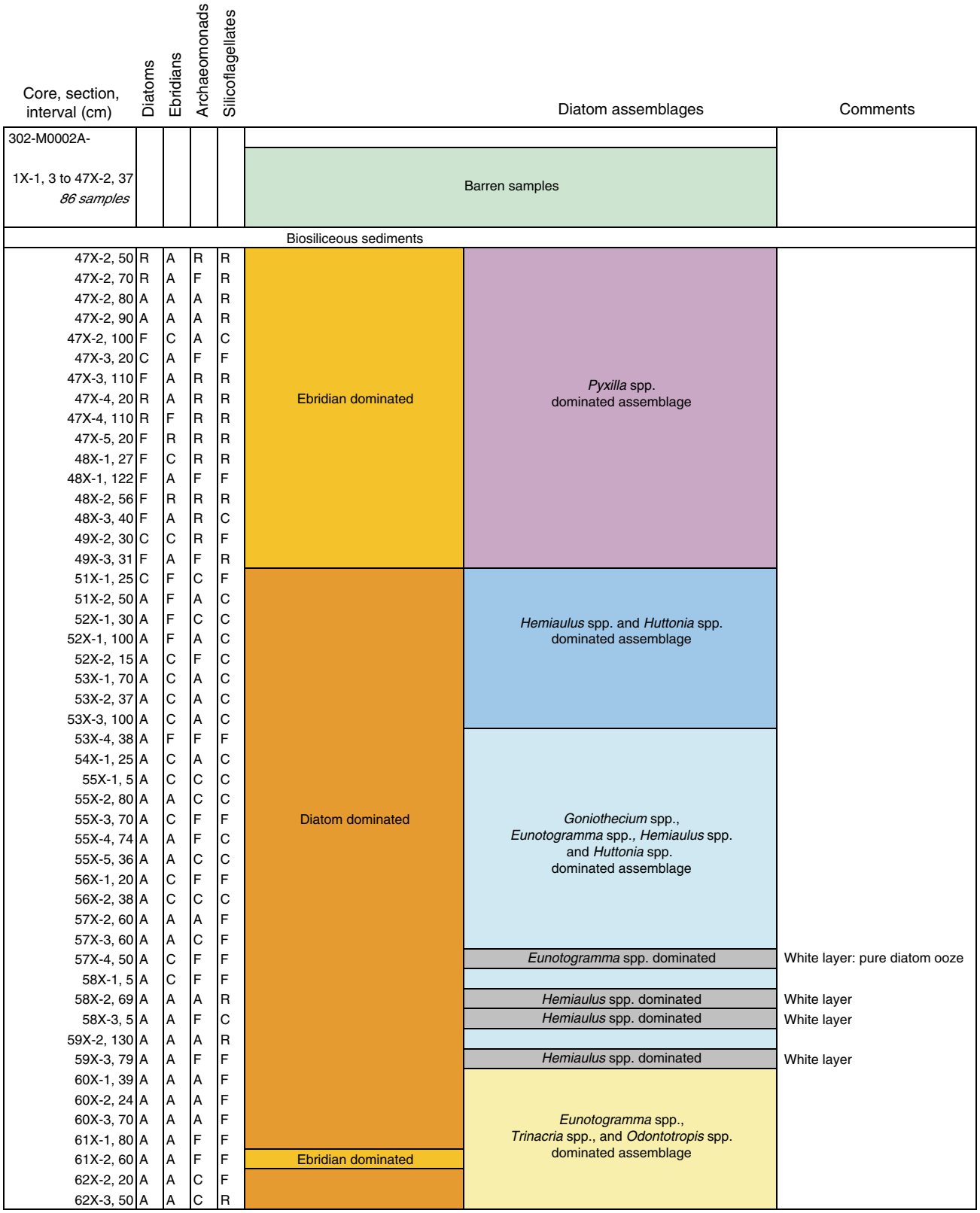

Figure F12. Occurrences of silicoflagellates and ebridians, silicoflagellate diversity, and an environmental reconstruction. **A.** Hole and core numbers and the top and bottom core depths. **B.** Abundance counts of silicoflagellate per column of microslides at 400× magnification in both coarse (>45 µm) and fine (<45 µm) fractions. **C.** Changes in silicoflagellate assemblage diversity; the Shannon indices (H: Shannon and Weaver, 1949) were calculated employing the paleontological statistic program PAST (Ryan et al., 1995). **D.** Estimated trend of seawater temperature changes employing *Dictyocha/Corbisema* ratios. **E.** Numbers of ebridian individuals, which may be indicators of biological productivity in relatively shallow marine waters (less than several hundred meters).

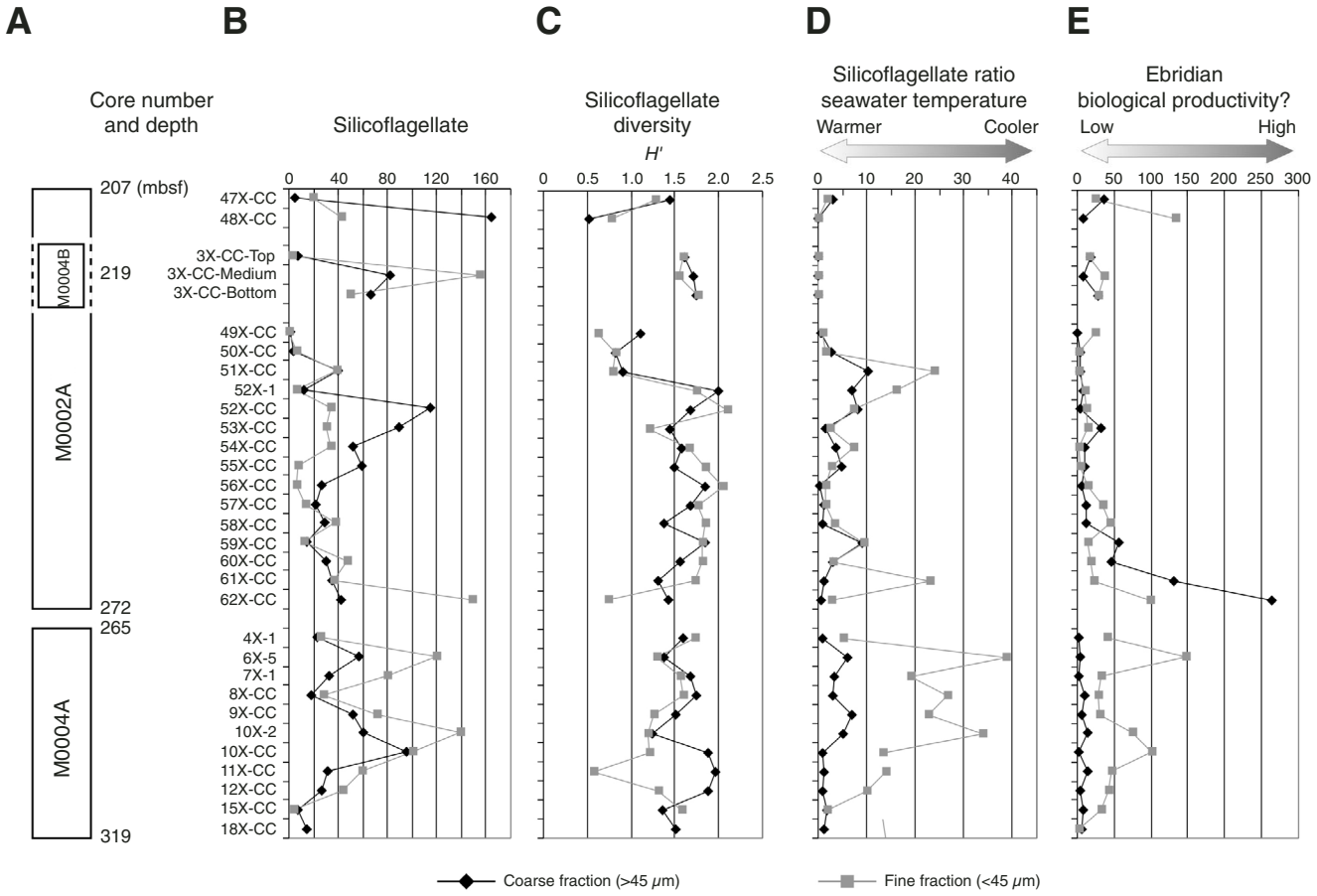

Figure F13. A. Gamma ray attenuation (GRA) bulk density and *P*-wave logger (PWL) data for Site M0002 plotted versus composite depth. Only one hole was cored. Outlying data points, due to section breaks or poor contact between the liner and core for PWL, were removed. (Continued on next three pages.)

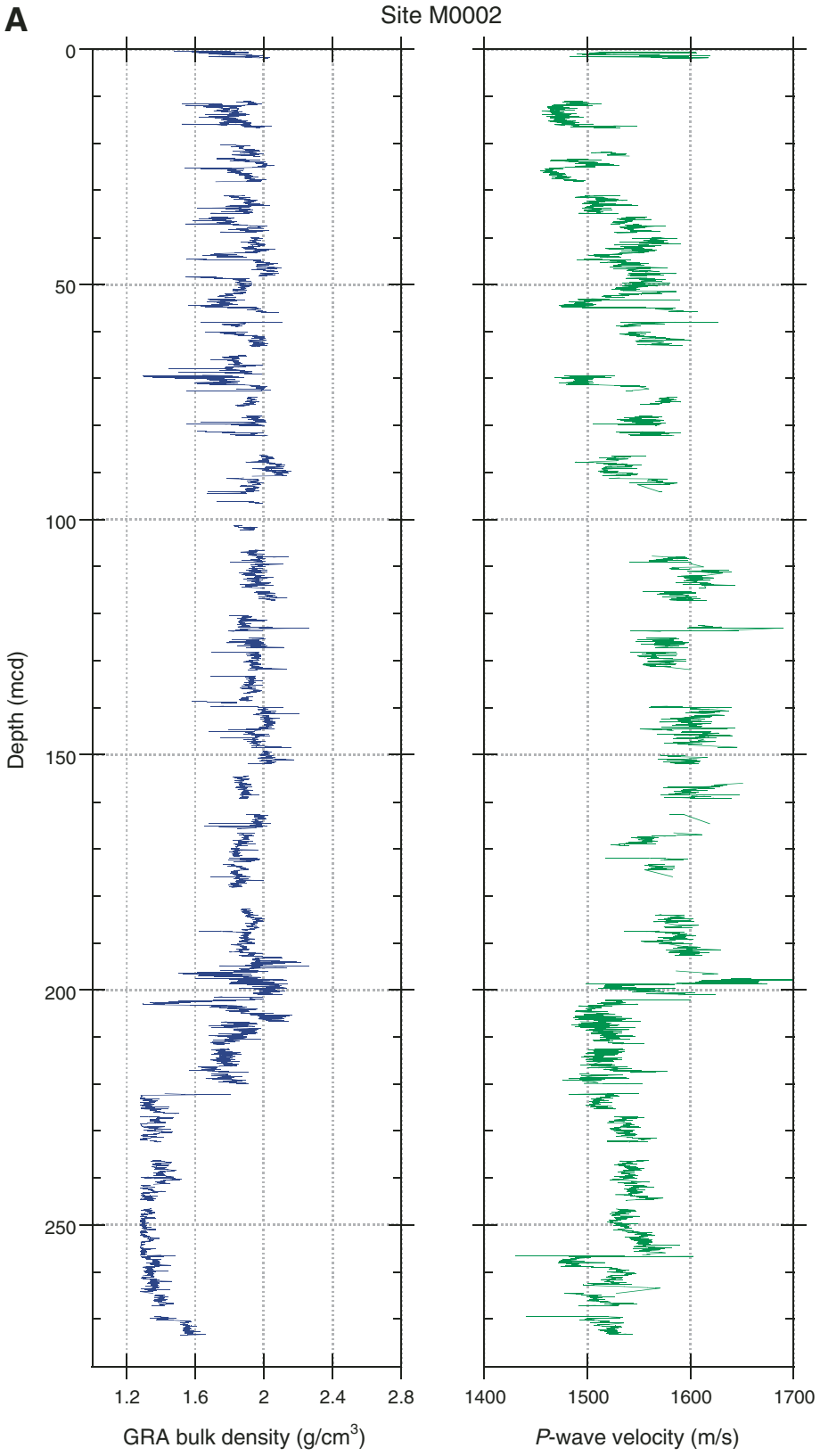

Figure F13 (continued). B. Magnetic susceptibility and electrical resistivity data for Site M0002 versus composite depth. Only one hole was cored. Outlying data points, due to section breaks, were removed.

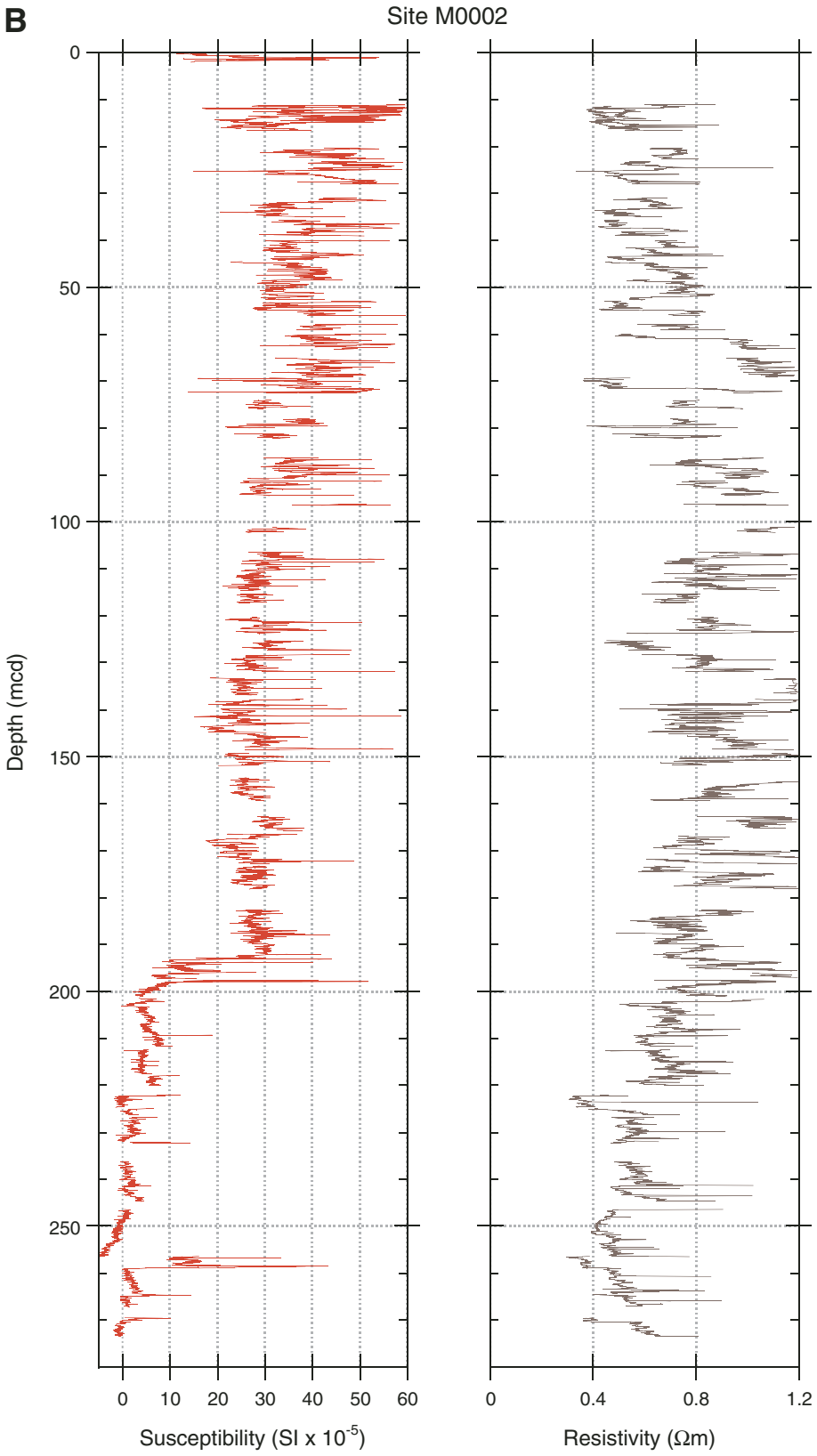

Figure F13 (continued). C. Color reflectance data for Site M0002 versus composite depth.

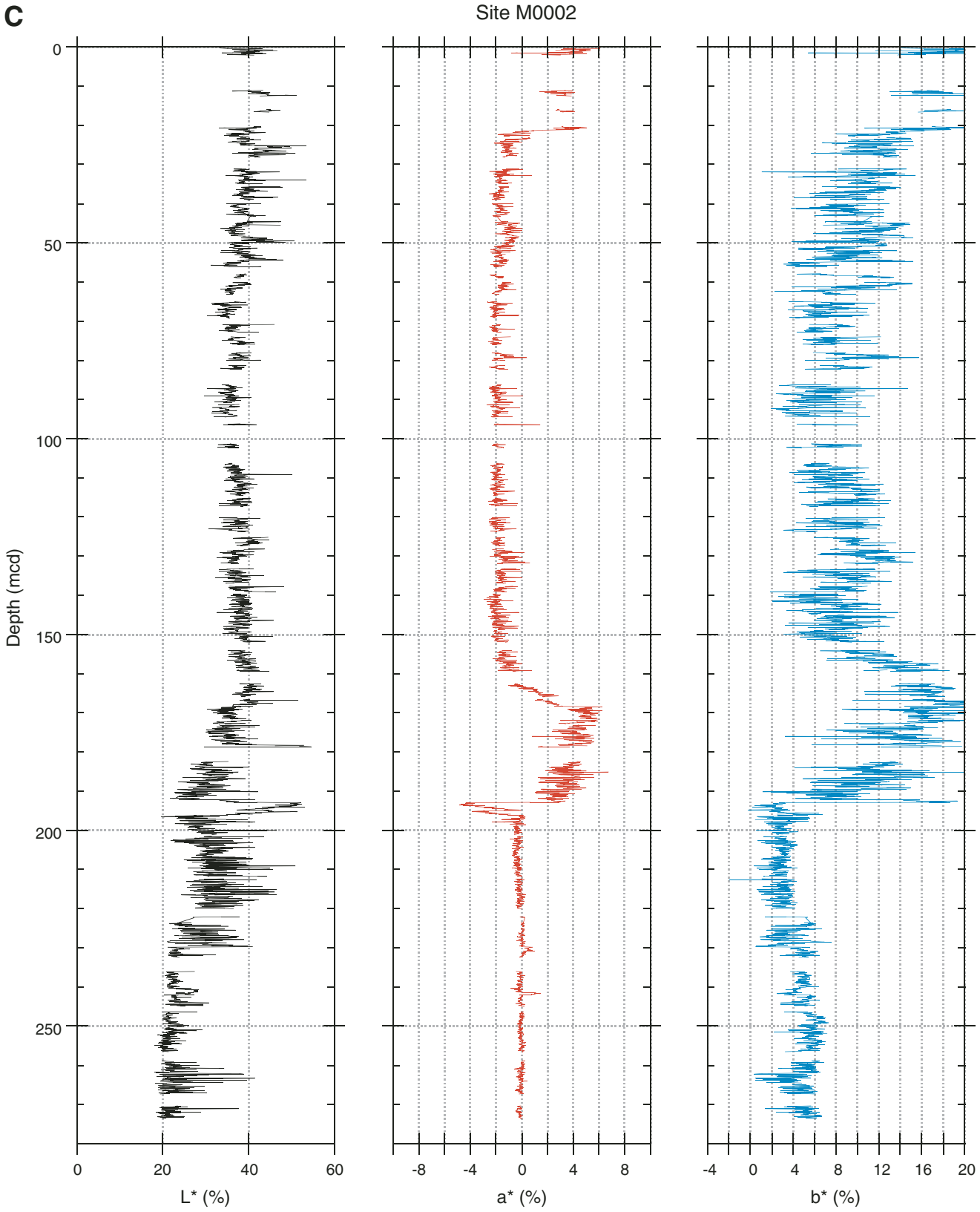

Figure F13 (continued). D. Natural gamma ray (NGR) data for Site M0002 versus composite depth.

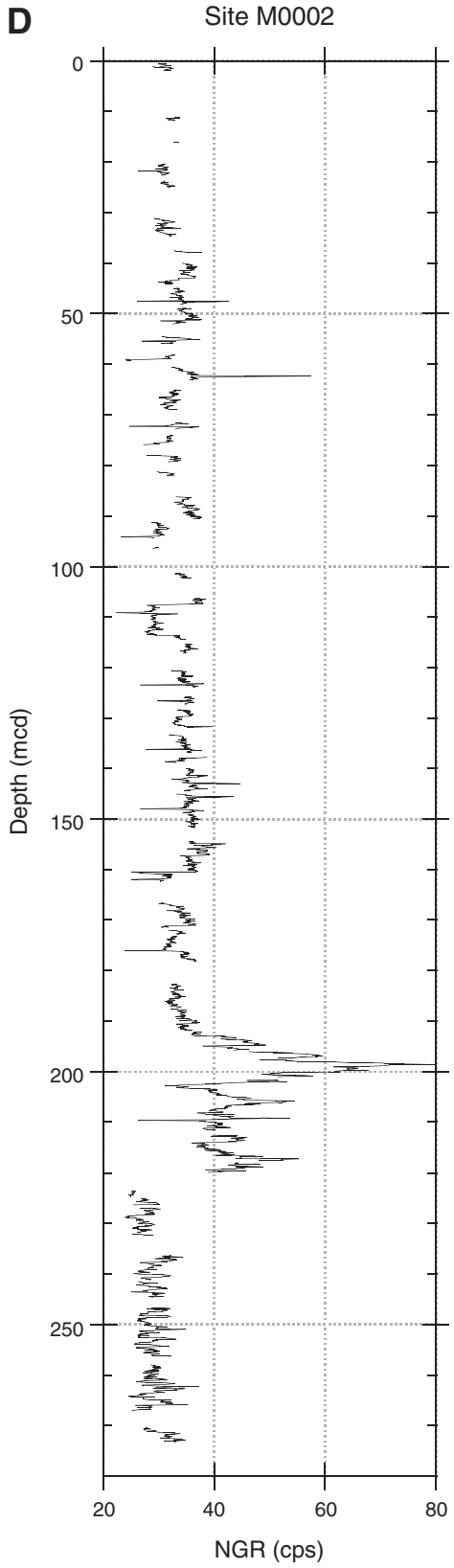

Figure F14. A. Gamma ray attenuation (GRA) bulk density and *P*-wave logger (PWL) data for Site M0003 plotted versus composite depth. Only one hole was cored. Outlying data points, due to section breaks or poor contact between the liner and core for PWL, were removed. (Continued on next three pages.)

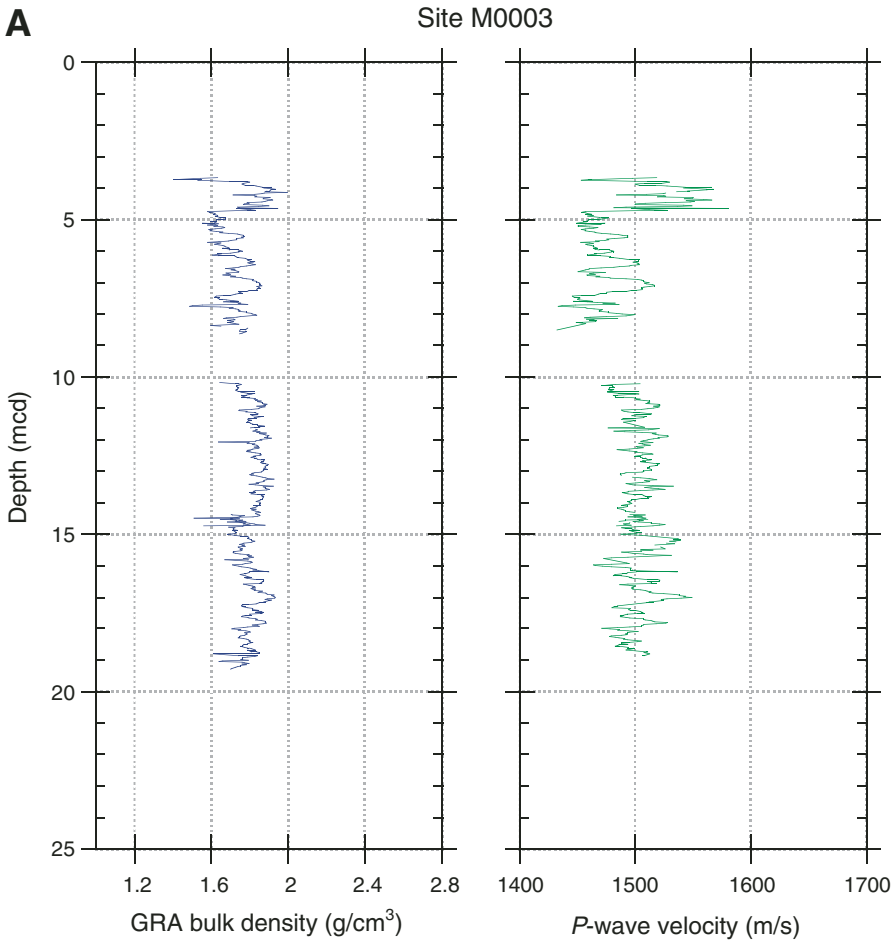

Figure F14 (continued). B. Magnetic susceptibility and electrical resistivity data for Site M0003 plotted versus composite depth. Only one hole was cored. Outlying data points, due to section breaks, were removed.

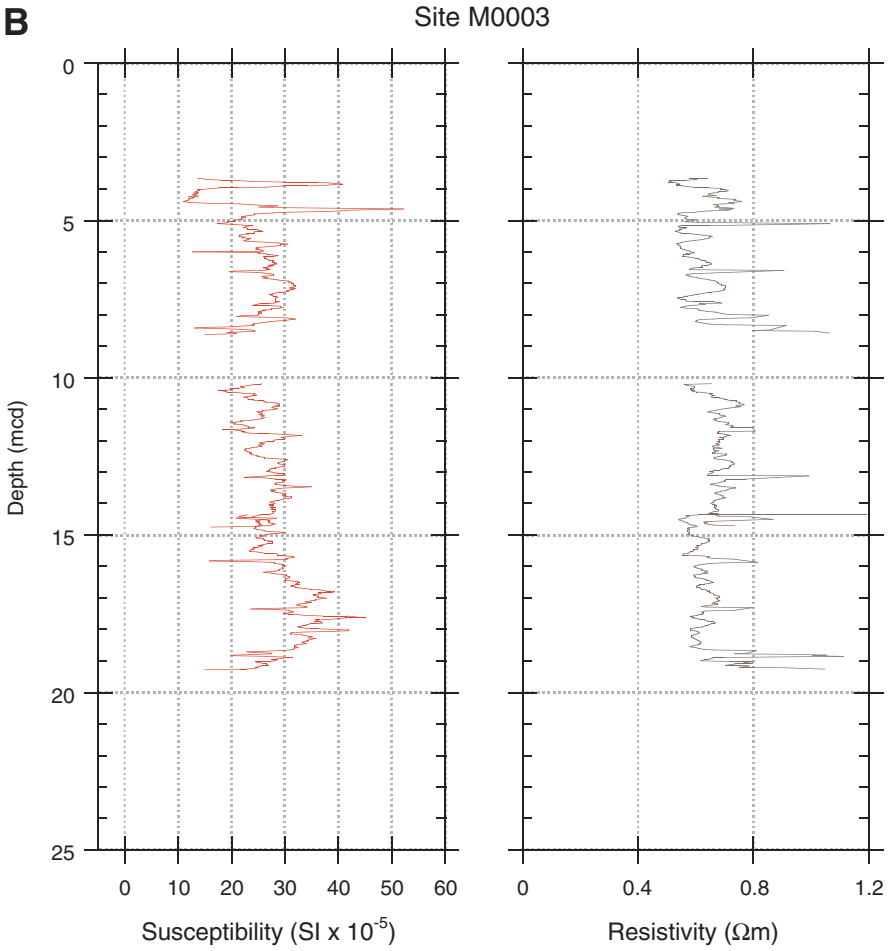

Figure F14 (continued). C. Color reflectance data for Site M0003 plotted versus composite depth.

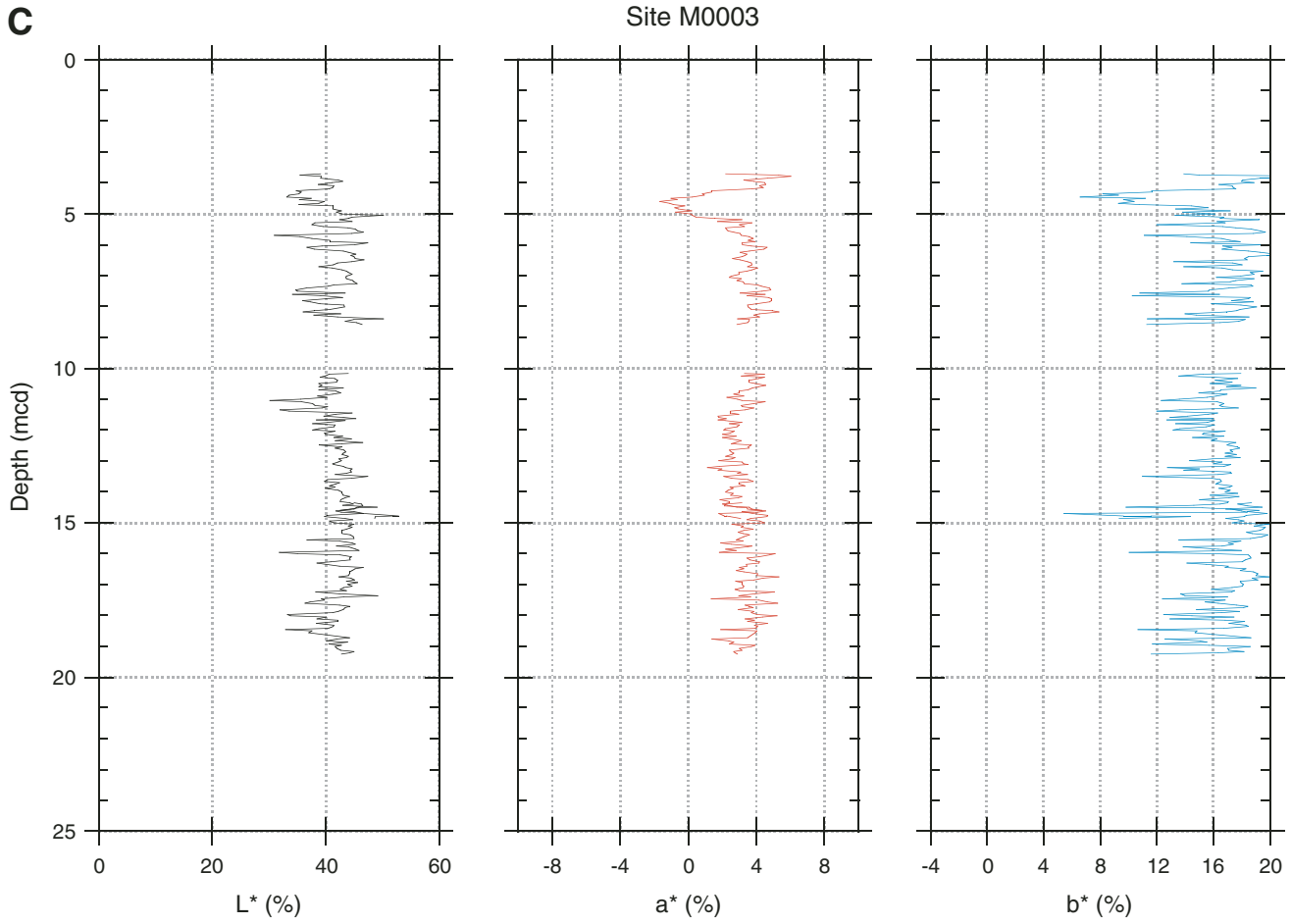

Figure F14 (continued). D. Natural gamma ray (NGR) data for Site M0003 plotted versus composite depth.

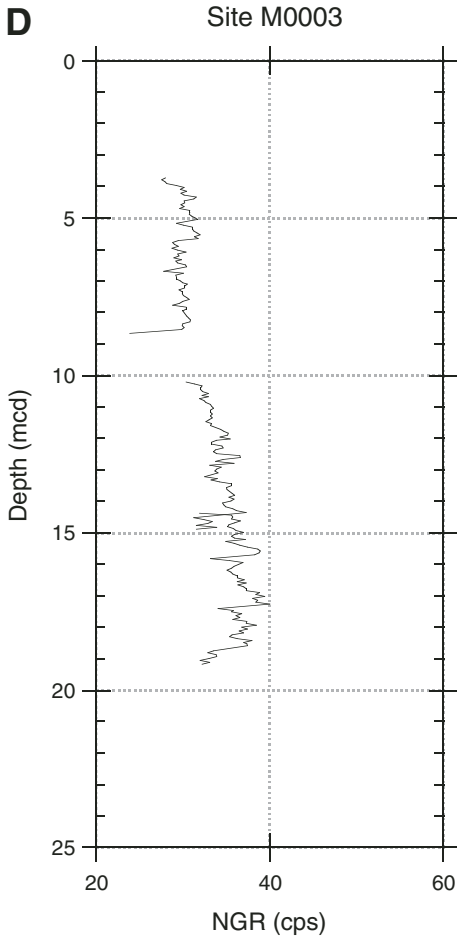

Figure F15. A. Gamma ray attenuation (GRA) bulk density and *P*-wave logger (PWL) data for Site M0004 plotted versus composite depth. No cores were retrieved between 50 and 200 mcd. Outlying data points, due to section breaks or poor contact between the liner and core for PWL, were removed. (Continued on next three pages.)

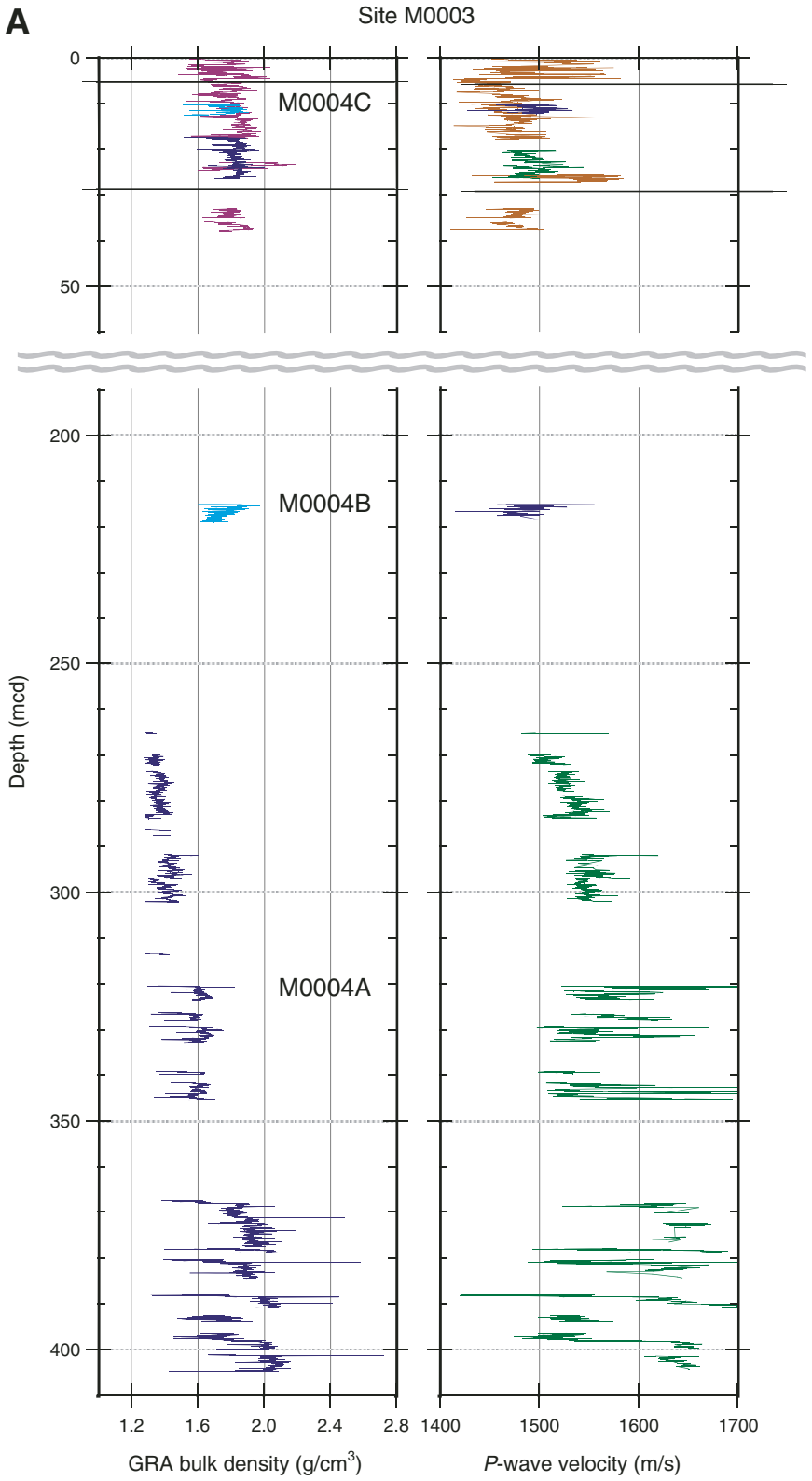

Figure F15 (continued). B. Magnetic susceptibility and electrical resistivity data for Site M0004 plotted versus composite depth. No cores were retrieved between 50 and 200 mcd. Outlying data points, due to section breaks, were removed.

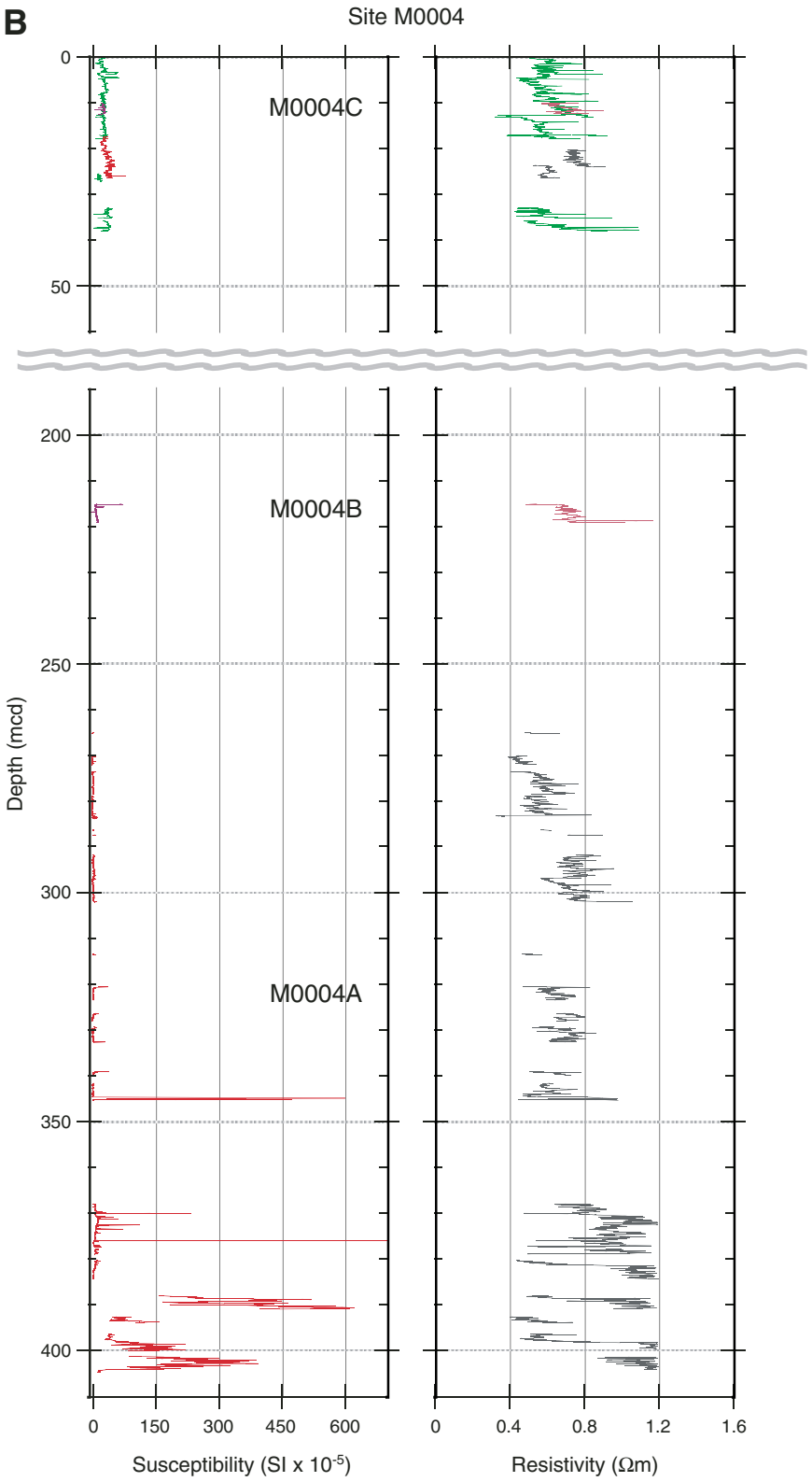

Figure F15 (continued). C. Color reflectance data for Site M0004 versus composite depth.

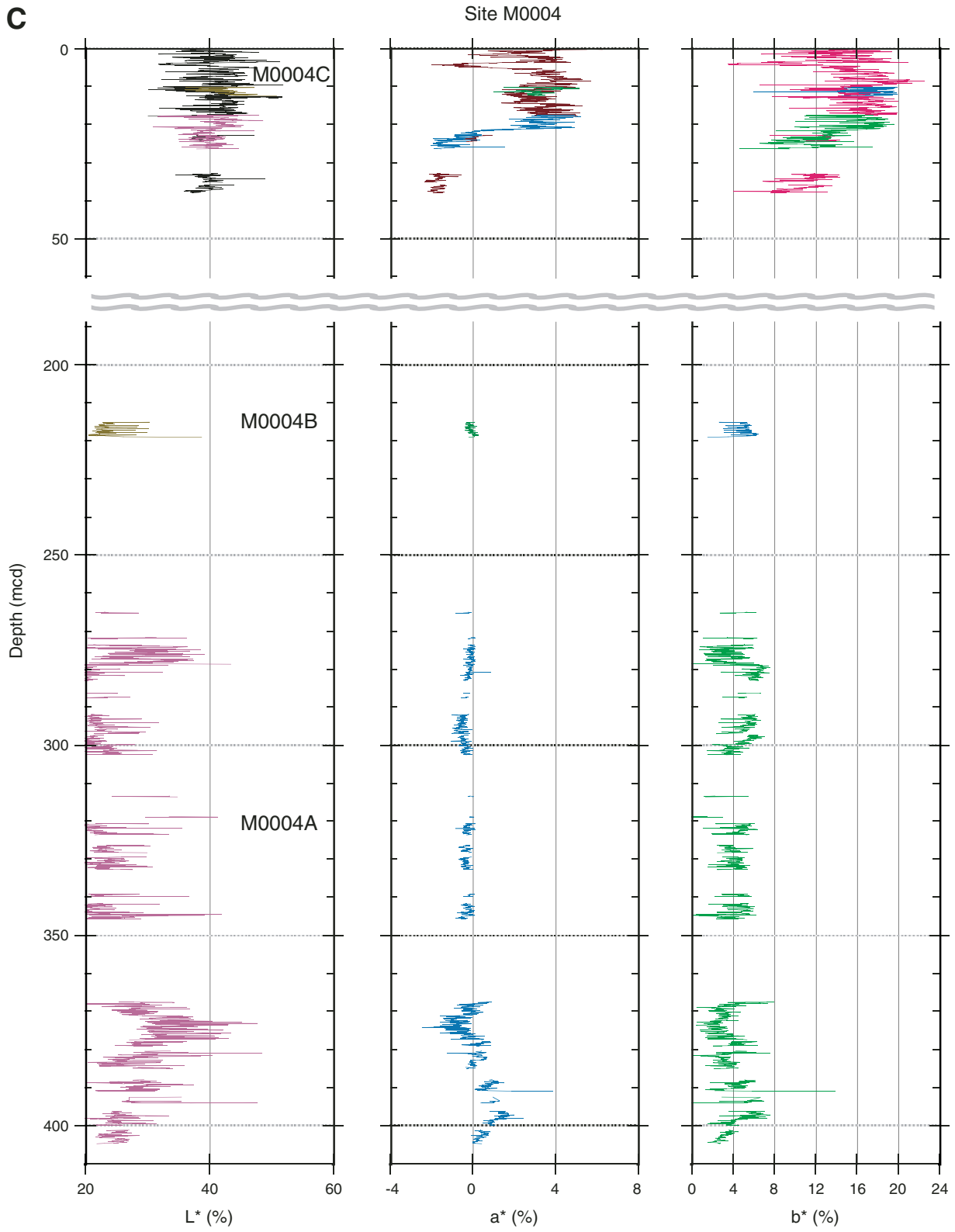

Figure F15 (continued). D. Natural gamma ray (NGR) data for Site M0004 versus composite depth.

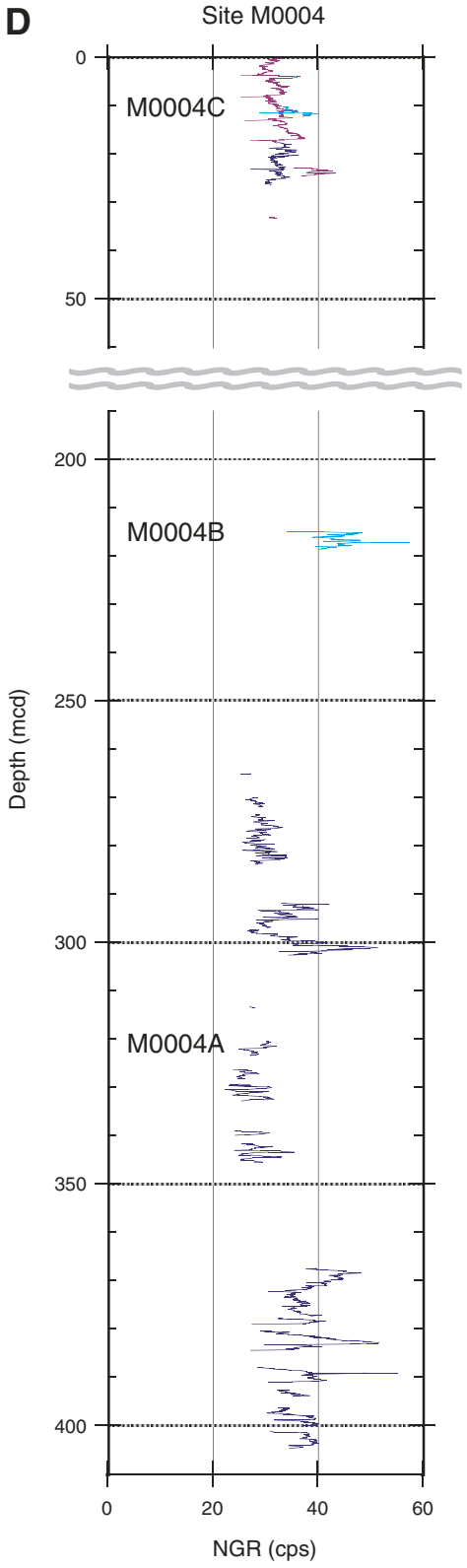

Figure F16. A. Gamma ray attenuation (GRA) bulk density data for upper 50 mcd from all holes. Densities from different sites are offset for better readability as follows: Hole M0002A = not offset, Hole M0003A = offset by +0.2 g/cm³, Hole M0004A = offset by +0.4 g/cm³, Hole M0004B = offset by +0.6 g/cm³, Hole M0004C = offset by +0.8 g/cm³. (Continued on next eight pages.)

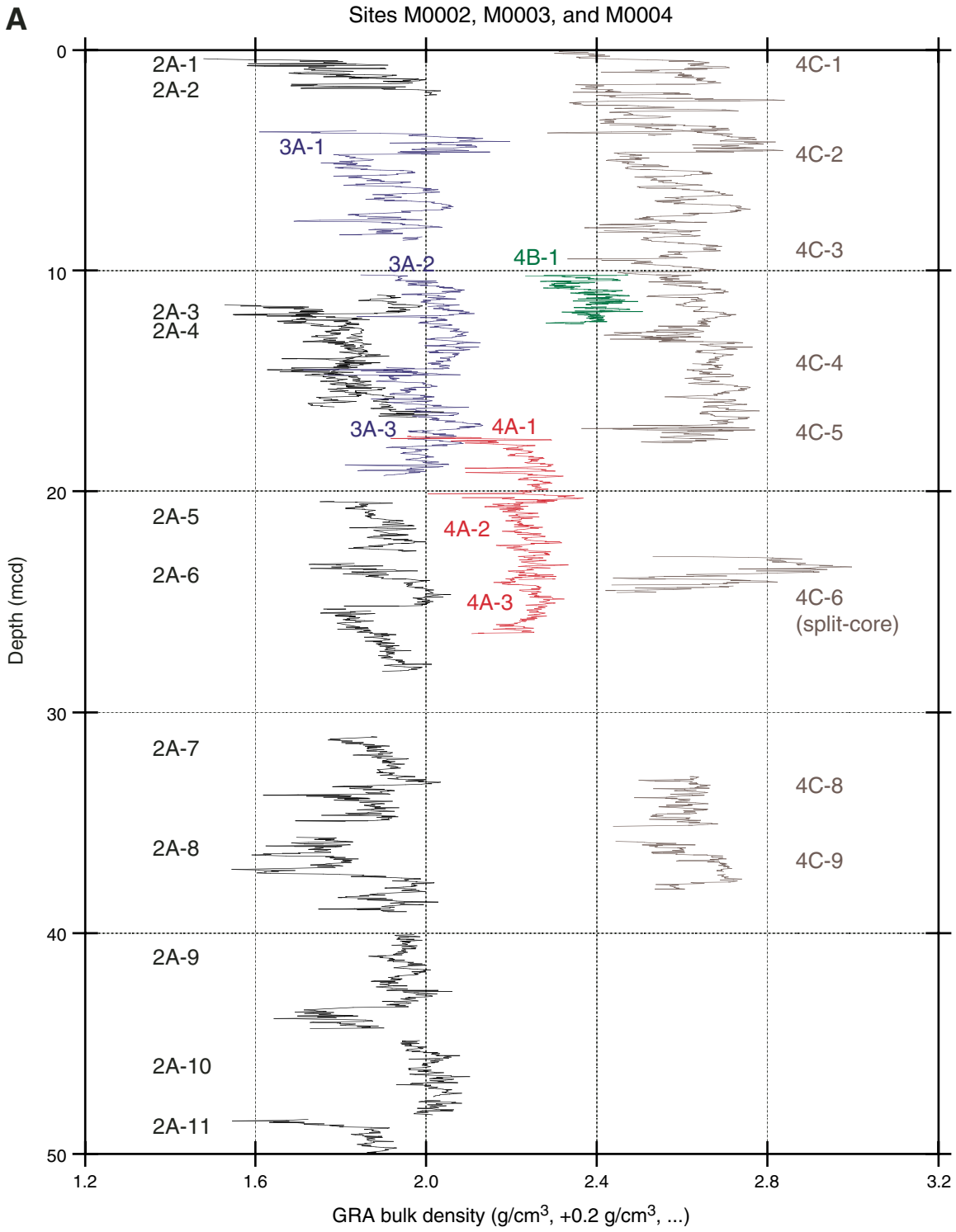

Figure F16 (continued). B. Magnetic susceptibility (MS) data for upper 50 mcd from all holes. MS data from different sites are offset for better readability as follows: Hole M0002A = not offset, Hole M0003A = offset by +20 units, Hole M0004A = offset by +40 units, Hole M0004B = offset by +60 units, Hole M0004C = offset by +80 units.

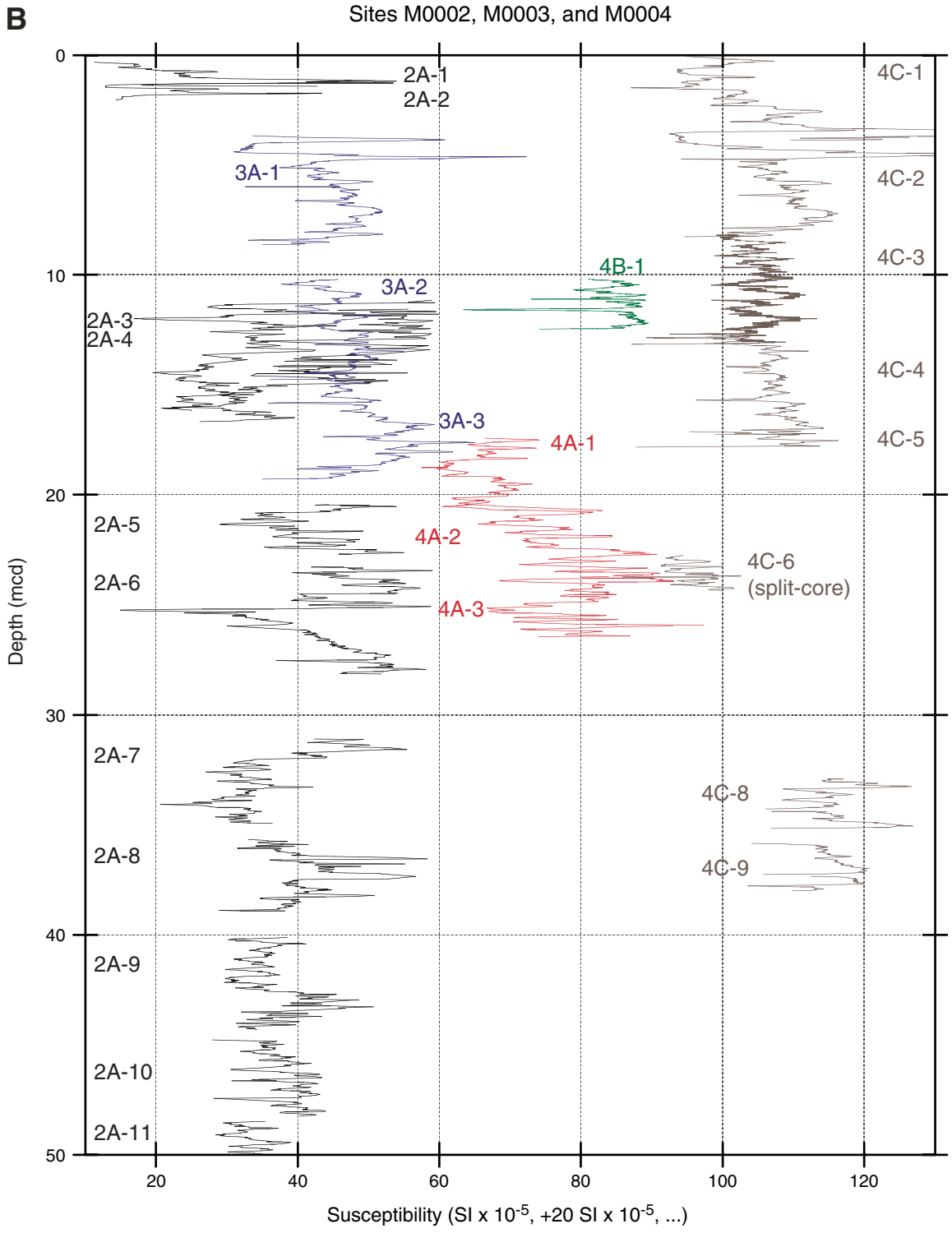

Figure F16 (continued). C. *P*-wave velocity data for upper 50 mcd from all holes. Velocity data from different sites are offset for better readability as follows: Hole M0002A = not offset, Hole M0003A = offset by +100 units, Hole M0004A = offset by +200 units, Hole M0004B = offset by +300 units, Hole M0004C = offset by +400 units.

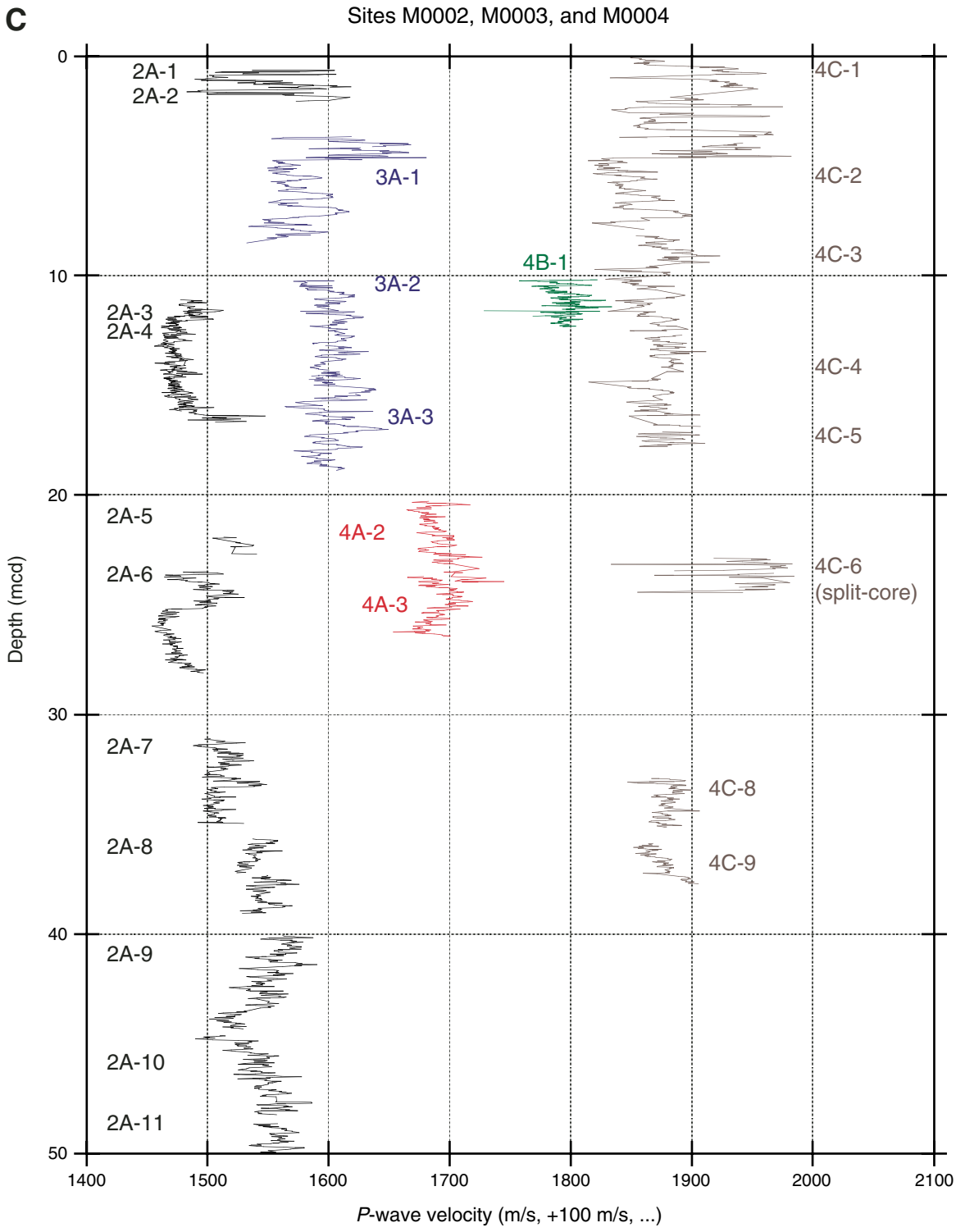

Figure F16 (continued). D. Electrical resistivity data for upper 40 m from all holes. Resistivity data from different sites are offset for better readability as follows: Hole M0002A = not offset, Hole M0003A = offset by +0.2 units, Hole M0004A = offset by +0.4 units, Hole M0004B = offset by +0.6 units, Hole M0004C = offset by +0.8 units.

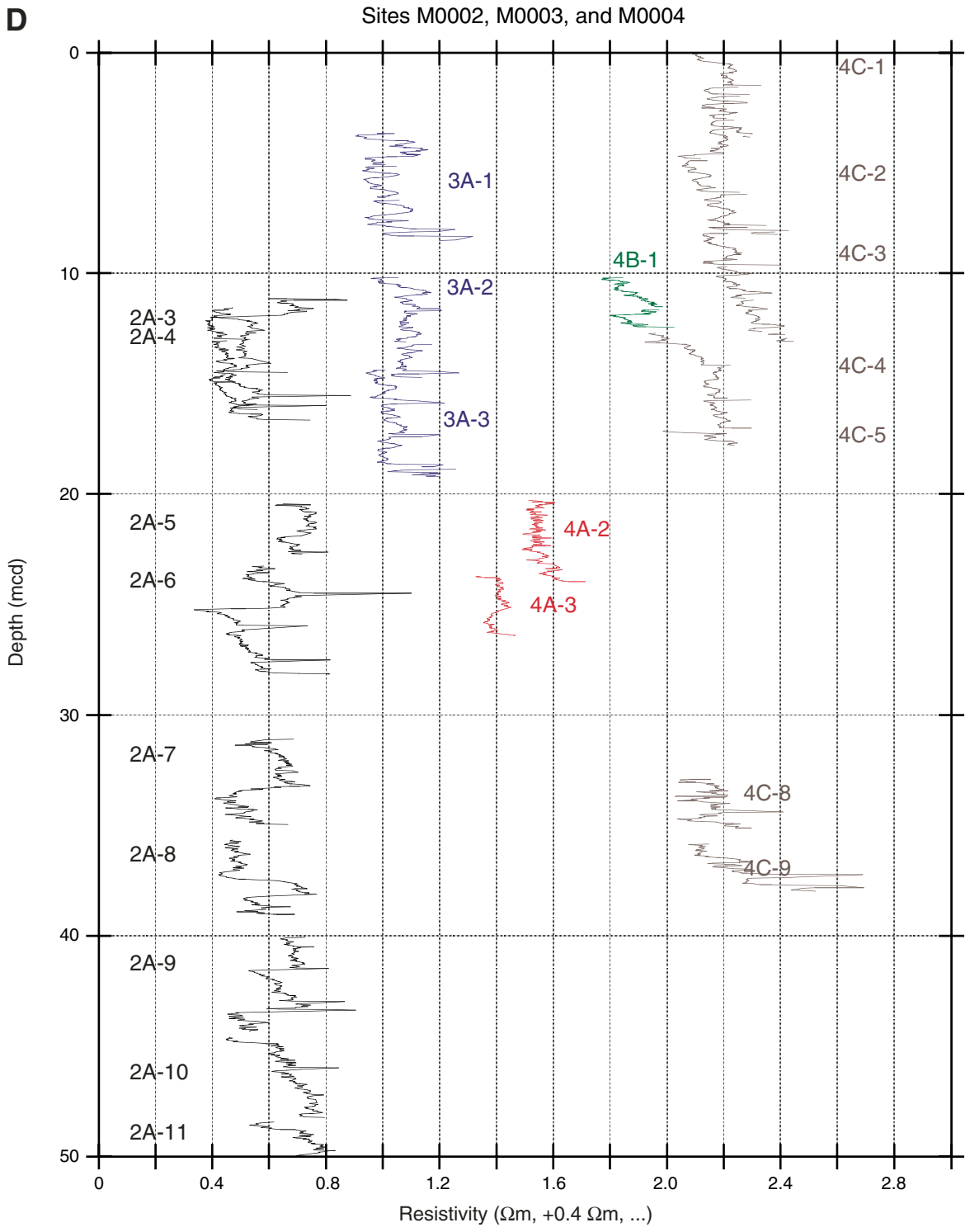

Figure F16 (continued). E. Color reflectance (L*) data for upper 50 mcd from all holes. L* data from different sites are offset for better readability as follows: Hole M0002A = not offset, Hole M0003A = offset by +10%, Hole M0004A = offset by +20%, Hole M0004B = offset by +30%, Hole M0004C = offset by +40%.

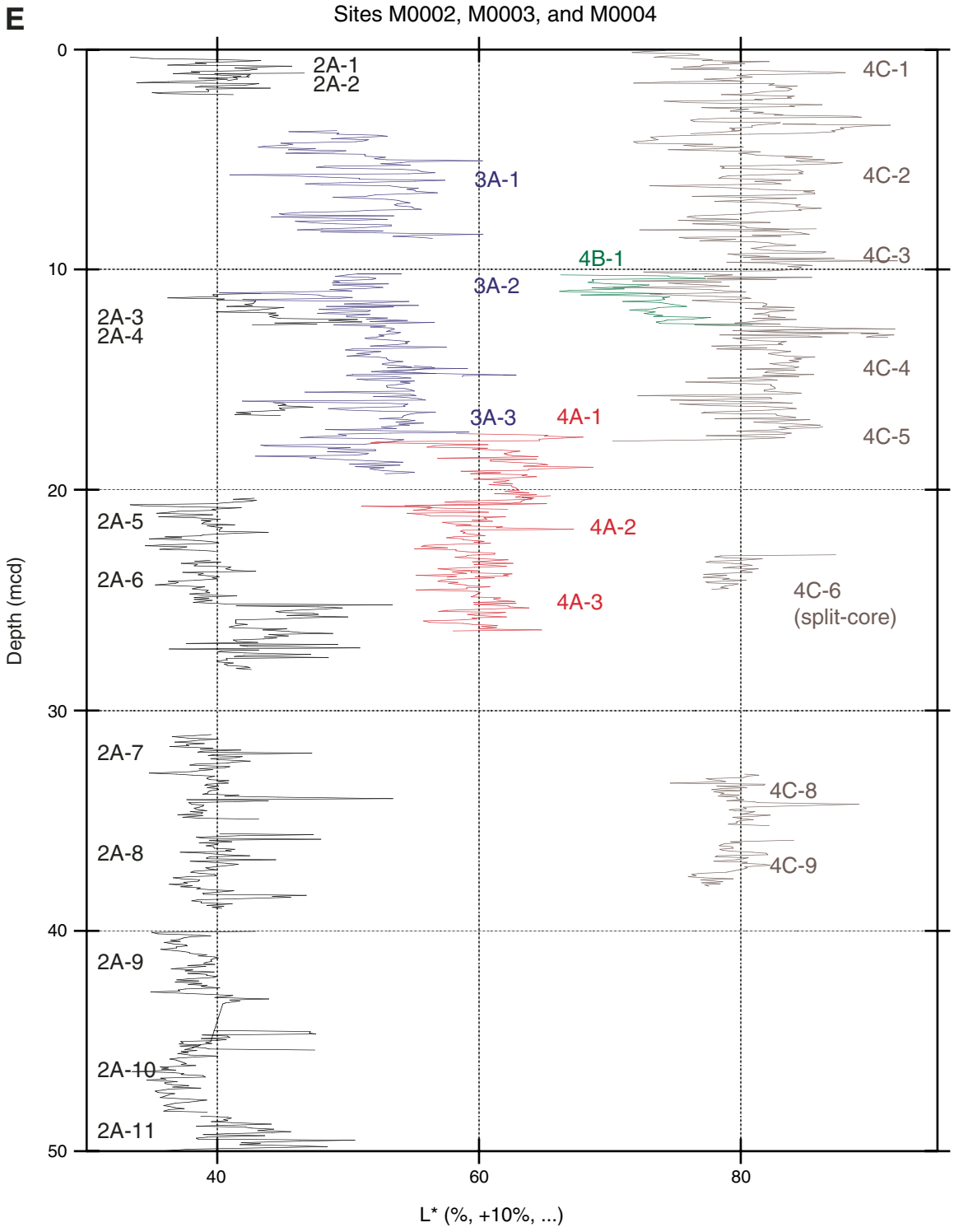

Figure F16 (continued). F. Chromaticity (a*) data for upper 50 mcd from all holes. a* data from different sites are offset for better readability as follows: Hole M0002A = not offset, Hole M0003A = offset by +4%, Hole M0004A = offset by +8%, Hole M0004B = offset by +12%, Hole M0004C = offset by +16%.

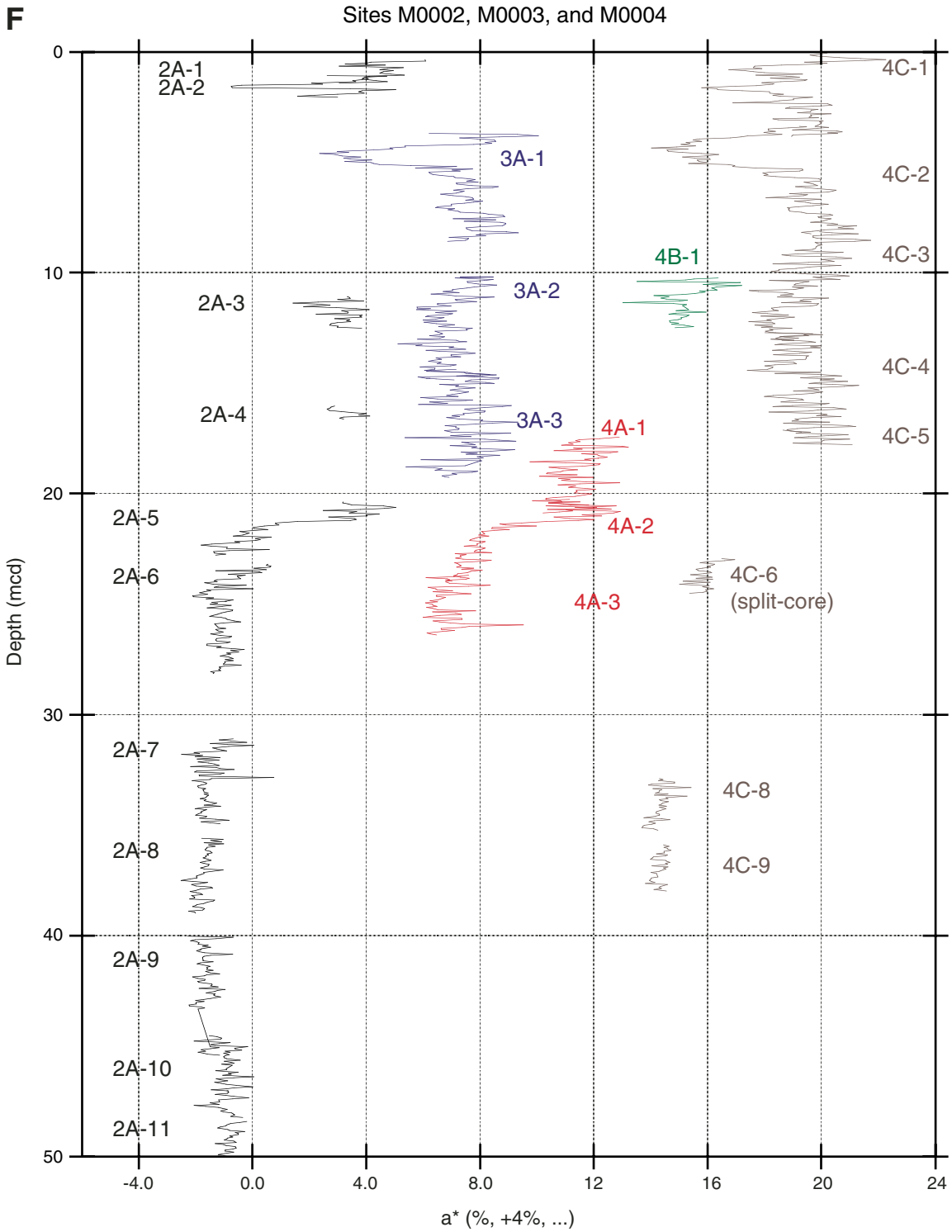

Figure F16 (continued). G. Chromaticity (b*) data for upper 50 mcd from all holes. b* data from different sites are offset for better readability as follows: Hole M0002A = not offset, Hole M0003A = offset by +4%, Hole M0004A = offset by +8%, Hole M0004B = offset by +12%, Hole M0004C = offset by +16%.

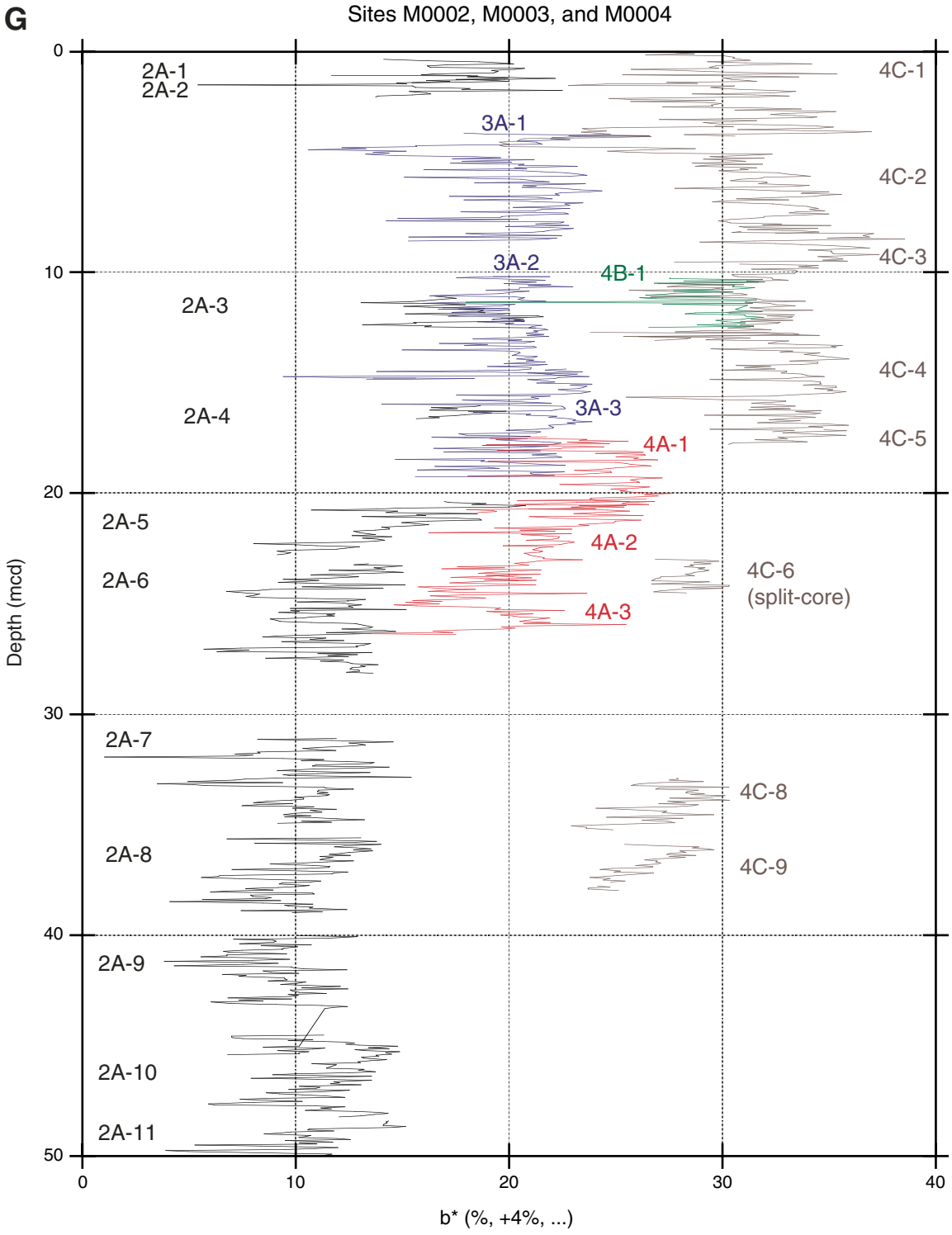

Figure F16 (continued). H. Natural gamma ray (NGR) data for upper 50 mcd from all holes. NGR data from different sites are offset for better readability as follows: Hole M0002A = not offset, Hole M0003A = offset by +10 cps, Hole M0004A = offset by +20 cps, Hole M0004B = offset by +30 cps, Hole M0004C = offset by +40 cps.

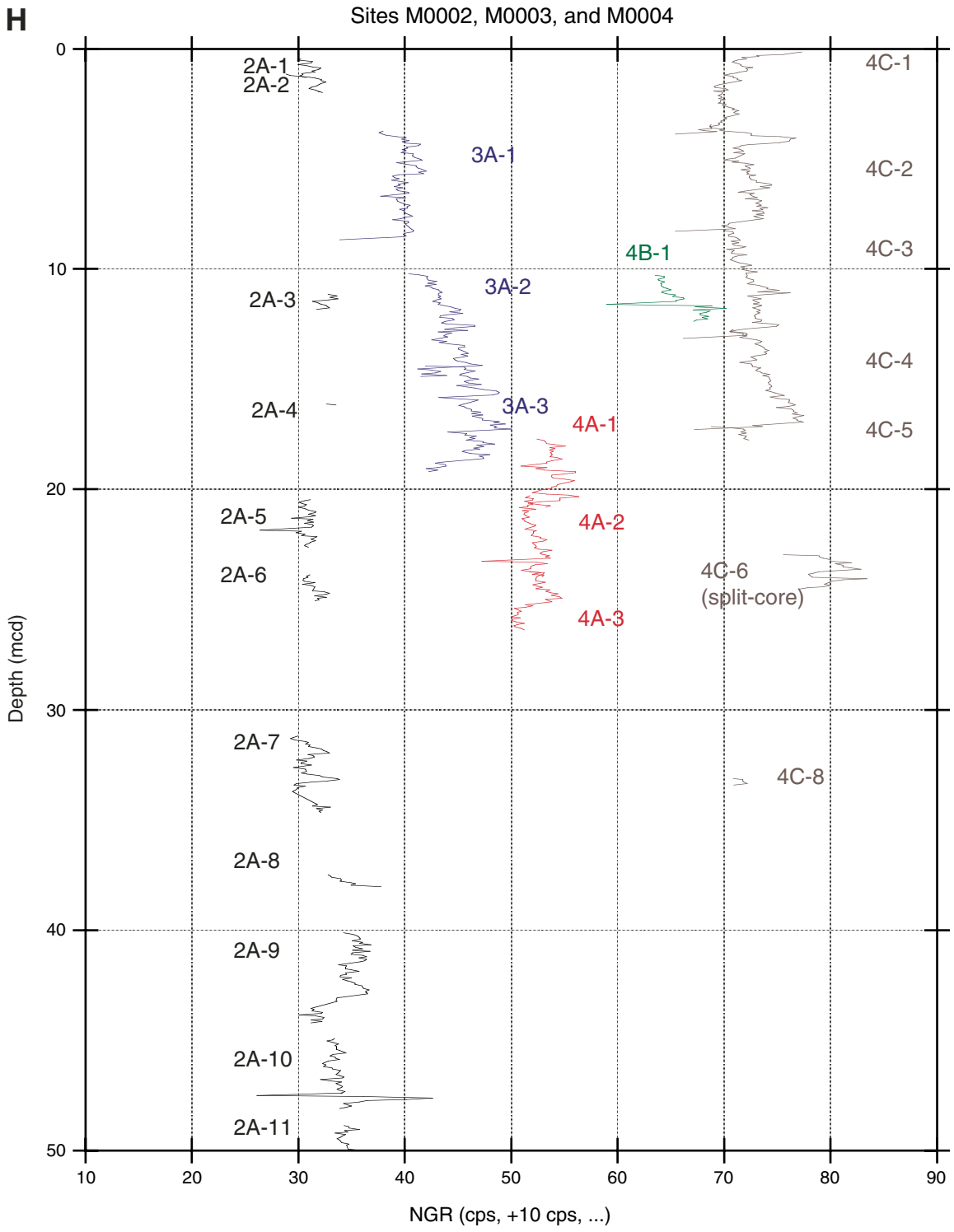

Figure F16 (continued). I. Magnetic inclination data for upper 30 mcd from all holes. Inclination data from different sites are offset for better readability as follows: Hole M0002A = not offset, Hole M0003A = offset by 180°, Hole M0004A = offset by 360°, Hole M0004B = offset by 540°, Hole M0004C = offset by 720°. Question marks = a zone of currently uncertain inclination.

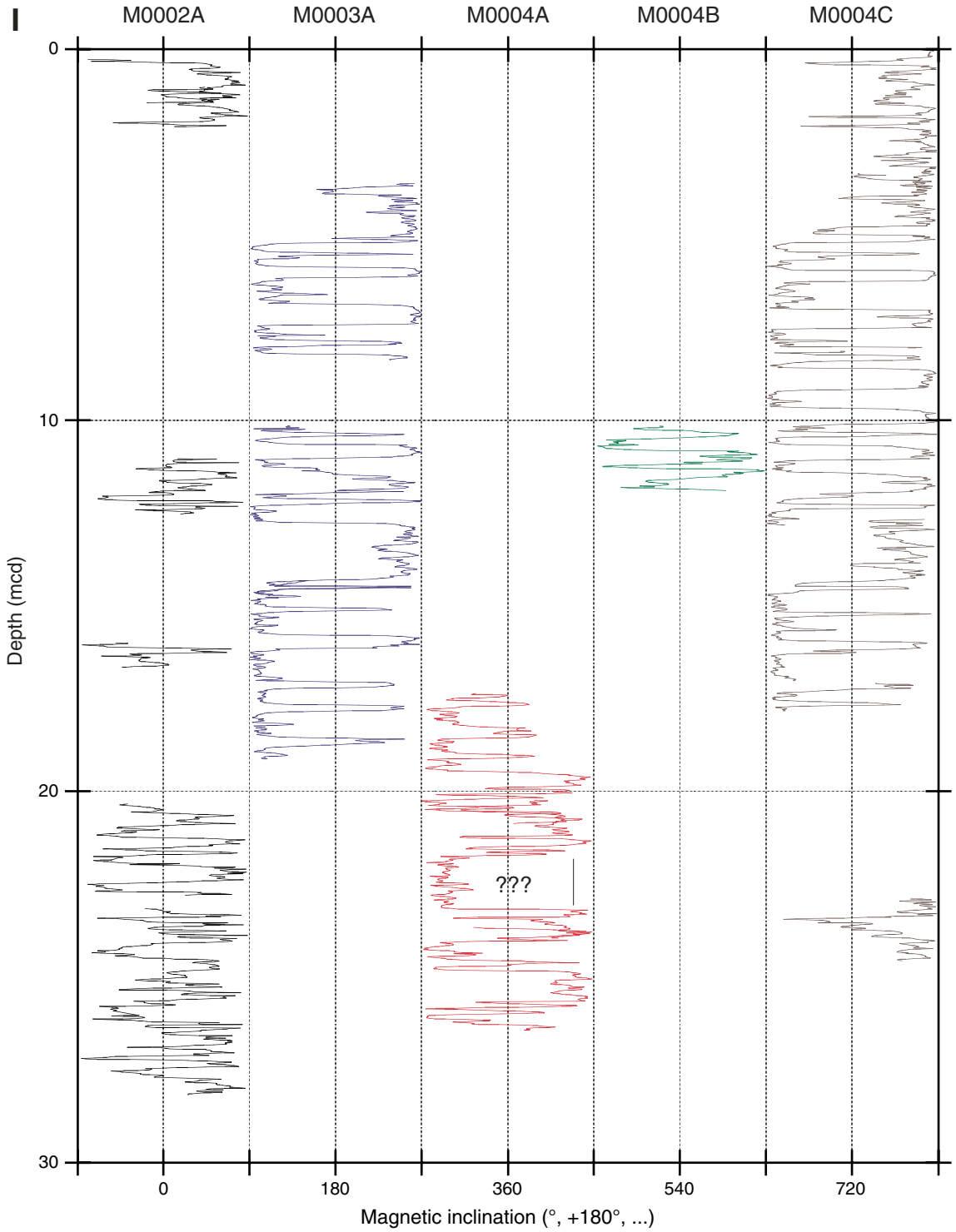

Figure F17. A. Spliced complete data sets for gamma ray attenuation (GRA) bulk density, magnetic susceptibility, *P*-wave velocity, and electrical resistivity on a composite depth scale. The construction of the splice follows Table T26. (Continued on next page.)

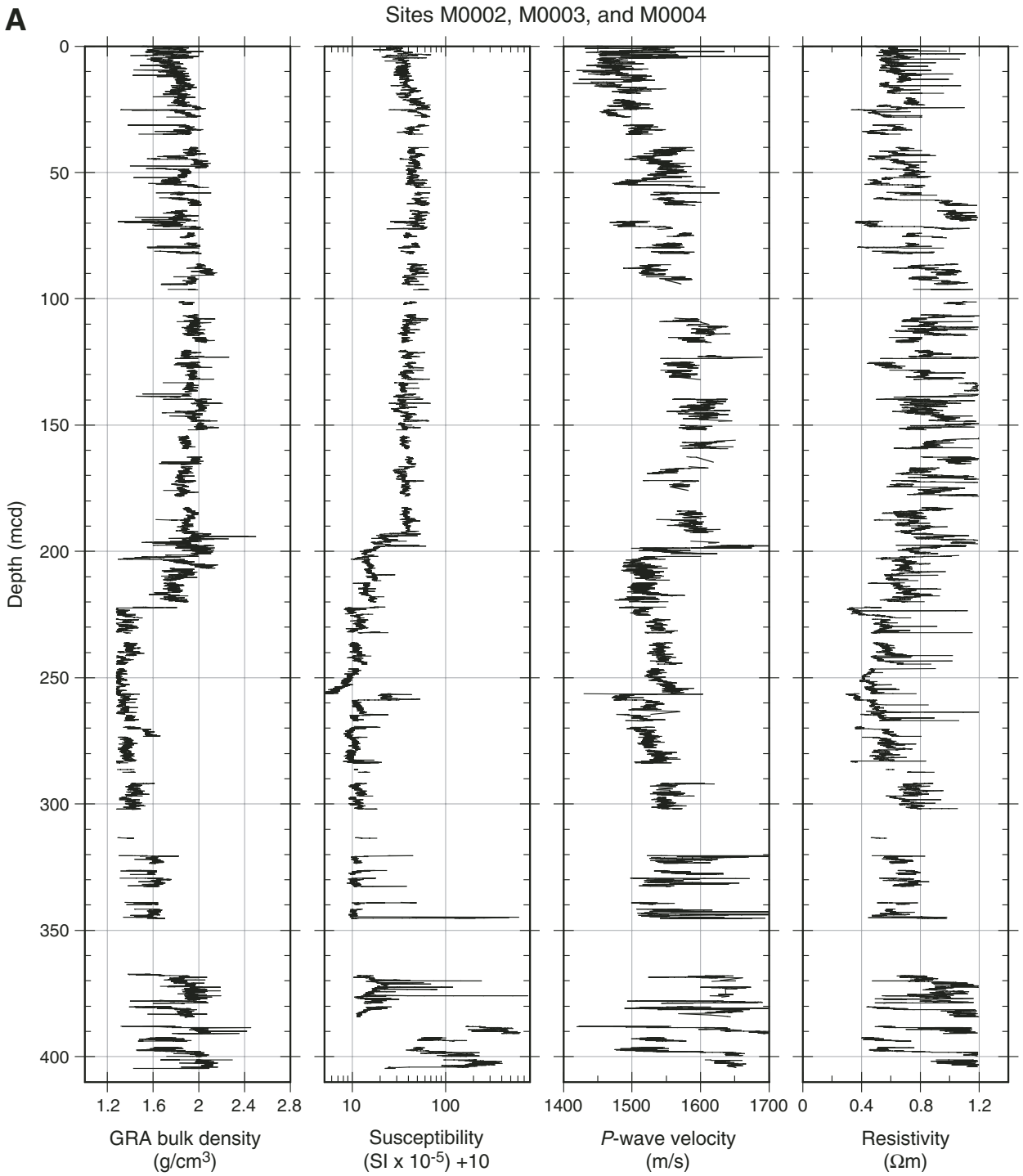

Figure F17 (continued). B. Spliced complete data sets for color reflectance L*, chromaticity a* and b*, and natural gamma ray (NGR) counts on a composite depth scale. The construction of the splice follows Table T25.

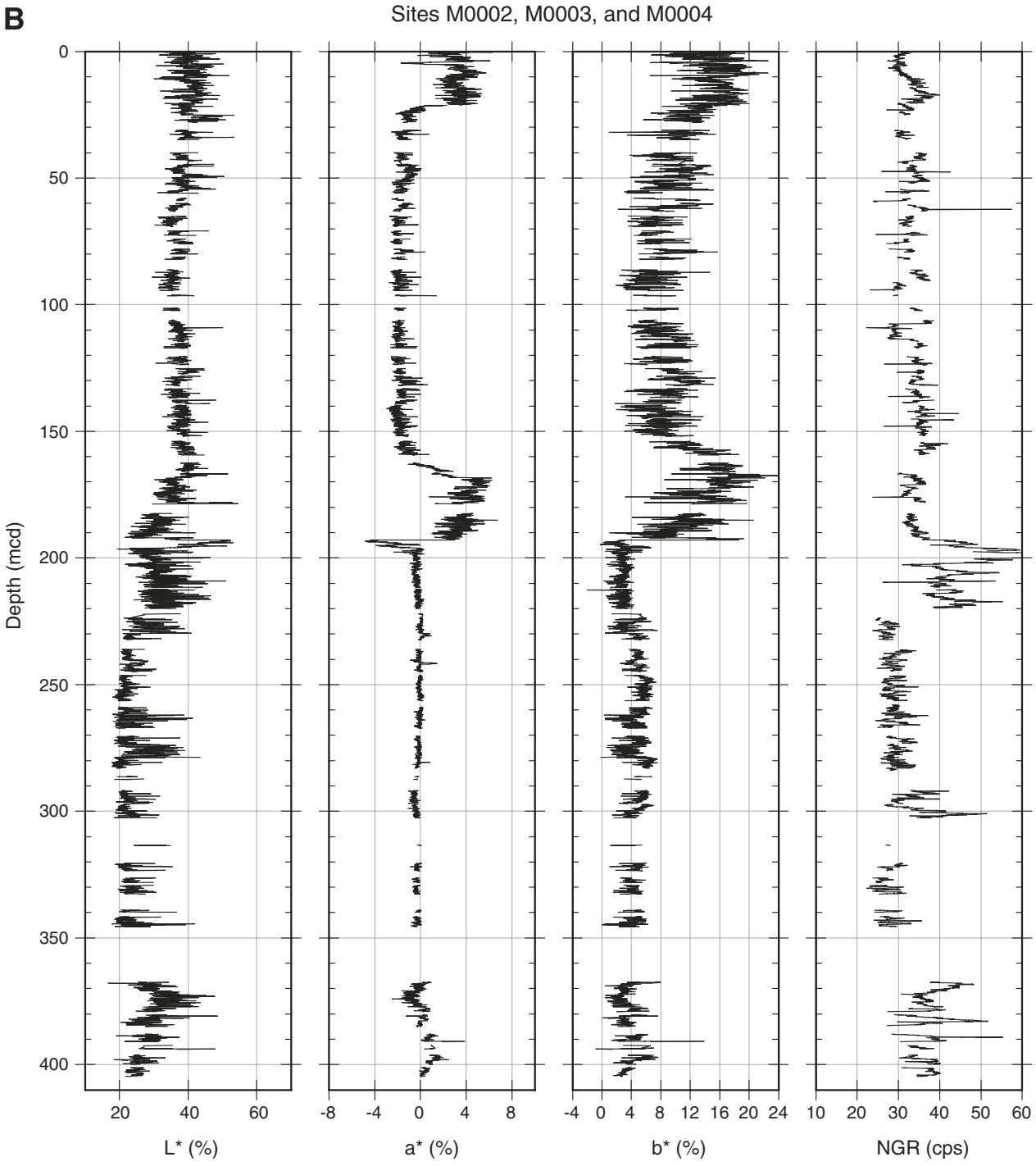

Figure F18. A. Location of Expedition 302 sites (red dot) on a paleoreconstruction at 50 Ma (from ODSN Web site: www.odsn.de). Shorelines are approximate and are based on reconstructions of Radionova et al. (2003), Radionova and Khokhlova (2000), and Bice and Marotzke (2002). NA = North America, Gr = Greenland, E = Europe, A = Asia. (Continued on next page.)

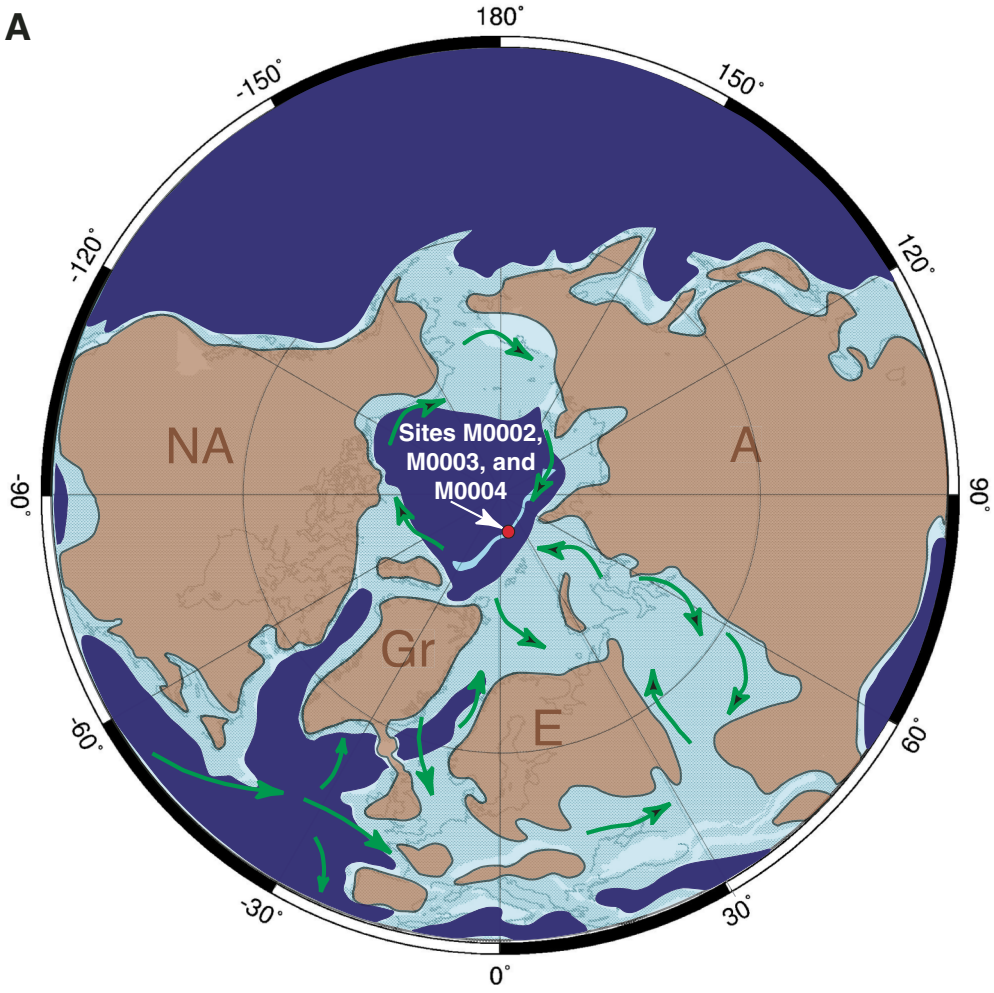

Figure F18 (continued). B. Detailed plot of Expedition 302 site locations.

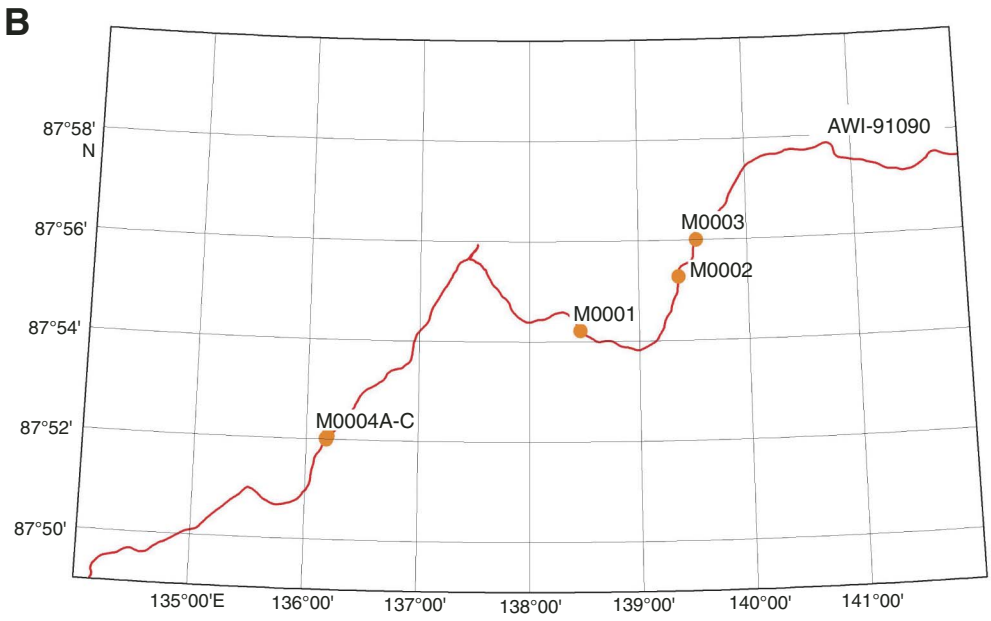

Figure F19. Depth of stratigraphic datums versus their estimated age. Squares enclose those datums used in calculating average linear sedimentation rates. The calculated rates are noted along the linear segments of the sedimentation rate curve. Lithostratigraphic units are noted in the column at the extreme right of the figure. Intervals in which hiatuses are suspected are shaded.

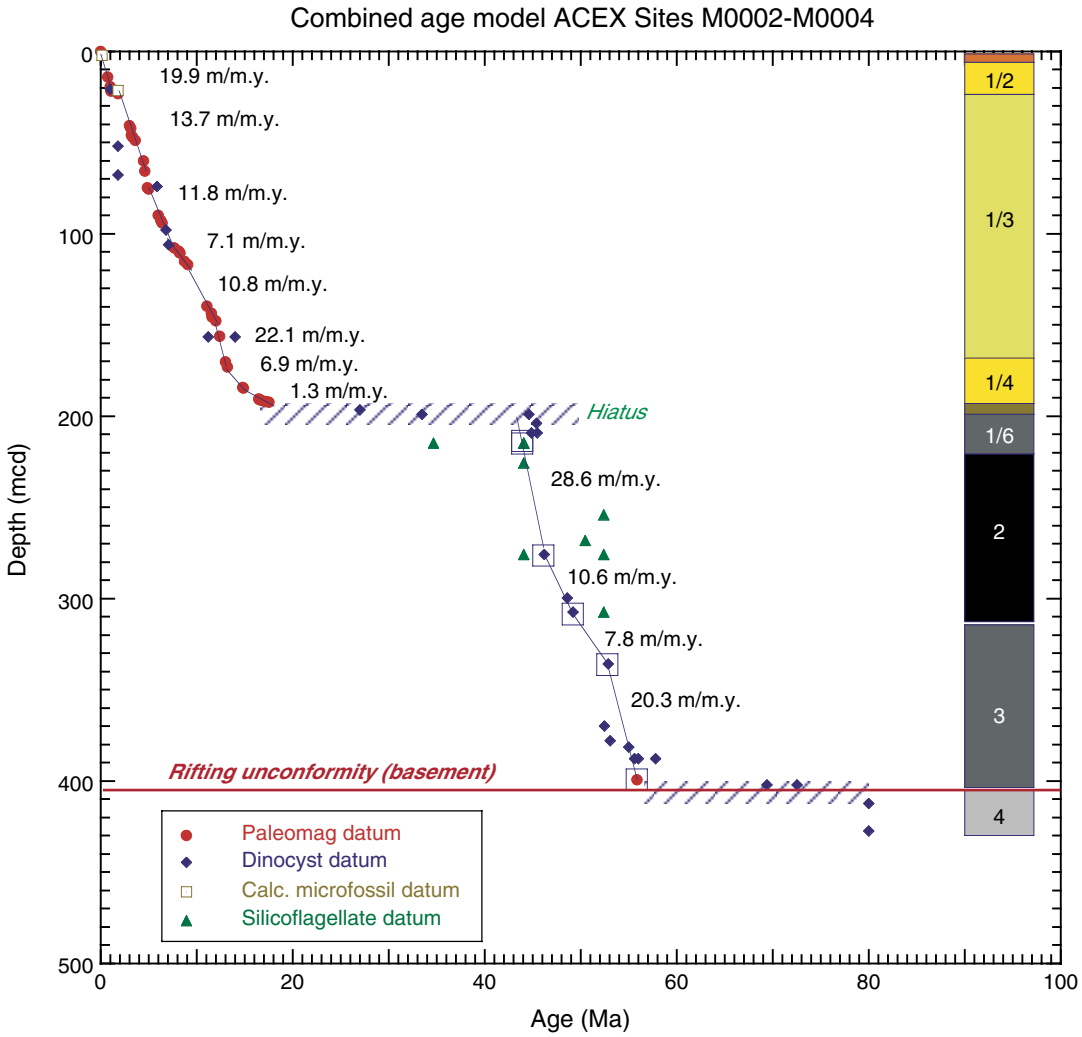

Figure F20. Caliper log from the Formation MicroScanner plotted in logging mbsf for the open-hole section of Hole M0004B along with composite core recovery for the expedition.

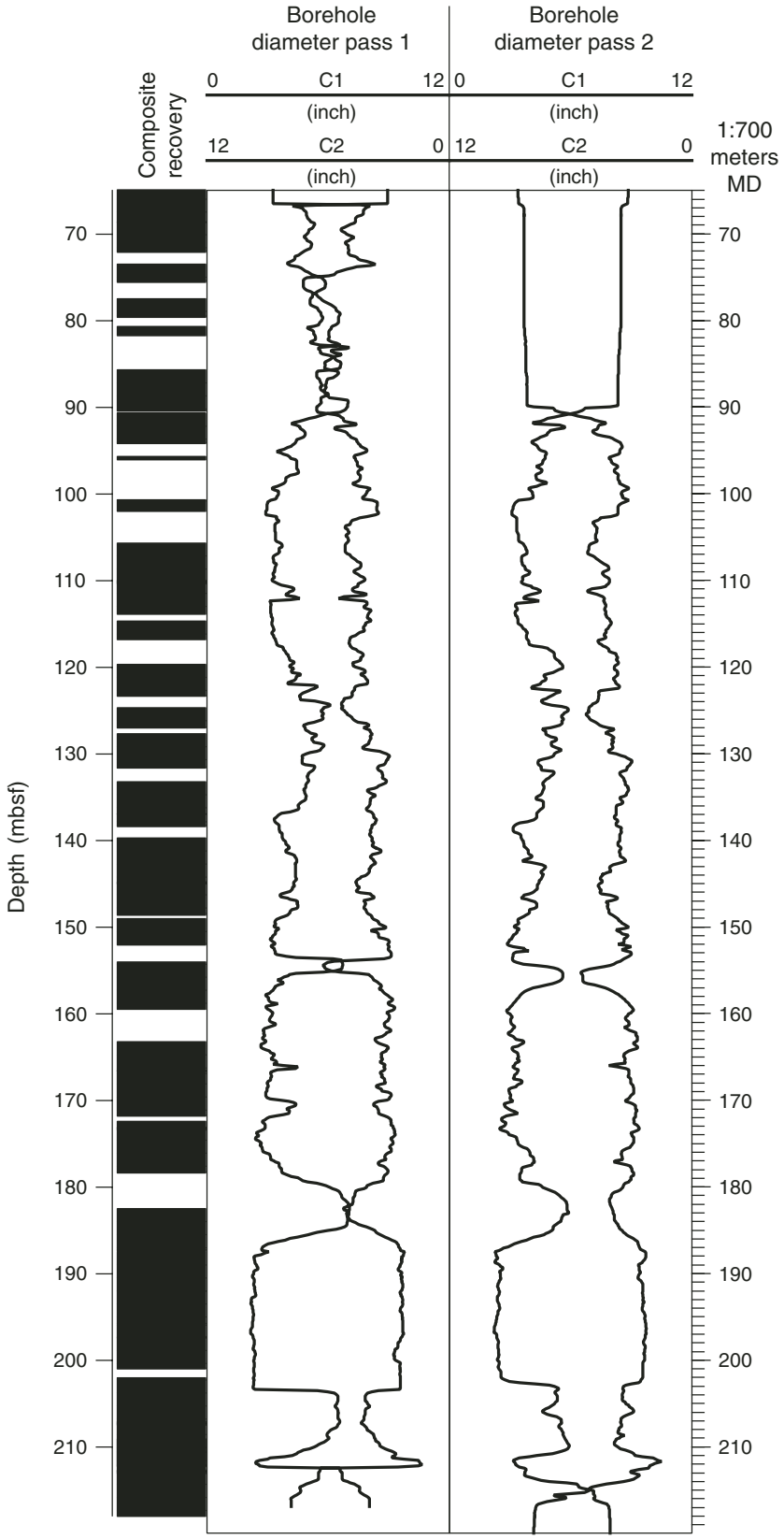

Figure F21. Formation MicroScanner (FMS) resistivity images from a section of Hole M0004B. Drilling artifacts, fine dark lines running at a constant angle across the image, obscure much of the detail of the borehole wall.

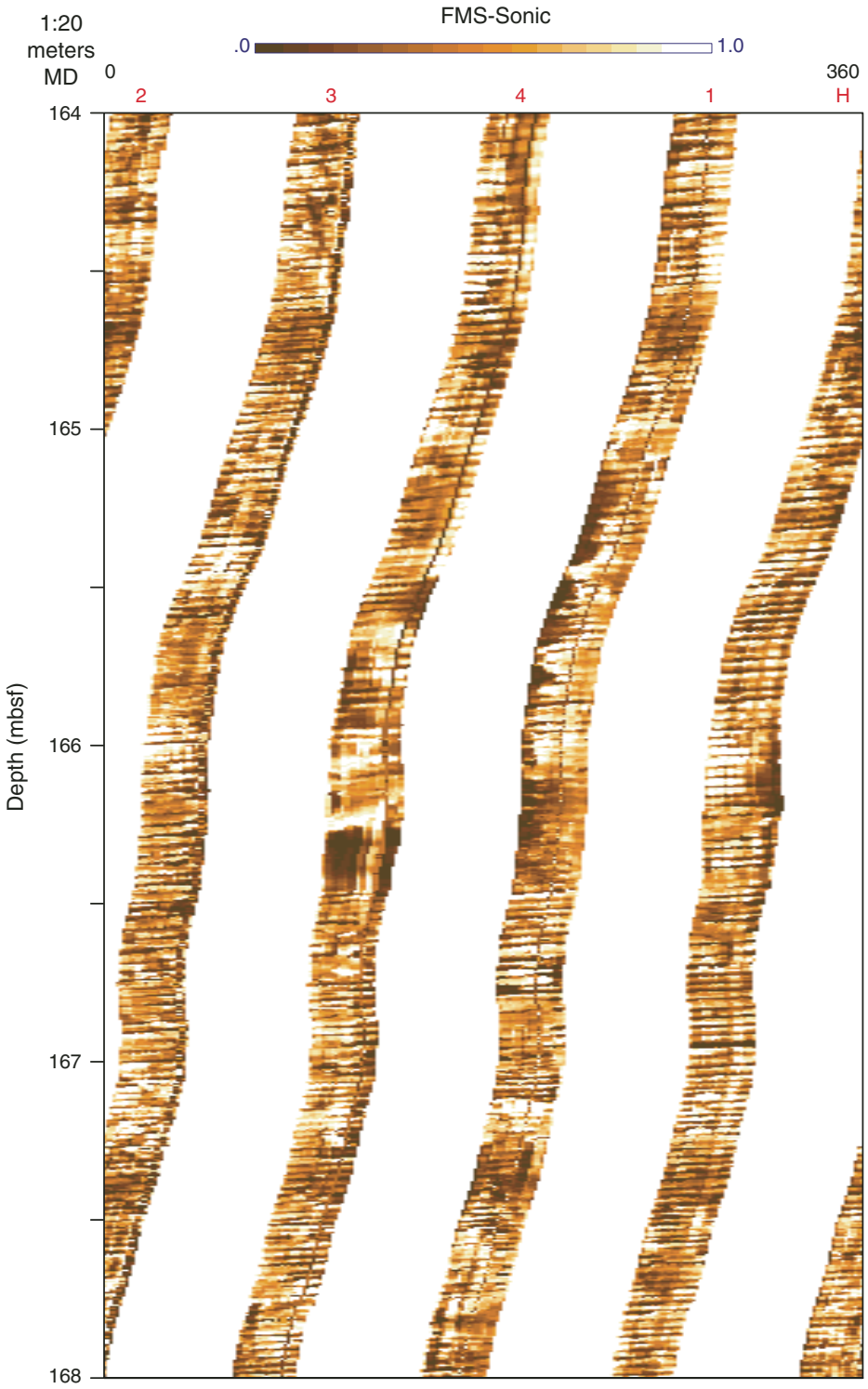

Figure F22. Split-core MSCL density data for Core 302-M0004C-6X shown with the two moisture and density (MAD) measurements taken from the core. The raw density values from the MSCL remain positively correlated with core thickness even after a correction has been applied in the processing software. The residual relationship between core thickness and density was used to detrend the raw values and obtain downcore density values that approach MAD values.

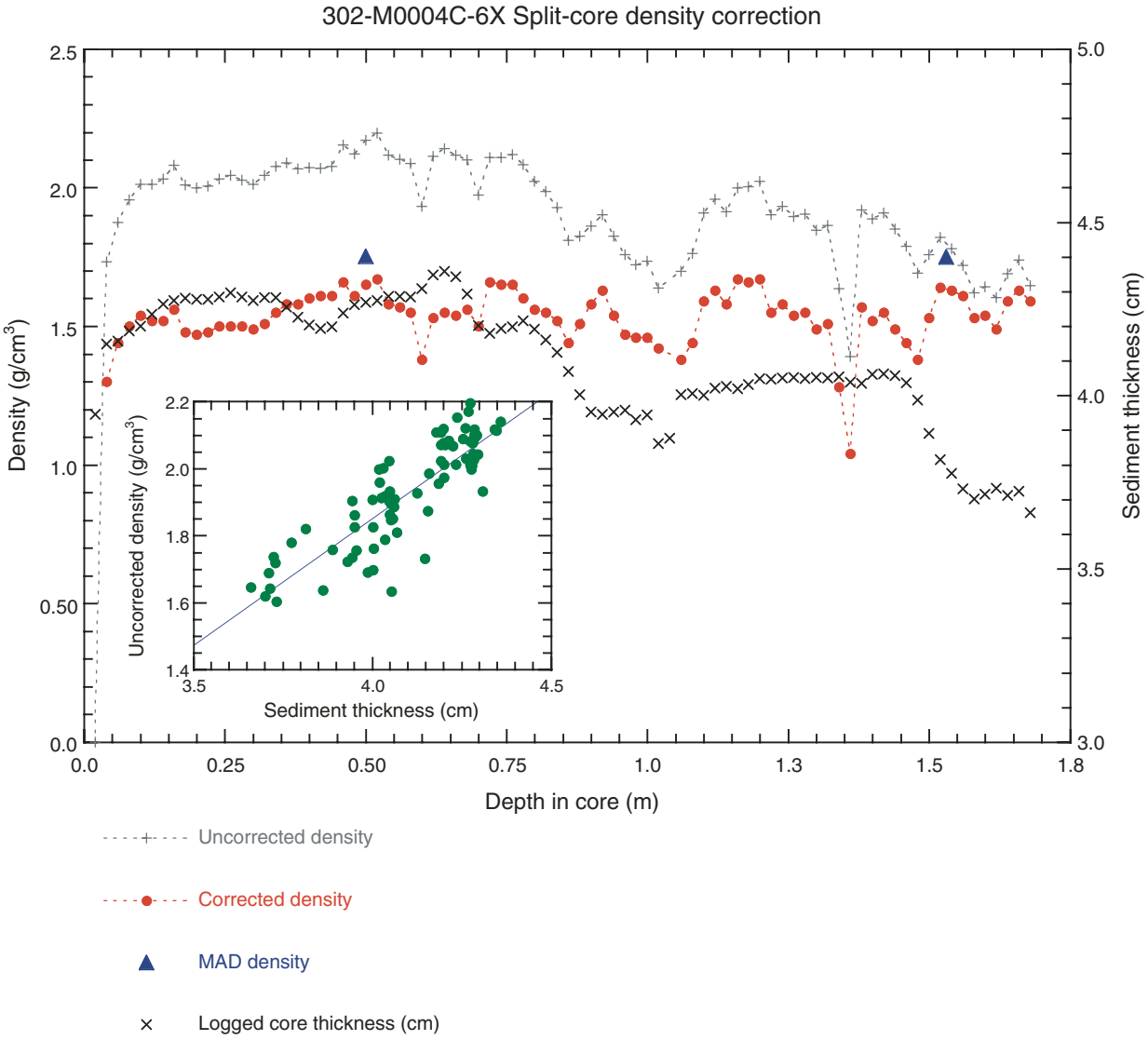

Figure F23. Offshore and onshore discrete sample moisture and density (MAD) measurements plotted with the MSCL bulk density curve.

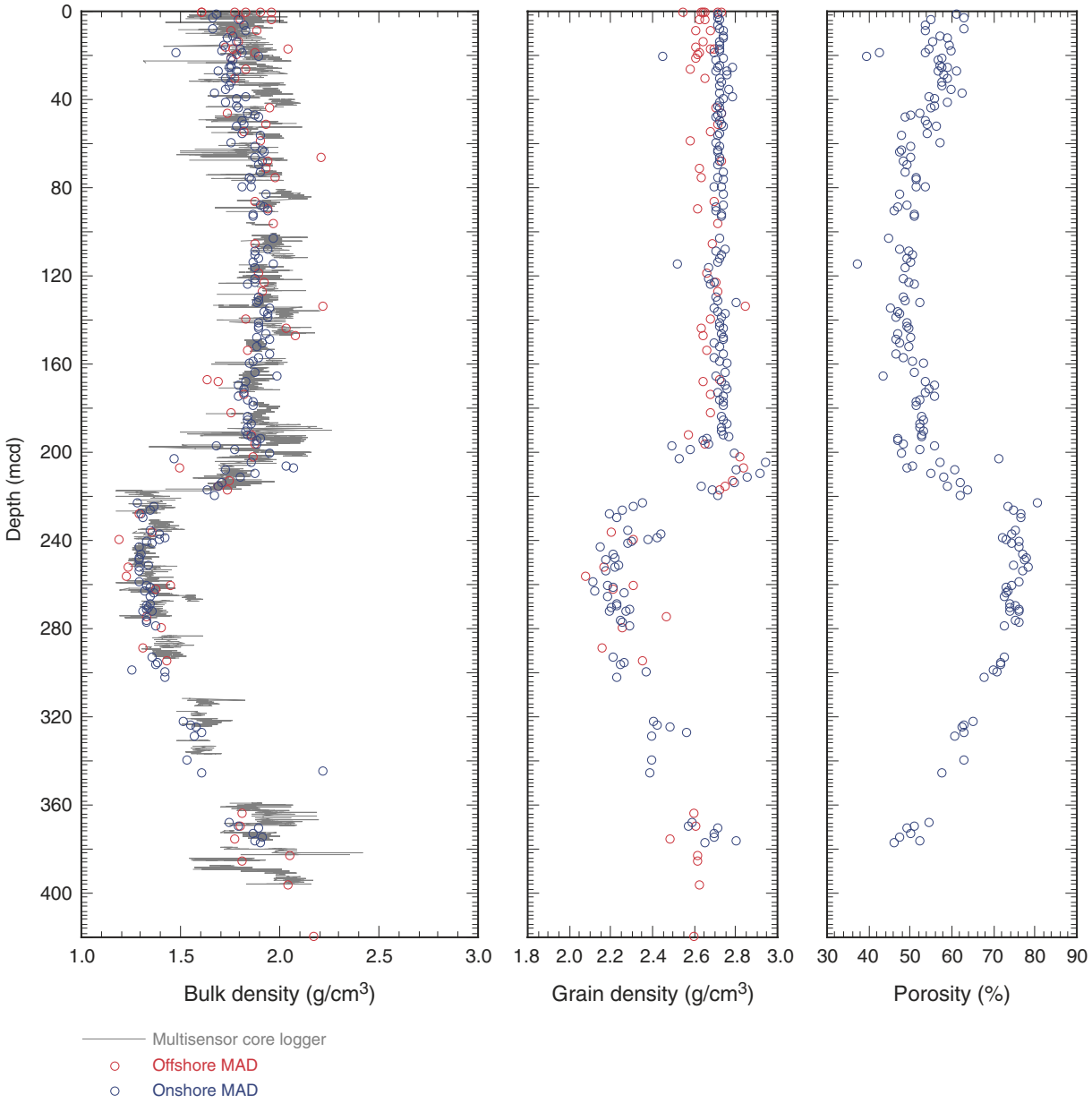

Figure F24. MSCL (offshore) and natural gamma ray (NGR) (onshore) data from Hole M0002A.

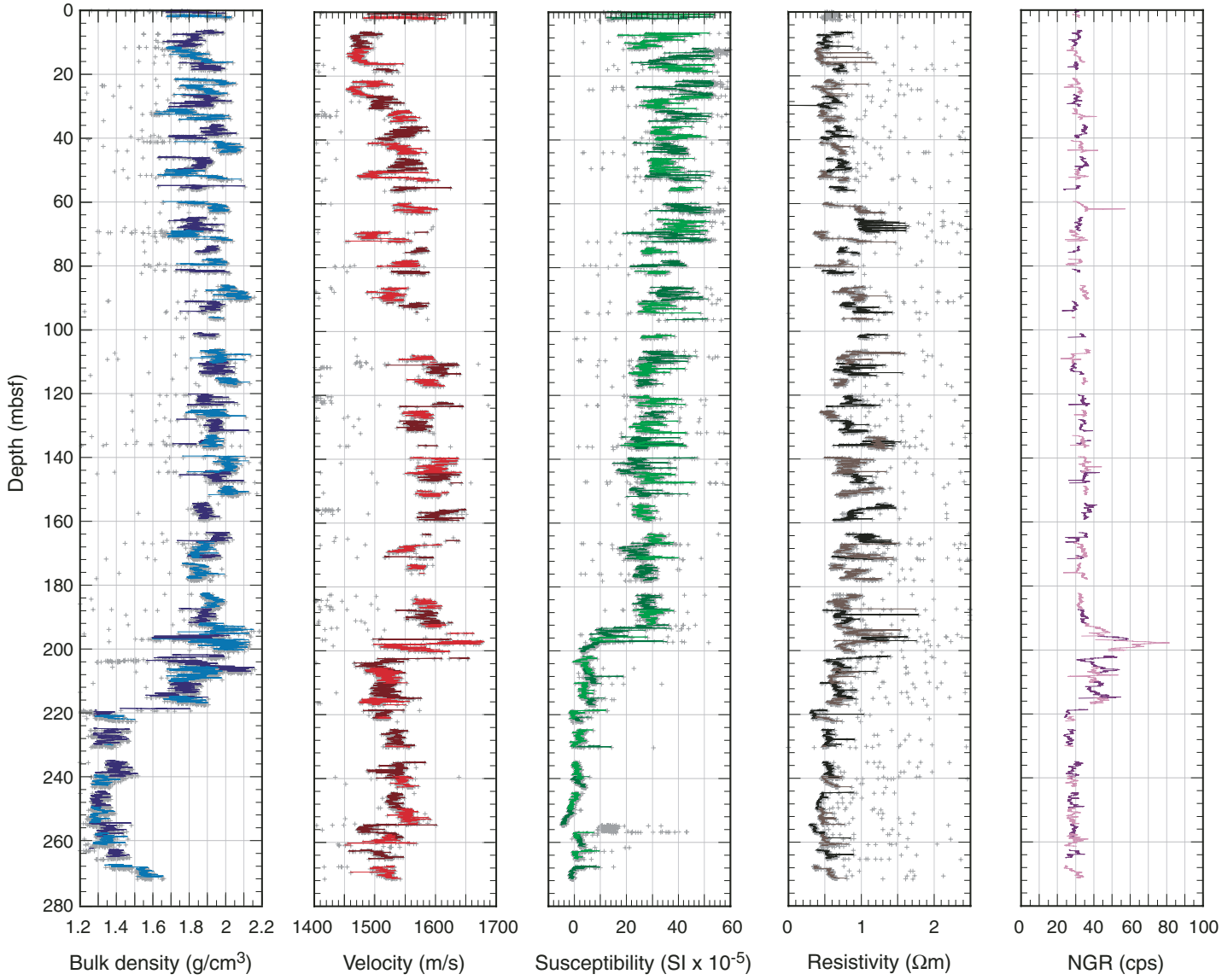

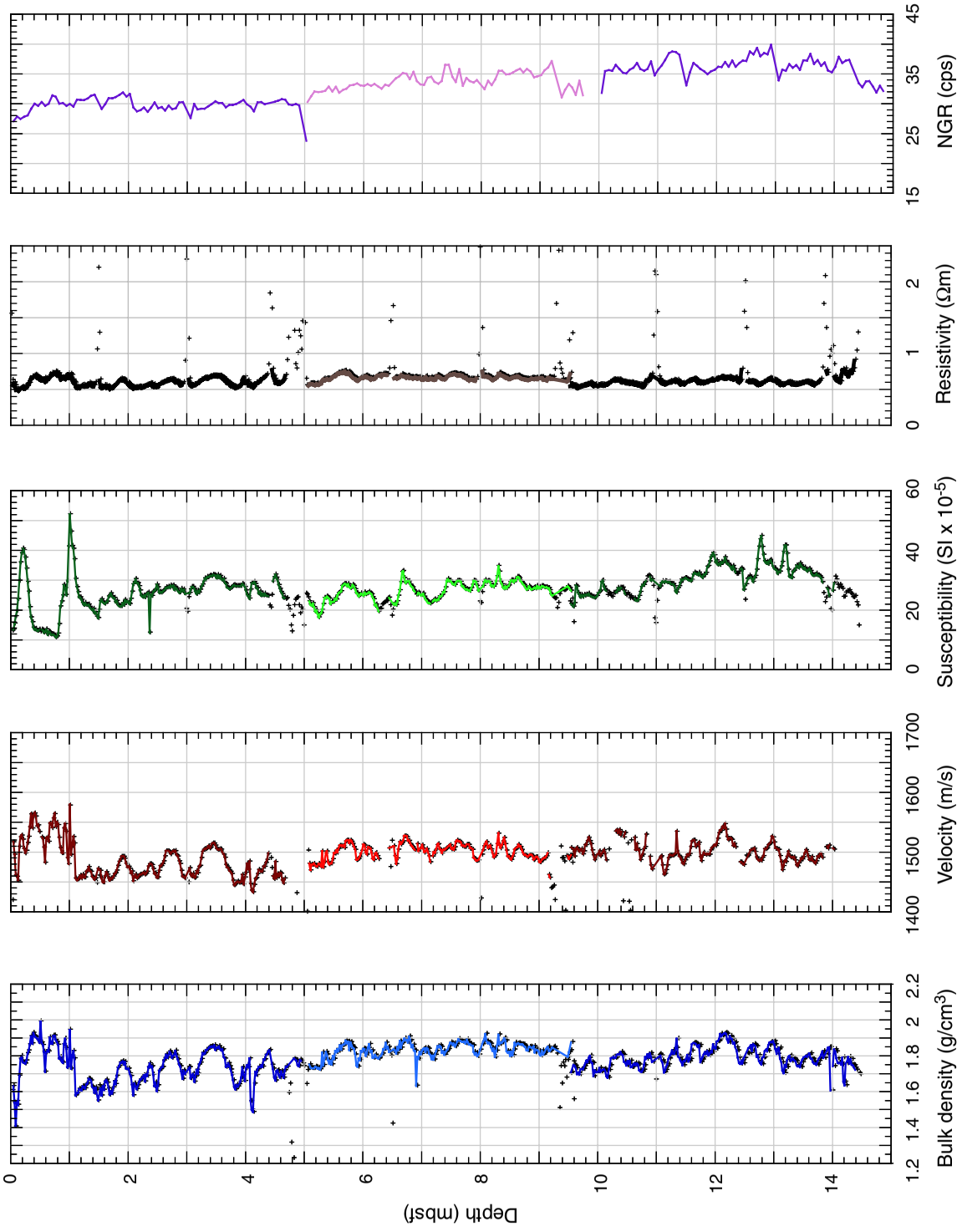

Figure F25. MSCL (offshore) and natural gamma ray (NGR) (onshore) data from Hole M0003A.

Figure F26. MSCL (offshore) and natural gamma ray (NGR) (onshore) data from Holes M0004A and M0004B.

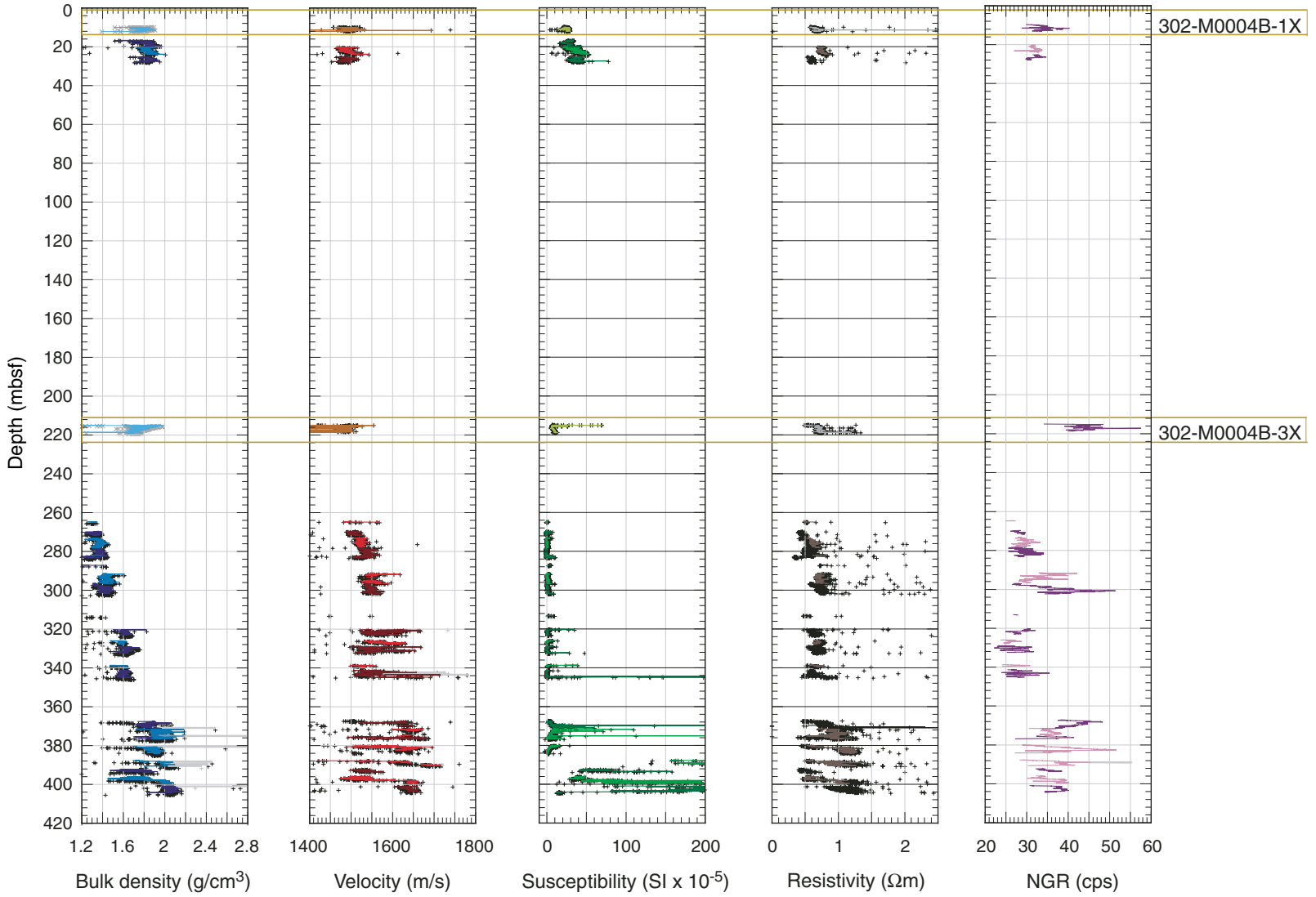

Figure F27. MSCL (offshore) and natural gamma (onshore) data from Hole M0004C.

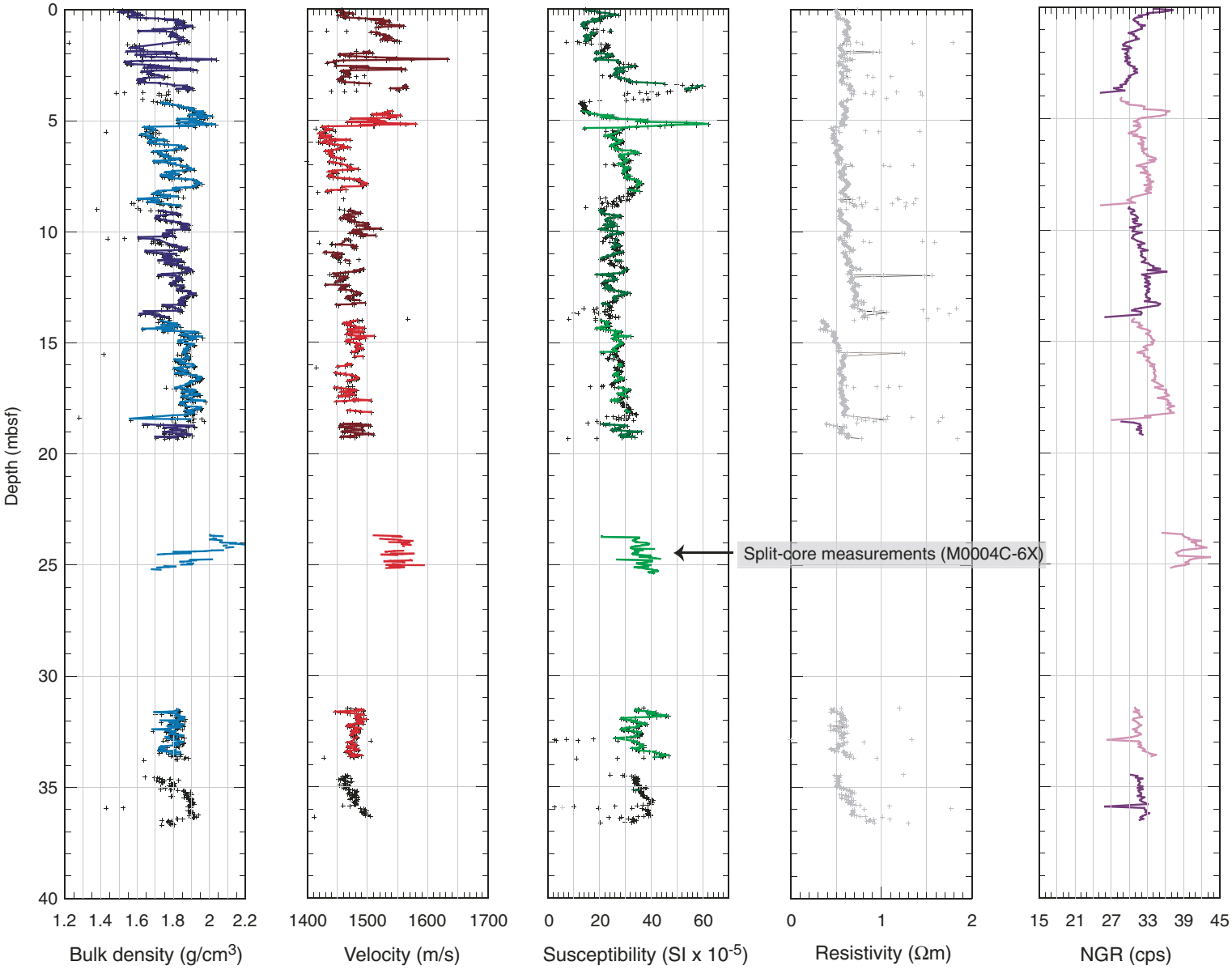

Figure F28. Downhole (Hole M0004B) and downcore (Hole M0002A) *P*-wave velocity data. Note that the data have not been depth-matched.

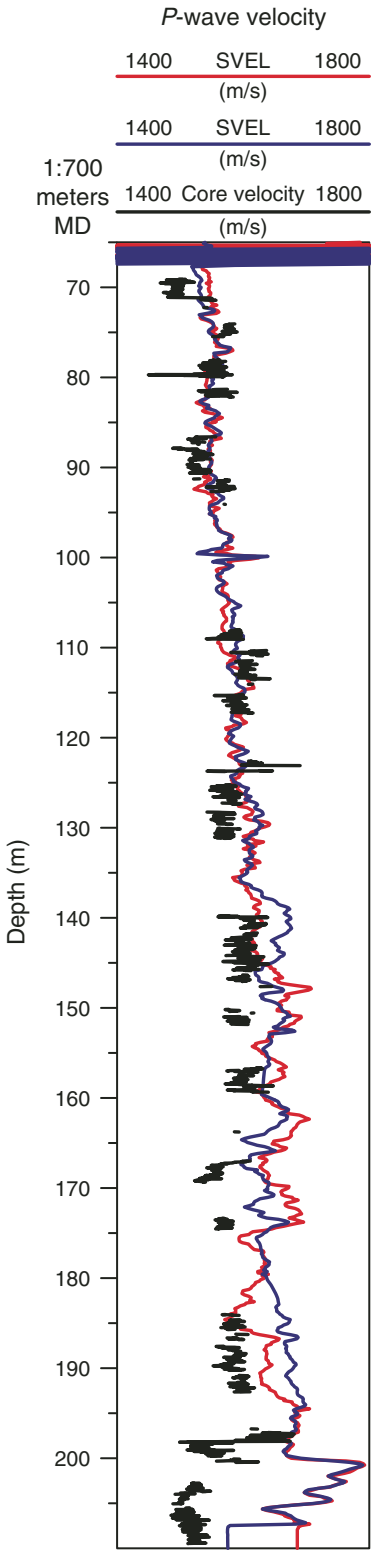

Figure F29. Color reflectance data, Hole M0002A.

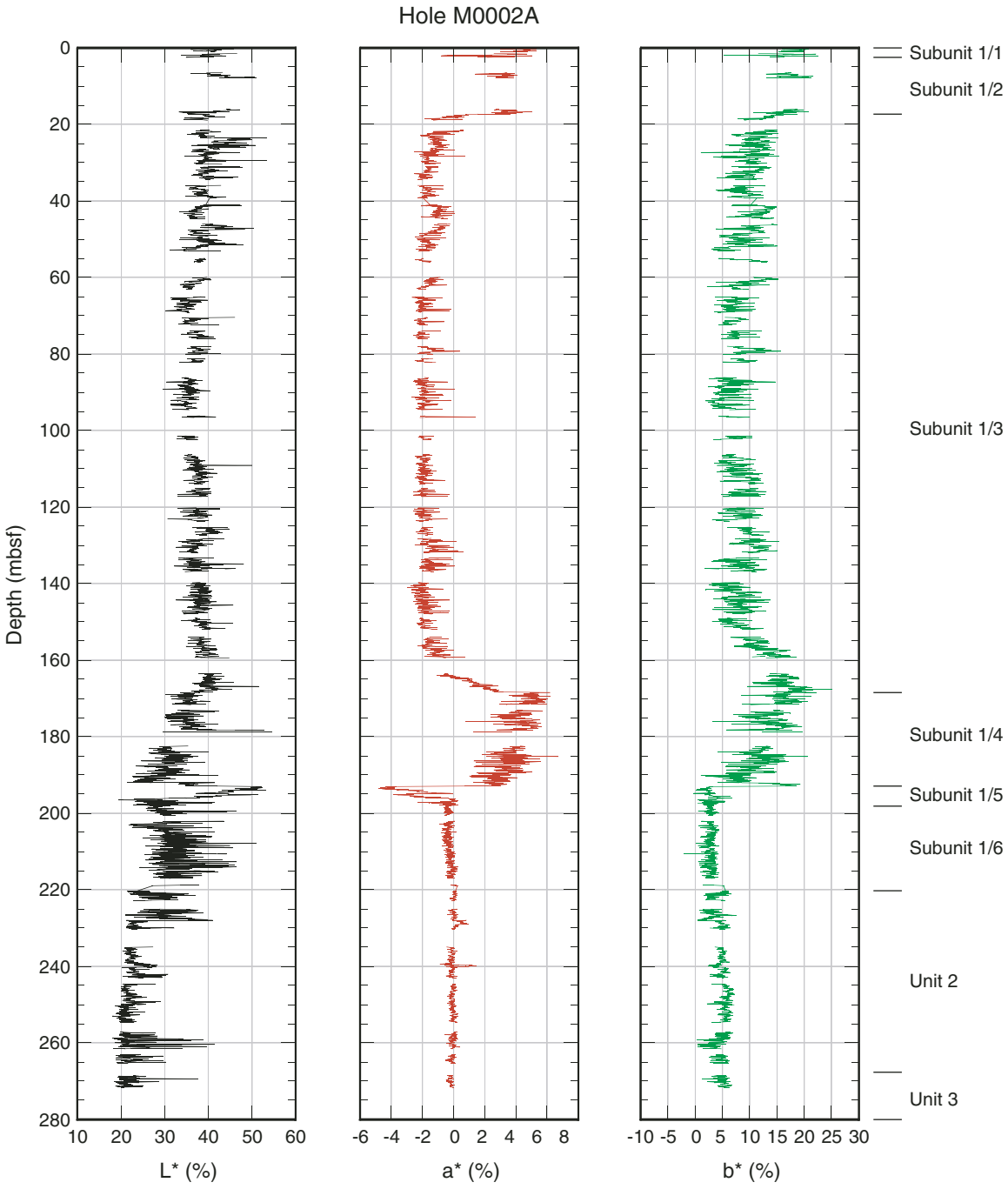

Figure F30. Color reflectance data, Hole M0003A.

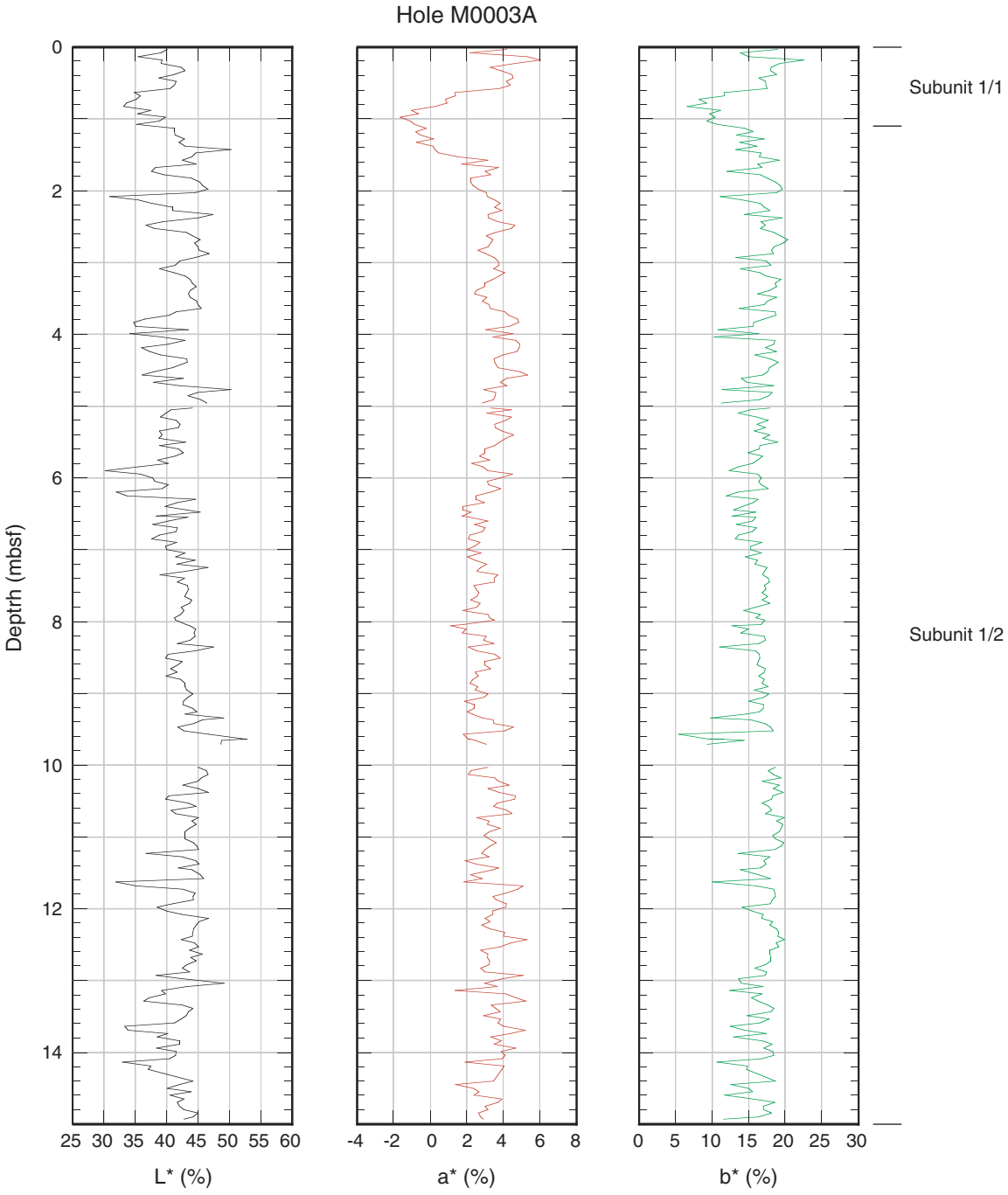

Figure F31. Color reflectance data, Hole M0004A and M0004B.

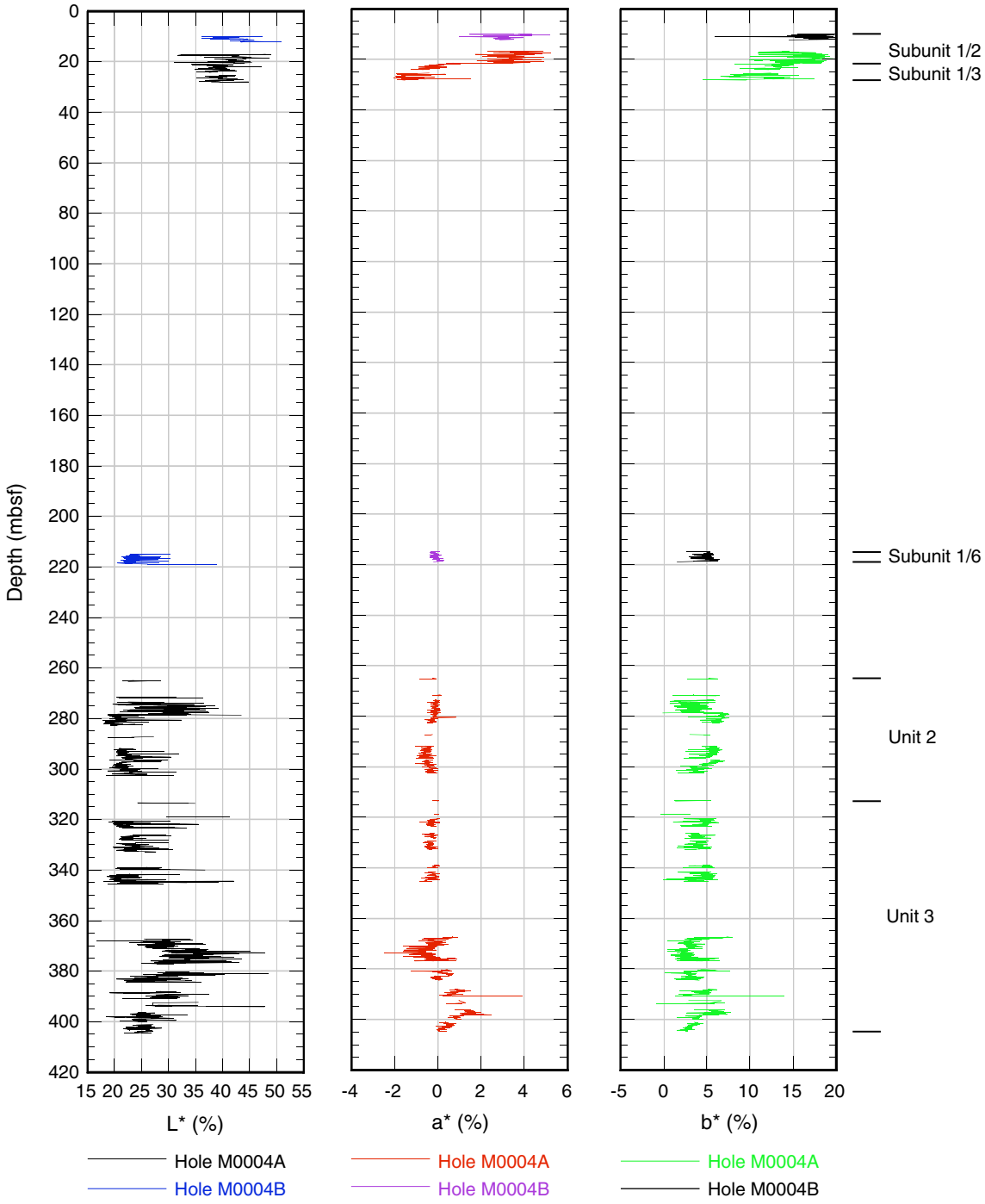

Figure F32. Color reflectance data, Hole M0004C.

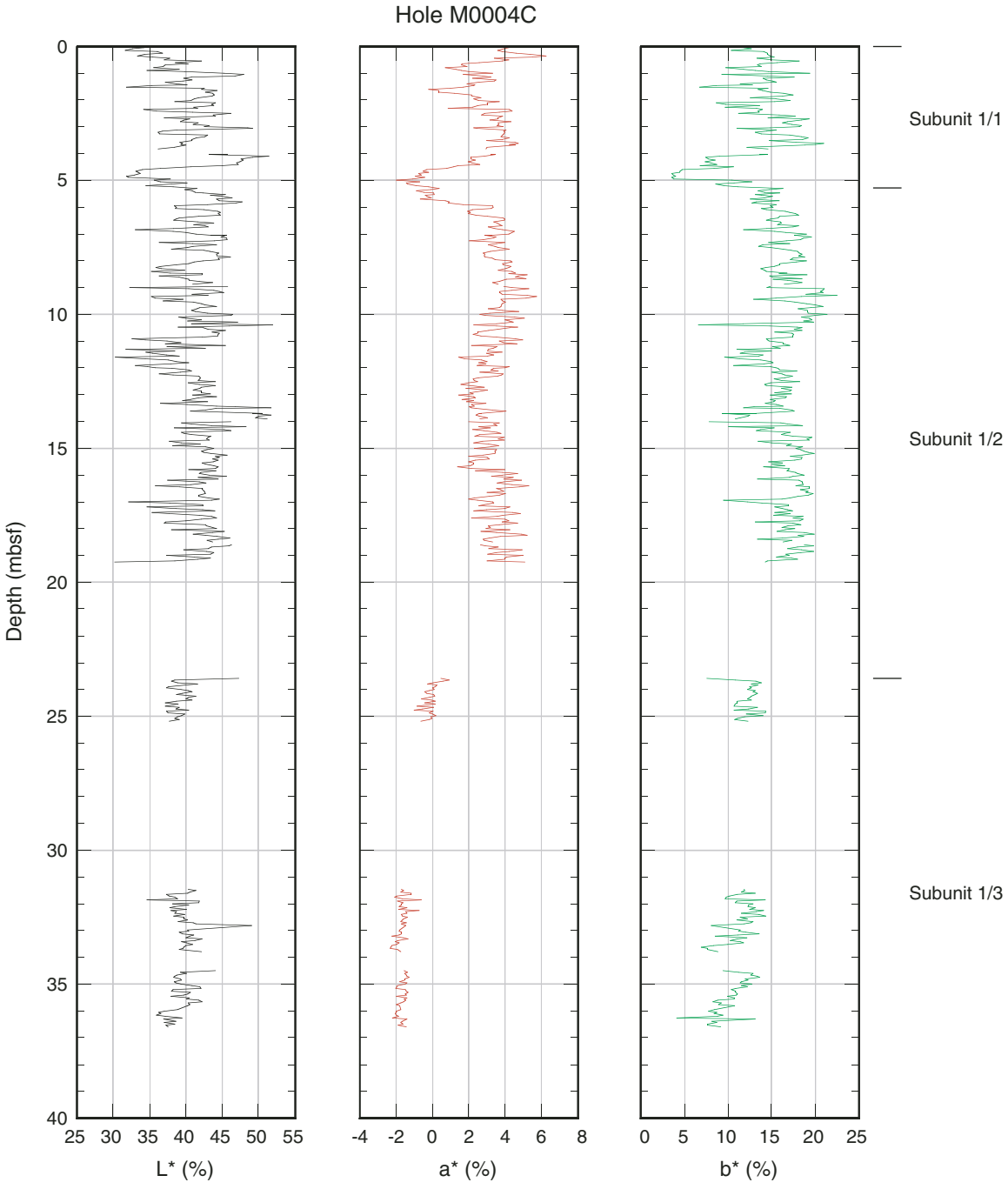

Figure F33. Downhole total and spectral gamma ray (SGR) (Hole M0004B) and downcore (Hole M0002A) total gamma ray data. The data have not been depth-matched. Note that the core total gamma radiation is given in cps and the downhole logging total gamma is given in gAPI units.

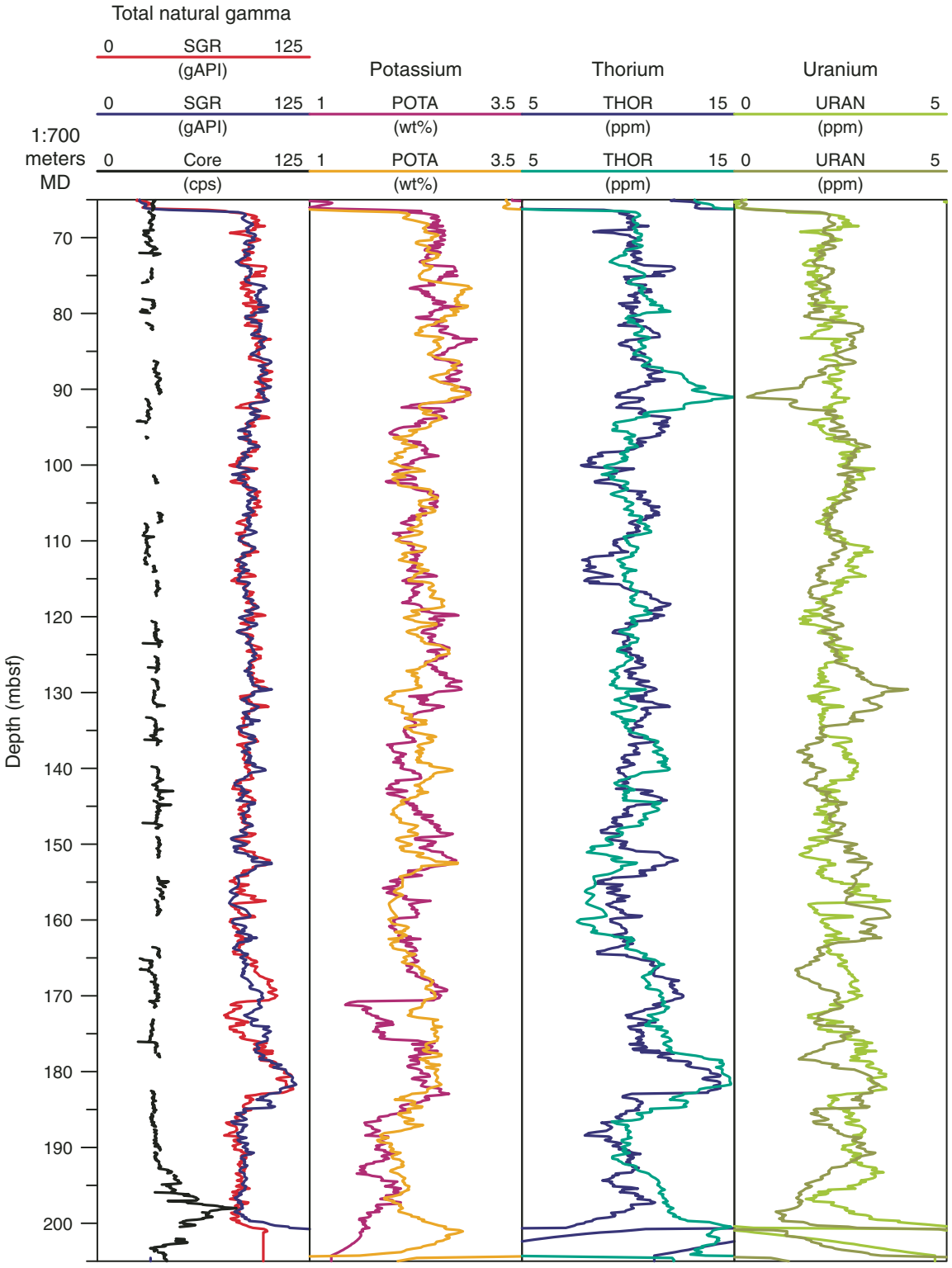

Figure F34. Bulk density, undrained shear strength, and consolidation index. MSCL = multisensor core logger, MAD = moisture and density.

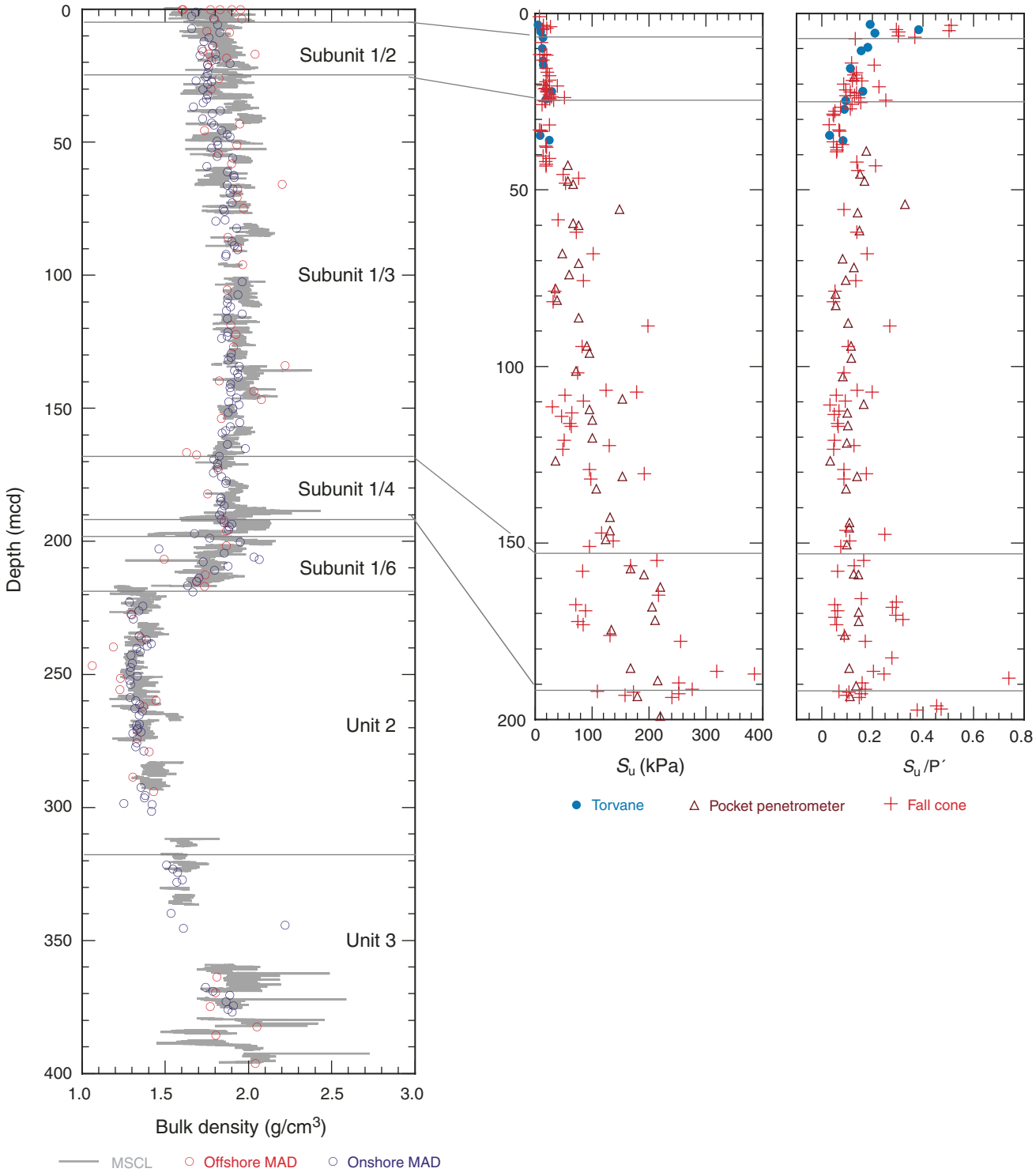

Figure F35. Average thermal conductivity measured on cores from Holes M0002A (blue) and M0004A (red).

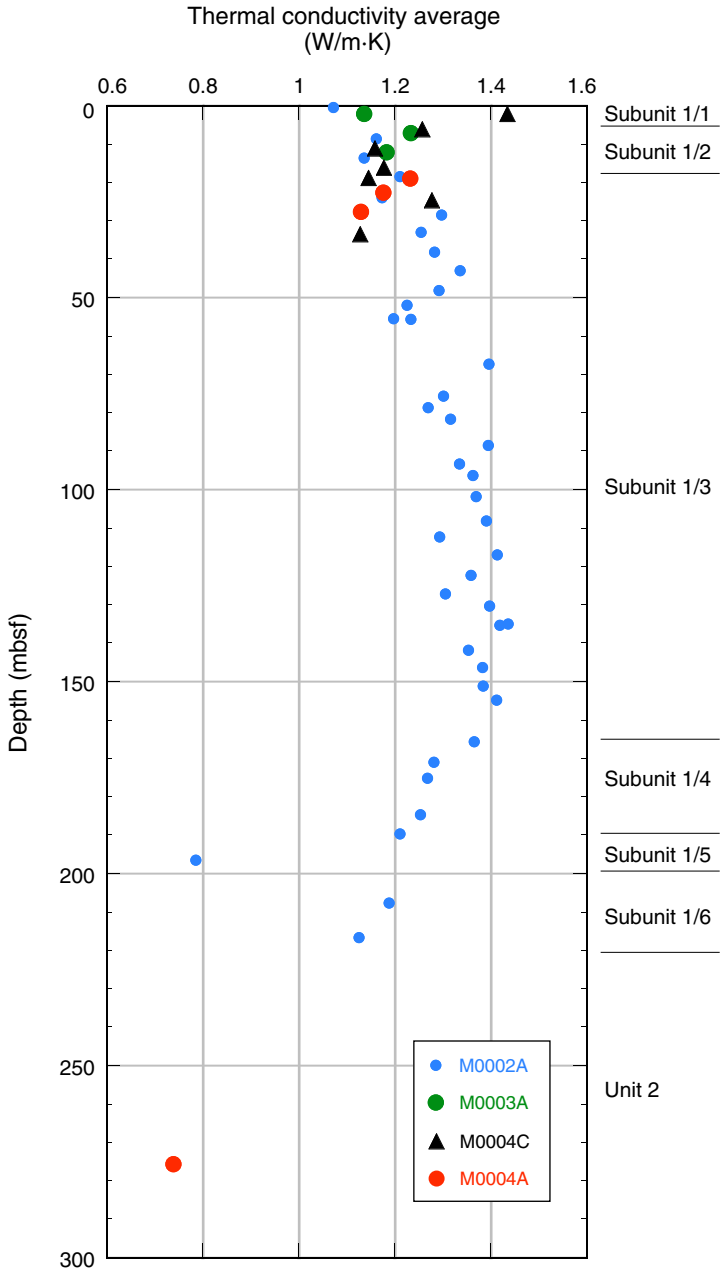

Figure F36. In situ recorded temperature measurements from the Lomonosov Ridge. Note that the regression excludes the measurement at 60 mbsf.

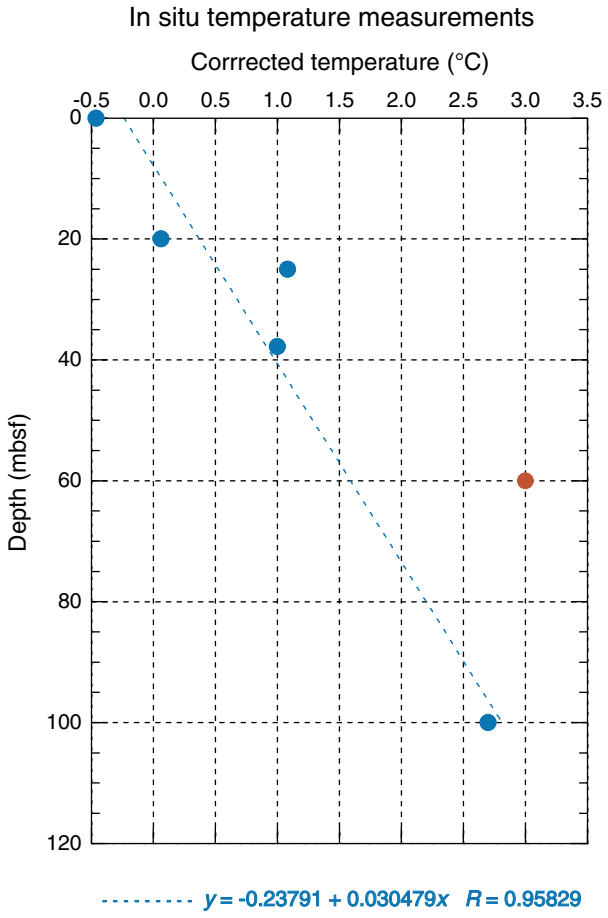

Figure F37. Raw in situ temperature data from the Adara and British Geological Survey (BGS) tools **A.** Adara at 25 mbsf. **B.** Adara at 37.8 mbsf. (Continued on next page.)

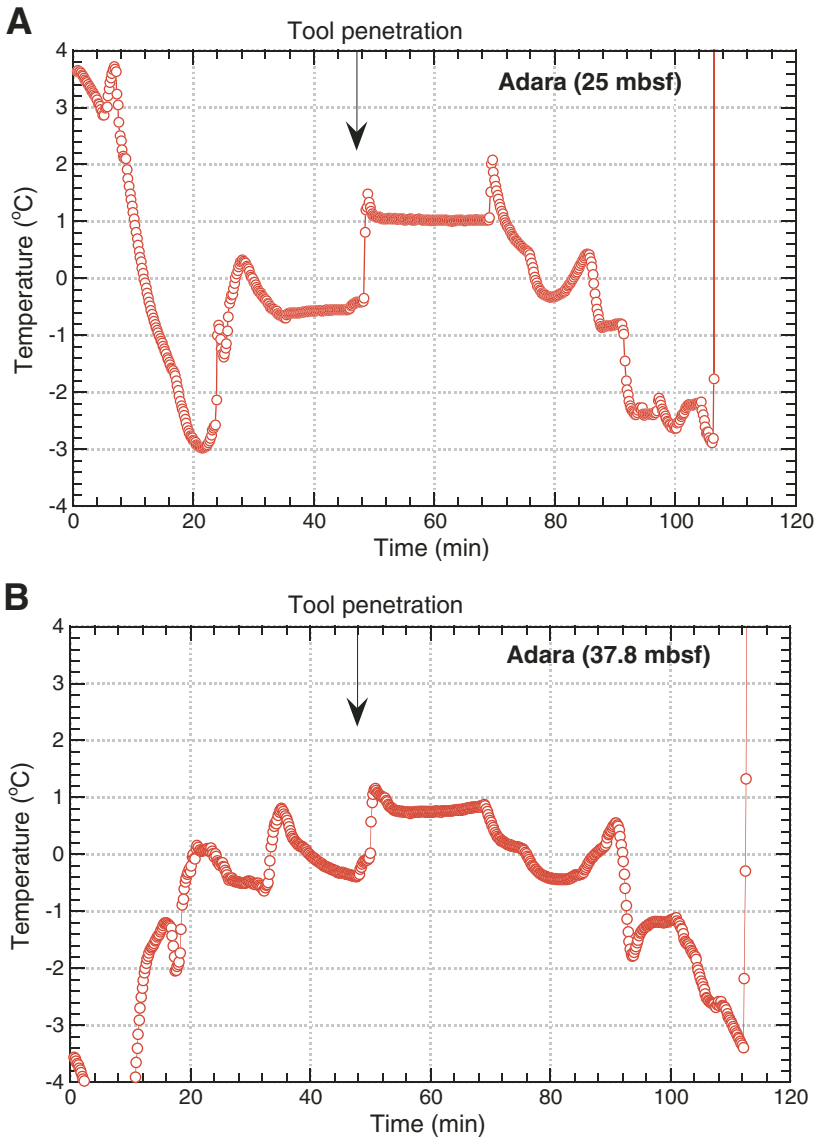

Figure F37 (continued). **C.** BGS at 20 mbsf. **D.** BGS at 60 mbsf. **E.** BGS at 100 mbsf.

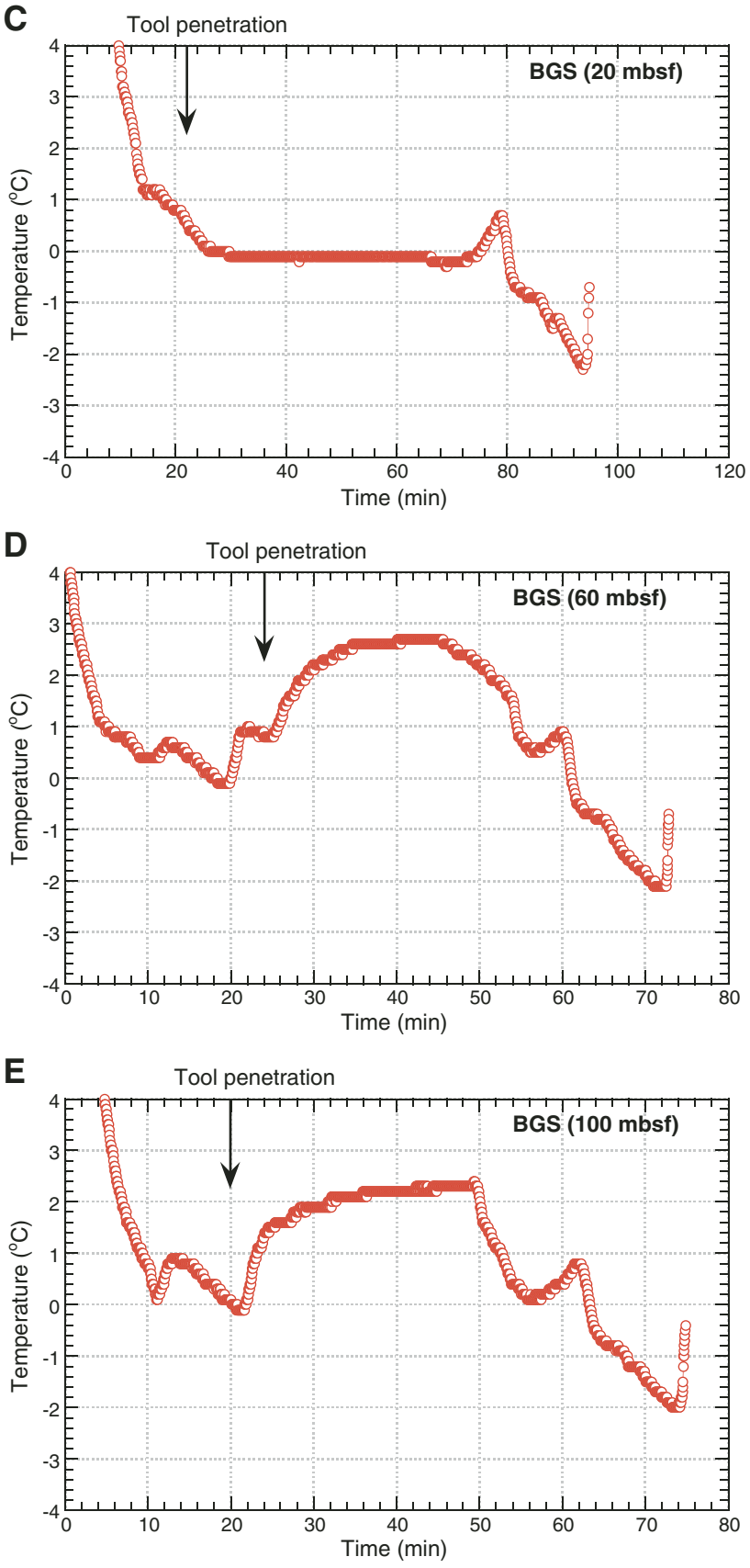

Figure F38. Alkalinity and ammonium profiles in the upper 45 m of sediment, showing location of samples collected by whole-round squeezing and Rhizone. Note the peak in alkalinity and the inflection in ammonium.

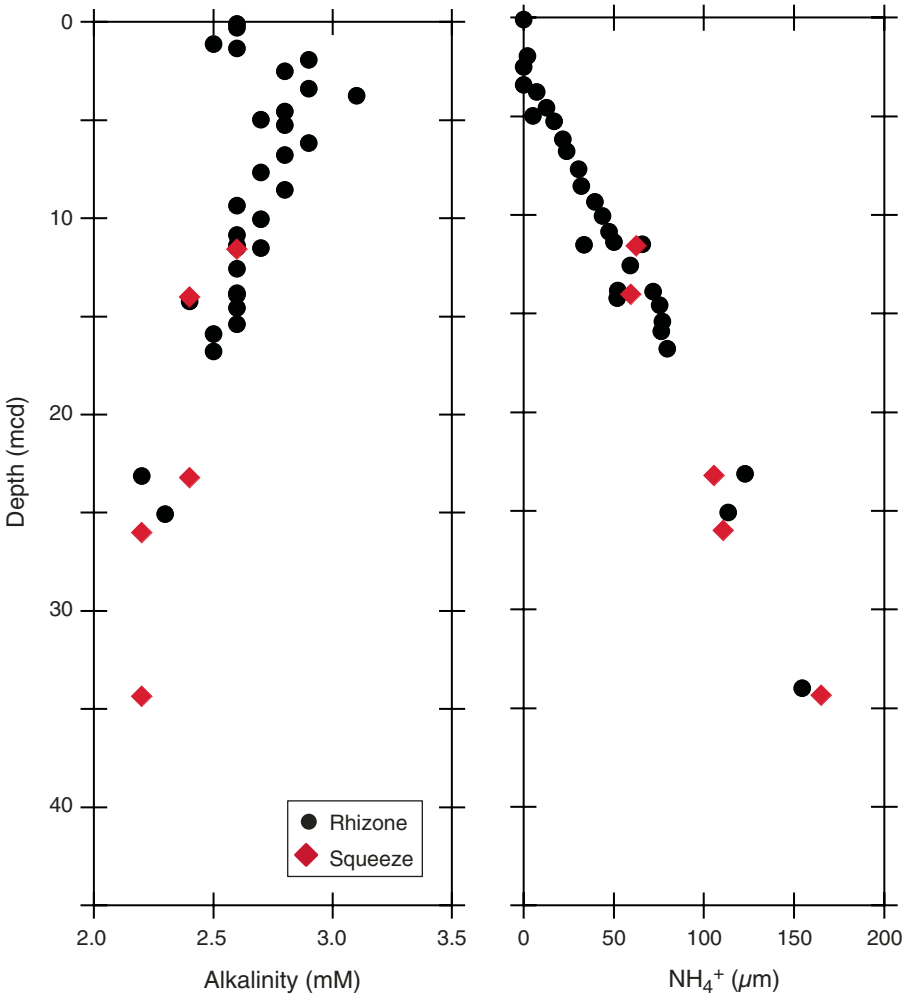

Figure F39. Profiles of dissolved constituents for the 400 m Cenozoic sediment sequence. Samples include those collected using whole-round squeezing and Rhizones. **A.** pH, alkalinity, Ca, Fe, Mg, and Mn. (Continued on next page.)

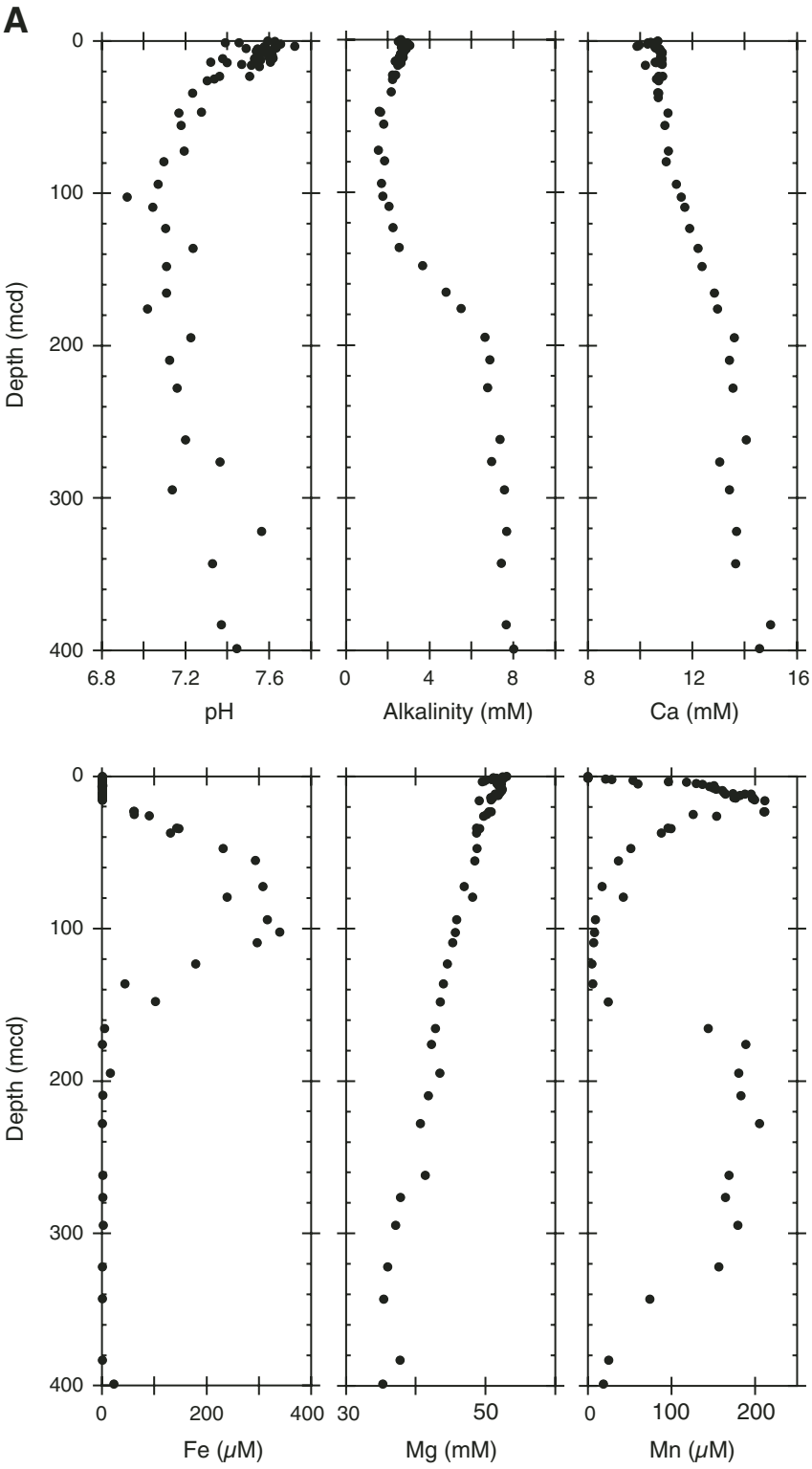

Figure F39 (continued). B. Ammonium, Na, S, sulfate, Si, and Sr.

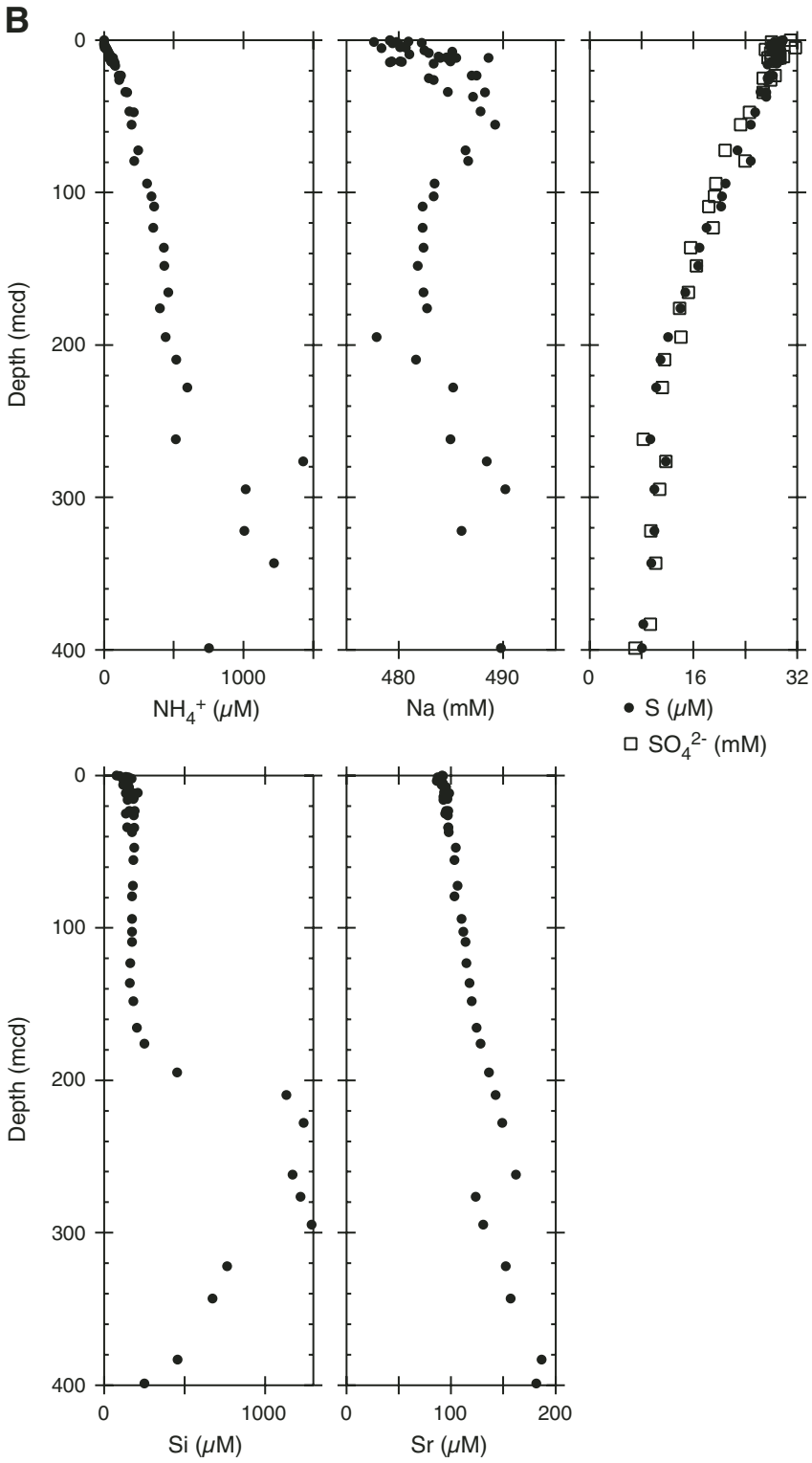

Figure F40. Elemental contents of sediment for the 400 m Cenozoic sequence. (Continued on next page.)

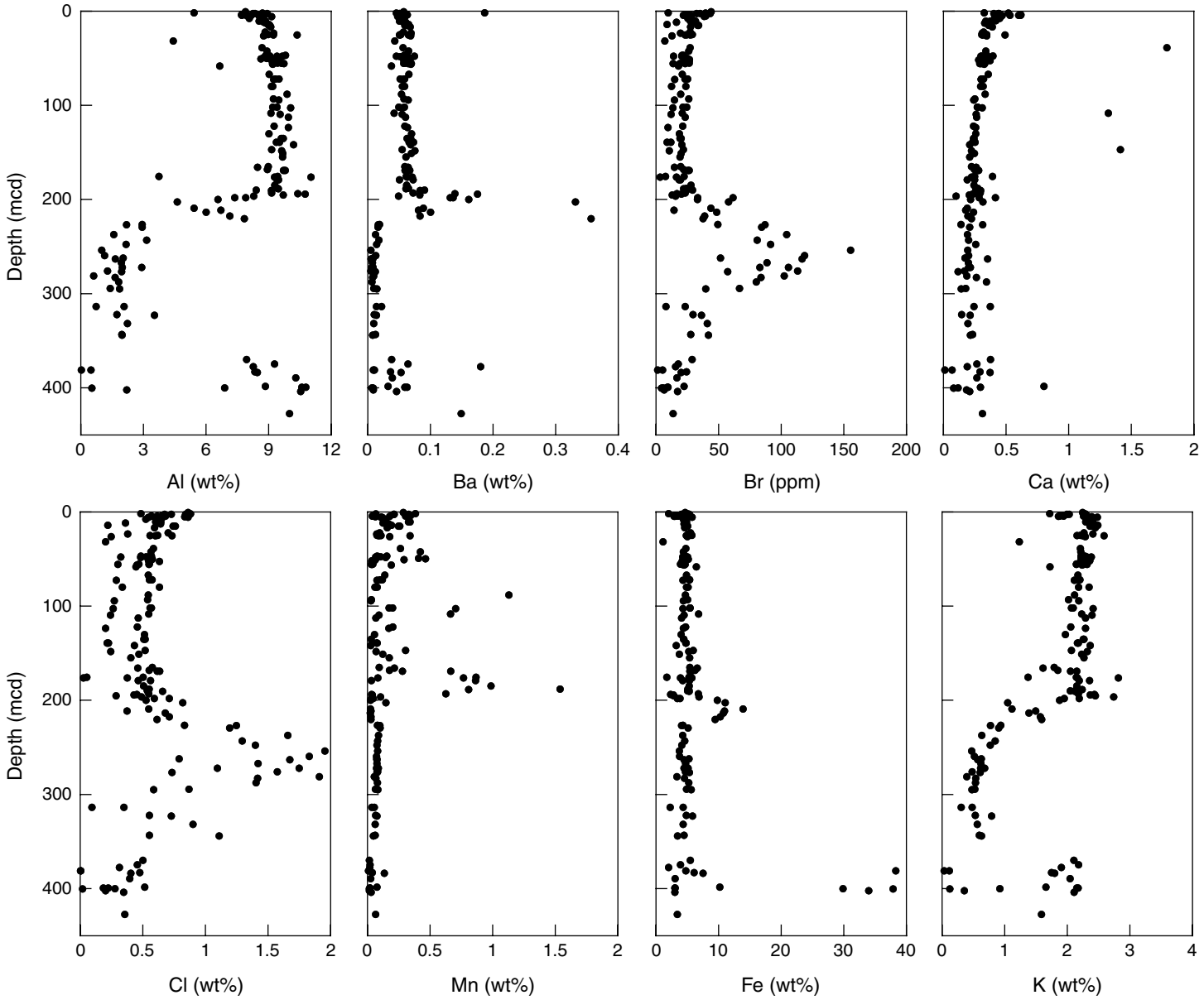

Figure F40 (continued).

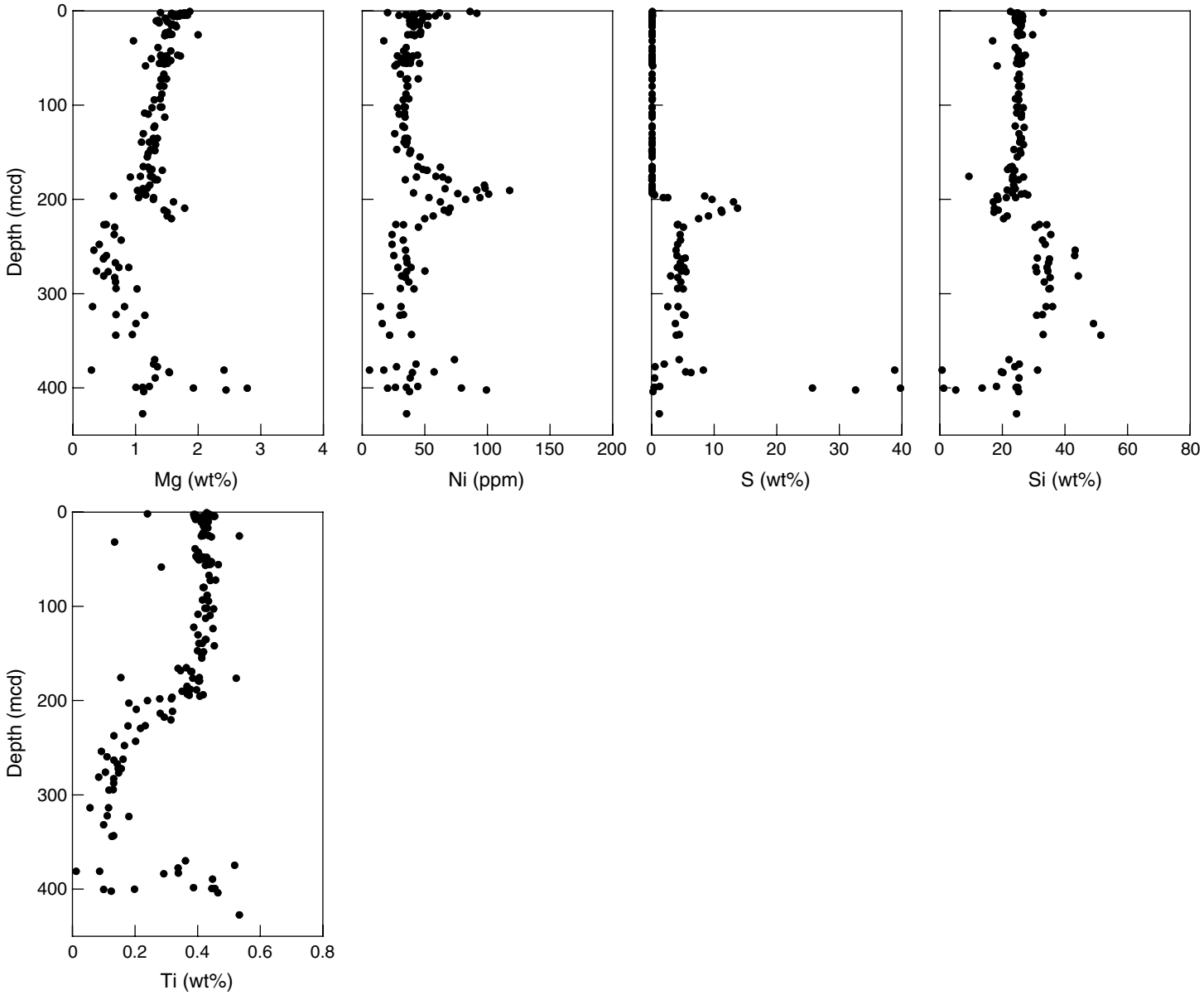

Figure F41. Ratios of Ti/Al, K/Al, Ca/Al, and Fe/Al in sediment for the 400 m Cenozoic sequence.

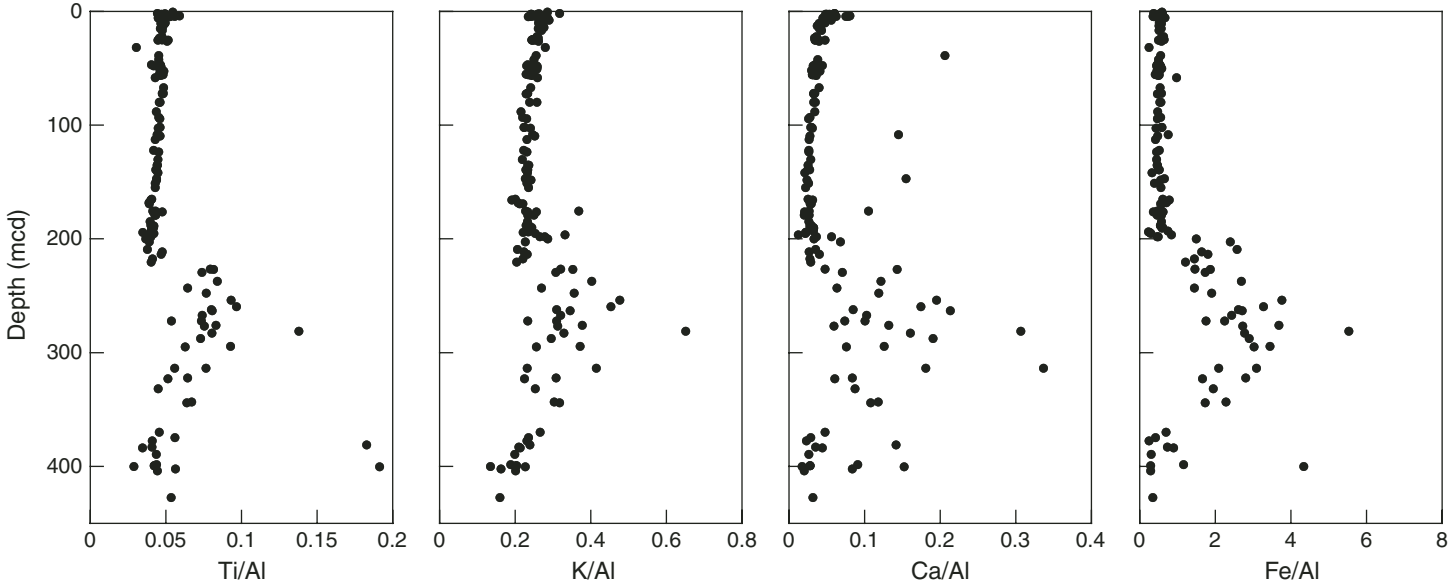

Figure F42. Total organic carbon (TOC) contents in sediment for the 400 m Cenozoic sequence. Only core catcher samples are shown here. Lithostratigraphic units and subunits are indicated.

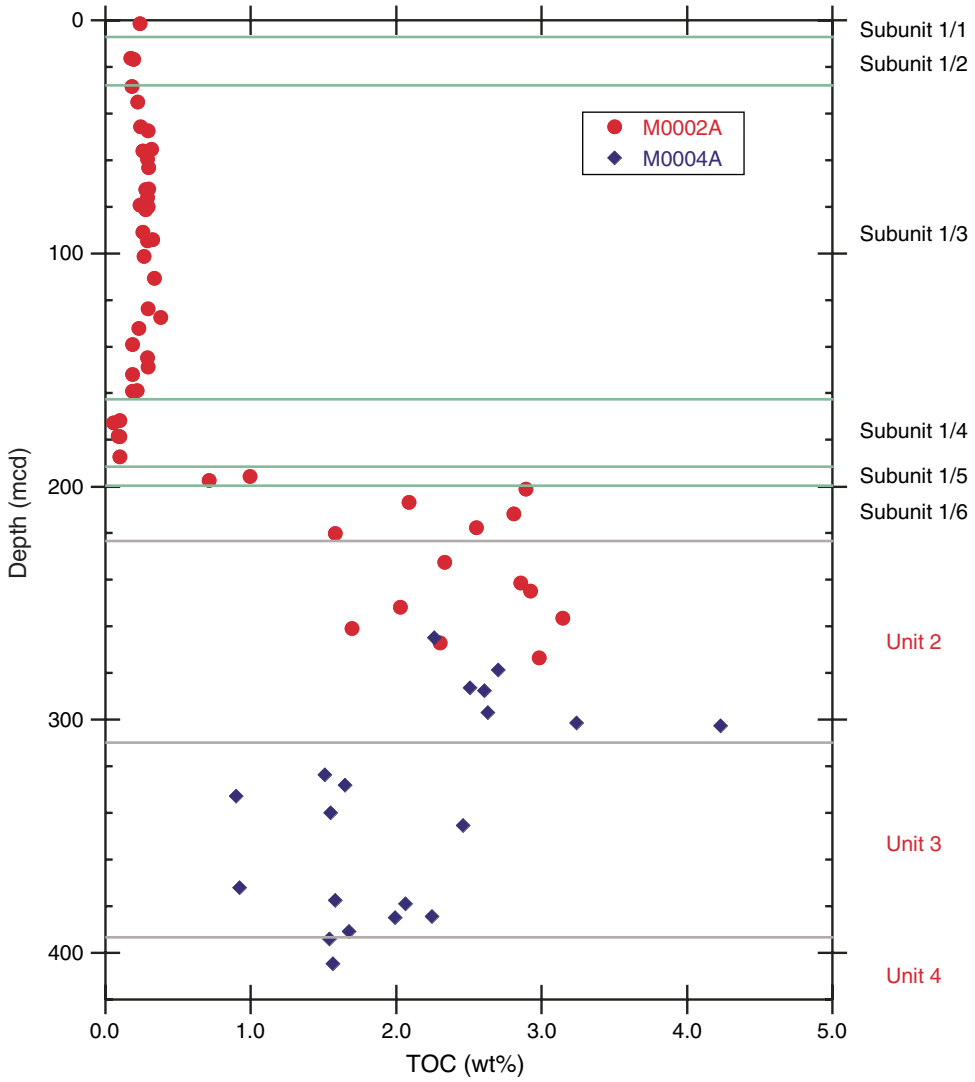

Figure F43. Results of Rock-Eval pyrolysis in core catcher samples for the 400 m Cenozoic sequence, plotted as hydrogen index versus oxygen index. Lithostratigraphic units are indicated. (Continued on next page.)

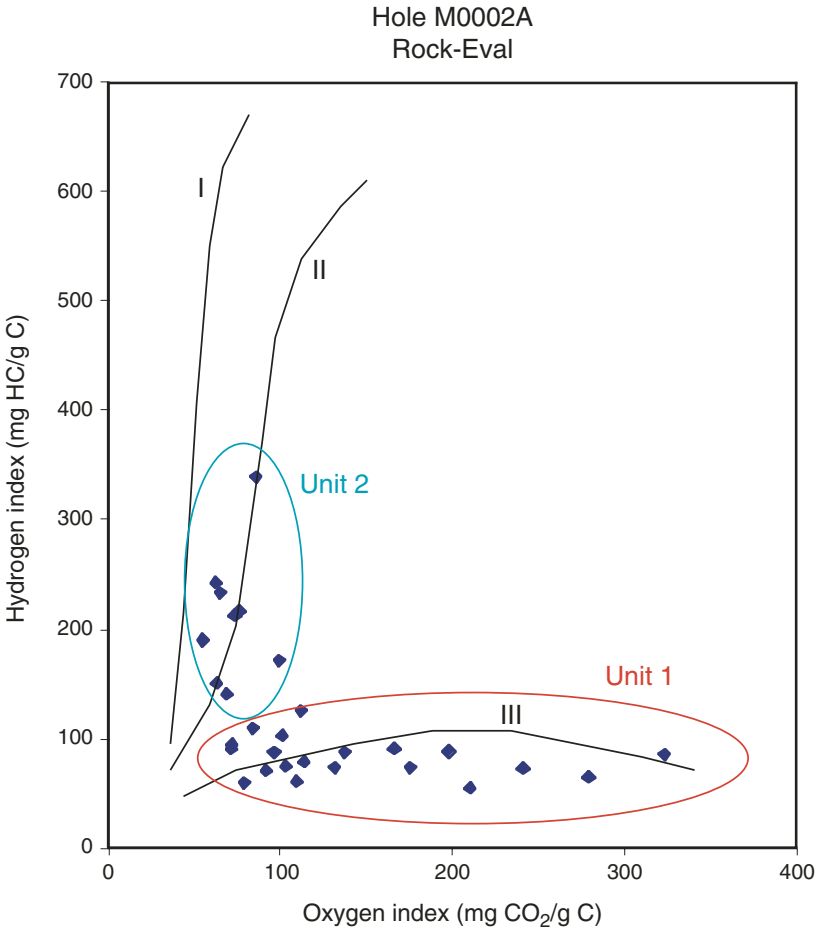

Figure F43 (continued).

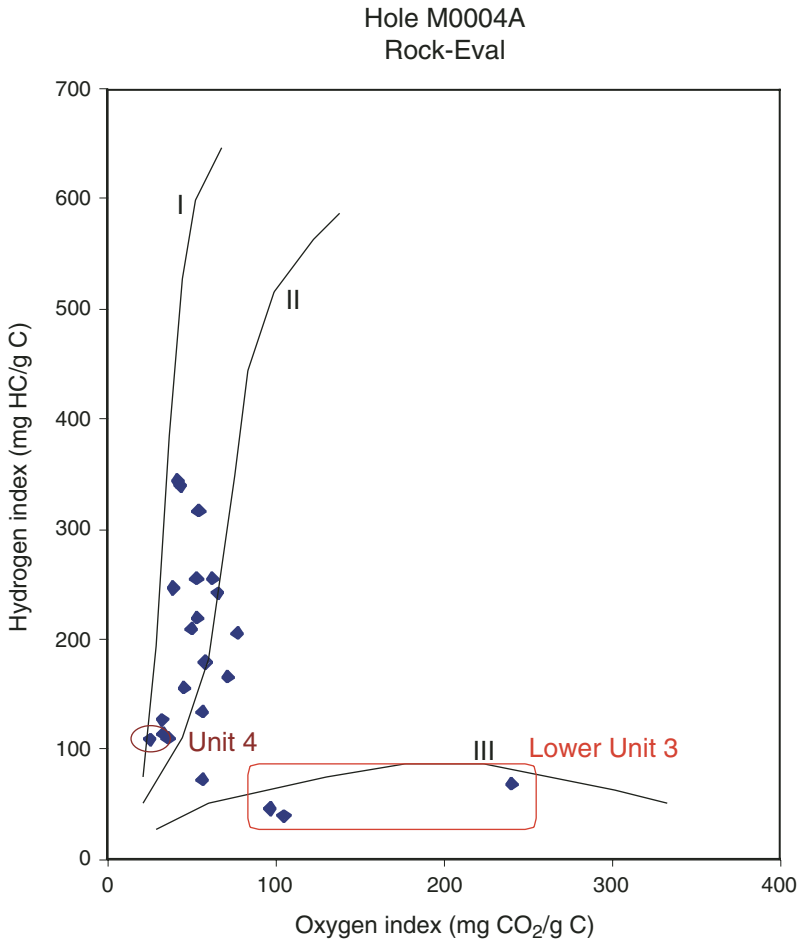

Figure F44. Hydrogen index from Rock-Eval pyrolysis plotted with depth for Holes M0002A and M0004A.

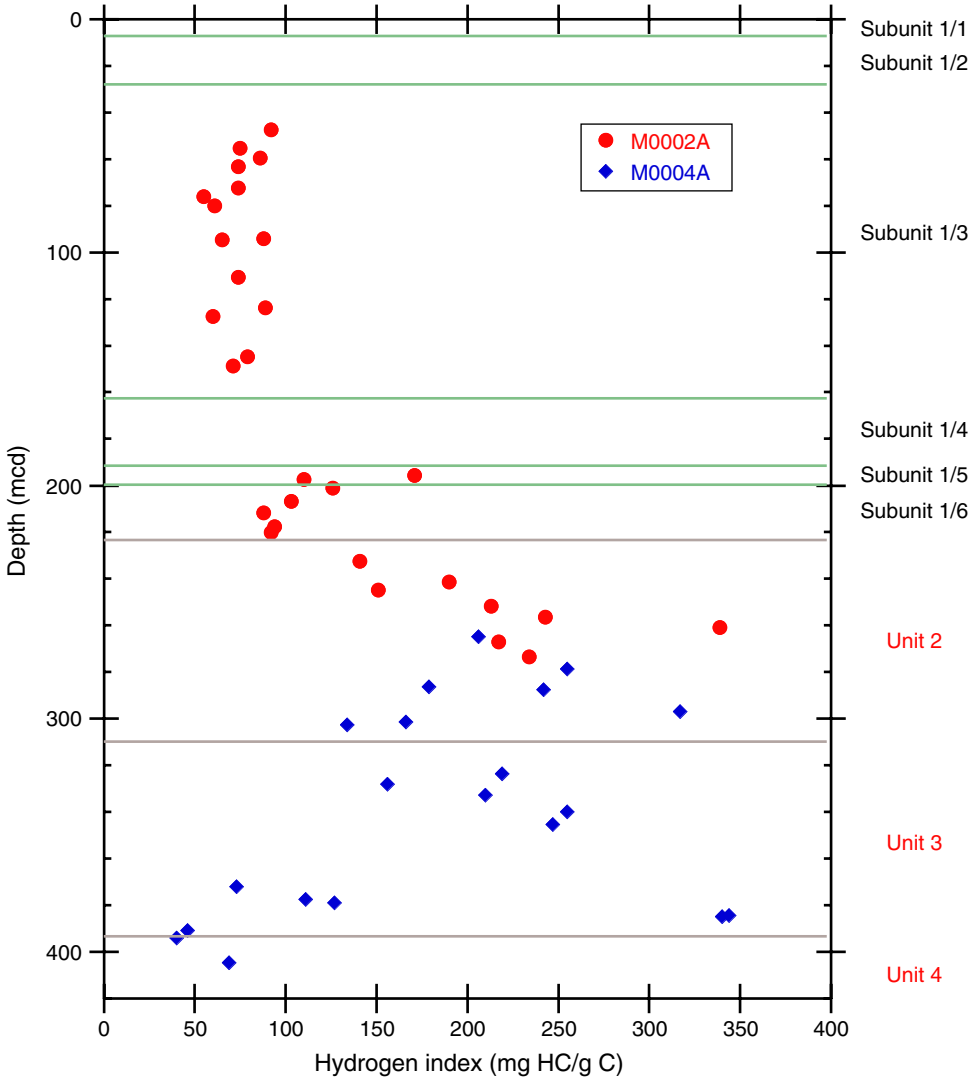

Figure F45. Variations with depth of natural remanent magnetization (NRM) intensity and whole-core magnetic susceptibility. Susceptibility has been offset by +10 to allow data to be plotted on a log scale.

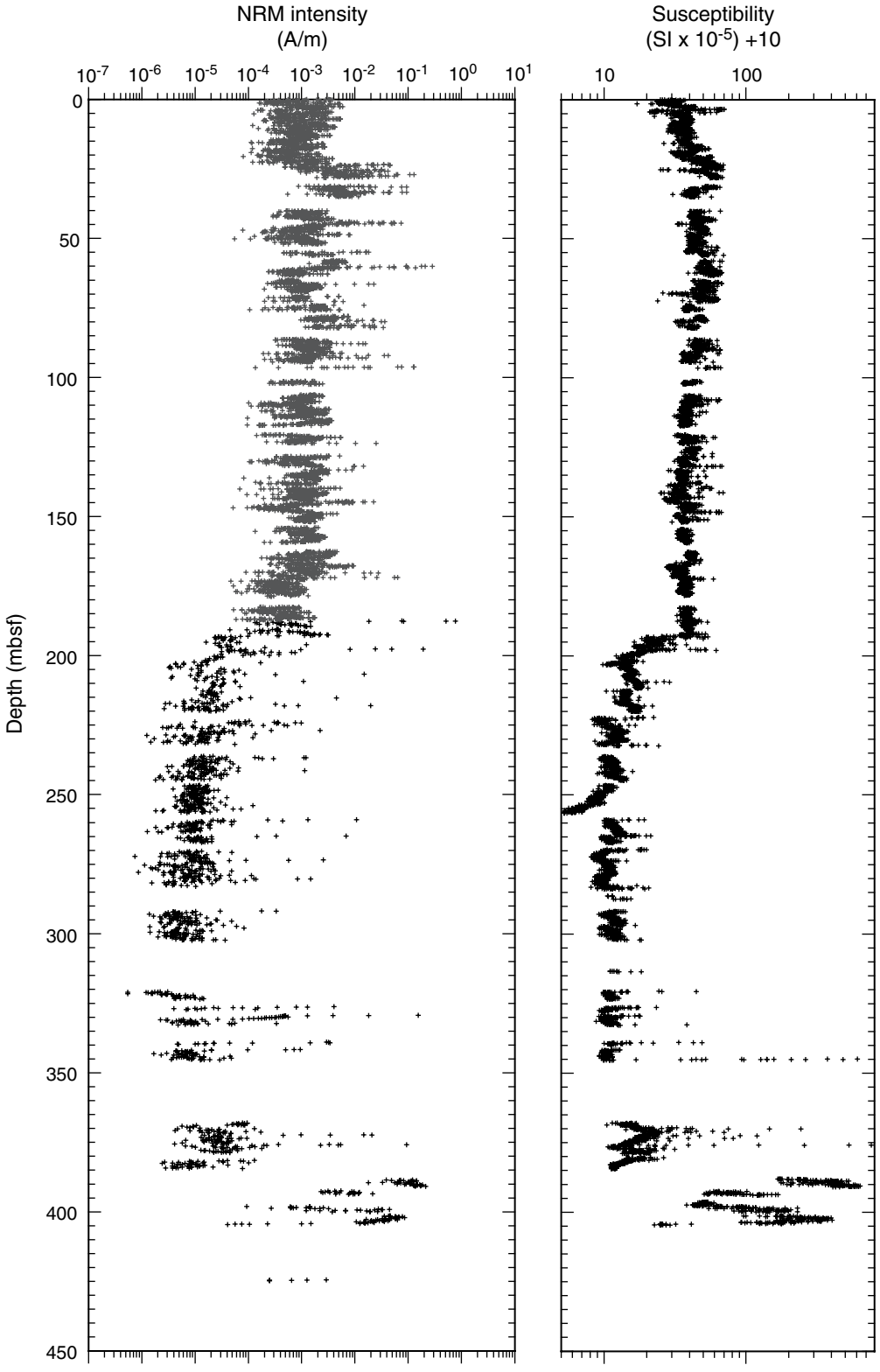

Figure F46. A. Variations with depth of natural remanent magnetization (NRM) inclination after alternating-field (AF) demagnetization at 30–55 mT and interpreted magnetic stratigraphic age in the interval 0–197 mcd. Black = normal polarity, white = reversed polarity. Shaded portions indicate intervals over which interpretations agree. Tie lines indicate possible interpretations. The preferred model is shown on the left. (Continued on next page.)

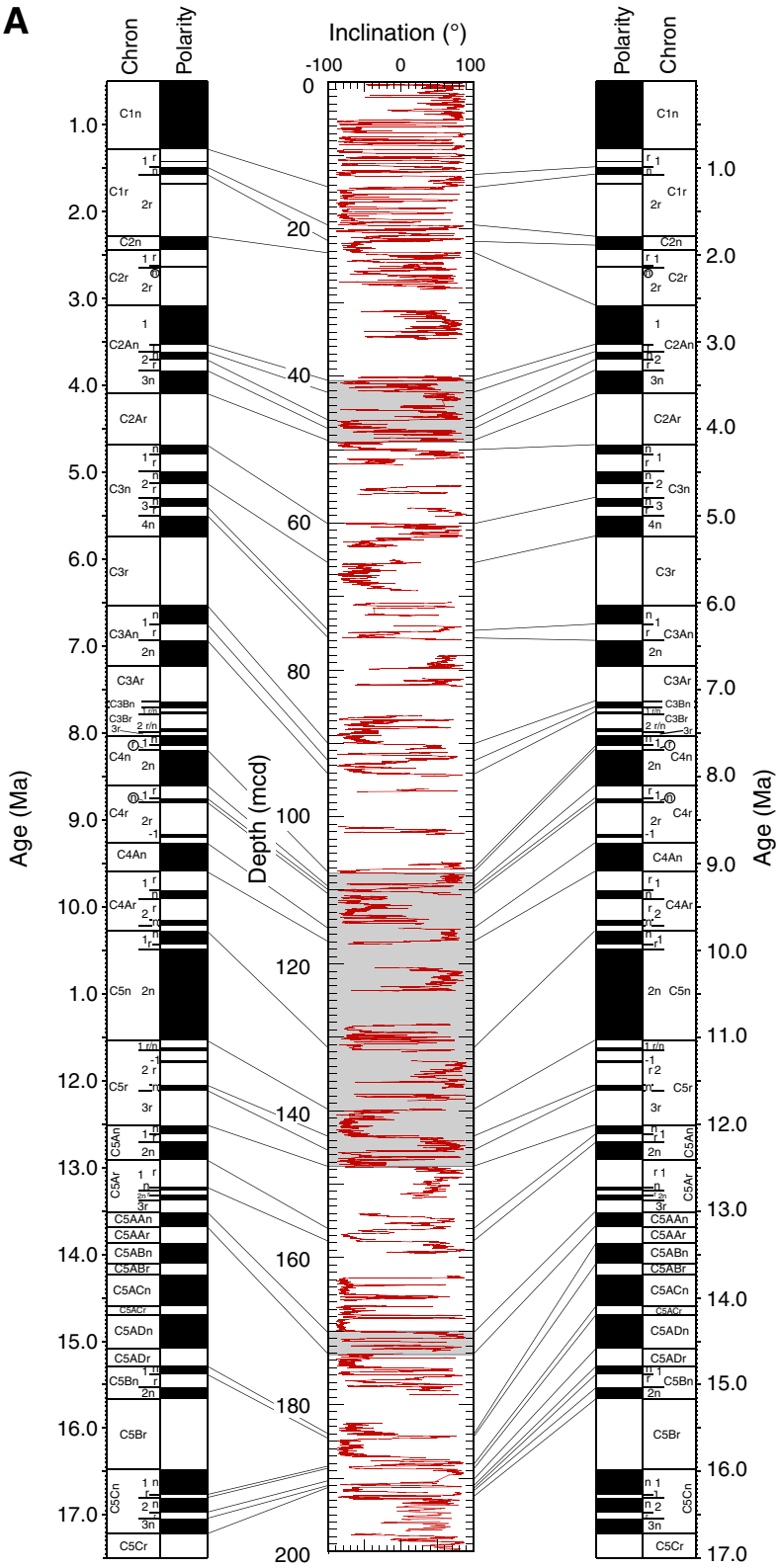

Figure F46 (continued). B. 0–70 mcd.

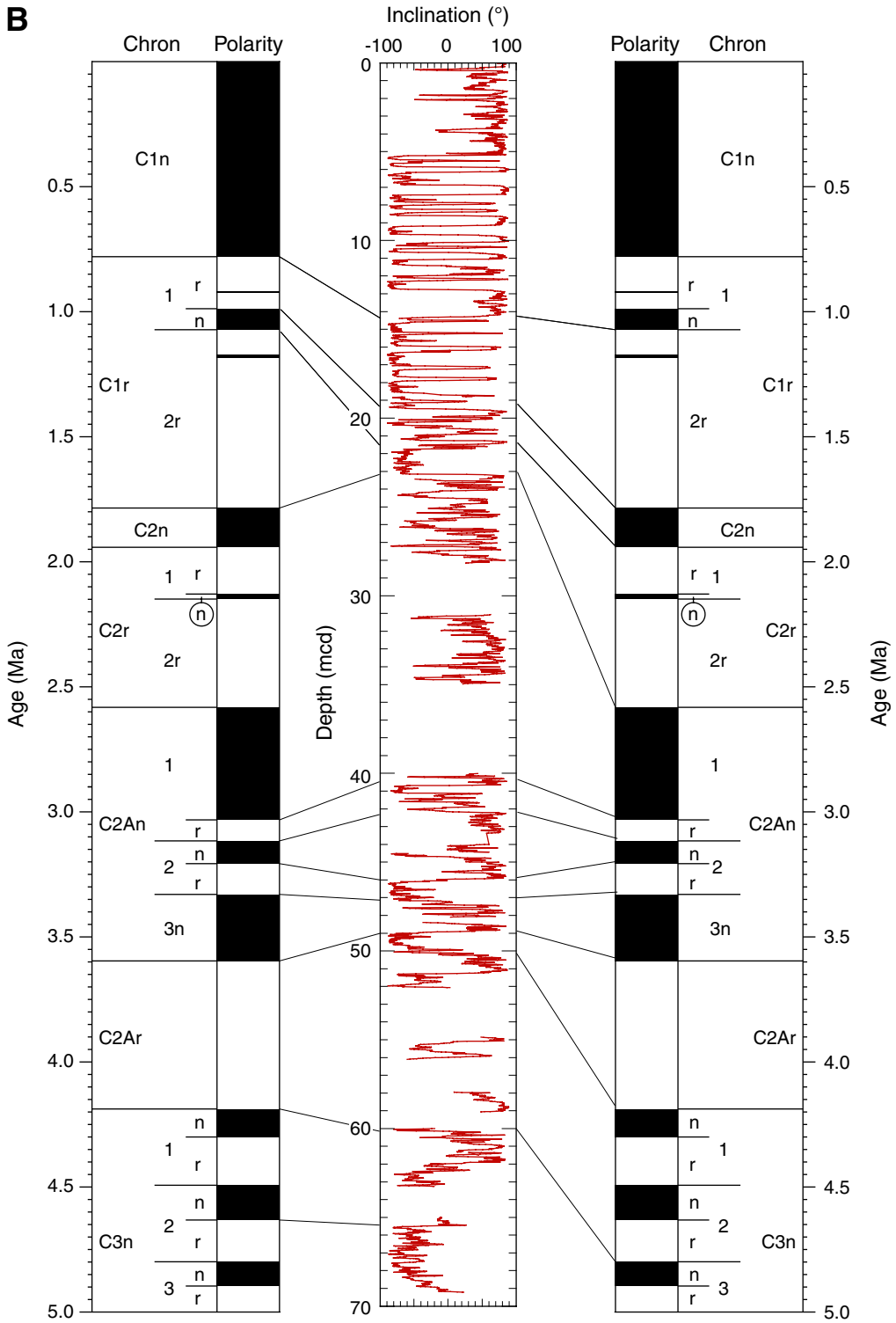

Figure F47. Variations with depth of magnetic inclination after AF demagnetization at 30–55 mT and interpreted paleomagnetic polarity for the interval 388–405 m. Black = normal polarity, white = reversed polarity, gray = missing recovery or indeterminate polarity.

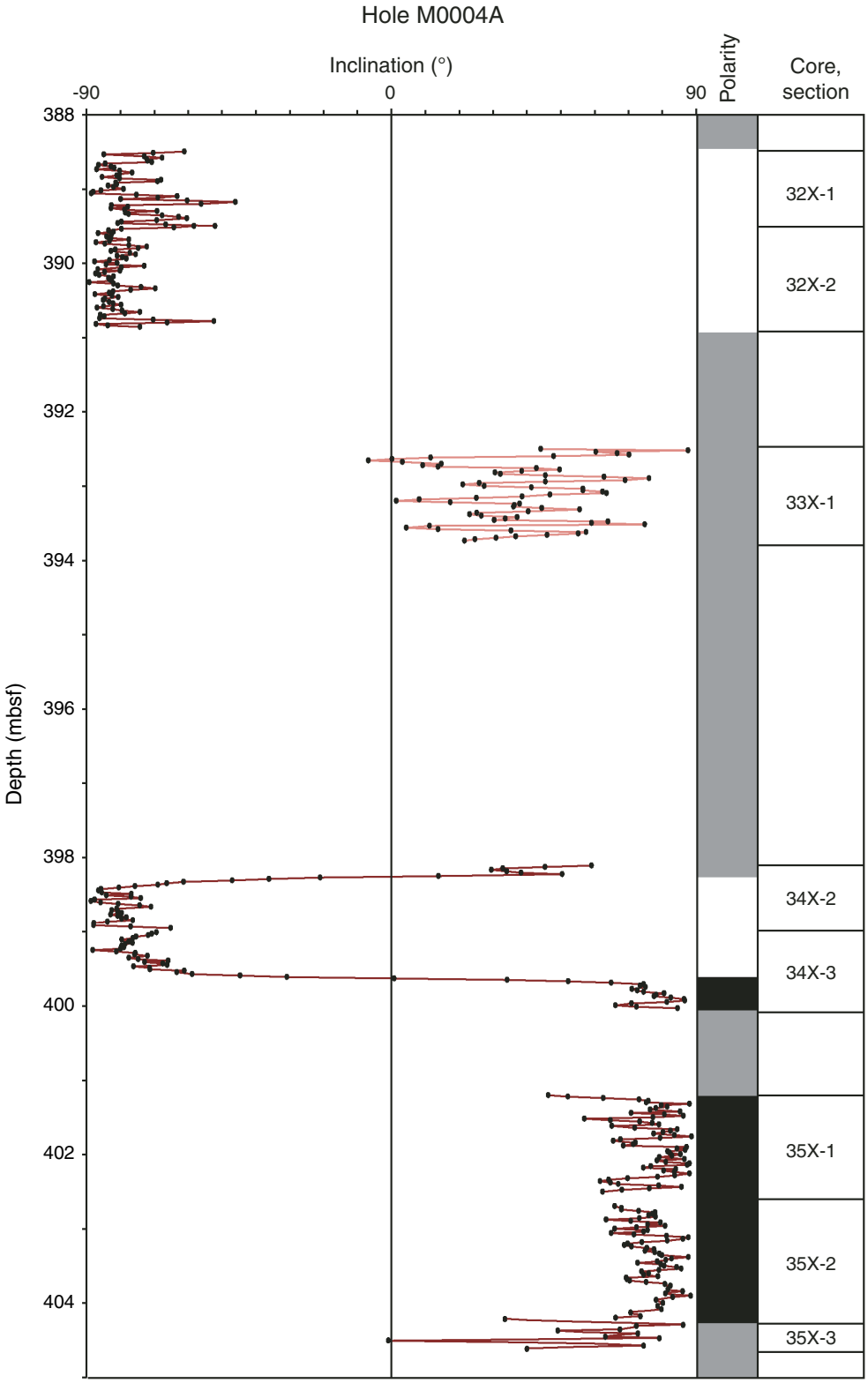

Table T1. Coring summary. (See table note. Continued on next three pages.)

Hole M0002A
Latitude: 87°55.271′N
Longitude: 139°21.901′E
Time in hole (h): 167 (17 August–24 August 2004)
Seafloor (drill pipe measurement from rig floor, m): 1211.09
Water depth (sonar, m): 1209
Total depth (drill pipe measurement from rig floor, m): 1481.2
Total penetration (meters below seafloor, mbsf): 270.1
Total length of cored section (m): 270.1
Total core recovered (m): 213.15
Core recovery (%): 78.9
Total number of cores (including cores having no recovery): 62
Oldest sediment cored:
Depth (mbsf): 270.1
Lithology: mud-bearing biosiliceous ooze
Age: middle Eocene

Hole M0003A
Latitude: 87°56.000′N
Longitude: 139°32.100′E
Time on hole (h): 41 (25 August–26 August 2004)
Seafloor (drill pipe measurement from rig floor, m): 1207.97
Water depth (sonar, m): 1206.2
Total depth (drill pipe measurement from rig floor, m): 1222.97
Total penetration (meters below seafloor, mbsf): 15
Total length of cored section (m): 15
Total core recovered (m): 14.85
Core recovery (%): 99
Total number of cores (including cores having no recovery): 3
Oldest sediment cored:
Depth (mbsf): 15
Lithology: silty clay
Age: late Pleistocene

Hole M0004A
Latitude: 87°51.995′N
Longitude: 136°10.641′E
Time on hole (h): 148 (27 August–2 September 2004)
Seafloor (drill pipe measurement from rig floor, m): 1289.73
Water depth (sonar, m): 1287.9
Total depth (drill pipe measurement from rig floor, m): 1717.6
Total penetration (m): 427.9
Total length of cored section (m): 157.59
Total core recovered (m): 78.41
Core recovery (%): 49.8
Total number of cores (including cores having no recovery): 42
Oldest sediment cored:
Depth (mbsf): 427.9
Lithology: silty sand
Age: Late Cretaceous

Hole M0004B
Latitude: 87°52.018′N
Longitude: 136°10.475′E
Time on hole (h): 38 (2 September–4 September 2004)
Seafloor (drill pipe measurement from rig floor, m): 1289.7
Water depth (sonar, m): 1287.9
Total depth (drill pipe measurement from rig floor, m): 1507.74
Total penetration (m): 218.0
Total length of cored section (m): 11
Total core recovered (m): 7.31
Core recovery (%): 66.5
Total number of cores (including cores having no recovery): 3
Oldest sediment cored:
Depth (mbsf): 218.0
Lithology: silty clay and clayey silt
Age: middle Eocene

Table T1 (continued).

Hole M0004C
Latitude: 87°52.065′N
Longitude: 136°11.381′E
Time on hole (h): 34 (4 September–5 September 2004)
Seafloor (drill pipe measurement from rig floor, m): 1289.7
Water depth (sonar, m): 1287.9
Total depth (drill pipe measurement from rig floor, m): 1327.03
Total penetration (m): 37.33
Total length of cored section (m): 37.33
Total core recovered (m): 25.33
Core recovery (%): 67.9
Number of cores (including cores having no recovery): 9
Oldest sediment cored:
Depth (mbsf): 37.33
Lithology: silty clay and silty mud
Age: Pliocene

Core	Date (2004)	Time (UTC)	Depth (mbsf) Top	Depth (mbsf) Bottom	Length (m) Cored	Length (m) Recovered	Recovery (%)
302-M0001A-							
1H	16 Aug	0801	0	0.31	0.31	0.31	100.0
				Cored totals:	0.31	0.31	100.0
302-M0002A-							
1X	19 Aug	1335	0	1.5	1.5	1.28	85.3
2X	19 Aug	1530	1.5	6.5	5	1.08	21.6
3X	19 Aug	1745	6.5	11.5	5	5.26	105.2
4X	19 Aug	2030	11.5	16.5	5	5.29	105.8
5X	19 Aug	2135	16.5	21.5	5	2.46	49.2
6X	19 Aug	2235	21.5	26.5	5	5.2	104.0
7X	20 Aug	0001	26.5	31	4.5	4.09	90.9
8X	20 Aug	0140	31	36	5	3.53	70.6
9X	20 Aug	0303	36	41	5	4.35	87.0
10X	20 Aug	0430	41	46	5	3.96	79.2
11X	20 Aug	0530	46	50	4	4.44	111.0
12X	20 Aug	0645	50	55	5	3.29	65.8
13X	20 Aug	0800	55	60	5	1.41	28.2
14X	20 Aug	0900	60	65	5	3.39	67.8
15X	20 Aug	1115	65	69	4	4.2	105.0
16X	20 Aug	1200	69	74	5	3.53	70.6
17X	20 Aug	1330	74	78	4	2.1	52.5
18X	20 Aug	1700	78	81.2	3.2	2.15	67.2
19X	20 Aug	1930	81.2	86.2	5	1.06	21.2
20X	20 Aug	2050	86.2	91.2	5	4.77	95.4
21X	20 Aug	2210	91.2	96.2	5	3.51	70.2
22X	20 Aug	2310	96.2	101.2	5	0.39	7.8
23X	21 Aug	0100	101.2	106.2	5	1.33	26.6
24X	21 Aug	0215	106.2	110.2	4	4.71	117.8
25X	21 Aug	1100	110.2	115.2	5	3.92	78.4
26X	21 Aug	1240	115.2	120.2	5	2.14	42.8
27X	21 Aug	1400	120.2	125.2	5	3.68	73.6
28X	21 Aug	1515	125.2	128.2	3	2.34	78.0
29X	21 Aug	1640	128.2	133.2	5	3.97	79.4
30X	21 Aug	1740	133.2	134.7	1.5	2.79	186.0
31X	21 Aug	1940	134.7	139.7	5	1.5	30.0
32X	21 Aug	2045	139.7	144.2	4.5	5.32	118.2
33X	21 Aug	2150	144.2	149	4.8	3.87	80.6
34X	21 Aug	2250	149	154	5	3.05	61.0
35X	21 Aug	2355	154	159	5	5.48	109.6
36X	22 Aug	0110	159	163.5	4.5	0.21	4.7
37X	22 Aug	0210	163.5	166.5	3	3.42	114.0
38X	22 Aug	0315	166.5	170.68	4.18	5.31	127.0
39X	22 Aug	0500	170.68	173.08	2.4	1.03	42.9
40X	22 Aug	0630	173.08	178.08	5	5.28	105.6
41X	22 Aug	0740	178.08	182.49	4.41	0.17	3.9
42X	22 Aug	0845	182.49	187.49	5	4.92	98.4
43X	22 Aug	1000	187.49	191.99	4.5	4.53	100.7
44X	22 Aug	1110	191.99	195.93	3.94	3.94	100.0
45X	22 Aug	1240	195.93	197	1.07	1.49	139.3
46X	22 Aug	1400	197	202	5	3.63	72.6
47X	22 Aug	1515	202	205.5	3.5	5.49	156.9

Table T1 (continued).

Core	Date (2004)	Time (UTC)	Depth (mbsf) Top	Depth (mbsf) Bottom	Length (m) Cored	Length (m) Recovered	Recovery (%)
48X	22 Aug	1630	205.5	210	4.5	5.2	115.6
49X	22 Aug	1745	210	215	5	5.5	110.0
50X	22 Aug	1910	215	218.74	3.74	2.24	59.9
51X	22 Aug	2010	218.74	220.94	2.2	2.68	121.8
52X	22 Aug	2120	220.94	225	4.06	1.95	48.0
53X	22 Aug	2225	225	230	5	5.29	105.8
54X	22 Aug	2330	230	235	5	0.51	10.2
55X	23 Aug	0040	235	239.6	4.6	5.4	117.4
56X	23 Aug	0145	239.6	244.6	5	3.64	72.8
57X	23 Aug	0315	244.6	249.6	5	5.57	111.4
58X	23 Aug	0500	249.6	254.6	5	5.22	104.4
59X	23 Aug	1650	254.6	257.6	3	4.47	149.0
60X	23 Aug	1830	257.6	262.6	5	4.55	91.0
61X	23 Aug	1940	262.6	267.6	5	2.58	51.6
62X	23 Aug	2050	267.6	270.1	2.5	4.09	163.6
				Cored totals:	270.1	213.15	78.9
302-M0003A-							
1H	26 Aug	0115	0	5	5	5.05	101.0
2H	26 Aug	0315	5	10	5	4.8	96.0
3H	26 Aug	1630	10	15	5	5	100.0
				Cored totals:	15	14.85	99.0
302-M0004A-							
1H	28 Aug	0140	17	20.5	3.5	3.53	100.9
2X	28 Aug	0345	20.5	25.5	5	3.79	75.8
3X	28 Aug	0450	25.5	30.5	5	2.79	55.8
4X	28 Aug	2335	265	270	5	0.33	6.6
5X	29 Aug	0050	270	273.5	3.5	2.11	60.3
6X	29 Aug	0210	273.5	278.5	5	5.28	105.6
7X	29 Aug	0320	278.5	282.3	3.8	5.18	136.3
8X	29 Aug	0430	282.3	287.3	5	0.28	5.6
9X	29 Aug	0550	287.3	291.85	4.55	0.36	7.9
10X	29 Aug	0715	291.85	297.3	5.45	5.34	98.0
11X	29 Aug	0835	297.3	301.35	4.05	5.43	134.1
12X	29 Aug	1000	301.35	306.35	5	0.02	0.4
13X	29 Aug	1115	306.35	310.85	4.5	0	0.0
14X	29 Aug	1300	310.85	313.35	2.5	0	0.0
15X	29 Aug	1530	313.35	315.35	2	0.26	13.0
16X	29 Aug	1820	315.35	318.8	3.45	0	0.0
17X	29 Aug	1950	318.8	318.81	0.01	0	0.0
18X	29 Aug	2120	318.8	320.53	1.73	0.16	9.2
19X	30 Aug	0030	320.53	326.28	5.75	3.17	55.1
20X	30 Aug	0550	326.28	329.28	3	2	66.7
21X	30 Aug	1230	329.28	330.18	0.9	3.58	397.8
22X	30 Aug	1550	339	341.6	2.6	0.98	37.7
23X	30 Aug	1230	341.6	345.6	4	4.07	101.8
24X	31 Aug	1550	355.6	360.6	5	0	0.0
25X	31 Aug	0050	360.6	365.6	5	0	0.0
26X	31 Aug	0300	365.6	367.4	1.8	0	0.0
27X	31 Aug	0700	367.4	371.8	4.4	4.85	110.2
28X	31 Aug	0900	371.8	375.8	4	5.23	130.8
29X	31 Aug	1100	375.8	380.3	4.5	1.32	29.3
30X	31 Aug	1240	380.3	383.2	2.9	4.24	146.2
31X	31 Aug	1405	383.2	388	4.8	0.55	11.5
32X	31 Aug	1540	388	392.5	4.5	3.04	67.6
33X	31 Aug	1710	392.5	396.25	3.75	1.65	44.0
34X	31 Aug	1850	396.25	401.2	4.95	3.89	78.6
35X	31 Aug	2035	401.2	405.7	4.5	3.59	79.8
36X	31 Aug	2210	405.7	410.7	5	0	0.0
37X	31 Aug	2340	410.7	415.1	4.4	0	0.0
38X	1 Sep	0115	415.1	420	4.9	0	0.0
39X	1 Sep	0315	420	424	4	0	0.0
40X	1 Sep	0450	424	424.5	0.5	0	0.0
41X	1 Sep	0815	424.5	426.6	2.1	0.33	15.7
42X	1 Sep	1030	426.6	427.9	1.3	1.06	81.5
				Cored totals:	157.59	78.41	49.8

Table T1 (continued).

Core	Date (2004)	Time (UTC)	Depth (mbsf) Top	Depth (mbsf) Bottom	Length (m) Cored	Length (m) Recovered	Recovery (%)
302-M0004B-							
1X	2 Sep	2230	10	15	5	2.31	46.2
2W	3 Sep	2000	212	215	3	1	33.3
3X	3 Sep	2350	215	218	3	4	133.3
				Cored totals:	11	7.31	66.5
302-M0004C-							
1H	4 Sep	1510	0	4	4	3.91	97.8
2H	4 Sep	2020	4	8.95	4.95	4.95	100.0
3H	4 Sep	2320	8.95	13.97	5.02	5.02	100.0
4H	5 Sep	0545	13.97	18.57	4.6	4.6	100.0
5X	5 Sep	0715	18.57	26.43	7.86	0.75	9.5
6X	5 Sep	0915	23.57	27.83	4.26	1.72	40.4
7X	5 Sep	1030	26.43	31.43	5	0	0.0
8X	5 Sep	1150	31.43	34.43	3	2.42	80.7
9X	5 Sep	1400	34.43	37.33	2.9	1.96	67.6
				Cored totals:	41.59	25.33	60.9

Note: UTC = Universal Time Coordinated.

Table T2. Breakdown of operational time while on site during Expedition 302.

Date (2004)	Time (h) T	P	D	W	B	TR	Total	Comments
15 Aug	8.50	2.50			2.00		13	Chicksan valve broken
16 Aug	6.00			5.00	13.00		24	Extended core barrel lost
17 Aug					24.00		24	BHA lost; chicksan valve broken
18 Aug				13.00	11.00		24	Repair of chicksan valve
19 Aug			9.58		14.42		24	
20 Aug			22.83	1.17			24	
21 Aug			15.83	8.17			24	
22 Aug			24.00				24	
23 Aug			10.00	14.00			24	
24 Aug	9.50	1.00		10.00		3.50	24	
25 Aug	10.67	1.00	1.00		11.33		24	Iron roughneck failed; reflective seismics (D)
26 Aug		3.50	4.25		16.25		24	Wireline termination failed
27 Aug	13.50		1.50		1.75	7.25	24	Chicksan valve broken third time
28 Aug			21.33		2.67		24	APC stuck
29 Aug			24.00				24	
30 Aug			24.00				24	
31 Aug			24.00				24	
1 Sept	4.75	5.42	11.67	1.00	1.17		24	
2 Sept	1.83		2.92		19.25		24	Logging failed, plugged bit
3 Sept			23.08	0.92			24	
4 Sept		5.50	12.67		5.83		24	Equipment frozen
5 Sept	8.33		8.75		6.92		24	APC stuck in BHA
6 Sept	5.00		6.50		8.00	4.50	24	Maintenance of ships; reflective seismics (D)
Totals:	68.1	18.9	247.9	53.3	137.6	15.3	541	
Percent:	12.6	3.5	45.8	9.8	25.4	2.8		

Notes: T = trip time, P = preparation time on rig floor, D = drill time, W = wait for better ice conditions, B = breakdown time, TR = transit time. BHA = bottom-hole assembly, APC = advanced piston corer. Approval was given to start running pipe on Site M0001 at 1100 h on 15 August.

Table T3. Summary of lithologic units and occurrences by section, Holes M0002A, M0003A, M0004A, M0004B, and M0004C.

Unit	General lithologies	Depth (mbsf)	Thickness (m)	Age	Core, Section, Interval (cm)
1	Brown, olive, gray, and black silty clay, silty mud, and clayey silt, with intervals of color banding and isolated sand lenses. Isolated pebbles throughout.	0.00–220.24	220.24	Holocene to middle Eocene	302-M0002A-1X-1, 0 cm, to 51X-1, 150 cm, (0–220.24 mbsf) 302-M0003A-1H-1, 0 cm, to H-CC, 5 cm (0–15 mbsf) 302-M0004A-1H-1, 0 cm, to 3X-2, 128 cm (17.0–28.28 mbsf) 302-M0004B-1X-1, 0 cm, to 1X-2, 85 cm (10.0–12.29 mbsf) 302-M0004B-3X-1, 0 cm, to 3X-CC, 25 cm (215.0–219.0 mbsf) 302-M0004C-1H-1, 0 cm, to 9X-CC, 25 cm (0–36.66 mbsf)
1/1	Brown silty clay, silty mud, and sandy mud, strong color banding, contains biogenic carbonate and isolated pebbles.	0.00–5.29	5.28	Holocene to late Pleistocene	302-M0002A-1X-1, 0 cm, to 2X-1, 108 cm (0–2.58 mbsf) 302-M0003A-1H-1, 0 cm, to 1H-1, 110 cm (0–1.1 mbsf) 302-M0004C-1H-1, 0 cm, to 2H-1, 129 cm (0–5.29 mbsf)
1/2	Brown silty clay, contains minor amounts of biogenic carbonate, with intervals of color banding and isolated sand lenses, isolated pebbles throughout.	2.58–23.59	21.01	late Pleistocene	302-M0002A-2X-1, 108 cm, to 5X-1, 88 cm (2.58–17.38 mbsf) 302-M0003A-1H-1, 110 cm, to 3H-CC, 15 cm (1.1–15.0 mbsf) 302-M0004A-1H-1, 0 cm, to 2X-1, 118 cm (17.0–21.68 mbsf) 302-M0004B-1X-1, 0 cm, to 1X-2, 85 cm (10.0–12.29 mbsf) 302-M0004C-2H-1, 129 cm, to 6X-1, 2 cm (5.29–23.59 mbsf)
1/3	Olive to olive-brown silty clay to silty mud, with color banding and occasional black microconcretions, sand lenses, and isolated pebbles occur throughout.	17.38–168.53	151.15	Pleistocene to middle Miocene	302-M0002A-5X-1, 88 cm, to 38X-3, 45 cm (17.38–168.53 mbsf) 302-M0004A-2X-1, 118 cm, to 3X-2, 128 cm (21.38–28.28 mbsf) 302-M0004C-6X-1, 2 cm, to 9X-CC, 25 cm (23.59–36.66 mbsf)
1/4	Brown silty clay with intervals of color banding and black microconcretions, sand lenses, and isolated pebbles occur throughout.	168.53–192.94	24.41	middle Miocene	302-M0002A-38X-3, 45 cm, to 44X-1, 95 cm (168.53–192.94 mbsf)
1/5	Firm silty clay, tilted gray to black "zebra-stripe" crosscutting couplets, occasional pyrite concretions, sand lenses, and isolated pebbles throughout.	192.94–198.13	5.19	middle Miocene (?)	302-M0002A-44X-1, 95 cm, to 46X-1, 113 cm (192.94–198.13 mbsf)
1/6	Very dark gray, firm homogeneous silty clay to clayey silt with disseminated pyrite and minor amounts of siliceous microfossils; isolated pebbles throughout.	198.13–220.24	22.11	middle Miocene to middle Eocene	302-M0002A-46X-1, 113 cm, to 51X-1, 150 cm, (198.13–220.24 mbsf) 302-M0004B-3X-1, 0 cm, to 3X-CC, 25 cm (215.0–219 mbsf)
2	Very dark gray, laminated, and cross-laminated mud-bearing biosiliceous ooze, with occasional isolated pebbles and pyrite lenses.	220.24–318.96	98.72	middle Eocene	302-M0002A-51X-1, 150 cm, to 62X-CC, 11 cm (220.24–267.71 mbsf) 302-M0004A-4X-1, 0 cm, to 15X-1, 26 cm (265.0–313.61 mbsf)
3	Very dark gray very firm clay to silty clay with occasional laminations and pyrite concretions and minor amounts of siliceous microfossils and biogenic opal.	318.96–404.75	85.97	late Paleocene to early Eocene	302-M0004A-15X-1, 26 cm, to 35X-CC, 18 cm (313.61–404.79 mbsf)
4	Very dark gray clayey mud, silty clay, and silty sand, with sandstone fragments and occasional pyrite concretions.	424.51–427.63	3.12	Late Cretaceous	302-M0004A-41X-1, 0 cm, to 42X-CC, 17 cm (424.50–427.63 mbsf)

Table T4. Core location and depth of isolated pebbles observed during core description, including both the working and archive half, Holes M0002A, M0003A, M0004A, and M0004C.

Core, section, interval (cm)	Depth (mbsf)	Diameter (cm)
302-M0002A-		
6X-2, 141	24.28	1.0
6X-3, 71	25.08	1.0
6X-3, 136	25.73	2.5
7X-1, 88	27.38	5.0
7X-1, 120	27.70	3.0
11X-1, 55	46.55	0.5
11X-1, 144	47.44	0.5
12X-3, 24	52.76	0.5
14X-2, 44	61.95	1.0
17X-2, 4	75.55	0.5
20X-2, 105	88.76	0.5
21X-3, 25	94.47	1.0
21X-CC, 11	94.68	1.0
22X-1, 21	96.41	5.5
23X-2, 109	102.42	2.0
24X-2, 25	107.94	<1.0
24X-3, 78	109.98	1.0
26X-1, 86	116.06	<1.0
26X-2, 12	116.82	1.0
26X-2, 17	116.87	<0.5
26X-2, 41	117.11	<0.5
29X-1, 5	128.25	3.0
29X-1, 92	129.12	2.5
29X-3, 51	131.71	<0.5
33X-3, 30	147.53	<0.5
34X-1, 48	149.48	1.5
34X-CC, 8	151.95	5.0
35X-2, 1.5	154.29	2.0
35X-4, 97	158.24	<0.5
35X-5, 39	159.18	0.5
39X-1, 9	170.77	1.0
40X-1, 105	174.13	0.5
40X-1, 123	174.31	1.0
42X-1, 68	183.17	2.0
43X-3, 73	191.22	1.5
44X-1, 18	192.17	2.0
45X-1, 80	196.73	1.5
47X-5, 45	207.24	1.0
48X-1, 50	206.00	<0.5
48X-1, 77	206.27	0.5
48X-1, 100	206.50	2.0
55X-3, 42	237.03	1.0
55X-3, 109	237.70	1.0
55X-4, 122	239.34	1.0
302-M0003A-		
1H-1, 40.5	0.41	<0.5
1H-1, 43	0.43	<0.5
1H-2, 56	2.06	0.5
3H-2, 97	12.47	1.0
3H-3, 45	13.46	<0.5
302-M0004A-		
1H-1, 32	17.32	1.0
1H-1, 70	17.70	2.5
1H-1, 96	17.96	1.0
2X-2, 50	22.50	1.5
3X-2, 36	27.36	1.0
302-M0004C-		
1H-1, 14.5	0.15	0.5
1H-2, 10	1.61	1.5
1H-3, 31.5	3.34	1.0
2H-1, 24.5	4.25	1.0
3H-1, 140	10.35	1.0
3H-2, 16.5	10.63	0.5
3H-3, 54	12.51	0.5

Table T5. Results of nannoplankton analysis, Hole M0002A.

Core, section, interval (cm)	Abundance
302-M0002A-	
1X-CC, 3–4	B
1X-CC, 8–9	B
3X-CC, 2–3	B
3X-CC, 5–6	B
3X-CC, 8–9	B
4X-CC, 1–2	B
4X-CC, 6–7	B
4X-CC, 10–11	B
6X-CC, 1–2	B
6X-CC, 3–4	B
6X-CC, 5–6	B
6X-CC, 10–11	B
6X-CC, 15–16	B
7X-CC, 1–2	B
7X-CC, 11–12	B
9X-CC, 3–4	B
10X-CC, 1–2	B
10X-CC, 7–8	B
10X-CC, 15–16	B
10X-CC, 23–24	B
12X-CC, 1–2	B
12X-CC, 11–12	B
13X-CC, 1–2	B
13X-CC, 6–7	B
14X-CC, 1–2	B
14X-CC, 9–10	B
16X-CC, 10–11	B
16X-CC, 17–18	B
17X-CC, 15–16	B
18X-CC, 10–11	B
19X-CC	B
20X-CC, 1–2	B
20X-CC, 7–8	B
21X-CC, 1–2	B
21X-CC, 9–10	B
21X-CC, 12–13	B
23X-CC, 1–2	B
23X-CC, 11–12	B
24X-CC, 1–2	B
24X-CC, 7–8	B
24X-CC, 12–13	B
24X-CC, 20–21	B
27X-CC, 1–2	B
27X-CC, 5–6	B
28X-CC, 6–7	B
29X-CC, 1–2	B
29X-CC, 8–9	B
30X-CC	B
31X-CC, 1–2	B
32X-CC, 1–2	B
32X-CC, 10–11	B
33X-CC, 1–2	B
34X-CC, 1–2	B
35X-CC, 2–3	B
36X-CC, 1–2	B
38X-CC, 2–3	B
39X-CC, 1–2	B
40X-CC, 1–2	B
41X-CC, 1–2	B
42X-CC, 1–3	B
43X-3, 152	B
44X-1, top	B
44X-CC, 13–14	B
45X-CC	B
46X-CC, 5–6	B
47X-CC	B
48X-CC	B
49X-CC	B
50X-CC	B
52X-CC	B
53X-CC	B
54X-CC	B
55X-CC	B
56X-CC	B
57X-CC	B
58X-CC	B
60X-CC	B
60X-1, top	B
62X-CC	B

Note: B = barren.

Table T6. Results of nannoplankton analysis, Hole M0004A.

Core, section, interval (cm)	Abundance
302-M0004A-	
4X-1, 0–1	B
6X-CC, 15–16	B
7X-1, 0–1	B
8X-CC, 2–3	B
9X-CC, 2–3	B
10X-2, 147–148	B
10X-CC, 13–14	B
11X-CC, 20–21	B
12X-CC, 1–2	B
15X-CC	B
18X-CC, 0–1	B
19X-CC, 13–14	B
20X-CC, 16–17	B
21X-CC, 15–16	B
22X-1, 0–1	B
22X-CC, 9–10	B
23X-1, 144–145	B
23X-CC, 18–19	B
24X-1, 0–1	B
27X-CC, 2–3	B
28X-CC, 2–3	B
29X-CC, 9–10	B
30X-CC, 9–10	B
31X-CC, 52–53	B
32X-CC, 15–16	B
33X-CC, 12–13	B
34X-CC, 1–2	B
35X-CC, 15–16	B
39X-CC, 0–1	B
41X-1, 0–1	B
41X-CC, 2–3	B
42X-CC, 3–4	B

Note: B = barren.

Table T7. Results of diatom analysis, Hole M0002A. (Continued on next page.)

Core, section, interval (cm)	Depth (mbsf)	Depth (mcd)	Abundance	Preservation	*Actinoptychus irregularis*	*Actinoptychus undulatus*	*Anaulus* spp.	*Brightwellia hyperborea*	*Coscinodiscus* spp.	*Costopyxis trochlea*	*Cymatosira* sp. 1	*Cymatosira* spp.	*Goniothecium coronatum*	*Goniothecium decoratum*	*Goniothecium loricatum*	*Goniothecium odontella* var. *danica*	*Goniothecium* spp.	*Hemiaulus danicus*	*Hemiaulus hostilis*	*Hemiaulus incisus*	*Hemiaulus kittonii*	*Hemiaulus polymorphus*	*Hemiaulus* sp. 1	*Hemiaulus* sp. (*gigantes*?)	*Hemiaulus* spp.	*Huttonia norwegica*	*Hyalodiscus subtilis*	*Kozloviella subrotunda*	*Monobranchia simplex*	*Monobranchia unicornuta*	*Navicula udintsevii*	*Neodelphineis pelagica*	*Nitzschia* spp.	*Odontotropis carinata*	*Paralia crenulata*	*Paralia ornata*	*Paralia simplex*	*Paralia sulcata*	*Pseudopodosira simplex*
302-M0002A-																																						
42X-CC, 0–1	187.26	187.26	B																																			
44X-CC, 14–15	195.88	195.88	B																																			
45X-CC, 15–16	197.40	197.40	B																																			
46X-CC, 6–7	200.61	201.18	R	M																					R													
47X-CC, 0–1	207.31	206.75	R	P																					F									C				
48X-CC, 7–8	210.66	211.80	R	M																														C				
49X-CC, 11–12	215.46	217.78	R	P																			R		R									C				
50X-CC, 0–1	217.15	220.03	R	P					R																									A				
51X-2, 117–118	221.43	224.75	A	G		3	4					1			6			18		4	17			2	25	5			1		1	1		+				1
52X-1, 140–150	222.39	226.41	A	G					+	1		+			4	+	1	9	2	2	17	1	11	1	22	7	+	+								+		
52X-CC*	222.89	226.91	A	G		2	5			8			2		10	28		4	2	2	4	2	+		16	1		1				1	+	+		+	2	
53X-CC*	230.29	232.11	A	G	1		12			2		15		+	14			17		3	4		4		20			+					+			1		
54X-CC*	230.51	232.53	A	G			8			3		1		1	22			15		1	8	1			30					+			+					
55X-CC, 0–1	240.32	241.39	A	G			4			2		5		2	5			4			+		49		10	1		+					+					
56X-CC*	243.24	245.06	A	G			1			1		+		4	4			1					73		9							1	+					
57X-CC*	250.11	251.93	A	G			1			+		8		+	9			6		2	+		60		6	1										+		
58X-CC*	254.82	256.64	A	G		2	2		+	1		41		12	12	+		1					4		10								1		1	1	+	
59X-CC, 0–1	258.99	260.81	A	G					+	+		5			9	+		2	+	2	+		67		5	5							1	+	1			
60X-CC*	262.15	265.09	A	G		1				1	+				12	12		7		3		1	5		5			2					6		+	1		
61X-CC, 0–1	265.30	267.18	A	G						1	+				4			1					70		13								+		3	+		
62X-CC*	271.69	273.51	A	G				+							2								79		+								1		2			

Notes: * = bag. † = without resting spore valves. Abundance: A = abundant, C = common, R = rare, B = barren. Preservation: G = good, M = moderate, P = poor, + = trace.

Table T7 (continued).

Core, section, interval (cm)	Depth (mbsf)	Depth (mcd)	Abundance	Preservation	*Pseudopyxilla* spp.	*Pseudostictodiscus picus*	*Pseudotriceratium radiosoreticulatum*	*Pterotheca aculeifera*	*Pterotheca carinifera*	*Rhizosolenia* spp.	*Riedelia claviger*	*Rocella praenitida*	*Sceptroneis* spp.	*Stephanogonia hanzawae*	*Stephanopyxis hyalomarginata*	*Stephanopyxis* spp.	*Triceratium inconspicuum* var. *trilobata*	*Trinacria cornuta*	*Trinacria* spp.	*Trochosira cornata*	*Trochosira spinosa*	*Trochosira* spp.	Genus et species indet. sp. 1	Genus et species indet. sp. 2	Resting spore sp. 1	*Syndendrium diadema*?	Total valves counted (%)†
302-M0002A-																											
42X-CC, 0–1	187.26	187.26	B																								
44X-CC, 14–15	195.88	195.88	B																								
45X-CC, 15–16	197.40	197.40	B																								
46X-CC, 6–7	200.61	201.18	R	M																							
47X-CC, 0–1	207.31	206.75	R	P	A																		R		A		
48X-CC, 7–8	210.66	211.80	R	M	A		A																				
49X-CC, 11–12	215.46	217.78	R	P	R											R									R		
50X-CC, 0–1	217.15	220.03	R	P	C											A			R								
51X-2, 117–118	221.43	224.75	A	G						2	1				4	3		+	1								100
52X-1, 140–150	222.39	226.41	A	G			+								5	10					4		3				100
52X-CC*	222.89	226.91	A	G			+	2			+				2	3	1		1		1				4	+	100
53X-CC*	230.29	232.11	A	G		1	2					+			+									4	+		100
54X-CC*	230.51	232.53	A	G							+		+		+	2							8				100
55X-CC, 0–1	240.32	241.39	A	G			+				+	+			7	11											100
56X-CC*	243.24	245.06	A	G								1			3	2											100
57X-CC*	250.11	251.93	A	G			1					1	1	+	2	2											100
58X-CC*	254.82	256.64	A	G		+						1		1	3	7											100
59X-CC, 0–1	258.99	260.81	A	G	+				1						+	+		+		2		+					100
60X-CC*	262.15	265.09	A	G	24	3					3	3		3	2	1		5									100
61X-CC, 0–1	265.30	267.18	A	G	3										2	2		+		1							100
62X-CC*	271.69	273.51	A	G	6	1		+				1		1	5	1		1							+		100

Table T8. Results of diatom analysis, Hole M0004A. (Continued on next page.)

Core, section, interval (cm)	Depth (mbsf)	Depth (mcd)	Abundance	Preservation	*Actinoptychus undulatus*	*Anaulus* spp.	*Brightwellia hyperborea*	*Cavitatus jouseanus*	*Coscinodiscus* spp.	*Costopyxis trochlea*	*Cymatosira praecompacta*	*Cymatosira* sp. 1	*Cymatosira* spp.	*Goniothecium loricatum*	*Goniothecium odontella* var. *danica*	*Hemiaulus danicus*	*Hemiaulus hostilis*	*Hemiaulus incisus*	*Hemiaulus kittonii*	*Hemiaulus* sp. 1	*Hemiaulus* spp.	*Huttonia norwegica*	*Odontotropsis carinata*	*Paralia crenulata*	*Paralia ornata*	*Paralia simplex*	*Pseudopyxilla* spp.	*Pseudostictodiscus picus*	*Pseudotriceratium radiosoreticulatum*	*Pterotheca aculeifera*	*Pterotheca carinifera*	*Pyxilla oligocenica*	*Rhizosolenia* spp.	*Riedelia claviger*
302-M0004A-																																		
2X-2	23.50	23.24	B	P																														
3X-1	27.01	25.18	B	P																														
4X-1	265.33	265.33	A	G				*				2	*	6	4	2		1	1	74	2	1	1		*		3			*				
6X-CC	278.78	278.78	A	G	8		*				*	*	*	6	4	4	1			8	6		*		*		29	5		10		2		5
7X-1	280.02	280.22	A	G							5	4	*	3	4	1	*			37	3	*	*		2		10	1		12		1	1	8
8X-CC	282.58	286.58	A	G	1				1	1	2	2		11		1	1			9	17		*		6	3	17			18				4
9X-CC	287.66	287.66	A	G	1	*					1	5		2		1					2	1	1	1	1	1	32	*		14	13	2		15
10X-2, 147–150	294.84	294.84	A	G							3	6		3	4		1			1	4		4		6		27	2		7	4			8
10X-CC	297.19	297.19	A	G		1				1	3			8	2					12	6		2		1	1	26	10		13	1			
11X-CC, 18–23	302.71	302.71	A	G					1	1	5	7		3	5					7	4		1		*		26	1		29				*
12X-CC	301.37	301.35	A	G						2	5	3								1	3		2	1	2	1	8	*		57	2	3		1
15X-CC	313.61	313.61	R	P										C						R	R		F		R			R		C		R		R
18X-CC	318.96	318.96	R	P					R					R									C					R	R	R				
19X-CC	323.70	323.70	R	P																														R
20X-CC	328.28	328.28	B	P																														
21X-CC	332.86	332.86	B	P																														
22X-CC	339.98	339.98	B	P																														

Notes: Abundance: A = abundant, C = common, R = rare, B = barren. Preservation: G = good, P = poor. * = without resting spore valves.

Table T8 (continued).

Core, section, interval (cm)	Depth (mbsf)	Depth (mcd)	Abundance	Preservation	*Riedelia* sp. (straight)	*Sceptroneis* spp.	*Stephanogonia hanzawae*	*Stephanopyxis hyalomarginata*	*Stephanopyxis* sp. 1	*Stephanopyxis* spp.	*Trinacria cornuta*	*Trochosira cornata*	Resting spore sp. 1	*Syndendrium diadema*?	Total valves counted* (%)
302-M0004A-															
2X-2	23.50	23.24	B	P											0
3X-1	27.01	25.18	B	P											0
4X-1	265.33	265.33	A	G		*	2	1		*		*	*	2	100
6X-CC	278.78	278.78	A	G	*		1	2	3	5	1			*	100
7X-1	280.02	280.22	A	G	1	2	*	1	2	1	1	*			100
8X-CC	282.58	286.58	A	G		*		1	1	2	2				100
9X-CC	287.66	287.66	A	G			1			2	4				100
10X-2, 147–150	294.84	294.84	A	G		*	10			4	6		1		100
10X-CC	297.19	297.19	A	G			6	*		2	5				100
11X-CC, 18–23	302.71	302.71	A	G	2		1	2		2	3			4	100
12X-CC	301.37	301.35	A	G			4			2	2	1	1	6	100
15X-CC	313.61	313.61	R	P				F		F	F				
18X-CC	318.96	318.96	R	P				R		T	C				
19X-CC	323.70	323.70	R	P											
20X-CC	328.28	328.28	B	P											0
21X-CC	332.86	332.86	B	P											0
22X-CC	339.98	339.98	B	P											0

Table T9. The occurrences of silicoflagellate taxa and total ebridians, Hole M0002A.

Core, section, interval (cm)	Depth (mbsf)	Depth (mcd)	Silicoflagellate abundance	Silicoflagellate preservation	Ebridian abundance	Ebridian preservation	*Corbisema apiculata*	*Corbisema bimucronata rotaria?*	*Corbisema glezerae*	*Corbisema hastata cunicula?*	*Corbisema hastata globulata*	*Corbisema hastata hastata*	*Corbisema hexacantha*	*Corbisema ovalis*	*Corbisema spinosa*	*Corbisema toxeuma*	*Corbisema* aff. *toxeuma*	*Dictyocha arctios*	*Dictyocha carentis incerta*	*Dictyocha crux crux*	*Dictyocha crux parvus*	*Dictyocha curta*	*Dictyocha deflandrei*	*Dictyocha deflandrei* (asperoid)	*Dictyocha frenguelli*	*Dictyocha frenguelli* (circular)	*Dictyocha lockerii*	*Dictyocha pentagona*	*Dictyocha pentagona* (small)	*Dictyocha rotundata*	*Dictyocha* aff. *subarctios*	*Dictyocha varians*	*Dictyocha* sp. A	*Dictyocha* sp. B	*Distephanus antiquus*	*Distephanus quinarius*	*Distephanus quinquangellus*	*Distephanus speculum*	*Mesocena apiculata inflata*	*Naviculopsis biapiculata*	*Naviculopsis constricta*	*Naviculopsis punctilia*	*Naviculopsis robusta*	Aberrant *(Corbisema)*
302-M0002A-																																										
45X-CC, 1–5	197.27	197.27	B	P	B	P																																				
46X-CC, 6–8	200.61	201.18	B	P	B	P																																				
47X-CC, 3–5	207.34	206.78	A	M	C	M	X			X	X	X	X		X					X	X		X				X							X	X						
48X-CC, 4–6	210.63	211.77	A	G	A	G	X				X	X	X		X		X																								
FO (*C. hexacantha* 44.1 Ma)																																										
49X-CC, 2–4	215.37	217.69	R	M	C	M	X		X	X	X				X	X		X					X		X							X	X	X		X		X	X	X		
50X-CC, 8–10	217.23	220.11	R	M	F	M	X				X	X						X					X	X	X	X		X				X		X		X		X	X			
51X-2, 117–118	221.43	224.75	A	G	F	G	X					X				X							X	X	X	X						X	X	X	X		X		X		X	
52X-1, 0–2	220.95	224.97	A	G	F	G	X				X	X			X	X			X				X	X	X			X				X	X	X								
52X-CC, 20–22	222.92	226.94	A	G	C	G	X			X	X	X			X	X		X				X	X	X	X		X	X				X	X	X	X							
53X-CC, 13–15	230.28	232.10	A	G	F	G	X		X		X	X				X		X					X	X	X			X				X	X	X								
54X-CC, 5–7	230.50	232.52	A	G	F	G	X		X		X	X				X		X	X				X		X			X				X	X	X								
55X-CC, 8–10	240.40	241.47	A	G	F	G	X		X	X	X	X				X		X					X	X	X	X		X				X	X	X	X							
56X-CC, 18–20	243.13	244.95	A	G	C	G	X	X	X	X	X	X		X		X		X		X			X	X	X	X		X	X				X	X		X						
57X-CC, 0–2	249.95	251.77	A	G	C	G	X		X		X	X						X		X			X	X	X	X		X	X					X	X		X	X				
58X-CC, 9–11	254.81	256.63	A	G	C	G	X				X	X				X			X	X			X	X	X	X		X	X	X			X									
59X-CC, 2–4	259.01	260.83	A	G	C	G	X					X				X		X	X	X			X		X			X	X				X	X								
60X-1, 0–2	257.61	260.55	A	G	C	G	X				X	X							X	X			X		X	X			X	X			X									
61X-CC, 0–1	265.30	267.18	A	G	A	G	X				X				X		X		X	X			X		X	X					X											X
62X-CC, 9–11	271.69	273.51	A	G	A	G	X			X	X	X			X		X	X	X	X		X	X		X				X	X		X									X		

Notes: All samples above Sample 302-M0002A-45X-CC are barren of silicoflagellates and ebridians. Abundance: A = abundant, C = common, F = few, R = rare, B = barren. Preservation: G = good, M = moderate, P = poor. FO = first occurrence.

Table T10. Occurrences of silicoflagellate taxa and total ebridians, Holes M0004A and M0004B.

Core, section, interval (cm)	Depth (mbsf)	Depth (mcd)	Silicoflagellate abundance	Silicoflagellate preservation	Ebridian abundance	Ebridian preservation	*Corbisema apiculata*	*Corbisema glezerae*	*Corbisema hastata cunicula?*	*Corbisema hastata globulata*	*Corbisema hastata hastata*	*Corbisema hexacantha*	*Corbisema ovalis*	*Corbisema spinosa*	*Corbisema toxeuma*	*Corbisema triacantha*	*Dictyocha arctios*	*Dictyocha carentis incerta*	*Dictyocha curta*	*Dictyocha deflandrei*	*Dictyocha deflandrei* (asperoid)	*Dictyocha frenguellii*	*Dictyocha frenguellii* (circular)	*Dictyocha pentagona*	*Dictyocha rotundata*	*Dictyocha varians*	*Dictyocha* sp. B	*Mesocena apiculata apiculata*	*Mesocena apiculata inflata*	*Mesocena inflata inflata* (no spine)	*Mesocena occidentalis*	Aberrant (*Corbisema*)
302-M0004A-																																
2X-1, 149–151	22.00	21.74	B	P	B	P																										
2X-2, 0–2	22.01	21.75	B	P	B	P																										
3X-1, 149–151	27.00	25.17	B	P	B	P																										
4X-1, 0–3	265.02	265.02	C	M	C	M	X	X		X	X		X		X		X	X		X	X	X	X		X		X					
6X-5, 16–18	278.77	278.77	C	G	A	G	X	X			X						X	X	X	X		X			X							
7X-1, 0–2	278.51	278.71	C	M	C	M	X								X		X	X	X	X		X	X		X				X			
8X-CC, 5–7	282.57	286.57	C	G	C	G	X	X		X	X						X	X	X	X		X			X					X		
9X-CC, 7–9	287.65	287.65	C	M	C	M	X	X		X	X						X	X	X	X		X			X							
10X-2, 147–150	294.84	294.84	C	M	A	M	X	X		X							X	X	X	X		X			X							
10X-CC, 3–5	297.08	297.08	A	M	A	M	X	X		X	X					X	X	X		X		X	X	X		X						X
11X-CC, 21–23	302.72	302.72	A	G	A	G	X	X		X	X					X				X	X	X	X			X		X	X			X
12X-CC, 0–2	301.36	301.36	A	G	C	G	X	X		X	X					X	X	X		X		X	X		X	X			X			X
15X-CC, 24–26	313.60	313.60	R	P	C	P	X	X			X		X						X	X	X	X										
18X-CC, 14–16	318.95	318.95	R	P	F	P	X	X			X		X				X			X		X										
19X-CC, 14–16	323.69	323.69	B	P	B	P																										
20X-CC, 19–21	328.27	328.27	B	P	B	P																										
21X-CC, 0–2	332.67	332.67	B	P	B	P																										
22X-1, 0–2	339.01	339.01	B	P	B	P																										
23X-1, 3–5	341.64	341.64	B	P	B	P																										
23X-CC, 20–22	345.66	345.66	B	P	B	P																										
27X-1, 3–5	367.44	367.44	B	P	B	P																										
28X-CC, 3–5	377.02	377.49	B	P	B	P																										
29X-CC, 3–5	377.04	379.04	B	P	B	P																										
30X-CC, 9–12	384.53	384.53	B	P	B	P																										
31X-CC, 53–55	383.74	385.24	B	P	B	P																										
32X-CC, 16–18	391.03	391.03	B	P	B	P																										
33X-CC, 13–15	394.14	394.14	B	P	B	P																										
34X-CC, 9–11	400.13	400.13	B	P	B	P																										
35X-CC, 16–18	404.78	404.78	B	P	B	P																										
39X-CC, 48–50	420.49	420.49	B	P	B	P																										
42X-CC, 11–13	427.55	427.55	B	P	B	P																										
302-M0004B-																																
1X-CC, 0–2	12.30	12.46	B	P	B	P																										
1X-CC, 0–2	12.30	12.46	B	P	B	P																										
3X-CC, 0–2	218.76	218.76	C	M	C	M			X	X		X		X																		X
3X-CC, 11–13	218.87	218.87	C	M	C	M				X	X	X		X																		
3X-CC, 22–24	218.98	218.98	C	M	C	M				X	X	X		X																		

Notes: Abundance: A = abundant, F = few, C = common, R = rare, B = barren. Preservation: G = good, M = moderate, P = poor.

Table T11. Results of radiolarian analysis, Hole M0002A.

Core, section, interval (cm)	Depth (mbsf)	Depth (mcd)	Abundance	Preservation	Epoch	*Calocyclas talwanii*	*Botryostrobis joides*	*Botryospera? pseudoantarctissa?*	*Lophocorys* sp.	*Pseudodictyophimus* sp.
302-M0002A-										
49X-CC, bottom	215.50	217.82	VR	M	l–m Eocene	+	+	+	+	+
50X-CC, 8–10	217.23	220.11	T	M	l–m Eocene	+		?		

Notes: Abundance: VR = very rare, T = trace. Preservation: M = moderate.

Table T12. Results of foraminifer and ostracode analyses, Hole M0002A.

Core, section, interval (cm)	Depth (mbsf)	Depth (mcd)	Abundance	Preservation	*Cyclammina pusilla*	*Rhabdammina* sp.	*Alveolophragmium polarensis*	*Cyclammina* ex gr. *cancellata*	*Recurvoides* spp.	Pyritized diatoms	Fish debris	Other
302-M0002A-												
12X-CC, 3–5	53.26	56.20	B									
13X-CC, 3–5	56.54	59.48	B									
14X-CC, 1–3	63.28	63.28	B									
16X-CC, 17–19	72.52	72.86	B									
17X-CC, 18–20	76.09	76.09	B									
18X-CC, 13–15	80.14	80.14	B									
19X-CC	81.20	82.26	B									
20X-CC, 7–9	90.96	90.96	B									
21X-CC, 12–14	94.70	94.70	B									
23X-CC, 10–13	101.45	101.45	R	P	X							
24X-CC, 20–24	110.90	110.90	B									
27X-CC, 6–8	123.87	123.87	B									
28X-CC, 8–10	127.53	127.53	B									
29X-CC, 10–12	132.14	132.14	B									
31X-CC	136.05	139.20	R			X						
32X-CC, 6–8	144.94	144.94	B									
33X-CC, 5–8	147.94	148.74	B									
34X-CC, 1–3	151.89	151.89	B									
35X-CC, 0–2	158.80	158.80	R			X	X					
36X-CC, 0–2	159.01	159.01	R									X
38X-CC, 0–3	171.72	171.72	B									
39X-CC, 1–3	171.50	172.70	R		X							X
40X-CC, 0–2	178.25	178.25	R		X			X				X
40X-CC, 8–10	178.33	178.33	R						X			
41X-CC, 1–3	178.60	178.60	B									
42X-CC, 1–3	187.27	187.27	R		X				X			X
44X-CC	195.73	195.93	B									
45X-CC	197.24	197.42	B									
46X-CC	200.54	201.20	B							X		
47X-CC	207.30	206.93	B							X		
48X-CC	210.58	211.84	B							X		
49X-CC	215.34	217.82	B							X		
50X-CC	217.14	220.12	B									
52X-CC	222.71	226.91	B									
53X-CC	230.14	232.11	B								X	
54X-CC	230.44	232.53	B								X	
55X-CC	240.31	241.48	B								X	
56X-CC	242.94	245.06	B								X	
57X-CC	249.94	251.93	B									
58X-CC	254.71	256.64	B								X	
60X-1, 0–5	257.60	262.05	B									
60X-CC	261.90	265.09	B								X	
62X-CC	271.59	273.51	B									

Notes: Abundance: R = rare, B = barren. Preservation: P = poor.

Table T13. Results of foraminifer and ostracode analyses, Hole M0004A. (Continued on next page.)

Core, section, interval (cm)	Depth (mbsf)	Depth (mcd)	Abundance	*Ammodiscus glabratus*	*Ammodiscus planus*	*Ammodiscus* spp.	*Convallina logani/dawsoni*	*Glaphyammina spirocompressa*	*Glomospirella?* sp.	*Haplophragmoides perexilis*	*Haplophragmoides reindeerensis*	*Haplophragmoides* spp.	*Hyperammina* sp.	*Jaculella* sp.	*Karrerulina* sp.	*Labrospira* sp.	*Lagenammina* sp.	*Miliammina* sp.	*Nothia* spp.	*Portatrochammina tagluensis*	*Psammosphaera* sp.	*Psammosphaera eocenica*	*Psammosphaera fusca*	*Psammosphaera trinitatensis*	*Recurvoides* cf. *obskiensis*	*Recurvoides rectangulatus*	*Recurvoides* spp.	*Reophax scorpiurus*	*Reophax subfusiformis*	*Reophax* spp.	*Reticulophragmium arcticum*	*Reticulophragmium boreale*	*Reticulorphragmium ministicoogense*	*Rhabdammina* sp.	*Rhizammina* sp.	*?Sculptobaculites* sp.	*Trochammina* (small species)	*Trochamminoides* sp.
302-M0004A-																																					
4X-CC	265.00	265.33	B																																		
6X-CC	278.60	278.78	B																																		
7X-CC	282.84	283.88	B																																		
8X-CC	282.51	286.58	B																																		
9X-CC	287.57	287.66	B																																		
10X-CC	297.04	297.19	B																																		
11X-CC	302.50	302.73	B																																		
12X-CC	301.35	301.35	B																																		
15X-CC	313.35	313.61	B																																		
18X-CC	318.80	318.96	B																																		
19X-CC	323.54	323.70	B																																		
20X-CC	328.07	328.28	B																																		
21X-CC	332.66	332.86	B																																		
22X-CC	339.85	339.98	B																																		
23X-CC	345.45	345.67	B																																		
23X*	345.45	345.67	B																																		
24X-CC	355.60	357.10	B																																		
27X†	372.20	372.25	B																																		
27X-CC	372.20	372.25				X?	X		X?	X		X					X?	X		X	X	X		X		X										
28X-CC	376.98	377.50							X	X		X																									
29X-CC	377.00	379.12				X	X							X	X								X					X		X	X						
30X-CC	384.42	384.54																																			
31X-CC	383.20	385.25																																			
32X-CC	390.86	391.04			X						X		X			X		X	X				X			X				X	X	X	X	X			
33X-CC	394.00	394.15			X						X					X		X?					X			X				X	X	X		X		X	
35X-CC	404.61	404.79			X	X												X								X						X	X				
39X-CC	420.00	421.50																																			X
41X-CC	424.78	424.83						X																	X		X							X			X
42X-CC, 1	427.43	427.66																									X										X
42X-CC, 2	427.43	427.66																									X										X

Notes: * = trim, † = cutting. A = abundant, F = few, C = common, R = rare, B = barren.

Table T13 (continued).

Core, section, interval (cm)	Depth (mbsf)	Depth (mcd)	Abundance	*Verneuilinoides macintyrei*	*Verneuilinoides* cf. *polystrophus*	*Verneuilinoides subtilis*	Indeterminate genus	*Avolla*	Ferromanganese micronodules?	Fish parts	Fish teeth	Large spores	Other	Comments
302-M0004A-														
4X-CC	265.00	265.33	B						1	C		R (2 types)		Little quartz
6X-CC	278.60	278.78	B							A	2	R		
7X-CC	282.84	283.88	B							F	1	Large	Iron?	Muddier
8X-CC	282.51	286.58	B						1	A			Iron?	
9X-CC	287.57	287.66	B					R					Pyrite diatom?	
10X-CC	297.04	297.19	B					C		A	4	?		
11X-CC	302.50	302.73	B					A						All *Azolla*
12X-CC	301.35	301.35	B					A						
15X-CC	313.35	313.61	B							R?			Lithified sediment; large pyrite	
18X-CC	318.80	318.96	B							R			Laminated; almost no quartz	
19X-CC	323.54	323.70	B							C		?		Possible spore contamination
20X-CC	328.07	328.28	B						1	C	1			
21X-CC	332.66	332.86	B							R	1	?		
22X-CC	339.85	339.98	B							R			Pyrite, laminae	
23X-CC	345.45	345.67	B							A			White sediment	
23X*	345.45	345.67	B							A			Phosphatic? grains	
24X-CC	355.60	357.10	B						1?	R			Flaser bedding?, metamorphic grains	
27X†	372.20	372.25	B							A		C	Abundant pyrite and tubes	
27X-CC	372.20	372.25				X							Quartz sand, pyrite	
28X-CC	376.98	377.50		X		X	X						Quartz, coarse, wood	
29X-CC	377.00	379.12												
30X-CC	384.42	384.54					X			C			Abundant pyrite	
31X-CC	383.20	385.25					X			C			Abundant pyrite, angular quartz	
32X-CC	390.86	391.04			X		X						Abundant pyrite, angular quartz	
33X-CC	394.00	394.15			X				X?				Pyrite, large metamorphic grains	
35X-CC	404.61	404.79											Poorly sorted sand, pyrite	
39X-CC	420.00	421.50											Much sand, pyrite, large concretions, bedrock grains	
41X-CC	424.78	424.83								R			Pyrite balls, pyritization; agglutinations	
42X-CC, 1	427.43	427.66								R			Sandstone clasts, pyrite, firm clay	
42X-CC, 2	427.43	427.66											Sandstone clasts, pyrite, firm clay	

Table T14. Results of Neogene foraminifer and ostracode analyses, Holes M0001A, M0002A, M0003A, M0004B, and M0004C.

Core, section, interval (cm)	Depth (mbsf)*	Depth (mcd)	*Alveolophragmium polarensis*	*Ammodiscus* spp.	*Cyclammina pusilla*	*Haplophragmoides carinatus*	*Recurvoides* sp.	*Reophax* sp.	*Rhizammina* sp.	*Trochammina* sp.	*Saccammina* sp.	*Neogloboquadrina pachyderma* (sinistral)	*Turborotalita quinqueloba*	*Cassidulina teretis*	Ostracodes
302-M0001A-															
1H-CC, 2–4	0.03	NA										X	X?	X	X
1H-CC, 14–16	0.15	NA										X			X
1H-CC, 26–28	0.27	NA			X										
1H-CC, 10–12	0.11	NA			X										
1H-CC, 20–22	0.21	NA			X										
302-M0002A-															
1X-CC, 6–8	1.26	1.54													
3X-CC, 7–9	11.73	16.27			X										
4X-CC, 11–13	16.79	16.79			X										
6X-CC, 11–13	26.65	28.31			X	X									
7X-CC, 12–16	30.57	35.14													
9X-CC, 4–8	41.52	45.59													
10X-CC, 14–18	44.90	48.41			X										
302-M0003A-															
2H-CC, 14–19	9.78	14.93			X	X				X	X				
3H-CC, 0–1	14.96	19.29								X					
3H-CC, 2–3	14.98	19.31								X					
3H-CC, 2–5	14.99	19.32	X		X							X			X
3H-CC, 4–5	15.00	19.33			X	X	X					X	X	X	
302-M0004B-															
1X-CC, 0–2	12.30	12.46			X							X			
302-M0004C-															
1H-CC, 0–2	3.73	3.73													
2H-CC, 0–2	8.73	8.08		X	X		X	X	X						
3H-CC, 0–2	13.67	12.86			X		X		X						
4H-CC, 0–2	18.33	17.04										X			
6X-CC, 0–2	24.61	23.94													
8X-CC, 0–2	33.76	35.20			X										
9X-CC, 0–2	36.37	37.76			X										

Notes: * = composite (upper). NA = not applicable.

Table T15. Palynological analysis, Hole M0001A.

Core, section, interval (cm)	Depth (mbsf)	Abundance	*n* palynomorphs	Bisaccate pollen	*?Brigantednium* spp.
302-M0001A-					
1H-CC, 0–2	0.01	R	7.00	4	3
1H-CC, 23–25	0.24	B			

Note: R = rare, B = barren.

Table T16. Palynological index events, Hole M0002A.

Dinocyst datum	Core, section, interval (cm) Top	Core, section, interval (cm) Bottom	Depth (mbsf) Top	Depth (mbsf) Bottom	Depth (mcd) Top	Depth (mcd) Bottom	Depth (mcd) Mean	Error (±m)	Proposed age (Ma)	Comment
	302-M0002A-	302-M0002A-								
LO *Filisphaera microornata*	10X-CC	12X-CC	44.74	53.22	48.47	56.23	52.35	3.88	1.77	
LO *Filisphaera* spp.	14X-CC	16X-CC	63.26	72.34	63.40	72.87	68.14	4.74	1.77	
LO *Evittosphaerula* sp. 2 Manum et al., 1986	16X-CC	17X-CC	72.34	75.90	72.87	76.10	74.49	1.62	5.9	
LO *Bitectatodinium*? *serratum*	21X-CC	23X-1, 11–13	94.57	101.20	94.71	101.33	98.02	3.31	6.84	
LO *Habibacysta tectata*	21X-CC	23X-1, 11–13	94.57	101.20	94.71	101.33	98.02	3.31	1.5	Too young
FO *Evittosphaerula* sp. 2 Manum et al., 1986	23X-1, 11–13	24X-CC	101.32	110.68	101.32	110.91	106.12	4.80	7.1	
FO *Bitectatodinium*? *serratum*	35X-1, 6–8	36X-CC	154.07	159.00	154.07	159.21	156.64	2.57	11.2	
FO *Habibacysta tectata*	35X-1, 6–8	36X-CC	154.07	159.00	154.07	159.21	156.64	2.57	14	
LO *Wetzeliella gochtii*	44X-CC	45X-CC	195.73	197.24	195.93	197.42	196.68	0.75	27	Reworked?
FO *Wetzeliella gochtii*	45X-CC	46X-CC	197.24	200.54	197.42	201.20	199.31	1.89	33.5	Reworked?
LO *Phthanoperidinium clithridium*	45X-CC	46X-CC	197.24	200.54	197.42	201.20	199.31	1.89	44.6	
LO *Lentinia* cf. *wetzelii*	46X-CC	47X-CC	200.54	207.30	201.20	206.93	204.07	2.87	45.4	
LO *Cerodinium depressum*	47X-CC	48X-CC	207.30	210.58	206.93	211.84	209.39	2.46	44.9	
LO *Thalassiphora delicata*	47X-CC	48X-CC	207.30	210.58	206.93	211.84	209.39	2.46	45.5	
FO *Phthanoperidinium clithridium*	62X-CC	Bottom	271.59	271.59	271.59	271.59	271.59	0.00	46.2	

Note: FO = first occurrence, LO = last occurrence.

Table T17. Palynological analysis, Hole M0002A. (Continued on next two pages.)

Core, section, interval (cm)	Depth (mbsf)	Depth (mcd)	Abundance	Preservation	*n* palynomorphs	Bisaccate pollen	Other pollen	Spores	Fungal spores	*Botryococcus* spp.	*Cymatiosphaera* spp.	*Cyclopsiella* spp.	*Leiosphaeridia* spp.	*Paralecaniella* spp.	*Pediastrum* spp.	*Pterospermella* spp.	*Tasmanites* spp.	Genus et sp. indet. A	Reworked Paleozoic	Reworked Mesozoic	Reworked Paleogene	Dinocysts indet.	*Areoligera tauloma*	*?Bataicasphaera* spp.
302-M0002A-																								
1X-CC, 4–6	1.24	1.52	C	M	111.50	18.5		12		41			3	2	13	1	1		5	7	1			
3X-CC, 5–7	11.71	16.25	B		0.00																			
4X-CC, 5–7	16.73	16.73	B		0.00																			
6X-CC, 7–9	26.61	28.27	B		0.00																			
7X-CC, 3–5	30.47	35.04	R	M	20.00	7				2									3	1	5			
9X-CC, 0–2	41.47	45.54	B		0.00																			
10X-CC, 0–2	44.75	48.26	R	M	1.00														1					
12X-CC, 5–7	53.28	56.22	R	M	35.00	3	3	3								1					3			
13X-CC, 5–7	56.56	59.50	R	M	1.00	1																		
14X-CC, 10–12	63.37	63.37	R	M	7.00					1							1		2		3			
16X-CC, 13–15	72.48	72.82	R	M	11.00	2				7									1					
17X-CC, 17–19	76.08	76.08	R	M	7.50	1.5				1									1					
18X-CC, 11–13	80.12	80.12	R	M	5.00	1				1									2					
19X-1, 0–1	81.21	81.21	B		0.00																			
20X-CC, 5–7	90.94	90.94	R	M	6.00	3				1							1		1					
21X-CC, 6–8	94.64	94.64	R	M	25.00	21				2									2					
23X-1, 11–13	101.32	101.32	R	M	66.00	13	1			4					1				5					1
24X-CC, 21–23	110.90	110.90	C	M	10.00	2	2			2							1		3					
27X-CC, 3–5	123.84	123.84	F	M	273.00	137	2	8	1	2					2				36	1		11		
28X-CC, 5–7	127.50	127.50	B		0.00																			
29X-CC, 5–7	132.09	132.09	B		0.00																			
31X-1, 0–1	134.71	137.71	R	M	20.00	11		2											5			2		
32X-CC, 8–10	144.96	144.96	R	M	25.00	8		1											3			5		3
33X-CC, 3–5	147.91	148.71	R	M	42.00	22		1											7			3		1
34X-CC, 13–15	152.01	152.01	B		0.00																			
35X-1, 6–8	154.07	154.07	R	M	16.00	3																4		2
36X-CC, 15–18	159.17	159.17	R	M	3.00																			
38X-CC, 0–2	171.71	171.71	B		0.00																			
39X-CC, 18–20	171.67	172.87	B		0.00																			
40X-CC, 0–2	178.25	178.25	B		0.00																			
40X-CC, 10–12	178.35	178.35	B		0.00																			
41X-CC, 0–2	178.59	178.59	B		0.00																			
42X-CC, 11–14	187.38	187.38	B		0.00																			
44X-2, 145–151	194.97	194.97	~B	M	14.00	2	2			3									1	3	1	2		
44X-CC, 13–15	195.87	195.87	R	M	159.00	103	5	11				X	2	1				4			3	5		
45X-CC, 16–18	197.41	197.41	A	M	389.00	215	23	14		2		X	1					2		1	3	1		
46X-CC, 7–9	200.62	201.19	A	M	589.00	345	76	24			1	X	8				11	46		1		9		5
47X-CC, 16–19	207.48	206.92	A	M	284.00	83	25	9			1	X	9			3	2	67		3		9		
48X-CC, 10–12	210.69	211.83	A	M	223.00	60	18	9		7		1	7	4				10		1		15		
49X-CC, 64–66	215.99	218.31	A	M	285.00	70	11	8		3		X	12	6		1		37				20	1	
50X-CC, 4–6	217.19	220.07	A	M	198.00	130	11	17		2		X	6					10				5		
52X-CC, 15–16	222.87	226.89	A	M	169.00	65	2	5		2		X	3					6				7		
53X-CC, 0–1	230.15	231.97	A	M	183.00	105	3	9		1		X	2					8		1		6		
54X-CC, 0–5	230.47	232.49	F	M	178.00	50	2	3		1	1	X	7					5				3		1
55X-CC, 0–5	240.34	241.41	F	M	355.00	65	7	12		5		X	20			1		60				2		
56X-CC, 0–5	242.97	244.79	F	M	280.00	55	3	7		2		X	20					160				5		
57X-CC, 0–5	249.97	251.79	F	M	267.00	60	5	8		1		X	15			1		125				5		
58X-CC, 0–5	254.74	256.56	F	M	256.00	52	2	4				X	17					134				6		
59X-CC, 3–5	259.02	260.84	A	M	244.00	6	4	10				64	84	2				4				34		
60X-CC, 0–25	262.03	264.97	A	M	127.00	8	2	4				2	8			1		8				10		
61X-CC, 0–1	265.30	267.18	A	M	290.00	100	4	4				2	8					2				5		
62X-CC, 2–4	271.62	273.44	A	M	243.00	24	1	2				2	14			8		100				5		

Notes: Abundance: A = abundant, C = common, F = few, R = rare, B = barren. Preservation: M = moderate. cpx = complex.

Table T17 (continued).

Core, section, interval (cm)	Depth (mbsf)	Depth (mcd)	Abundance	Preservation	*Bitectatodinium? serratum*	*?Brigantedinium* spp.	*Brigantedinium* spp.	*Cerebrocysta bartonensis*	*Cerebrocysta* sp.	*Cerebrocysta?* sp.	*Cerodinium depressum*	*Cribroperidinium tenuitabulatum*	*Deflandrea phosphoritica*	*Evittosphaerula* sp. 2 Manum et al.	*Filisphaera microornata*	*Filisphaera?* sp.	Genus et sp. indet. B	*Glaphyrocysta texta*	*Habibacysta tectata*	*Heteraulacacysta leptalea*	*Homotryblium tenuispinosum*	*Impagidinium dispertitum* cpx	*Impagidinium japonicum*	*Impagidinium pallidum*	*Impagidinium velorum*	*Impletosphaeridium* spp.	*Lejeunecysta* cf. *cinctoria*	*Lentinia* cf. *wetzelii*	*Lophocysta?* sp.
302-M0002A-																												
1X-CC, 4–6	1.24	1.52	C	M		7																						
3X-CC, 5–7	11.71	16.25	B																									
4X-CC, 5–7	16.73	16.73	B																									
6X-CC, 7–9	26.61	28.27	B																									
7X-CC, 3–5	30.47	35.04	R	M		2																						
9X-CC, 0–2	41.47	45.54	B																									
10X-CC, 0–2	44.75	48.26	R	M																								
12X-CC, 5–7	53.28	56.22	R	M											22													
13X-CC, 5–7	56.56	59.50	R	M																								
14X-CC, 10–12	63.37	63.37	R	M																								
16X-CC, 13–15	72.48	72.82	R	M												1												
17X-CC, 17–19	76.08	76.08	R	M										4														
18X-CC, 11–13	80.12	80.12	R	M										1														
19X-1, 0–1	81.21	81.21	B																									
20X-CC, 5–7	90.94	90.94	R	M																								
21X-CC, 6–8	94.64	94.64	R	M																								
23X-1, 11–13	101.32	101.32	R	M	13		1							6					10				7	2				
24X-CC, 21–23	110.90	110.90	C	M																								
27X-CC, 3–5	123.84	123.84	F	M					4	1						15			25				1	2	1			
28X-CC, 5–7	127.50	127.50	B																									
29X-CC, 5–7	132.09	132.09	B																									
31X-1, 0–1	134.71	137.71	R	M																								
32X-CC, 8–10	144.96	144.96	R	M															4				1					
33X-CC, 3–5	147.91	148.71	R	M												2			6									
34X-CC, 13–15	152.01	152.01	B																									
35X-1, 6–8	154.07	154.07	R	M	1														3						1			
36X-CC, 15–18	159.17	159.17	R	M						1												1						
38X-CC, 0–2	171.71	171.71	B																									
39X-CC, 18–20	171.67	172.87	B																									
40X-CC, 0–2	178.25	178.25	B																									
40X-CC, 10–12	178.35	178.35	B																									
41X-CC, 0–2	178.59	178.59	B																									
42X-CC, 11–14	187.38	187.38	B																									
44X-2, 145–151	194.97	194.97	~B	M																								
44X-CC, 13–15	195.87	195.87	R	M									1				5											2	
45X-CC, 16–18	197.41	197.41	A	M													125										?		
46X-CC, 7–9	200.62	201.19	A	M									1							1						4			
47X-CC, 16–19	207.48	206.92	A	M						1												40					1	4	
48X-CC, 10–12	210.69	211.83	A	M				2			1	1									3	7				6	1	8	
49X-CC, 64–66	215.99	218.31	A	M								3						1				4				25	3	1	1
50X-CC, 4–6	217.19	220.07	A	M																						5		1	
52X-CC, 15–16	222.87	226.89	A	M																		1				4		16	
53X-CC, 0–1	230.15	231.97	A	M								3														4	3	4	
54X-CC, 0–5	230.47	232.49	F	M																						5	2	17	
55X-CC, 0–5	240.34	241.41	F	M																		1						15	
56X-CC, 0–5	242.97	244.79	F	M							1	3															1	7	
57X-CC, 0–5	249.97	251.79	F	M								1															1	9	
58X-CC, 0–5	254.74	256.56	F	M								2																11	
59X-CC, 3–5	259.02	260.84	A	M																						6	6	4	
60X-CC, 0–25	262.03	264.97	A	M							8	4														14	4	1	
61X-CC, 0–1	265.30	267.18	A	M								2														2	6	1	
62X-CC, 2–4	271.62	273.44	A	M																						14	14	6	

Table T17 (continued).

Core, section, interval (cm)	Depth (mbsf)	Depth (mcd)	Abundance	Preservation	*Nematosphaeropsis labyrinthus*	*Nematosphaeropsis major*	*Operculodinium* cf. *centrocarpum*	*Operculodinium* cf. *microtrianium*	*?Operculodinium* sp.	*Operculodinium* cf. *janducheni*	*Palaeocystodinium golzowense*	*?Phelodinium* spp.	*Phthanoperidinium amoenum*	*Phthanoperidinium clithridium*	*Phthanoperidinium* spp. indet.	*Phthanoperidinium comatum*	*Phthanoperidinium echinatum* cpx	*Senegalinium* spp.	*?Systematophora* sp.	*Spiniferites ramosus*	*Svalbardella cooksoniae*	*Tectatodinium* sp.	*Thalassiphora delicata*	*Thalassiphora patula*	*Thallasiophora pelagica*	*Wetzeliella gochtii*	*Wetzeliella articulata* cpx
302-M0002A-																											
1X-CC, 4–6	1.24	1.52	C	M																							
3X-CC, 5–7	11.71	16.25	B																								
4X-CC, 5–7	16.73	16.73	B																								
6X-CC, 7–9	26.61	28.27	B																								
7X-CC, 3–5	30.47	35.04	R	M																							
9X-CC, 0–2	41.47	45.54	B																								
10X-CC, 0–2	44.75	48.26	R	M																							
12X-CC, 5–7	53.28	56.22	R	M																							
13X-CC, 5–7	56.56	59.50	R	M																							
14X-CC, 10–12	63.37	63.37	R	M																							
16X-CC, 13–15	72.48	72.82	R	M																							
17X-CC, 17–19	76.08	76.08	R	M																							
18X-CC, 11–13	80.12	80.12	R	M																							
19X-1, 0–1	81.21	81.21	B																								
20X-CC, 5–7	90.94	90.94	R	M																							
21X-CC, 6–8	94.64	94.64	R	M																							
23X-1, 11–13	101.32	101.32	R	M	1	1																					
24X-CC, 21–23	110.90	110.90	C	M																							
27X-CC, 3–5	123.84	123.84	F	M	20															4							
28X-CC, 5–7	127.50	127.50	B																								
29X-CC, 5–7	132.09	132.09	B																								
31X-1, 0–1	134.71	137.71	R	M																							
32X-CC, 8–10	144.96	144.96	R	M																							
33X-CC, 3–5	147.91	148.71	R	M																							
34X-CC, 13–15	152.01	152.01	B																								
35X-1, 6–8	154.07	154.07	R	M	1					1																	
36X-CC, 15–18	159.17	159.17	R	M					1																		
38X-CC, 0–2	171.71	171.71	B																								
39X-CC, 18–20	171.67	172.87	B																								
40X-CC, 0–2	178.25	178.25	B																								
40X-CC, 10–12	178.35	178.35	B																								
41X-CC, 0–2	178.59	178.59	B																								
42X-CC, 11–14	187.38	187.38	B																								
44X-2, 145–151	194.97	194.97	~B	M																							
44X-CC, 13–15	195.87	195.87	R	M									1					10		1	5						
45X-CC, 16–18	197.41	197.41	A	M																						1	1
46X-CC, 7–9	200.62	201.19	A	M			4					1		5	4		25	18									
47X-CC, 16–19	207.48	206.92	A	M								2			9		2	2	9			2			1		
48X-CC, 10–12	210.69	211.83	A	M										5	12	2		27	7	2			3	3			1
49X-CC, 64–66	215.99	218.31	A	M										1	8	7	17	33	7				4				1
50X-CC, 4–6	217.19	220.07	A	M													4	7									
52X-CC, 15–16	222.87	226.89	A	M										1			25	29		2			1				
53X-CC, 0–1	230.15	231.97	A	M													18	15		1							
54X-CC, 0–5	230.47	232.49	F	M										1		1	12	66		1							
55X-CC, 0–5	240.34	241.41	F	M										6	5	3	2	150		1							
56X-CC, 0–5	242.97	244.79	F	M													1	15									
57X-CC, 0–5	249.97	251.79	F	M										1	4	2	7	21		1							
58X-CC, 0–5	254.74	256.56	F	M												2	9	17									
59X-CC, 3–5	259.02	260.84	A	M							2					2	8	8									
60X-CC, 0–25	262.03	264.97	A	M				4						1		1	6	40		1							
61X-CC, 0–1	265.30	267.18	A	M				8			1						1	142		2							
62X-CC, 2–4	271.62	273.44	A	M				18						1				30		4							

Table T18. Palynological analysis, Hole M0003A.

Core, section, interval (cm)	Depth (mbsf)	Depth (mcd)	Abundance	*n* palynomorphs	Bisaccate pollen
302-M0003A-					
1H-CC, 25–27	5.04	8.66	R	1.00	1
2H-CC, 17–19	9.79	14.94	B		
3H-CC, 3–5	14.99	19.32	R	1	1

Note: R = rare, B = barren.

Table T19. Results of palynological analysis, Hole M0004A. (Continued on next two pages.)

Core, section, interval (cm)	Depth* (mbsf)	Depth* (mcd)	Abundance	Preservation	*n* palynomorphs	Bisaccate pollen	Other pollen	Spores	*Azolla* remains	Fungal spores	*Botryococcus* spp.	*Cymatiosphaera* spp.	*Cyclopsiella* spp.	*Leiosphaeridia* spp.	*Palambages* spp.	*Paralecaniella* spp.	*Pediastrum* spp.	*Pterospermella* spp.	*Tasmanites* spp.	Gen. et. sp. indet. A	Reworked Paleozoic	Reworked Mesozoic	Reworked Paleogene	Caved Paleogene	Dinocysts indet.	*Areoligera* spp.	*Apectodinium augustum*	*Apectodinium homomorphum*	*Apectodinium hyperacanthum*	*Apectodinium parvum*	*Apectodinium quinquelatum*	*Caligodinium amiculum*	*Cerodinium*? sp.	*Cerodinium depressum*
302-M0004A-																																		
4X-1, 0–1	265.01	265.01	A	M	268.00	66	2	2	6					28	10			1		4	2	2			20									1
6X-CC, 15–17	278.76	278.76	A	M	228.00	60	8	14	2					16	1			1		8					20									
7X-1, 0–1	278.51	278.71	A	M	133.00	36	2	6						6				2		2					4									8
8X-CC, 3–5	282.55	286.55	A	M	224.00	2		1		1				2	1			1		2					5									1
9X-CC, 3–5	287.61	287.61	A	M	253.00	4	1	2	3					4				1		4					5									2
10X-2, 147–150	294.84	294.84	A	M	224.00	90	4	5	1					9	1			1		1		1			5									1
10X-CC, 13–15	297.18	297.18	A	M	224.00	10			3					5				1		2					5									2
11X-CC, 20–22	302.71	302.71	A	M	291.00	1		1	175					1	1			1		2					5	2								3
12X-CC, 0–2	301.36	301.36	A	M	444.00				350					5	8					6					5									
15X-CC, 0–26	313.48	313.48	A	M	212.00									5																				
18X-CC, 0–1	318.81	318.81	A	M	433.00	2								3											1									
19X-CC, 13–16	323.69	323.69	A	M	228.00																				1									
20X-CC, 16–21	328.26	328.26	A	M	322.00	2								5											2									
21X-CC, 15–20	332.84	332.84	A	M	199.00	3	1					2		11											2									
22X-1, 0–1	339.01	339.01	A	M	212.00																				5									
22X-CC, 9–13	339.96	339.96	A	M	291.00	22	21	5		1				1				1		1					5									
23X-1, 144–150	343.07	343.07	A	M	188.00	5	3	3												1					5									
23X-CC, 18–22	345.65	345.65	A	M	287.00	11	2	1						1				1	1	2					5									
24X-1, 0–1	355.61	355.61	A	M	208.00	7	1							1				1							5									1
27X-1, 0–1	367.41	367.41	A	M	223.00	1	9	11		1				3				7							5							9		
27X-CC, 2–4	372.23	372.23	A	M	268.00	135	11	26										2							5							1	33	
28X-CC, 2–4	377.01	377.48	A	M	116.00	42	11	46				2						2							4									
29X-CC, 9–11	377.10	379.10	A	M	129.00	26	22	55										3							5									
30X-CC, 9–11	384.52	384.52	A	M	184.00	1	23	16										9							5		10	19	32	6	2			
31X-CC, 52–54	383.73	385.23	A	M	160.00	13	17	8								2		2							5		21	14	15	6	4			1
32X-CC, 15–17	391.02	391.02	A	M	159.00	100	4	8										2						1	2									
33X-CC, 12–14	394.13	394.13	P	M	90.00	40	4	5																1	3									
34X-CC, 0–2	400.04	400.04	P	M	116.00	70	6	16																										
35X-CC, 15–18	404.78	404.78	P	M	158.00	100	20	35														2?												
39X-CC, 0–1	421.50	421.50	P	M	191.00	15	20	50																	5									
41X-1, 0–1	424.51	424.51	B		0.00																													
41X-CC, 2–4	424.81	424.81	B		0.00																													
42X-CC, 3–5	427.47	427.47	A	M	23.00	5	1	1																6										
42X-CC, 9–11	427.53	427.53	A	M	25.00	5	1	1																2										

Notes: * = provisional. Abundance: A = abundant, P = poor, B = barren. Preservation: M = moderate.

Table T19 (continued).

Core, section, interval (cm)	Depth* (mbsf)	Depth* (mcd)	Abundance	Preservation	*Cerodinium striatum–D. denticulata*	*Cerodinium speciosum*	*Cerodinium wardenense*	*Chatangiella* spp.	*Cribroperidinium tenuitabulatum*	*Deflandrea oebisfeldensis*	*Deflandrea phosphoritica*	*Diphyes colligerum*	cf. *Paralecaniella*	*Glaphyrocysta ordinata*	*Hystrichokolpoma* sp.	*Hystrichosphaeridium tubiferum*	*Impagidinium* spp.	*Impletosphaeridium* spp.	*Lejeunecysta* cf. *cinctoria*	*Lentinia* cf. *wetzelii*	*Membranisphaera* spp.	*Oligosphaeridium complex*	*Operculodinium* cf. *microtrianium*	*Operculodinium* spp.	*Palaeocystodinium golzowense*	*Palaeohystrichophora infusorioides*	*Phthanoperidinium clithridium*	*Phthanoperidinium* spp. indet.	*Senegalinium* spp.	*Senoniasphaera* spp.	*Spiniferites ramosus*	*Thalassiphora delicata*	*Thallasiophora pelagica*	*Wetzeliella articulata*	*Wetzeliella astra*	*Wetzeliella hampdenensis*
302-M0004A-																																				
4X-1, 0–1	265.01	265.01	A	M	1				1									4	1	12			1		1		?	1	94		8						
6X-CC, 15–17	278.76	278.76	A	M	10												4	4	20	6			20						32		2						
7X-1, 0–1	278.51	278.71	A	M	10													1	16	4			2		4				22		4	4				
8X-CC, 3–5	282.55	286.55	A	M	3						15							1	2	1			1		1			1	180		1	2				
9X-CC, 3–5	287.61	287.61	A	M	5				1		5							2	5	2			1		1				200		1	1				3
10X-2, 147–150	294.84	294.84	A	M	4													5	11	3			2		2				75		1	2				
10X-CC, 13–15	297.18	297.18	A	M	14				2		46						23	1	1				1		1				90		1		16			
11X-CC, 20–22	302.71	302.71	A	M	15						2						3	3	1				3						70			1	1			
12X-CC, 0–2	301.36	301.36	A	M	7				4								5												50		1	2				1
15X-CC, 0–26	313.48	313.48	A	M	40												2												165							
18X-CC, 0–1	318.81	318.81	A	M	8	1								2			2	1											411		2					
19X-CC, 13–16	323.69	323.69	A	M	10									1			1						7						205		3					
20X-CC, 16–21	328.26	328.26	A	M	25									3			1	4					12						267		1					
21X-CC, 15–20	332.84	332.84	A	M	7									1				5					1						165		1					
22X-1, 0–1	339.01	339.01	A	M	1	1			1	1				1					1				1						200							
22X-CC, 9–13	339.96	339.96	A	M	6									1			4						7						215		1					
23X-1, 144–150	343.07	343.07	A	M	1												4						1						150		5		10			
23X-CC, 18–22	345.65	345.65	A	M	3												4						6						250							
24X-1, 0–1	355.61	355.61	A	M	1									1			3						16	12					150		2		2	4		1
27X-1, 0–1	367.41	367.41	A	M						50			61									1		3					36		2		3	15	6	
27X-CC, 2–4	372.23	372.23	A	M										2		3													49		1					
28X-CC, 2–4	377.01	377.48	A	M										1															8							
29X-CC, 9–11	377.10	379.10	A	M			1											1											15		1					
30X-CC, 9–11	384.52	384.52	A	M			38			2		1			3	1		2							1				8		4	1				
31X-CC, 52–54	383.73	385.23	A	M		1	16			2					2			7											24							
32X-CC, 15–17	391.02	391.02	A	M	22																								20							
33X-CC, 12–14	394.13	394.13	P	M	9												1	3			4								20							
34X-CC, 0–2	400.04	400.04	P	M	1													1											22							
35X-CC, 15–18	404.78	404.78	P	M				2																		1										
39X-CC, 0–1	421.50	421.50	P	M				100																					1							
41X-1, 0–1	424.51	424.51	B																																	
41X-CC, 2–4	424.81	424.81	B																																	
42X-CC, 3–5	427.47	427.47	A	M				10																												
42X-CC, 9–11	427.53	427.53	A	M				15																						1						

Table T19 (continued).

Core, section, interval (cm)	Depth* (mbsf)	Depth* (mcd)	Abundance	Preservation	Total dinocysts	Total *Apectodinium*	*Apectodinium* (%)	Dinocysts (%)	*Azolla* (%)
302-M0004A-									
4X-1, 0–1	265.01	265.01	A	M	145	0	0.0	54	2.2
6X-CC, 15–17	278.76	278.76	A	M	118	0	0.0	52	0.9
7X-1, 0–1	278.51	278.71	A	M	79	0	0.0	59	0
8X-CC, 3–5	282.55	286.55	A	M	214	0	0.0	96	0
9X-CC, 3–5	287.61	287.61	A	M	234	0	0.0	92	1.2
10X-2, 147–150	294.84	294.84	A	M	111	0	0.0	50	0.4
10X-CC, 13–15	297.18	297.18	A	M	203	0	0.0	91	1.3
11X-CC, 20–22	302.71	302.71	A	M	109	0	0.0	37	60
12X-CC, 0–2	301.36	301.36	A	M	75	0	0.0	17	79
15X-CC, 0–26	313.48	313.48	A	M	207	0	0.0	98	0
18X-CC, 0–1	318.81	318.81	A	M	428	0	0.0	99	0
19X-CC, 13–16	323.69	323.69	A	M	228	0	0.0	100	0
20X-CC, 16–21	328.26	328.26	A	M	315	0	0.0	98	0
21X-CC, 15–20	332.84	332.84	A	M	182	0	0.0	91	0
22X-1, 0–1	339.01	339.01	A	M	212	0	0.0	100	0
22X-CC, 9–13	339.96	339.96	A	M	239	0	0.0	82	0
23X-1, 144–150	343.07	343.07	A	M	176	0	0.0	94	0
23X-CC, 18–22	345.65	345.65	A	M	268	0	0.0	93	0
24X-1, 0–1	355.61	355.61	A	M	198	0	0.0	95	0
27X-1, 0–1	367.41	367.41	A	M	191	0	0.0	86	0
27X-CC, 2–4	372.23	372.23	A	M	94	0	0.0	35	0
28X-CC, 2–4	377.01	377.48	A	M	13	0	0.0	11	0
29X-CC, 9–11	377.10	379.10	A	M	23	0	0.0	18	0
30X-CC, 9–11	384.52	384.52	A	M	135	69	51.1	73	0
31X-CC, 52–54	383.73	385.23	A	M	118	60	50.8	74	0
32X-CC, 15–17	391.02	391.02	A	M	44	0	0.0	28	0
33X-CC, 12–14	394.13	394.13	P	M	40	0	0.0	44	0
34X-CC, 0–2	400.04	400.04	P	M	24	0	0.0	21	0
35X-CC, 15–18	404.78	404.78	P	M	3	0	0.0	1.9	0
39X-CC, 0–1	421.50	421.50	P	M	106	0	0.0	55	0
41X-1, 0–1	424.51	424.51	B		0	0	0.0	0	0
41X-CC, 2–4	424.81	424.81	B		0	0	0.0	0	0
42X-CC, 3–5	427.47	427.47	A	M	10	0	0.0	43	0
42X-CC, 9–11	427.53	427.53	A	M	16	0	0.0	64	0

Table T20. Palynological index events, Hole M0004A.

Dinocyst datum	Core, section, interval (cm) Top	Core, section, interval (cm) Bottom	Depth (mbsf) Top	Depth (mbsf) Bottom	Depth (mcd) Top	Depth (mcd) Bottom	Depth (mcd) Mean	Error (±m)	Proposed age (Ma)	Comment
	302-M0004A-	302-M0004A-								
FO *Phthanoperidinium clithridium*	4X-1, 0	6X-CC	265.00	278.60	265.00	278.78	271.89	6.89	46.1	
LO *Azolla* spp.	10X-CC	11X-CC	297.04	302.50	297.19	302.73	299.96	2.77	48.6	
FO *Deflandrea phosphoritica*	11X-CC	12X-CC	302.50	301.35	302.73	301.35	302.04	0.69	54	Too old
LO *Glaphyrocysta ordinata*	15X-CC	18X-CC	313.35	318.80	313.61	318.96	316.29	2.68	39.6–43.4	Too young
LO *Deflandrea oebisfeldensis*	21X-CC	22X-1, 0–1	332.66	339.01	332.86	339.01	335.94	3.08	52.9	
LO *Hystrichosphaeridium tubiferum*	27X-1, 1	27X-CC	367.42	372.20	367.42	372.25	369.83	2.42	46.3	Too young
LO *Cerodinium wardense*	28X-CC	29X-CC	376.98	377.00	377.50	379.12	378.31	0.81	53.1	
LO *Apectodinium augustum*	29X-CC	30X-CC	377.00	384.42	379.12	384.54	381.83	2.71	55	
FO *Hystrichosphaeridium tubiferum*	30X-CC	31X-CC	384.42	383.20	384.54	385.25	384.90	0.36	56	
FO *Diphyes colligerum*	30X-CC	31X-CC	384.42	383.20	384.54	385.25	384.90	0.36	58.9	Too old
FO *Apectodinium augustum*	31X-CC	32X-CC	383.20	390.86	385.25	391.04	388.15	2.90	55.6	
FO *Cerodinium wardense*	31X-CC	32X-CC	383.20	390.86	385.25	391.04	388.15	2.90	56	
FO *Deflandrea oebisfeldense*	31X-CC	32X-CC	383.20	390.86	385.25	391.04	388.15	2.90	57.8	

Note: FO = first occurrence, LO = last occurrence.

Table T21. Palynological analysis, Hole M0004B.

Core, section, interval (cm)	Depth (mbsf)	Depth (mcd)	Abundance	Preservation	*n* palynomorphs	Bisaccate pollen	Other pollen	Spores	*Botryococcus* spp.	*Cymatiosphaera* spp.	*Leiosphaeridia* spp.	*Paralecaniella* spp.	*Tasmanites* spp.	Dinocysts indet.	*Impagidinium* spp.	*Lentinia* cf. *wetzelii*	*Phthanoperidinium* spp. indet.	*Senegalinium* spp.	Total dinocysts
302-M0004B-																			
1X-CC, 0–2	12.30	12.46	B																
3X-CC, 11–13	218.87	218.87	A	M	236	11		19	60	1	16		2	1	1	1	4	120	127

Notes: Abundance: A = abundant, B = barren. Preservation: M = moderate.

Table T22. Palynological analysis, Hole M0004C.

Core, section, interval (cm)	Depth (mbsf)	Depth (mcd)	Abundance	Preservation	*n* palynomorphs	Bisaccate pollen	Other pollen	Spores	*Botryococcus* spp.	Reworked Mesozoic	Reworked Paleogene	*Habibacysts tectata*
302-M0004C-												
1H-CC, 3–5	3.76	3.76	B									
2H-CC, 3–5	8.76	8.11	B									
3H-CC, 3–5	13.70	12.89	B									
4H-CC, 19–24	18.54	17.25	B									
6X-2, 148–150	26.09	25.42	R	M	6.00	2			1			3
8X-CC, 7–10	33.84	35.28	R	M	16.00	9	2	1	1	2	1	
9X-CC, 27–29	36.64	38.03	R	M	1.00	1						

Notes: Abundance: R = rare, B = barren. Preservation: M = moderate.

Table T23. Palynological index events, Hole M0004C.

Dinocyst datum	Core, section Top	Core, section Bottom	Depth (mbsf) Top	Depth (mbsf) Bottom	Depth (mcd) Top	Depth (mcd) Bottom	Depth (mcd) Mean	Error (±m)	Proposed age (Ma)
LO *Habibacysta tectata*	302-M0004C-5X-CC	302-M0004C-6X-2	19.32	25.29	17.84	24.62	21.23	3.39	1

Note: LO = last occurrence.

Table T24. Disturbance, Holes M0002A, M0004A, and M0004C.

Core, section, interval (cm)	Quality
302-M0002A-	
3X-1, 0–8	Slurry
3X-1, 90–150	Slurry
3X-2	Slurry
3X-3	Slurry
3X-4	Flow-in
4X-1	Slurry
4X-2	Slurry
4X-3, 0–20	Slurry
4X-3, 20–150	Flow-in
4X-4, 0–30	Flow-in
4X-4, 30–end	Good
6X-1, 0–50	Disturbed
6X-2, 67–145	Slurry
6X-3	Slurry
6X-4	Flow-in
6X-2, 72–110	Disturbed
6X-2, 110–end	Slurry
7X-3	Flow-in
8X-1	Slurry/Biscuits
8X-2, 0–23	Slurry
8X-3	Flow-in
9X-4	Slurry
9X-5, 10–end	Slurry/Biscuits
10X-1. 0–34	Slurry
11X-1, 0–40	Disturbed
11X-3, 72–end	Slurry
12X-1, 0–152	Slurry/Biscuits
12X-2, 0–40	Disturbed
14X-1, 0–56	Disturbed
14X-1, 56–90	Slightly disturbed
16X-1	Slurry
16X-2, 0–10	Slurry
16X-2, 10–50	Disturbed
18X-2, 16–42	Disturbed
28X-1	Flow-in
28X-2	Flow-in
32X-4, 30–end	Disturbed
46X-2, 0–12	Disturbed
51X-1	Slurry
51X-2	Slurry
54X-1, 0–12	Disturbed
54X-1, 12–end	Slightly disturbed
55X-1	Disturbed
59X-1	Slurry
59X-2, 0–100	Disturbed
59X-3	Slightly disturbed
60X-2	Broken liner
60X-4	Disturbed
61X-1, 0–40	Slurry
62X-2, 0–90	Slurry
48X–51X	Biscuiting
60X–62X	Biscuiting
302-M0004A-	
1H-1, 0–30	Disturbed, shattered liner
1H-2	Shattered liner
1H-3	Shattered liner
1H-4	Shattered liner
7X-4	Slurry
8X-1	Disturbed
15X-1	Disturbed
27X-1, 0–61	Slurry
29X-1, 0–30	Disturbed
34X-1	Disturbed
41X-1	Disturbed
41X-2	Disturbed
302-M0004C-	
4H-1, 0–15	Slightly disturbed
8X-1, 0–20	Disturbed
8X, 55–end	Disturbed
8X-2	Flow-in
9X-1	Flow-in
9X-2	Flow-in
9X-3	Flow-in

Notes: Qualitative assessment ranges from good > slightly disturbed > disturbed > slurry biscuits > slurry. Flow-in = very distinct disturbance.

Table T25. Vertical core offset (affine), Holes M0002A, M0003A, M0004A, M0004B, and M0004C.

Core	Offset (m)	Depth adjusted? (yes/no)
302-M0002A-		
1X	0.28	Y
2X	–0.47	Y
3X	4.54	Y
4X	0.00	N
5X	3.84	Y
6X	1.66	Y
7X	4.57	N
8X	4.57	N
9X	4.01	Y
10X	3.51	Y
11X	2.39	Y
12X	2.94	Y
13X	2.94	N
14X	0.00	N
15X	0.00	N
16X	0.34	Y
17X	0.00	N
18X	0.00	N
19X	0.00	N
20X	0.00	N
21X	0.00	N
22X	0.00	N
23X	0.00	N
24X	0.00	N
25X	0.50	Y
26X	0.00	N
27X	0.00	N
28X	0.00	N
29X	0.00	N
30X	0.00	N
31X	3.00	Y
32X	0.00	N
33X	0.80	Y
34X	0.00	N
35X	0.00	N
36X	0.00	N
37X	–1.00	Y
38X	0.00	N
39X	1.20	Y
40X	0.00	N
41X	0.00	N
42X	0.00	N
43X	0.00	N
44X	0.00	N
45X	0.00	N
46X	0.57	Y
47X	–0.56	Y
48X	1.14	Y
49X	2.32	Y
50X	2.88	Y
51X	3.32	Y
52X	4.02	Y
53X	1.82	N
54X	2.02	Y
55X	1.07	Y
56X	1.82	Y
57X	1.82	N
58X	1.82	N
59X	1.82	N
60X	2.94	Y
61X	1.88	Y
62X	1.82	N
302-M0003A-		
1H	3.62	Y
2H	5.15	Y
3H	4.33	Y
302-M0004A-		
1H	0.37	Y
2X	–0.26	Y
3X	–1.83	Y
4X	0.00	N
5X	0.00	N
6X	0.00	N
7X	0.20	Y
8X	4.00	Y
9X	0.00	N
10X	0.00	N
11X	0.00	N
12X	0.00	N
15X	0.00	N
18X	0.00	N
19X	0.00	N
20X	0.00	N
21X	0.00	N
22X	0.00	N
23X	0.00	N
27X	0.00	N
28X	0.47	Y
29X	2.00	Y
30X	0.00	N
31X	1.50	Y
32X	0.00	N
33X	0.00	N
34X	0.00	N
35X	0.00	N
36X	0.00	N
37X	0.00	N
38X	0.00	N
39X	0.00	N
41X	0.00	N
42X	0.00	N
302-M0004B-		
1X	0.16	Y
2X	0.00	N
3X	0.00	N
302-M0004C-		
1H	0.00	N
2H	–0.65	Y
3H	–0.81	Y
4H	–1.29	Y
5X	–1.48	Y
6X	–0.67	Y
8X	1.44	Y
9X	1.39	Y

Table T26. Splice tie table. (See table notes. Continued on next page.)

Hole, core, section, interval (cm)	Depth (mbsf)	Depth (mcd)		Hole, core, section, interval (cm)	Depth (mbsf)	Depth (mcd)
302-				302-		
M0004C-1H-1, 0	0.00					
M0004C-1H-3, 64	3.66	3.66	Tie to	M0003A-1H-1, 4	0.04	3.66
M0003A-1H-4, 27	4.69	8.31	Tie to	M0004C-3H-1, 17	9.12	8.31
M0004C-3H-3, 27	12.24	11.43	Tie to	M0003A-2H-1, 128	6.28	11.43
M0003A-2H-3, 125	9.25	14.4	Tie to	M0004C-4H-2, 22	15.69	14.4
M0004C-4H-3, 69	17.66	16.37	Tie to	M0003A-3H-2, 57	12.04	16.37
M0003A-3H-4, 24	14.47	18.8	Tie to	M0004A-1H-1, 1	18.43	18.8
M0004A-1H-3, 1	20.20	20.57	Tie to	M0002A-5X-1, 23	16.73	20.57
M0002A-5X-1, 89	17.39	21.23	Tie to	M0004A-2X-1, 1	21.49	21.23
M0004A-2X-3, 0	23.69	23.43	Tie to	M0002A-6X-1, 27	21.77	23.43
M0002A-6X-4, 65	26.52	28.18	Append to	M0002A-7X-1, 0	26.5	31.07
M0002A-7X-4, 65	30.40	34.97	Append to	M0002A-9X-1, 0	36	40.01
M0002A-9X-5, 44	41.43	45.44	Append to	M0002A-10X-1, 0	41	44.51
M0002A-10X-3, 73	44.73	48.24	Append to	M0002A-11X-1, 0	46	48.39
M0002A-11X-3, 141	50.41	52.8	Append to	M0002A-12X-1, 0	50.02	52.96
M0002A-12X-3, 67	53.19	56.13	Append to	M0002A-13X-1, 0	55	57.94
M0002A-13X-1, 144	56.44	59.38	Append to	M0002A-14X-1, 0	60	60
M0002A-14X-3, 75	63.26	63.26	Append to	M0002A-15X-1, 0	65	65
M0002A-15X-3, 121	69.22	69.22	Append to	M0002A-16X-1, 0	69	69.34
M0002A-16X-CC, 8	72.42	72.76	Append to	M0002A-17X-1, 0	74	74
M0002A-17X-CC, 13	76.03	76.03	Append to	M0002A-18X-1, 0	78	78
M0002A-18X-CC, 8	80.08	80.08	Append to	M0002A-19X-1, 0	81.2	81.2
M0002A-19X-1, 103	82.23	82.23	Append to	M0002A-20X-1, 0	86.2	86.2
M0002A-20X-4, 13	90.85	90.85	Append to	M0002A-21X-1, 0	91.2	91.2
M0002A-21X-3, 33	94.55	94.55	Append to	M0002A-22X-1, 0	96.2	96.2
M0002A-22X-1, 38	96.58	96.58	Append to	M0002A-23X-1, 0	99.83	99.83
M0002A-23X-2, 108	102.41	102.41	Append to	M0002A-24X-1, 0	106.2	106.2
M0002A-24X-3, 143	110.63	110.63	Append to	M0002A-25X-1, 0	110.2	110.7
M0002A-25X-3, 85	114.08	114.58	Append to	M0002A-26X-1, 0	115.2	115.2
M0002A-26X-2, 63	117.33	117.33	Append to	M0002A-27X-1, 0	120.5	120.5
M0002A-27X-3, 42	123.93	123.93	Append to	M0002A-28X-1, 0	125.2	125.2
M0002A-28X-2, 68	127.38	127.38	Append to	M0002A-29X-1, 0	128.2	128.2
M0002A-29X-3, 78	131.98	131.98	Append to	M0002A-30X-1, 0	133.2	133.2
M0002A-30X-3, 73	136.94	136.94	Append to	M0002A-31X-1, 0	134.7	137.7
M0002A-31X-3, 11	136.16	139.16	Append to	M0002A-32X-1, 0	139.7	139.7
M0002A-32X-4, 63	144.85	144.85	Append to	M0002A-33X-1, 0	144.2	145
M0002A-33X-CC, 13	148.00	148.8	Append to	M0002A-34X-1, 0	149	149
M0002A-34X-CC, 8	151.95	151.95	Append to	M0002A-35X-1, 0	152.77	152.77
M0002A-35X-5, 63	159.42	159.42	Append to	M0002A-37X-1, 0	163.5	162.5
M0002A-37X-3, 38	166.90	165.9	Append to	M0002A-38X-1, 0	166.5	166.5
M0002A-38X-5, 54	171.66	171.66	Append to	M0002A-39X-1, 0	170.68	171.88
M0002A-39X-CC, 17	171.65	172.85	Append to	M0002A-40X-1, 0	173.08	173.08
M0002A-40X-CC, 10	178.34	178.34	Append to	M0002A-41X-1, 0	178.58	178.58
M0002A-41X-1, 13	178.71	178.71	Append to	M0002A-42X-1, 0	182.49	182.49
M0002A-42X-CC, 8	187.33	187.33	Append to	M0002A-43X-1, 0	187.49	187.49
M0002A-43X-3, 151	192.00	192	Append to	M0002A-44X-1, 0	191.99	191.99
M0002A-44X-4, 13	195.86	195.86	Append to	M0002A-45X-1, 0	195.93	195.93
M0002A-45X-2, 13	197.40	197.4	Append to	M0002A-46X-1, 0	197	197.57
M0002A-46X-3, 53	200.53	201.1	Append to	M0002A-47X-1, 0	202	201.44
M0002A-47X-CC, 13	207.43	206.87	Append to	M0002A-48X-1, 0	205.5	206.64
M0002A-48X-CC, 8	210.66	211.8	Append to	M0002A-49X-1, 0	210	212.32
M0002A-49X-CC, 13	215.47	217.79	Append to	M0002A-50X-1, 0	215	217.88
M0002A-50X-2, 63	217.14	220.02	Append to	M0002A-51X-1, 0	218.74	222.06
M0002A-51X-2, 113	221.38	224.7	Append to	M0002A-52X-1, 0	220.94	224.96
M0002A-52X-CC, 16	222.87	226.89	Append to	M0002A-53X-1, 7	225.07	226.89
M0002A-53X-CC, 8	230.22	232.04	Append to	M0002A-54X-1, 0	230	232.02
M0002A-54X-1, 38	230.38	232.4	Append to	M0002A-55X-1, 0	235	236.07
M0002A-55X-5, 66	240.29	241.36	Append to	M0002A-56X-1, 0	239.6	241.42
M0002A-56X-CC, 18	243.12	244.94	Append to	M0002A-57X-1, 0	244.6	246.42
M0002A-57X-5, 61	249.90	251.72	Append to	M0002A-58X-1, 27	249.9	251.72
M0002A-58X-4, 53	254.66	256.48	Append to	M0002A-59X-1, 0	254.6	256.42
M0002A-59X-3, 129	258.92	260.74	Append to	M0002A-60X-1, 19	257.8	260.74
M0002A-60X-3, 98	261.60	264.54	Append to	M0002A-61X-1, 0	262.6	264.48
M0002A-61X-CC, 13	265.42	267.3	Append to	M0002A-62X-1, 0	267.6	269.42
M0002A-62X-3, 98	271.59	273.41	Append to	M0004A-6X-1, 0	273.5	273.5
M0004A-6X-5, 10	278.70	278.7	Append to	M0004A-7X-1, 0	278.5	278.7
M0004A-7X-4, 83	283.68	283.88	Append to	M0004A-8X-1, 0	282.3	286.3

Table T26 (continued).

Hole, core, section, interval (cm)	Depth (mbsf)	Depth (mcd)		Hole, core, section, interval (cm)	Depth (mbsf)	Depth (mcd)
M0004A-8X-1, 20	282.50	286.5	Append to	M0004A-9X-1, 0.00	287.3	287.3
M0004A-9X-1, 26	287.56	287.56	Append to	M0004A-10X-1, 0.00	291.85	291.85
M0004A-10X-4, 67	297.00	297	Append to	M0004A-11X-1, 0.00	297.3	297.3
M0004A-11X-4, 84	302.67	302.67	Append to	M0004A-15X-1, 0.00	313.35	313.35
M0004A-15X-1, 26	313.61	313.61	Append to	M0004A-19X-1, 0.00	320.53	320.53
M0004A-19X-2, 151	323.53	323.53	Append to	M0004A-20X-1, 0.00	326.28	326.28
M0004A-20X-CC, 17	328.24	328.24	Append to	M0004A-21X-1, 0.00	329.28	329.28
M0004A-21X-4, 15	332.84	332.84	Append to	M0004A-22X-1, 0.00	339	339
M0004A-22X-1, 96	339.96	339.96	Append to	M0004A-23X-1, 0.00	341.6	341.6
M0004A-23X-CC, 16	345.61	345.61	Append to	M0004A-27X-1, 0.00	367.4	367.4
M0004A-27X-4, 29	372.24	372.24	Append to	M0004A-28X-1, 0.00	371.8	372.27
M0004A-28X-4, 65	377.04	377.51	Append to	M0004A-29X-1, 0.00	375.8	377.8
M0004A-29X-1, 132	377.12	379.12	Append to	M0004A-30X-1, 0.00	380.3	380.3
M0004A-30X-3, 120	384.53	384.53	Append to	M0004A-31X-1, 0.00	383.2	384.7
M0004A-31X-CC, 43	383.63	385.13	Append to	M0004A-32X-1, 0.00	388	388
M0004A-32X-3, 14	391.02	391.02	Append to	M0004A-33X-1, 0.00	392.5	392.5
M0004A-33X-CC, 8	394.08	394.08	Append to	M0004A-34X-1, 0.00	396.25	396.25
M0004A-34X-3, 101	400.03	400.03	Append to	M0004A-35X-1, 0.00	401.2	401.2
M0004A-35X-4, 13	404.76	404.76	Append to	M0004A-41X-1, 0.00	424.5	424.5
M0004A-41X-1, 26	424.76	424.76	Append to	M0004A-42X-1, 0.00	426.6	426.6
M0004A-42X-1, 72	427.32	427.32				

Notes: Site numbers were adjusted to be the same, with dummy hole letters, for import of different sites into Splicer. This table shows the actual site and hole numbers and letters. This table is also available in **ASCII.**

Table T27. Dynocysts and organic microfossils, Holes M0002A, M0004A, and M0004C.

Datum	Hole, core, section, interval (cm)		Depth (mbsf)		Depth (mcd)			Error (mcd)	Literature age (Ma)
	Top	Bottom	Top	Bottom	Top	Bottom	Mean		
	302-	302-							
LO *Habibacysta tectata*	M0004C-5X-CC	M0004C-6X-2	18.57	24.60	17.09	24.62	20.86	3.75	1
LO *Filisphaera microornata*	M0002A-10X-CC	M0002A-12X-CC	44.74	53.22	48.25	56.16	52.21	1.02	1.77
LO *Filisphaera* spp.	M0002A-14X-CC	M0002A-16X-CC	63.26	72.34	63.26	72.68	67.97	4.37	1.77
LO *Evittosphaerula* sp. 2 Manum et al., 1986	M0002A-16X-CC	M0002A-17X-CC	72.34	75.90	72.68	75.90	74.29	1.61	5.9
LO *Bitectatodinium? serratum*	M0002A-21X-CC	M0002A-23X-1, 11–13	94.57	101.20	94.57	101.20	97.89	3.32	6.84
FO *Evittosphaerula* sp. 2 Manum et al., 1986	M0002A-23X-1,11–13	M0002A-24X-CC	101.32	110.68	101.32	110.68	106.00	4.68	7.1
FO *Bitectatodinium? serratum*	M0002A-35X-1, 6–8	M0002A-36X-CC	154.07	159.00	154.07	159.00	156.54	2.47	11.2
FO *Habibacysta tectata*	M0002A-35X-1, 6–8	M0002A-36X-CC	154.07	159.00	154.07	159.00	156.54	2.47	14
LO *Wetzeliella gochtii*	M0002A-44X-CC	M0002A-45X-CC	195.73	197.24	195.73	197.24	196.49	0.76	27.
FO *Wetzeliella gochtii*	M0002A-45X-CC	M0002A-46X-CC	197.24	200.54	197.24	201.11	199.18	1.37	33.5
LO *Phthanoperidinium clithridium*	M0002A-45X-CC	M0002A-46X-CC	197.24	200.54	197.24	201.11	199.18	1.37	44.6
LO *Lentinia* cf. *wetzelii*	M0002A-46X-CC	M0002A-47X-CC	200.54	207.30	201.11	206.74	203.93	3.38	45.4
LO *Cerodinium depressum*	M0002A-47X-CC	M0002A-48X-CC	207.30	210.58	206.74	211.72	209.23	1.35	44.9
LO *Thalassiphora delicata*	M0002A-47X-CC	M0002A-48X-CC	207.30	210.58	206.74	211.72	209.23	1.35	45.5
FO *Phthanoperidinium clithridium*	M0002A-62X-CC	M0004A-6X-CC	271.59	278.60	273.41	278.60	276.01	2.60	46.2
LO *Azolla* spp.	M0004A-10X-CC	M0004A-11X-CC	297.04	302.50	297.04	302.50	299.77	2.09	48.6
FO *Azolla* spp.	M0004A-12XCC	M0004A-15X-CC	301.35	313.35	301.35	313.35	307.35	6.00	49.2
LO *Deflandrea oebisfeldensis*	M0004A-21XCC	M0004A-22X1, 0–1	332.66	339.00	332.66	339.00	335.83	3.58	52.9
FO *Wetzeliella articulata* cpx	M0004A-27X-1	M0004A-27X-CC	367.40	372.20	367.40	372.20	369.80	2.41	52.48
LO *Cerodinium wardense*	M0004A-28X-CC	M0004A-29X-CC	376.98	377.00	377.45	379.00	378.23	0.05	53.1
LO *Apectodinium augustum*	M0004A-29X-CC	M0004A-30X-CC	377.00	384.42	379.00	384.42	381.71	3.71	55
FO *Apectodinium augustum*	M0004A-31X-CC	M0004A-32X-CC	383.20	390.86	384.70	390.86	387.78	3.66	55.6
FO *Cerodinium wardenense*	M0004A-31X-CC	M0004A-32X-CC	383.20	390.86	384.70	390.86	387.78	3.66	56
FO *Deflandrea oebisfeldensis*	M0004A-31X-CC	M0004A-32X-CC	383.20	390.86	384.70	390.86	387.78	3.66	57.8
LO *Palaeohystrichophora infusorioides*	M0004A-34X-CC	M0004A-35X-CC	400.03	404.61	400.03	404.61	402.32	2.32	69.42
LO *Chatangiella verrucosa* cpx	M0004A-34X-CC	M0004A-35X-CC	400.03	404.61	400.03	404.61	402.32	2.32	72.5
LO Abundant *Chatangiella* spp.	M0004A-35X-CC	M0004A-39X-CC	404.61	420.00	404.61	420.00	412.31	8.37	80
FO Abundant *Chatangiella* spp.	M0004A-42X-CC, 2	M0004A, Bottom	427.43	427.43	427.43	427.43	427.43	0.00	87.5
FO *Chatangiella verrucosa* cpx	M0004A-42X-CC, 2	M0004A, Bottom	427.43	427.43	427.43	427.43	427.43	0.00	93.5

Notes: FO = first occurrence, LO = last occurrence. cpx = complex.

Table T28. Silicoflagellates, Holes M0002A and M0004A.

Datum	Hole, core, section Top	Hole, core, section Bottom	Depth (mbsf) Top	Depth (mbsf) Bottom	Depth (mcd) Top	Depth (mcd) Bottom	Depth (mcd) Mean	Error (mcd)	Literature age (Ma)
	302-	302-							
FO *Corbisema hexacantha*	M0002A-48X-CC	M0002A-49X-CC	210.58	215.34	211.72	217.66	214.69	0.65	44.1
LO *Naviculopsis punctilia*	M0002A-48X-CC	M0002A-49X-CC	210.58	215.34	211.72	217.66	214.69	2.77	34.7
LO *Dictyocha frenguellii*	M0002A-48X-CC	M0002A-49X-CC	210.58	215.34	211.72	217.66	214.69	0.65	34.7
LO *Corbisema toxeuma*	M0002A-48X-CC	M0002A-49X-CC	210.58	215.34	211.72	217.66	214.69	0.65	44.1
FO *Naviculopsis punctilia*	M0002A-51X-CC	M0002A-52X-CC	220.25	222.71	224.74	226.73	225.74	3.03	44.1
FO *Distephanus* spp.	M0002A-57X-CC	M0002A-58X-CC	249.94	254.71	251.76	256.53	254.15	0.57	52.4
FO *Corbisema spinosa*	M0004A-4X-CC	M0004A-5X-CC	265.00	271.50	265.00	271.50	268.25	3.25	50.5
FO *Corbisema toxeuma*	M0002A-62X-CC	M0004A-6X-CC	271.59	278.60	273.41	278.60	276.01	2.60	52.4
FO *Corbisema ovalis*	M0002A-62X-CC	M0004A-6X-CC	271.59	278.60	273.41	278.60	276.01	2.60	44.1
FO *Mesocena apiculata inflata*	M0004A-12X-CC	M0004A-15X-CC	301.35	313.35	301.35	313.35	307.35	6.00	52.4

Note: FO = first occurrence, LO = last occurrence.

Table T29. Diatoms, Hole M0004A.

Datum	Hole, core, section, interval (cm) Top	Hole, core, section, interval (cm) Bottom	Depth (mbsf) Top	Depth (mbsf) Bottom	Depth (mcd) Top	Depth (mcd) Bottom	Depth (mcd) Mean	Error (mcd)	Epoch
	302-	302-							
Pyxilla oligoceananica var. *oligoceanica*	M0004A-10X-5, 14	M0004A-12X-1, 1	297.18	301.49	297.18	301.49	299.34	2.16	Eocene

Table T30. Calcareous microfossils, Holes M0003A and M0004C.

Datum	Hole, core, sample, interval (cm) Top	Hole, core, sample, interval (cm) Bottom	Depth (mbsf) Top	Depth (mbsf) Bottom	Depth (mcd) Top	Depth (mcd) Bottom	Depth (mcd) Mean	Error (mcd)	Literature Age (Ma)
	302-	302-							
FO *Neogloboquadrina pachyderma* (sinistral)	M0003A-3H-CC	M0004C-6X-CC	14.95	24.60	19.28	23.93	21.61	3.00	1.8
FO *Emilliani huxleyi*	M0004C-1H-2, 2	M0004C-1H-2, 153	1.53	3.04	1.53	3.04	2.285	0.755	0.125
FO *Gephyrocapsa* spp.	M0004C-1H-2, 2	M0004C-1H-2, 153	1.53	3.04	1.53	3.04	2.285	0.755	0.125

Note: FO = first occurrence.

Table T31. Paleomagnetic chron boundaries, Holes M0002A and M0004A.

Datum	Hole, core, section, interval (cm) Top	Mean depth (mcd)	Literature age (Ma)
	302-		
B C1n (B/M)	M0004A-2H-2, 111	14.3	0.781
T C1r.1n	M0004A-2H-3, 116	19.48	0.988
B C1r.1n	M0004A-1H-2, 60	21.73	1.072
T C2n	M0004A-2X-1, 1.5	23.18	1.778
B C2An.1n	M0004A-2X-2, 1.4	40.68	3.032
T C2An.2n	M0002A-9X-1, 67	42.17	3.116
B C2An.2n	M0002A-9X-2, 66	46.11	3.207
T C2An.3n	M0002A-10X-1 18	47.19	3.33
B C2An.3n	M0002A-10X-1 126	48.92	3.596
T C3n.1n	M0002A-11X-1, 53	60.15	4.493
B C3n.2n	M0002A-11X-1, 17	65.53	4.631
B C3n.3n	M0002A-14X-1, 15	74.84	4.896
T C3n.4n	M0002A-15X-1, 53	75.68	4.997
T C3An.1n	M0002A-17X-1, 84	90.1	6.033
B C3An.1n	M0002A-17X-1, 17	92.57	6.252
T C3An.2n	M0002A-20X-3, 98	94.2	6.436
T C4n.2n	M0002A-21X-1, 137	107.71	7.695
T C4n.2n	M0002A-21X-3, 6	109.62	8.108
T C4r.1n	M0002A-24X-2, 94	110.19	8.254
B C4r.1n	M0002A-24X-2, 2	110.7	8.3
T C4An	M0002A-24X-3, 49	115.21	8.769
B C4An	M0002A-24X-3, 106	117.05	9.098
T C5n	M0002A-25X-2, 0	131.68	9.779
B C5n	M0002A-26X-1, 1	139.95	11.04
T C5r.2n	M0002A-26X-2, 34	143.66	11.554
B C5r.2n	M0002A-29X-3, 46	145.6	11.614
T C5An	M0002A-32X-2, 25	147.71	12.014
B C5An.2n	M0002A-32X-3, 95	156.19	12.415
T C5Ar.1n	M0002A-33X-1, 60	157.83	12.73
T C5AAn	M0002A-33X-2 120	170.18	13.015
B C5AAn	M0002A-35X-3, 50	173.08	13.183
T C5Bn.1n	M0002A-35X-4, 64	184.26	14.784
B C5Bn.1n	M0002A-38X-3, 58	184.55	14.877
B C5Cn.1n	M0002A-40X-2, 0	188.38	16.268
T C5Cn.2n	M0002A-42X-1, 27	188.76	16.303
B C5Cn.2n	M0002A-42X-2, 56	190.49	16.472
T C5Cn.3n	M0002A-43X-3, 75	191.03	16.543
B C5Cn.3n	M0002A-43X-3, 144	191.24	16.721
T C5Dn	M0002A-43X-3, 43	191.93	17.235
B C5Dn	M0002A-44X-1, 60	192.42	17.533
T C25n	M0004A-34X-3, 60	399.6	55.904

Notes: T = top, B = bottom. All belong to paleomagnetic taxon group.

Table T32. Paleomagnetic chron boundaries, Holes M0002A and M0004A. (**See table notes.** Continued on next page.)

Datum	Taxon group	Hole, core, section, interval (cm) Top	Hole, core, section, interval (cm) Bottom	Depth (mbsf) Top	Depth (mbsf) Bottom	Depth (mcd) Top	Depth (mcd) Bottom	Depth (mcd) Mean	Error (mcd)	Literature age (Ma)
		302-	302-							
B C1n (B/M)	Paleomagnetic	M0004A-2H-2, 111						14.3		0.781
T C1r.1n	Paleomagnetic	M0004A-2H-3, 116						19.48		0.988
B C1r.1n	Paleomagnetic	M0004A-1H-2, 60						21.73		1.072
T C2n	Paleomagnetic	M0004A-2X-1, 1.5						23.18		1.778
B C2An.1n	Paleomagnetic	M0004A-2X-2, 1.4						40.68		3.032
T C2An.2n	Paleomagnetic	M0002A-9X-1, 67						42.17		3.116
B C2An.2n	Paleomagnetic	M0002A-9X-2, 66						46.11		3.207
T C2An.3n	Paleomagnetic	M0002A-10X-1 18						47.19		3.33
B C2An.3n	Paleomagnetic	M0002A-10X-1 126						48.92		3.596
T C3n.1n	Paleomagnetic	M0002A-11X-1, 53						60.15		4.493
B C3n.2n	Paleomagnetic	M0002A-11X-1, 17						65.53		4.631
B C3n.3n	Paleomagnetic	M0002A-14X-1, 15						74.84		4.896
T C3n.4n	Paleomagnetic	M0002A-15X-1, 53						75.68		4.997
T C3An.1n	Paleomagnetic	M0002A-17X-1, 84						90.1		6.033
B C3An.1n	Paleomagnetic	M0002A-17X-1, 17						92.57		6.252
T C3An.2n	Paleomagnetic	M0002A-20X-3, 98						94.2		6.436
T C4n.2n	Paleomagnetic	M0002A-21X-1, 137						107.71		7.695
T C4n.2n	Paleomagnetic	M0002A-21X-3, 6						109.62		8.108
T C4r.1n	Paleomagnetic	M0002A-24X-2, 94						110.19		8.254
B C4r.1n	Paleomagnetic	M0002A-24X-2, 2						110.7		8.3
T C4An	Paleomagnetic	M0002A-24X-3, 49						115.21		8.769
B C4An	Paleomagnetic	M0002A-24X-3, 106						117.05		9.098
T C5n	Paleomagnetic	M0002A-25X-2, 0						131.68		9.779
B C5n	Paleomagnetic	M0002A-26X-1, 1						139.95		11.04
T C5r.2n	Paleomagnetic	M0002A-26X-2, 34						143.66		11.554
B C5r.2n	Paleomagnetic	M0002A-29X-3, 46						145.6		11.614
T C5An	Paleomagnetic	M0002A-32X-2, 25						147.71		12.014
B C5An.2n	Paleomagnetic	M0002A-32X-3, 95						156.19		12.415
T C5Ar.1n	Paleomagnetic	M0002A-33X-1, 60						157.83		12.73
T C5AAn	Paleomagnetic	M0002A-33X-2 120						170.18		13.015
B C5AAn	Paleomagnetic	M0002A-35X-3, 50						173.08		13.183
T C5Bn.1n	Paleomagnetic	M0002A-35X-4, 64						184.26		14.784
B C5Bn.1n	Paleomagnetic	M0002A-38X-3, 58						184.55		14.877
B C5Cn.1n	Paleomagnetic	M0002A-40X-2, 0						188.38		16.268
T C5Cn.2n	Paleomagnetic	M0002A-42X-1, 27						188.76		16.303
B C5Cn.2n	Paleomagnetic	M0002A-42X-2, 56						190.49		16.472
T C5Cn.3n	Paleomagnetic	M0002A-43X-3, 75						191.03		16.543
B C5Cn.3n	Paleomagnetic	M0002A-43X-3, 144						191.24		16.721
T C5Dn	Paleomagnetic	M0002A-43X-3, 43						191.93		17.235
B C5Dn	Paleomagnetic	M0002A-44X-1, 60						192.42		17.533
FO *Corbisema hexacantha*	Silicoflagellate	M0002A-48X-CC	M0002A-49X-CC	210.58	215.34	211.72	217.66	214.69	0.65	44.1
FO *Phthanoperidinium clithridium*	Dinocyst	M0002A-62X-CC	M0004A-6X-CC	271.59	278.60	273.41	278.60	276.01	2.60	46.2
LO *Azolla* spp.	Hydropterid fern	M0004A-10X-CC	M0004A-11X-CC	297.04	302.50	297.04	302.50	299.77	2.09	48.6
FO *Azolla* spp.	Hydropterid fern	M0004A-12X-CC	M0004A-15X-CC	301.35	313.35	301.35	313.35	307.35	6.00	49.2
LO *Deflandrea oebisfeldensis*	Dinocyst	M0004A-21X-CC	M0004A-22X-1, 0–1	332.66	339.00	332.66	339.00	335.83	3.58	52.9
FO *Wetzeliella articulata* cpx	Dinocyst	M0004A-27X-1	M0004A-27X-CC	367.40	372.20	367.40	372.20	369.80	2.41	52.48
LO *Cerodinium wardense*	Dinocyst	M0004A-28X-CC	M0004A-29X-CC	376.98	377.00	377.45	379.00	378.23	0.05	53.1
LO *Apectodinium augustum*	Dinocyst	M0004A-29X-CC	M0004A-30X-CC	377.00	384.42	379.00	384.42	381.71	3.71	55
FO *Apectodinium augustum*	Dinocyst	M0004A-31X-CC	M0004A-32X-CC	383.20	390.86	384.70	390.86	387.78	3.66	55.6

Table T32 (continued).

Datum	Taxon group	Hole, core, section, interval (cm) Top	Hole, core, section, interval (cm) Bottom	Depth (mbsf) Top	Depth (mbsf) Bottom	Depth (mcd) Top	Depth (mcd) Bottom	Depth (mcd) Mean	Error (mcd)	Literature age (Ma)
		302-	302-							
FO *Cerodinium wardenense*	Dinocyst	M0004A-31X-CC	M0004A-32X-CC	383.20	390.86	384.70	390.86	387.78	3.66	56
FO *Deflandrea oebisfeldensis*	Dinocyst	M0004A-31X-CC	M0004A-32X-CC	383.20	390.86	384.70	390.86	387.78	3.66	57.8
LO *Palaeohystrichophora infusorioides*	Dinocyst	M0004A-34X-CC	M0004A-35X-CC	400.03	404.61	400.03	404.61	402.32	2.32	69.42
LO *Chatangiella verrucosa* cpx	Dinocyst	M0004A-34X-CC	M0004A-35X-CC	400.03	404.61	400.03	404.61	402.32	2.32	72.5
LO Abundant *Chatangiella* spp.	Dinocyst	M0004A-35X-CC	M0004A-39X-CC	404.61	420.00	404.61	420.00	412.31	8.37	80
T C25n	Paleomagnetic	M0004A-34X-3, 60						399.6		55.904

Notes: T = top, B = bottom. FO = first occurrence, LO = last occurrence. cpx = complex.

Table T33. Sedimentation rates.

Age (Ma)		Sedimentation rate (m/m.y.)
Top	Bottom	
0	1.072	19.9
1.072	1.778	2.1
1.778	4.493	13.74
4.493	4.997	31.9
4.997	7.695	11.8
7.695	9.098	7.1
9.098	12.014	10.8
12.014	13.015	22.1
13.015	14.877	6.9
14.877	16.543	3.9
16.543	17.533	1.3
		Hiatus
44.1	46.2	29.6
46.2	49.2	10.6
49.2	52.9	7.8
52.9	55.9	20.3
69.42	93.5	1.2

Table T34. Physical properties, Holes M0001A, M0002A, M0003A, M0004A, M0004B, and M0004C.

Core, section, interval (cm)	Depth (mbsf)	Depth (mcd)	Density (g/cm³) Bulk	Density (g/cm³) Pycnometer
302-M0001A-				
1H-CC, 25	0.25		1.60	2.64
302-M0002A-				
1X-CC, 6	1.25	1.53	1.96	2.61
3X-CC, 5	11.7	16.24	2.04	2.66
4X-CC, 5	16.72	16.72	1.76	2.69
5X-1, 150	18	21.84	1.78	2.60
6X-CC, 10	26.63	28.29	1.82	2.57
7X-CC, 10	30.53	35.1	1.77	2.64
9X-CC, 8			1.73	2.72
10X-CC, 18	44.92	48.43	1.94	2.69
12X-CC, 4	53.26	56.2	1.93	2.71
13X-CC, 6	56.56	59.5	1.82	2.66
14X-CC, 8	63.34	63.34	1.90	2.57
10X-2, 150	44	47.51		2.68
12X-2, 150	53.02	55.96		2.73
16X-CC, 3	72.37	72.71	1.93	2.72
17X-CC, 3	75.93	75.93	1.93	2.61
18X-CC, 3	80.03	80.03	1.97	2.63
19X-CC, 6			1.95	2.71
20X-CC, 5	90.93	90.93	1.87	2.69
21X-CC, 7	94.64	94.64	1.93	2.61
18X-2, 151	80.96	80.96	2.64	2.69
16X-2, 55	71.05	71.39	2.20	2.64
21X-2, 151	94.22	94.22	2.57	2.69
23X-1, 5	101.25	101.25	1.96	2.70
24X-CC, 13.5	110.815	110.815	1.87	2.68
27X-CC, 5	123.85	123.85	1.90	2.65
28X-CC, 4.5	127.485	127.485	1.92	2.69
29X-CC, 6.5	132.095	132.095	1.91	2.70
32X-CC, 5	144.92	144.92	1.82	2.66
33X-CC, 3	147.9	148.7	2.03	2.63
31X-CC, 1	136.06	139.06	2.22	2.83
34X-CC, 2.5	151.895	151.895	2.07	2.63
35X-CC, 1			1.90	2.63
36X-CC, 3.5	159.035	159.035	1.83	2.65
38X-CC, 3	171.73	171.73	1.63	2.72
39X-CC, 2	171.5	172.7	1.69	2.63
40X-CC, 9	178.33	178.33	1.82	2.65
41X-CC, 1			1.60	2.64
42X-CC, 1.5	187.265	187.265	1.75	2.67
44X-CC, 1.5			1.77	2.54
45X-CC, 1	197.25	197.25	1.85	2.57
46X-CC, 2.5	200.565	201.135	1.875	2.64
47X-CC, 2	207.32	206.76	1.86	2.81
48X-CC, 2.5	210.605	211.745	1.49	2.82
49X-CC, 2.5	215.365	217.685	1.74	2.77
50X-CC, 2.5	217.165	220.045	1.695	2.73
54X-CC, 1	230.45	232.47	1.29	
55X-CC, 2.5	240.335	241.405	1.35	2.20
56X-CC, 1	242.95	244.77	1.18	2.30
57X-CC, 1	249.95	251.77	1.06	2.28
58X-CC, 1	254.72	256.54	1.23	2.17
59X-CC, 1	258.99	260.81	1.22	2.08
60X-CC, 1	261.91	264.85	1.44	2.30
61X-CC, 1	265.3	267.18	1.37	2.21
302-M0003A-				
1H-CC, 2.5	4.805	8.425	1.88	2.60
2H-CC, 2.5	9.635	14.785	1.72	2.59
3H-CC, 2.5	14.975	19.305	1.75	2.60
302-M0004A-				
4X-CC, 1			1.33	2.18
6X-CC, 3			1.05	2.16
8X-CC, 2.5	282.535	286.535	1.33	2.48
9X-CC, 3	287.6	287.6	1.40	2.25
10X-CC, 3.5	297.075	297.075	1.30	2.15
11X-CC, 3	302.53	302.53	1.43	2.34
12X-CC, 1	301.36		1.35	2.38
19X-CC, 1	323.55	323.55		2.38
20X-CC, 1	328.08	328.08		2.46
21X-CC, 1	332.67	332.67		2.31
22X-CC, 1	339.86	339.86		2.39
23X-CC, 1	345.46	345.46		2.44
27X-CC, 2.5	372.225	372.225	1.81	2.59
28X-CC, 1	376.99	377.46		2.57
29X-CC, 1	377.01	379.01	1.80	2.60
30X-CC, 1	384.43	384.43		2.51
31X-CC, 1	383.21	384.71	1.77	2.48
32X-CC, 1	390.87	390.87	2.05	2.61
33X-CC, 1	394.01	394.01	1.80	2.60
35X-CC, 1	404.62	404.62	2.04	2.62
41X-CC, 1	424.79	424.79		2.63
42X-CC, 2.5	427.455	427.455	2.17	2.59
302-M0004B-				
3X-CC, 12	218.87	218.87	1.73	2.71
302-M0004C-				
1H-CC, 1	3.73	3.73	1.79	2.64
2H-CC, 1	8.73	8.08	1.75	2.67
3H-CC, 1	13.67	12.86	1.79	2.63
4H-CC, 1	18.33	17.04	1.87	2.61
6X-CC, 1			1.83	2.71

Table T35. Moisture and density, Holes M0002A, M0004A, and M0004C. (Continued on next two pages.)

Core, section, interval (cm)	Depth (mbsf)	Depth (mcd)	Water content (wt%) Wet	Water content (wt%) Dry	Density (g/cm^3) Bulk	Density (g/cm^3) Dry	Density (g/cm^3) Grain	Porosity (%)	Void ratio
302-M0002A-									
6X-1, 100–102	22.5	24.16	0.326	0.483	1.777	1.198	2.756	0.565	1.3
6X-2, 66–68	23.53	25.19	0.338	0.511	1.753	1.16	2.754	0.579	1.374
6X-3, 100–102	25.37	27.03	0.349	0.536	1.724	1.123	2.72	0.587	1.423
7X-1, 100–102	27.5	32.07	0.334	0.502	1.754	1.168	2.73	0.572	1.337
7X-2, 100–102	29	33.57	0.337	0.507	1.746	1.158	2.717	0.574	1.346
7X-3, 89–91	30.39	34.96	0.353	0.546	1.726	1.117	2.758	0.595	1.469
8X-1, 100–102	32	36.57	0.382	0.617	1.667	1.031	2.719	0.621	1.638
8X-2, 100–102	33.5	38.07	0.304	0.436	1.829	1.274	2.783	0.542	1.185
8X-3, 85–87	34.45	39.02	0.32	0.472	1.781	1.21	2.733	0.557	1.259
9X-1, 100–102	37	41.01	0.349	0.537	1.722	1.12	2.715	0.587	1.423
9X-2, 100–102	38.5	42.51	0.319	0.469	1.776	1.21	2.709	0.554	1.24
9X-3, 30–32	39.3	43.31	0.312	0.453	1.792	1.233	2.716	0.546	1.203
10X-2, 100–102	43.5	47.01	0.274	0.377	1.868	1.356	2.709	0.5	0.998
10X-1, 100–102	42	45.51	0.29	0.409	1.838	1.304	2.725	0.521	1.089
10X-3, 30–32	44.3	47.81	0.263	0.357	1.887	1.391	2.698	0.485	0.94
11X-1, 100–102	47	49.39	0.303	0.435	1.809	1.26	2.715	0.536	1.154
11X-2, 100–102	48.49	50.88	0.303	0.436	1.814	1.263	2.731	0.537	1.162
11X-3, 60–62	49.6	51.99	0.323	0.477	1.776	1.202	2.735	0.56	1.274
12X-2, 60–62	52.12	55.06	0.304	0.436	1.81	1.261	2.722	0.537	1.159
12X-3, 30–32	52.82	55.76	0.257	0.346	1.903	1.414	2.709	0.478	0.916
13X-1, 100–102	56	58.94	0.334	0.501	1.747	1.164	2.705	0.57	1.324
14X-1, 100–102	61	61	0.274	0.378	1.87	1.357	2.718	0.501	1.002
14X-2, 80–82	62.31	62.31	0.255	0.342	1.909	1.423	2.707	0.475	0.903
14X-3, 60–62	63.11	63.11	0.253	0.338	1.913	1.43	2.709	0.472	0.895
15X-1, 100–102	66	66	0.274	0.378	1.869	1.356	2.716	0.501	1.003
15X-2, 100–102	67.51	67.51	0.258	0.347	1.905	1.414	2.715	0.479	0.92
15X-3, 100–102	69	69	0.265	0.361	1.887	1.386	2.711	0.489	0.956
16X-2, 100–102	71.5	71.84	0.282	0.394	1.869	1.341	2.768	0.516	1.064
16X-3, 20–22	72.21	72.55	0.263	0.356	1.9	1.401	2.732	0.487	0.95
17X-1, 100–102	75	75	0.284	0.397	1.846	1.321	2.71	0.512	1.051
17X-2, 20–22	75.71	75.71	0.284	0.396	1.855	1.329	2.736	0.514	1.059
18X-1, 100–102	79	79	0.281	0.392	1.857	1.334	2.724	0.51	1.042
18X-2, 10–12	79.55	79.55	0.304	0.437	1.802	1.254	2.696	0.535	1.15
19X-1, 98–102	82.18	82.18	0.251	0.335	1.927	1.443	2.737	0.473	0.896
20X-1, 100–102	87.2	87.2	0.265	0.36	1.898	1.396	2.74	0.491	0.963
20X-2, 100–102	88.71	88.71	0.251	0.336	1.913	1.432	2.699	0.469	0.885
20X-3, 100–102	90.21	90.21	0.243	0.321	1.933	1.463	2.705	0.459	0.849
21X-1, 80–82	92	92	0.278	0.385	1.864	1.345	2.725	0.506	1.026
21X-2, 100–102	93.71	93.71	0.279	0.388	1.862	1.342	2.727	0.508	1.032
23X-2, 100–102	102.33	102.33	0.234	0.305	1.959	1.501	2.715	0.447	0.809
24X-1, 100–102	107.2	107.2	0.25	0.333	1.934	1.451	2.745	0.471	0.892
24X-2, 100–102	108.69	108.69	0.27	0.37	1.873	1.367	2.703	0.494	0.978
24X-3, 110–112	110.3	110.3	0.276	0.38	1.87	1.355	2.727	0.503	1.013
25X-1, 100–102	111.2	111.7	0.265	0.36	1.891	1.39	2.721	0.489	0.957
25X-2, 100–102	112.71	113.21	0.274	0.378	1.866	1.354	2.707	0.5	0.999
25X-3, 70–72	113.92	114.42	0.194	0.241	1.96	1.58	2.514	0.372	0.591
26X-1, 100–102	116.2	116.2	0.265	0.361	1.871	1.375	2.667	0.484	0.94
27X-1, 100–102	121.2	121.2	0.263	0.357	1.874	1.381	2.663	0.482	0.929
27X-2, 100–102	122.7	122.7	0.27	0.37	1.869	1.364	2.692	0.493	0.974
27X-3, 40–42	123.61	123.61	0.284	0.396	1.836	1.315	2.675	0.508	1.034
29X-1, 100–102	129.2	129.2	0.261	0.353	1.894	1.399	2.704	0.483	0.932
29X-2, 100–102	130.7	130.7	0.262	0.355	1.892	1.397	2.706	0.484	0.938
29X-3, 70–72	131.9	131.9	0.283	0.395	1.878	1.346	2.802	0.52	1.082
30X-1, 100–102	134.2	134.2	0.237	0.31	1.943	1.483	2.694	0.45	0.817
30X-2, 100–102	135.71	135.71	0.251	0.336	1.915	1.434	2.706	0.47	0.888
30X-3, 50–52	136.71	136.71	0.25	0.334	1.933	1.45	2.748	0.472	0.896
31X-1, 50–52	135.2	138.2	0.246	0.325	1.936	1.46	2.725	0.464	0.866
32X-1, 100–102	140.7	140.7	0.264	0.359	1.891	1.391	2.717	0.488	0.952
32X-2, 100–102	142.2	142.2	0.267	0.364	1.887	1.383	2.721	0.492	0.967
32X-3, 100–102	143.71	143.71	0.267	0.365	1.892	1.386	2.739	0.494	0.977
33X-1, 100–102	145.2	146	0.249	0.332	1.927	1.447	2.725	0.469	0.883
33X-2, 100–102	146.71	147.51	0.272	0.374	1.88	1.368	2.734	0.5	0.998
33X-3, 50–52	147.73	148.53	0.245	0.324	1.941	1.466	2.734	0.464	0.865
34X-1, 100–102	150	150	0.253	0.339	1.905	1.423	2.689	0.471	0.89
34X-2, 100–102	151.5	151.5	0.271	0.371	1.876	1.368	2.715	0.496	0.985
35X-2, 97–99	155.24	155.24	0.243	0.321	1.945	1.472	2.735	0.462	0.858
35X-3, 100–102	156.76	156.76	0.262	0.355	1.888	1.394	2.694	0.483	0.933

Table T35 (continued).

Core, section, interval (cm)	Depth (mbsf)	Depth (mcd)	Water content (wt%) Wet	Water content (wt%) Dry	Density (g/cm³) Bulk	Density (g/cm³) Dry	Density (g/cm³) Grain	Porosity (%)	Void ratio
35X-4, 100–102	158.27	158.27	0.277	0.383	1.862	1.346	2.714	0.504	1.016
35X-5, 40–42	159.19	159.19	0.294	0.417	1.84	1.299	2.756	0.529	1.122
37X-1, 100–102	164.5	163.5	0.279	0.386	1.87	1.349	2.746	0.509	1.035
37X-2, 100–102	166.01	165.01	0.223	0.287	1.979	1.537	2.704	0.431	0.759
38X-2, 100–102	167.89	167.89	0.299	0.427	1.821	1.276	2.73	0.533	1.14
38X-3, 100–102	169.08	169.08	0.317	0.464	1.792	1.224	2.747	0.554	1.243
38X-4, 110–112	170.69	170.69	0.308	0.444	1.813	1.255	2.757	0.545	1.196
39X-1, 30–32	170.98	172.18	0.301	0.431	1.812	1.266	2.712	0.533	1.142
40X-1, 100–102	174.08	174.08	0.318	0.466	1.787	1.219	2.738	0.555	1.246
40X-2, 100–102	175.58	175.58	0.291	0.41	1.836	1.302	2.719	0.521	1.088
40X-3, 100–102	177.09	177.09	0.28	0.389	1.865	1.342	2.74	0.51	1.041
40X-4, 50–52	178.09	178.09	0.281	0.391	1.862	1.339	2.738	0.511	1.045
42X-1, 100–102	183.49	183.49	0.295	0.418	1.831	1.292	2.731	0.527	1.114
42X-2, 100–102	184.99	184.99	0.295	0.419	1.833	1.292	2.738	0.528	1.12
42X-3, 100–102	186.49	186.49	0.288	0.405	1.852	1.318	2.753	0.521	1.089
43X-1, 100–102	188.49	188.49	0.291	0.41	1.838	1.303	2.728	0.522	1.093
43X-2, 100–102	189.98	189.98	0.298	0.425	1.823	1.279	2.728	0.531	1.132
43X-3, 100–102	191.49	191.49	0.294	0.416	1.835	1.296	2.737	0.527	1.113
44X-2, 100–102	194.49	194.49	0.256	0.344	1.881	1.399	2.641	0.47	0.887
44X-1, 84–86	192.83	192.83	0.291	0.411	1.85	1.311	2.765	0.526	1.108
44X-1, 142–146	193.41	193.41	0.252	0.336	1.897	1.42	2.658	0.466	0.873
44X-3, 60–62	195.6	195.6	0.261	0.354	1.878	1.387	2.663	0.479	0.92
45X-1, 100–102	196.93	196.93	0.341	0.517	1.673	1.103	2.486	0.556	1.254
46X-1, 100–102	198	198.57	0.303	0.436	1.766	1.23	2.581	0.523	1.098
46X-2, 100–102	199.5	200.07	0.25	0.334	1.949	1.461	2.792	0.477	0.911
47X-2, 100–102	203.26	202.7	0.498	0.991	1.46	0.734	2.527	0.71	2.444
47X-3, 100–102	204.76	204.2	0.314	0.457	1.853	1.272	2.942	0.568	1.313
47X-4, 100–102	206.27	205.71	0.253	0.338	2.031	1.518	3.045	0.502	1.006
47X-5, 40–42	207.19	206.63	0.244	0.322	2.063	1.56	3.063	0.491	0.963
48X-1, 90–92	206.4	207.54	0.359	0.56	1.726	1.106	2.801	0.605	1.532
48X-2, 100–102	208	209.14	0.3	0.428	1.874	1.312	2.909	0.549	1.217
48X-3, 100–102	209.51	210.65	0.331	0.494	1.793	1.2	2.852	0.579	1.377
49X-2, 100–102	211.15	213.47	0.371	0.59	1.701	1.07	2.79	0.617	1.608
49X-3, 100–102	212.65	214.97	0.356	0.553	1.687	1.087	2.627	0.586	1.418
49X-4, 100–102	214.16	216.48	0.398	0.661	1.632	0.982	2.685	0.634	1.733
50X-1, 100–102	216	218.88	0.382	0.617	1.664	1.029	2.708	0.62	1.632
51X-2, 102–104	221.27	224.59	0.641	1.789	1.283	0.46	2.344	0.804	4.096
52X-1, 102–104	221.96	225.98	0.551	1.229	1.363	0.612	2.301	0.734	2.762
53X-1, 102–104	226.02	227.84	0.569	1.321	1.339	0.577	2.254	0.744	2.908
53X-2, 102–104	227.54	229.36	0.603	1.521	1.298	0.515	2.185	0.764	3.245
53X-3, 102–104	229.04	230.86	0.599	1.491	1.307	0.525	2.225	0.764	3.24
55X-2, 102–104	236.12	237.19	0.572	1.339	1.34	0.573	2.28	0.749	2.981
55X-3, 102–104	237.63	238.7	0.549	1.217	1.386	0.625	2.436	0.743	2.896
55X-4, 102–104	239.14	240.21	0.523	1.096	1.413	0.674	2.42	0.721	2.589
55X-5, 42–44	240.05	241.12	0.539	1.168	1.387	0.64	2.37	0.73	2.703
56X-1, 42–44	240.02	241.84	0.588	1.424	1.327	0.547	2.292	0.761	3.188
56X-2, 102–104	241.25	243.07	0.563	1.286	1.349	0.59	2.278	0.741	2.862
56X-3, 102–104	242.76	244.58	0.603	1.52	1.292	0.513	2.145	0.761	3.184
57X-2, 102–104	245.75	247.57	0.604	1.527	1.3	0.514	2.207	0.767	3.292
57X-3, 102–104	247.25	249.07	0.617	1.609	1.29	0.494	2.218	0.777	3.486
57X-4, 102–104	248.76	250.58	0.613	1.584	1.287	0.498	2.173	0.771	3.361
58X-1, 102–104	250.62	252.44	0.575	1.351	1.33	0.566	2.23	0.746	2.943
58X-2, 102–104	252.12	253.94	0.621	1.64	1.285	0.487	2.211	0.78	3.541
58X-3, 102–104	253.63	255.45	0.608	1.552	1.291	0.506	2.169	0.767	3.288
59X-3, 102–104	258.63	260.45	0.605	1.532	1.286	0.508	2.112	0.76	3.159
60X-1, 100–102	258.6	261.54	0.575	1.355	1.321	0.561	2.178	0.742	2.882
60X-2, 100–102	260.11	263.05	0.554	1.244	1.345	0.599	2.204	0.728	2.676
60X-3, 90–92	261.52	264.46	0.572	1.334	1.315	0.563	2.117	0.734	2.757
61X-1, 100–102	263.6	265.48	0.548	1.211	1.36	0.615	2.257	0.727	2.669
61X-2, 100–102	265.11	266.99	0.555	1.248	1.34	0.596	2.18	0.726	2.656
62X-1, 100–102	268.6	270.42	0.56	1.275	1.343	0.59	2.227	0.735	2.773
62X-2, 100–102	270.11	271.93	0.564	1.291	1.336	0.583	2.2	0.735	2.774
62X-3, 90–92	271.51	273.33	0.559	1.267	1.351	0.596	2.268	0.737	2.805
302-M0004A-									
1H-1, 100–102	18	18.37	0.358	0.558	1.706	1.095	2.714	0.596	1.478
1H-2, 100–102	19.51	19.88	0.303	0.435	1.804	1.257	2.696	0.534	1.145
2X-1, 100–102	21.5	21.24	0.214	0.272	1.887	1.484	2.448	0.394	0.65
3X-1, 102–104	26.52	24.69	0.338	0.51	1.741	1.153	2.706	0.574	1.347

Table T35 (continued).

Core, section, interval (cm)	Depth (mbsf)	Depth (mcd)	Water content (wt%) Wet	Water content (wt%) Dry	Density (g/cm³) Bulk	Density (g/cm³) Dry	Density (g/cm³) Grain	Porosity (%)	Void ratio
2X-2, 100–102	23	22.74	0.328	0.488	1.758	1.182	2.704	0.563	1.288
3X-2, 102–104	28.02	26.19	0.37	0.587	1.682	1.06	2.698	0.607	1.546
6X-1, 102–104	274.52	274.52	0.579	1.375	1.325	0.558	2.222	0.749	2.983
6X-2, 102–104	276.02	276.02	0.585	1.408	1.328	0.552	2.285	0.759	3.142
6X-3, 102–104	277.53	277.53	0.597	1.484	1.303	0.525	2.191	0.76	3.175
7X-1, 102–104	279.52	279.72	0.581	1.385	1.327	0.556	2.245	0.752	3.036
7X-2, 102–104	281.04	281.24	0.587	1.421	1.321	0.546	2.25	0.757	3.122
7X-3, 102–104	282.55	282.75	0.542	1.186	1.37	0.627	2.288	0.726	2.65
10X-1, 102–104	292.87	292.87	0.548	1.212	1.352	0.611	2.208	0.723	2.614
10X-3, 102–104	295.87	295.87	0.531	1.133	1.377	0.646	2.262	0.715	2.503
10X-4, 42–44	296.78	296.78	0.532	1.138	1.373	0.642	2.243	0.714	2.493
11X-1, 102–104	298.32	298.32	0.573	1.341	1.249	0.534	1.772	0.699	2.322
11X-2, 102–104	299.82	299.82	0.51	1.039	1.418	0.696	2.365	0.706	2.4
11X-3, 102–104	301.33	301.33	0.489	0.957	1.415	0.723	2.228	0.675	2.082
19X-1, 102–104	321.55	321.55	0.442	0.791	1.506	0.841	2.397	0.649	1.851
19X-1, 102–104	321.55	321.55	0.416	0.712	1.544	0.902	2.418	0.627	1.682
19X-2, 82–92	322.85	322.85	0.406	0.684	1.572	0.933	2.478	0.623	1.655
20X-1, 82–92	327.1	327.1	0.399	0.665	1.601	0.961	2.56	0.625	1.663
20X-2, 72–82	327.99	327.99	0.395	0.652	1.567	0.949	2.396	0.604	1.526
21X-1, 102–104	330.3	330.3	0.433	0.763	1.514	0.858	2.384	0.64	1.777
21X-2, 102–104	331.83	331.83	0.429	0.75	1.544	0.882	2.494	0.646	1.827
22X-1, 60–62	339.6	339.6	0.419	0.722	1.533	0.89	2.39	0.627	1.684
22X-1, 100–102	340	340	0.427	0.746	1.506	0.862	2.321	0.629	1.692
23X-2, 100–102	344.11	344.11	0.449	0.814	2.218	1.223	44.034	0.972	35.015
23X-3, 70–72	345.31	345.31	0.365	0.574	1.607	1.021	2.386	0.572	1.338
27X-1, 110–112	368.5	368.5	0.319	0.468	1.74	1.185	2.588	0.542	1.184
27X-2, 100–102	369.9	369.9	0.291	0.411	1.784	1.264	2.569	0.508	1.032
27X-3, 102–104	371.42	371.42	0.265	0.361	1.886	1.386	2.71	0.489	0.956
28X-1, 102–104	372.82	373.29	0.273	0.375	1.864	1.355	2.692	0.497	0.987
28X-2, 102–104	374.32	374.79	0.254	0.34	1.906	1.422	2.695	0.472	0.895
28X-3, 102–104	375.85	376.32	0.284	0.396	1.875	1.342	2.795	0.52	1.082
28X-4, 42–44	376.75	377.22	0.248	0.329	1.9	1.429	2.645	0.46	0.851
302-M0004C-									
1H-1, 100–102	1	1	0.371	0.591	1.681	1.057	2.707	0.61	1.562
1H-2, 100–102	2.51	2.51	0.387	0.632	1.655	1.014	2.712	0.626	1.674
1H-3, 40–42	3.42	3.42	0.313	0.455	1.79	1.23	2.715	0.547	1.207
2H-1, 100–102	5	4.35	0.301	0.43	1.812	1.267	2.708	0.532	1.136
2H-2, 100–102	6.5	5.85	0.389	0.636	1.655	1.011	2.72	0.628	1.69
2H-3, 100–102	8.01	7.36	0.299	0.426	1.826	1.281	2.738	0.532	1.138
3H-1, 100–102	9.95	9.14	0.332	0.496	1.761	1.177	2.739	0.57	1.327
3H-2, 100–102	11.46	10.65	0.348	0.534	1.729	1.127	2.732	0.587	1.423
3H-3, 100–102	12.97	12.16	0.318	0.466	1.781	1.214	2.718	0.553	1.238
4H-1, 70–72	14.67	13.38	0.352	0.544	1.717	1.113	2.718	0.591	1.443
4H-2, 100–102	16.47	15.18	0.309	0.447	1.8	1.244	2.722	0.543	1.189
4H-3, 100–102	17.97	16.68	0.295	0.419	1.469	1.035	1.797	0.424	0.736
5X-1, 50–52	19.07	17.59	0.335	0.503	1.753	1.166	2.732	0.573	1.343
6X-1, 50–52	24.07	23.4	0.334	0.501	1.753	1.168	2.722	0.571	1.331
6X-2, 50–52	25.1	24.43	0.344	0.524	1.749	1.148	2.781	0.587	1.424

Table T36. Shear strength, Holes M0003A, M0004C, M0004A, and M0002A. (See table note. Continued on next two pages.)

Core, section, interval (cm)	Depth (mbsf)	Depth (mcd)	Instrument	Strength (tons/ft^2)	Shear strength (kPa)	S_u/P'
302-M0003A-						
1H-3, 150	4.51	6.63	Torvane	0.15	14.37	0.38
2H-3, 150	9.51	13.16	Torvane	0.15	14.37	0.18
302-M0004C-						
1H-3, 0	3.02	3.02	Torvane	0.05	4.79	0.19
2H-2, 0	5.5	4.85	Torvane	0.1	9.58	0.21
3H-2, 0	10.46	9.65	Torvane	0.14	13.41	0.15
4H-2, 0	15.47	14.18	Torvane	0.15	14.37	0.11
6H-2, 0	24.6	23.93	Torvane	0.2	19.16	0.09
8H-2, 150	34.44	34.38	Torvane	0.09	8.62	0.03
9H-1, 150	35.93	35.82	Torvane	0.26	24.91	0.08
302-M0004A-						
2H-2, 0	22	21.74	Torvane	0.3	29.40	0.16
3H-1, 150	27	23.67	Torvane	0.2	19.60	0.09
302-M0002A-						
5H-1, 150	18	20.34	Pock.Pen.	0.4	19.16	0.13
9H-3, 0	39	43.01	Pock.Pen.	1.2	57.48	0.18
10H-3, 150	45.5	47.51	Pock.Pen.	1.2	57.48	0.15
11H-1, 150	47.5	48.39	Pock.Pen.	1.4	67.06	0.17
12H-3, 150	54.02	55.46	Pock.Pen.	3.1	148.48	0.33
13H-CC, 0	56.5	59.44	Pock.Pen.	1.4	67.06	0.14
14H-1, 150	61.5	60	Pock.Pen.	1.6	76.63	0.15
15H-3, 150	69.5	68	Pock.Pen.	1	47.90	0.08
16H-2, 150	72	70.84	Pock.Pen.	1.6	76.63	0.13
17H-1, 150	75.5	74	Pock.Pen.	1.25	59.87	0.10
18H-1, 150	79.5	78	Pock.Pen.	0.75	35.92	0.05
19H-1, 150	82.7	81.2	Pock.Pen.	0.8	38.32	0.06
20H-1, 150	87.7	86.2	Pock.Pen.	1.6	76.63	0.10
21H-3, 0	94.22	94.22	Pock.Pen.	1.9	91.00	0.12
22H-1, 150	97.7	96.2	Pock.Pen.	2	95.79	0.12
23H-2, 150	102.83	101.33	Pock.Pen.	1.5	71.85	0.08
24H-3, 150	110.7	109.2	Pock.Pen.	3.2	153.27	0.17
25H-2, 150	113.21	112.21	Pock.Pen.	2	95.79	0.10
26H-1, 150	116.7	115.2	Pock.Pen.	2.1	100.58	0.10
27H-1, 150	121.7	120.2	Pock.Pen.	2.1	100.58	0.10
28H-2, 0	126.7	126.7	Pock.Pen.	0.75	35.92	0.03
29H-3, 0	131.2	131.2	Pock.Pen.	3.2	153.27	0.14
30H-2, 0	134.71	134.71	Pock.Pen.	2.25	107.77	0.10
32H-3, 150	144.21	142.71	Pock.Pen.	2.75	131.72	0.11
33H-2, 0	145.71	146.51	Pock.Pen.	2.75	131.72	0.11
34H-1, 150	150.5	149	Pock.Pen.	2.6	124.53	0.10
35H-4, 150	158.77	157.27	Pock.Pen.	3.5	167.64	0.13
36H-CC, 0	159	159	Pock.Pen.	4	191.59	0.14
37H-1, 0	163.5	162.5	Pock.Pen.	>4.6	>220	
38H-3, 150	169.58	168.08	Pock.Pen.	4.3	205.96	0.15
39H-1, 150	172.18	171.88	Pock.Pen.	4.4	210.75	0.15
40H-2, 150	176.08	174.58	Pock.Pen.	2.8	134.11	0.09
42H-3, 0	185.49	185.49	Pock.Pen.	3.5	167.64	0.11
43H-2, 150	190.48	188.98	Pock.Pen.	4.5	215.53	0.14
44H-2, 0	193.49	193.49	Pock.Pen.	3.75	179.61	0.11
46H-2, 150	200	199.07	Pock.Pen.	>4.6	>220	
47H-2, 150	203.76	201.7	Pock.Pen.	~4.6	>220	
48H-1	205.5	206.64	Pock.Pen.	>4.6	>220	
49H-1	210	212.32	Pock.Pen.	>4.6	>220	
50H-1	215	217.88	Pock.Pen.	>4.6	>220	
52H-1	220.94	224.96	Pock.Pen.	>4.6	>220	
53H-3, 150	229.52	229.84	Pock.Pen.	3.75	179.61	
55H-5, 150	241.13	240.7	Pock.Pen.	>4.6	>220	
56H-3, 150	243.24	243.56	Pock.Pen.	2.75	131.72	0.07
57H-3, 150	247.73	248.05	Pock.Pen.	>4.6	>220	
59H-3, 150	259.11	259.43	Pock.Pen.	>4.6	>220	
60H-1, 150	259.1	260.54	Pock.Pen.	2.75	131.72	0.06
61H-3, 150	265.61	265.99	Pock.Pen.	>4.6	>220	
1H-1, 66	0.66	0.94	Fall cone	9.31	7.74	1.41
3H-1, 69	7.19	11.73	Fall cone	9.18	7.97	0.13
5H-2, 40	18.41	22.25	Fall cone	5.62	21.25	0.14

Table T36 (continued).

Core, section, interval (cm)	Depth (mbsf)	Depth (mcd)	Instrument	Strength (tons/ft^2)	Shear strength (kPa)	S_u/P'
5H-1, 92	17.42	21.26	Fall cone	6.02	18.52	0.13
6H-1, 105.5	22.555	24.215	Fall cone	5.10	25.81	0.14
6H-2, 44	23.31	24.97	Fall cone	6.00	18.65	0.10
7H-1, 53	27.03	31.6	Fall cone	5.13	25.51	0.11
7H-2, 56	28.56	33.13	Fall cone	7.93	10.67	0.04
7H-2, 90	28.9	33.47	Fall cone	7.68	11.38	0.05
8H-2, 52	33.02	37.59	Fall cone	5.97	18.83	0.07
8H-2, 89	33.39	37.96	Fall cone	5.80	19.95	0.07
9H-1, 41	36.41	40.42	Fall cone	6.90	14.10	0.05
9H-1, 111	37.11	41.12	Fall cone	5.15	25.31	0.08
9H-2, 42	37.92	41.93	Fall cone	5.97	18.83	0.06
9H-2, 123	38.73	42.74	Fall cone	5.86	19.55	0.06
9H-3, 24	39.24	43.25	Fall cone	5.92	19.15	0.06
10H-1, 108	42.08	45.59	Fall cone	3.70	49.03	0.14
10H-2, 67	43.17	46.68	Fall cone	2.96	76.61	0.21
10H-3, 53	44.53	48.04	Fall cone	3.55	53.26	0.14
12H-3, 33	52.85	55.79	Fall cone	0.93	776.10	1.76
13H-1, 55	55.55	58.49	Fall cone	4.06	40.72	0.09
14H-2, 50	62.01	62.01	Fall cone	3.05	72.16	0.14
15H-3, 10	68.1	68.1	Fall cone	2.56	102.42	0.18
16H-3, 15	72.16	72.5	Fall cone	0.97	713.41	1.19
17H-2, 20	75.71	75.71	Fall cone	2.81	85.01	0.13
18H-1, 70	78.7	78.7	Fall cone	4.41	34.52	0.05
19H-1, 50	81.7	81.7	Fall cone	4.60	31.72	0.05
20H-2, 80	88.51	88.51	Fall cone	1.84	198.27	0.27
21H-3, 16	94.38	94.38	Fall cone	2.85	82.64	0.11
23H-2, 51	101.84	101.84	Fall cone	3.00	74.58	0.09
24H-1, 55	106.75	106.75	Fall cone	2.32	124.71	0.14
24H-1, 110	107.3	107.3	Fall cone	1.94	178.35	0.20
24H-2, 50	108.19	108.19	Fall cone	3.58	52.37	0.06
24H-3, 62	109.82	109.82	Fall cone	2.81	85.01	0.09
25H-1, 75	110.95	111.45	Fall cone	4.71	30.26	0.03
25H-2, 96	112.67	113.17	Fall cone	3.23	64.34	0.07
25H-3, 40	113.62	114.12	Fall cone	3.79	46.73	0.05
26H-1, 93	116.13	116.13	Fall cone	3.32	60.90	0.06
26H-2, 27	116.97	116.97	Fall cone	3.25	63.55	0.07
27H-1, 70	120.9	120.9	Fall cone	3.62	51.22	0.05
27H-2, 73	122.43	122.43	Fall cone	2.27	130.27	0.13
27H-3, 27	123.48	123.48	Fall cone	3.71	48.77	0.05
29H-1, 100	129.2	129.2	Fall cone	2.65	95.59	0.09
29H-2, 69	130.39	130.39	Fall cone	1.87	191.96	0.18
29H-3, 74	131.94	131.94	Fall cone	2.62	97.79	0.09
30H-1, 84	134.04	134.04	Fall cone	1.14	516.50	0.46
30H-2, 67	135.38	135.38	Fall cone	1.07	586.30	0.52
30H-3, 35	136.56	136.56	Fall cone	1.28	409.70	0.36
31H-1, 52	135.22	138.22	Fall cone	1.40	342.47	0.30
33H-1, 80	145	145.8	Fall cone	1.08	575.49	0.48
33H-2, 72	146.43	147.23	Fall cone	2.40	116.54	0.10
33H-3, 30	147.53	148.33	Fall cone	1.48	306.45	0.25
34H-CC, 5	151.92	151.92	Fall cone	1.13	525.69	0.42
34H-1, 45	149.45	149.45	Fall cone	2.21	137.44	0.11
34H-2, 50	151	151	Fall cone	2.65	95.59	0.08
34H-CC, 5	151.92	151.92	Fall cone	0.75	1193.33	0.94
35H-1, 10	154.1	154.1	Fall cone	0.61	1803.95	1.40
35H-2, 67	154.94	154.94	Fall cone	1.77	214.26	0.17
35H-3, 67	156.43	156.43	Fall cone	2.00	167.81	0.13
35H-4, 79	158.06	158.06	Fall cone	2.84	83.22	0.06
37H-1, 70	164.2	163.2	Fall cone	1.10	554.75	0.41
37H-2, 77	165.78	164.78	Fall cone	1.76	216.70	0.16
37H-3, 22	166.74	165.74	Fall cone	0.35	5479.59	3.94
38H-1, 20	166.7	166.7	Fall cone	1.28	409.70	0.29
38H-2, 60	167.49	167.49	Fall cone	3.07	71.22	0.05
38H-3, 20	168.28	168.28	Fall cone	1.31	391.15	0.28
38H-3, 110	169.18	169.18	Fall cone	2.75	88.76	0.06
38H-4, 86	170.45	170.45	Fall cone	1.27	416.18	0.29
38H-5, 25	171.36	171.36	Fall cone	1.06	597.41	0.42
39H-1, 40	171.08	172.28	Fall cone	2.99	75.08	0.05
39H-CC, 14	171.62	172.82	Fall cone	1.21	458.47	0.32
40H-1, 10	173.18	173.18	Fall cone	2.82	84.41	0.06

Table T36 (continued).

Core, section, interval (cm)	Depth (mbsf)	Depth (mcd)	Instrument	Strength (tons/ft^2)	Shear strength (kPa)	S_u/P'
40H-4, 30	177.89	177.89	Fall cone	1.62	255.77	0.17
40H-2, 10	174.68	174.68	Fall cone	0.80	1048.83	0.72
40H-3, 10	176.19	176.19	Fall cone	2.26	131.42	0.09
42H-1, 10	182.59	182.59	Fall cone	1.26	422.81	0.28
42H-2, 110	185.09	185.09	Fall cone	0.63	1691.23	1.10
42H-3, 90	186.39	186.39	Fall cone	1.45	319.26	0.21
42H-4, 13	187.13	187.13	Fall cone	1.32	385.24	0.25
43H-1, 80	188.29	188.29	Fall cone	0.76	1162.14	0.74
43H-2, 70	189.68	189.68	Fall cone	1.63	252.64	0.16
43H-3, 100	191.49	191.49	Fall cone	1.56	275.83	0.17
44H-1, 5	192.04	192.04	Fall cone	2.48	109.14	0.07
44H-1, 30	192.29	192.29	Fall cone	1.97	172.96	0.11
44H-1, 75	192.74	192.74	Fall cone	1.63	252.64	0.16
44H-1, 120	193.19	193.19	Fall cone	2.06	158.18	0.10
44H-2, 30	193.79	193.79	Fall cone	1.67	240.69	0.15
44H-2, 130	194.79	194.79	Fall cone	0.62	1746.23	1.08
44H-3, 40	195.4	195.4	Fall cone	0.32	6555.17	4.02
44H-4, 8	195.81	195.81	Fall cone	0.14	34247.41	20.98
45H-1, 17	196.1	196.1	Fall cone	0.95	743.77	0.45
45H-1, 50	196.43	196.43	Fall cone	0.36	5179.39	3.16
45H-1, 110	197.03	197.03	Fall cone	0.93	776.10	0.47
46H-1, 124	198.24	198.81	Fall cone	0.36	5179.39	3.13
46H-1, 34	197.34	197.91	Fall cone	1.04	620.61	0.38
46H-2, 97	199.47	200.04	Fall cone	0.26	9929.72	5.97
46H-3, 27	200.27	200.84	Fall cone	0.49	2795.71	1.67
47H-2, 40	202.66	202.1	Fall cone	0.14	34247.41	20.27
47H-5, 27	207.06	206.5	Fall cone	0.24	11653.63	6.75
49H-2, 63	210.78	213.1	Fall cone	0.93	776.10	0.44
49H-3, 60	212.25	214.57	Fall cone	1.11	544.80	0.31
49H-4, 24	213.4	215.72	Fall cone	0.63	1691.23	0.95
52H-1, 70	221.64	225.66	Fall cone	0.34	5806.65	3.14
302-M0003A-						
1H-4, 20	4.64	8.26	Fall cone	7.67	11.41	0.30
2H-1, 141	6.41	11.56	Fall cone	6.45	16.13	0.30
2H-2, 20	6.7	11.85	Fall cone	5.71	20.59	0.37
3H-4, 27	14.64	18.97	Fall cone	5.14	25.41	0.21
3H-2, 82.5	12.325	16.655	Fall cone	5.60	21.40	0.21
302-M0004A-						
1H-2, 48	18.99	19.36	Fall cone	5.92	19.15	0.12
1H-3, 31	20.03	20.4	Fall cone	6.81	14.47	0.09
2H-1, 118	21.68	21.42	Fall cone	6.24	17.24	0.10
2H-1, 32	20.82	20.56	Fall cone	4.13	39.35	0.23
2H-2, 24	22.24	21.98	Fall cone	5.68	20.81	0.11
2H-2, 122	23.22	22.96	Fall cone	5.16	25.21	0.13
2H-3, 39	23.89	23.63	Fall cone	4.80	29.13	0.15
3H-1, 30	25.8	23.97	Fall cone	5.10	25.81	0.12
3H-1, 116	26.66	24.83	Fall cone	6.35	16.65	0.07
3H-2, 69	27.69	25.86	Fall cone	7.47	12.03	0.05
302-M0004C-						
1H-3, 38.5	3.405	3.405	Fall cone	6.80	14.52	0.51
2H-1, 129	5.29	4.64	Fall cone	7.06	13.47	0.31
2H-1, 87	4.87	4.22	Fall cone	5.73	20.44	0.50
1H-CC, 6	3.78	3.78	Fall cone	5.00	26.85	0.85
3H-CC, 40	14.06	13.25	Fall cone	6.97	13.82	0.12
4H-2, 136	16.83	15.54	Fall cone	5.91	19.22	0.14
5H-1, 59	19.16	17.68	Fall cone	5.14	25.41	0.16
6H-1, 98	24.55	23.88	Fall cone	3.60	51.79	0.25
6H-2, 62	25.22	24.55	Fall cone	4.54	32.57	0.15
8H-1, 11	31.54	32.98	Fall cone	9.27	7.81	0.03

Note: Pock.Pen. = pocket penetrometer.

Table T37. Thermal conductivity, Holes M0002A, M0003A, M0004A, and M0004C. (See table note. Continued on next page.)

Core, section, interval (cm)	Depth (mbsf)	Depth (mcd)	Thermal conductivity (W/m·K) Average	1	2	3	Probe type	Temperature (°C)
302-M0002A-								
1X, 1–60	0.6	0.88	1.073	1.063	1.084	—	V10269	15.00
3X, 2–75	8.75	13.29	1.163	1.176	1.157	1.156	V10269	15.00
4X, 2–75	13.75	13.75	1.137	1.134	1.141	1.138	V10269	14.00
5X, 2–55	18.56	22.4	1.212	—	1.211	1.213	V10269	15.00
6X, 2–120	24.07	25.73	1.175	1.177	1.168	1.179	V10269	15.00
7X, 2–55	28.55	33.12	1.298	1.299	1.299	1.295	V10269	16.64
8X, 2–55	33.05	37.62	1.255	1.255	1.256	1.253	V10269	19.18
9X, 2–78	38.28	42.29	1.284	1.285	1.282	—	V10269	18.44
10X, 2–58	43.08	46.59	1.337	1.350	1.327	1.335	V10269	17.70
11X, 2–75	48.24	50.63	1.293	1.293	1.290	1.297	V10269	17.66
12X, 2–50	52.02	54.96	1.226	1.238	1.220	1.219	V10269	17.80
13X, 1–60	55.6	58.54	1.199	1.199			V10269	18.02
13X, 1–80	55.8	58.74	1.234	1.176	1.234*	—	V10269	19.20
15X, 2–80	67.31	67.31	1.397	1.391	1.402	—	V10269	17.95
17X, 2–20	75.71	75.71	1.302	1.294	1.311	1.302	V10269	17.93
18X, 1–75	78.75	78.75	1.270	1.273	1.271	1.267	V10269	17.97
19X, 1–50	81.7	81.7	1.317	1.311	1.318	1.322	V10269	17.80
20X, 2–75	88.46	88.46	1.396	1.401	1.391	1.396	V10269	17.29
21X, 2–75	93.46	93.46	1.336	1.336	1.338	1.336	V10269	17.52
22X, 1–20	96.4	96.4	1.364	1.375	1.355	1.363	V10269	16.90
23X, 2–60	101.93	101.93	1.370	1.352	1.382	1.377	V10269	17.10
24X, 2–60	108.29	108.29	1.392	1.391	1.394	1.391	V10269	19.02
25X, 2–75	112.46	112.96	1.295	1.290	1.300	—	V10269	18.84
26X, 2–32	117.02	117.02	1.414	1.422	1.417	1.403	V10269	18.52
27X, 2–70	122.4	122.4	1.360	1.362	1.363	1.311	V10269	17.83
28X, 2–57	127.27	127.27	1.306	1.298	1.308	1.311	V10269	17.74
29X, 2–75	130.45	130.45	1.398	1.391	1.403	1.399	V10269	17.29
30X, 2–72	135.43	135.43	1.419	1.413	1.424	1.420	V10269	17.09
31X, 1–45	135.15	138.15	1.437	1.429	1.445	1.436	V10269	17.00
32X, 2–75	141.95	141.95	1.354	1.346	1.362	1.354	V10269	17.07
33X, 2–70	146.41	147.21	1.384	1.391	1.378	1.384	V10269	16.51
34X, 2–65	151.15	151.15	1.385	1.374	1.396	1.385	V10269	16.23
35X, 2–75	155.02	155.02	1.413	1.389	1.435	1.415	V10269	15.50
37X, 2–75	165.76	164.76	1.366	1.388	1.355	1.357	V10269	15.16
38X, 2–75	167.64	167.64	—	—	—	—	V10269	17.510
39X, 1–40	171.08	172.28	1.283	1.283	1.284	1.281	V10269	16.41
40X, 2–75	175.33	175.33	1.269	1.260	1.277	1.268	V10269	16.47
42X, 2–75	184.74	184.74	1.254	1.253	1.255	1.255	V10269	16.28
43X, 2–75	189.73	189.73	1.212	1.204	1.218	1.216	V10269	15.90
44X, 2–75	194.24	194.24	—	—	—	—	V10269	15.70
45X, 1–75	196.68	196.68	0.786	0.786	0.793	0.780	V10269	16.52
46X, 2–90	199.4	199.97	—	—	—	—	V10269	—
47X, 2–84	203.1	202.54	—	—	—	—	V10269	—
48X, 2–70	207.7	208.84	1.189	1.189	—	—	V10269	—
49X, 2–75	210.9	213.22	—	—	—	—	V10269	—
50X, 2–30	216.81	219.69	1.126	1.127	—	1.125	V10269	
302-M0003A-								
1H, 2–75	2.25	5.87	1.137	1.137	1.138	1.136	V10269	16.25
2H, 2–75	7.25	12.4	1.234	1.233	1.234	1.234	V10269	16.4
3H, 2–75	12.25	16.58	1.184	1.184	—	—	V10269	17.5
302-M0004A-								
1H, 2–60	19.11	19.48	1.233	1.239	1.232	1.228	V10209	19.15
2X, 2–77	22.77	22.51	1.177	1.177	—	—	V10209	19.04
3X, 2–62	27.62	25.79	1.130	1.127	1.134	—	V10209	19.04
6X, 2–75	275.75	275.75	0.739	0.739	—	—	V10209	14.48
7X, 2–75	280.77	280.97	—	—	—	—	V10209	—
10X, 2–75	294.1	294.1	—	—	—	—	V10209	—
11X, 2–75	299.55	299.55	—	—	—	—	V10209	—
19X, 2–75	322.78	322.78	—	—	—	—	V10209	15.74
302-M0004C-								
1H, 2–70	2.21	2.21	1.436	1.431	1.448	1.430	—	17.5
2H, 2–75	6.25	5.6	1.258	1.261	1.255		—	16.8
3H, 2–75	11.21	10.4	1.160	1.164	1.159	1.166	—	15
4H, 2–75	16.22	14.93	1.178	1.178	1.177	1.179	—	
5X, 1–40	18.97	17.49	1.147	1.147	1.147	1.148	—	16.7

Table T37 (continued).

Core, section, interval (cm)	Depth (mbsf)	Depth (mcd)	Thermal conductivity (W/m·K) Average	1	2	3	Probe type	Temperature (°C)
6X, 2–22	24.82	24.15	1.278	1.274	1.283	1.277	—	16.4
8X, 2–60	33.54	34.98	1.129	1.127	1.133	1.127	—	16.7
9X, 2–20	36.13	37.52					—	16.9

Note: * = good LET > 800.

Table T38. In situ recorded temperature measurements from the Lomonsov Ridge.

Depth (mbsf)	Mudline (°C) In	Mudline (°C) Out	Temperature (°C)	Adjustment	Corrected temperature (°C)	Tool type
0	–0.46	NA	NA	0.00	–0.46	Calculated from Adara
20	–0.20	NA	–0.10	0.26	0.06	BGS
25	–0.40	–0.55	1.02	0.06	1.08	Adara
37.8	–0.45	–0.45	0.99	0.01	1.00	Adara
60	–0.10	NA	2.65	0.36	3.00	BGS
100	0.00	NA	2.25	0.46	2.70	BGS

Notes: Regression excludes the measurement at 60 mbsf. BGS = British Geological Survey. NA = not available.

Table T39. Pore water chemistry, Holes M0001A, M0002A, M0003A, M0004A, M0004B, and M0004C. (See table notes. Continued on next two pages.)

Core, section, interval (cm)	Sample type	Depth (mbsf)*	Depth (mcd)†	Salinity (ppt)	pH	Alkalinity (mM)	NH_4^+ (µm)	B (µm)	Ba (µm)	Ca (mM)
Surface seawater (n = 5)	—	—	—	34	7.8	2.2	0	472	0.5	9.5
Drill mud (filtered)	—	—	—	34	NA	NA	13	NA	NA	NA
302-M0001A-										
1H-CC‡, 4–14	Rhizone	5.10	—	35	7.6	2.7	9	577	0.6	9.6
302-M0002A-										
1X-1, 80–91	Rhizone	0.86	1.14	37	7.5	2.5	NA	639	0.5	10.3
2X-1, 86–96	Rhizone	2.41	1.94	40	7.7	2.9	2	725	0.5	10.3
3X-2, 124–133	Rhizone	9.29	13.83	37	7.5	2.6	52	679	0.6	10.6
3X-2, 145–150	Squeezer	9.48	14.02	38	7.3	2.4	60	681	0.6	10.7
4X-2, 120–125	Rhizone	14.23	14.23	37	7.4	2.4	52	689	0.6	10.6
6X-2, 50–60	Rhizone	23.42	25.08	37	7.3	2.3	114	600	0.5	10.6
6X-2, 145–150	Squeezer	24.35	26.01	38	7.3	2.2	111	671	0.5	10.7
7X-2, 137–147	Rhizone	29.42	33.99	39	NA	NA	155	672	0.5	10.7
10X-2, 72–83	Rhizone	43.28	46.79	NA	7.3	1.6	181	NA	NA	NA
10X-2, 144–150	Squeezer	43.97	47.48	37	7.2	1.7	215	693	0.6	11.1
12X-2, 92–100	Squeezer	52.48	55.42	37	7.2	1.8	199	712	0.6	10.9
16X-2, 144–150	Squeezer	71.97	72.31	38	7.2	1.6	247	689	0.6	11.1
18X-1, 138–145	Squeezer	79.42	79.42	NA	7.1	1.8	217	670	0.6	11.0
21X-2, 143–150	Squeezer	94.18	94.18	38	7.1	1.7	308	673	0.6	11.4
23X-2, 114–120	Squeezer	102.50	102.50	37	6.9	1.8	341	628	0.7	11.6
24X-2, 144–151	Squeezer	109.17	109.17	37	7.0	2.1	359	639	0.7	11.7
27X-2, 144–150	Squeezer	123.17	123.17	36	7.1	2.3	353	620	0.7	11.9
30X-2, 144–150	Squeezer	136.18	136.18	38	7.2	2.6	428	620	0.7	12.2
33X-2, 144–150	Squeezer	147.18	147.98	37	7.1	3.7	431	626	0.8	12.4
37X-2, 143–150	Squeezer	166.48	165.48	36	7.1	4.8	461	588	0.7	12.8
40X-2, 144–151	Squeezer	176.06	176.06	36	7.0	5.5	403	600	0.8	13.0
44X-2, 146–151	Squeezer	194.98	194.98	NA	7.2	6.7	443	610	1.0	13.6
48X-2, 140–151	Squeezer	208.46	209.60	NA	7.1	6.9	519	530	1.2	13.4
52X-2, 140–151	Squeezer	223.91	227.93	36	7.2	6.8	597	537	0.9	13.6
60X-1, 140–151	Squeezer	259.06	262.00	35	7.2	7.4	516	471	0.9	14.1
302-M0003A-										
1H-1, 131–141	Rhizone	1.36	4.98	NA	7.5	2.7	5	712	0.6	10.7
2H-1, 130–142	Rhizone	6.36	11.51	NA	7.6	2.7	34	684	0.6	10.8
302-M0004A-										
2X-2, 135–145	Rhizone	23.40	23.14	NA	7.5	2.2	123	628	0.6	10.7
2X-2, 145–150	Squeezer	23.48	23.22	38	7.4	2.4	106	636	0.6	10.9
6X-2, 145–151	Squeezer	276.48	276.48	37	7.4	7.0	1427	504	0.9	13.1
10X-2, 143–150	Squeezer	294.82	294.82	NA	7.1	7.6	1018	496	1.0	13.4
19X-1, 144–151	Squeezer	322.01	322.01	NA	7.6	7.7	1005	471	1.5	13.7
23X-1, 144–150	Squeezer	343.07	343.07	NA	7.3	7.4	1221	445	NA	13.7
30X-2, 143–152	Squeezer	383.29	383.29	NA	7.4	7.7	NA	369	NA	15.0
34X-2, 144–150	Squeezer	398.98	398.98	NA	7.4	8.0	754	379	2.3	14.6
302-M0004B-										
1X-1, 127–137	Rhizone	11.32	11.48	NA	7.4	2.6	66	650	0.7	10.8
1X-1, 139–144	Squeezer	11.42	11.58	NA	7.5	2.6	62	721	0.6	10.8
302-M0004C-										
1H-1, 10	Rhizone	0.10	0.10	NA	7.6	2.6	0	710	0.5	10.7
1H-1, 30	Rhizone	0.30	0.30	NA	7.6	2.6	NA	763	0.5	10.7
1H-1, 80	Rhizone	0.80	0.80	NA	NA	NA	NA	815	0.5	10.4
1H-1, 135	Rhizone	1.35	1.35	NA	7.4	2.6	NA	702	0.6	10.5
1H-2, 40	Rhizone	1.91	1.91	NA	NA	NA	NA	775	0.7	10.5
1H-2, 100	Rhizone	2.51	2.51	NA	7.6	2.8	0	708	NA	10.0
1H-3, 39	Rhizone	3.41	3.41	NA	7.7	2.9	0	739	NA	9.9
2H-1, 40–43	Rhizone	4.42	3.77	NA	7.6	3.1	7	702	0.5	10.6
2H-1, 120–123	Rhizone	5.22	4.57	NA	7.6	2.8	13	744	0.6	10.6
2H-2, 40–43	Rhizone	5.92	5.27	NA	7.5	2.8	17	704	0.6	10.7
2H-2, 130–134	Rhizone	6.82	6.17	NA	7.6	2.9	22	746	0.2	10.8
2H-3, 40–43	Rhizone	7.43	6.78	NA	7.5	2.8	24	699	0.6	10.7
2H-3, 130–134	Rhizone	8.33	7.68	NA	7.6	2.7	31	764	0.8	10.8
3H-1, 39–43	Rhizone	9.36	8.55	NA	7.6	2.8	32	694	0.8	10.8
3H-1, 119–124	Rhizone	10.17	9.36	NA	7.6	2.6	40	705	0.8	10.8
3H-2, 39–43	Rhizone	10.87	10.06	NA	7.6	2.7	44	NA	NA	NA
3H-2, 119–124	Rhizone	11.68	10.87	NA	7.6	2.6	47	710	0.8	10.8
3H-3, 20–23	Rhizone	12.19	11.38	NA	7.6	2.6	50	802	1.2	10.8
3H-3, 140–143	Rhizone	13.39	12.58	NA	7.6	2.6	59	757	0.9	10.8

Table T39 (continued).

Core, section, interval (cm)	Fe (μm)	K (mM)	Mg (mM)	Mn (μm)	Na (mM)	S (mM)	Si (μm)	Sr (μm)	Cl^- (mM)	SO_4^{2-} (mM)	PO_4^{3-} (μm)	ZnAc PPT (color)
Surface seawater (n = 5)	0.4	9	49	0.0	419	26.2	59	77.6	499	22.9	2.3	NA
Drill mud (filtered)	NA	NA	NA	NA	NA	NA	NA	NA	NA	NA	NA	NA
302-M0001A-												
1H-CC‡	0.3	10	47	64.9	NA	26.4	117	81.0	NA	NA	NA	NA
302-M0002A-												
1X-1, 80–91	0.4	11	52	-0.0	478	28.5	150	87.5	565	28.1	2.1	NA
2X-1, 86–96	0.6	12	51	28.5	479	28.6	169	88.5	NA	NA	NA	NA
3X-2, 124–133	1.0	11	51	175.4	480	28.1	153	93.0	565	28.0	5.9	NA
3X-2, 145–150	0.8	11	51	174.5	479	28.6	180	94.6	NA	NA	NA	NA
4X-2, 120–125	0.9	11	51	176.7	480	28.4	148	93.4	NA	NA	NA	NA
6X-2, 50–60	61.8	11	50	125.6	483	27.4	134	94.5	564	26.8	8.3	NA
6X-2, 145–150	90.2	11	50	153.8	483	27.6	183	97.0	566	27.9	2.4	None
7X-2, 137–147	142.7	10	49	95.7	485	26.4	143	97.4	NA	NA	NA	NA
10X-2, 72–83	NA	NA	NA	NA	488	NA	NA	NA	NA	NA	NA	NA
10X-2, 144–150	232.2	9	49	51.3	NA	25.5	186	104.5	565	24.6	3.0	None
12X-2, 92–100	293.7	9	49	36.4	489	24.8	180	103.4	565	23.3	3.1	Orange
16X-2, 144–150	308.3	8	47	16.9	486	22.8	177	106.4	565	20.9	3.9	Orange
18X-1, 138–145	239.2	9	48	42.2	487	24.8	174	103.6	566	23.9	3.0	Orange
21X-2, 143–150	316.8	7	46	8.8	483	20.9	172	110.1	567	19.5	2.5	Orange
23X-2, 114–120	339.8	7	46	8.0	483	20.4	172	111.8	568	19.2	2.5	Orange
24X-2, 144–151	296.9	7	45	6.6	482	20.3	173	114.1	567	18.3	2.2	Orange
27X-2, 144–150	179.6	7	45	4.8	482	18.0	162	114.9	564	19.0	2.5	Orange
30X-2, 144–150	44.0	7	44	5.8	482	17.0	158	117.7	564	15.6	2.9	Orange
33X-2, 144–150	102.1	7	44	24.1	482	16.7	180	120.0	567	16.5	1.8	Orange
37X-2, 143–150	5.3	6	43	143.9	482	14.8	203	124.6	567	15.2	5.8	None
40X-2, 144–151	0.5	7	42	189.0	483	14.0	248	128.3	567	13.9	3.7	NA
44X-2, 146–151	15.5	6	43	180.0	478	12.1	454	136.4	566	14.0	3.8	NA
48X-2, 140–151	1.4	6	42	182.7	482	10.9	1133	142.6	564	11.6	16.0	White
52X-2, 140–151	0.9	7	41	205.0	485	10.2	1242	149.1	565	11.2	38.9	White
60X-1, 140–151	1.5	6	41	168.7	485	9.4	1172	162.1	564	8.3	14.4	White
302-M0003A-												
1H-1, 131–141	0.6	12	52	59.8	481	29.2	146	92.1	567	31.7	2.3	NA
2H-1, 130–142	0.3	11	52	164.5	484	28.9	137	98.2	566	29.0	NA	NA
302-M0004A-												
2X-2, 135–145	61.2	10	51	210.3	487	27.7	157	95.2	NA	NA	NA	NA
2X-2, 145–150	61.8	10	51	211.3	487	28.3	188	97.6	565	28.5	7.2	NA
6X-2, 145–151	1.8	6	38	164.7	488	11.7	1221	123.8	567	11.8	19.0	NA
10X-2, 143–150	1.9	5	37	179.2	490	10.0	1289	130.8	568	10.8	19.2	White
19X-1, 144–151	0.8	5	36	156.8	486	10.0	765	152.6	569	9.5	19.8	NA
23X-1, 144–150	0.4	11	35	73.7	NA	9.5	674	157.1	567	10.2	12.5	NA
30X-2, 143–152	0.5	16	38	24.6	NA	8.3	456	186.8	568	9.4	4.7	NA
34X-2, 144–150	22.4	4	35	18.4	490	8.1	250	181.8	569	7.0	1.4	White
302-M0004B-												
1X-1, 127–137	0.5	11	52	187.9	489	29.0	133	94.4	566	29.3	3.1	NA
1X-1, 139–144	0.3	11	51	195.3	485	29.2	180	96.3	566	27.5	2.7	NA
302-M0004C-												
1H-1, 10	0.5	12	53	0.0	479	29.8	75	91.4	565	31.0	1.8	NA
1H-1, 30	0.6	12	52	0.1	479	29.6	96	92.3	NA	NA	NA	NA
1H-1, 80	0.4	12	51	0.0	481	29.7	134	91.1	NA	NA	NA	NA
1H-1, 135	0.3	12	53	-0.0	480	29.5	134	89.9	NA	NA	NA	NA
1H-2, 40	0.6	12	52	21.0	482	29.5	148	90.0	NA	NA	NA	NA
1H-2, 100	0.3	14	50	54.1	NA	28.0	118	88.1	NA	NA	NA	NA
1H-3, 39	0.3	14	50	96.3	NA	27.9	127	86.4	NA	NA	NA	NA
2H-1, 40–43	0.4	12	52	117.7	480	29.4	143	89.7	NA	NA	NA	NA
2H-1, 120–123	1.1	12	52	129.6	480	29.4	139	90.1	NA	NA	NA	NA
2H-2, 40–43	0.5	12	52	137.1	478	29.4	141	92.3	565	28.2	NA	NA
2H-2, 130–134	1.5	12	52	150.9	NA	28.2	118	91.1	566	27.1	NA	NA
2H-3, 40–43	0.2	12	52	145.3	482	29.3	134	93.2	NA	NA	NA	NA
2H-3, 130–134	0.5	12	52	149.7	485	29.3	154	95.5	NA	NA	NA	NA
3H-1, 39–43	0.5	11	52	153.4	483	29.3	153	94.2	565	27.9	3.8	NA
3H-1, 119–124	0.4	11	52	160.8	481	29.2	154	93.9	566	29.2	NA	NA
3H-2, 39–43	NA	NA	NA	NA	NA	NA	NA	NA	NA	NA	NA	NA
3H-2, 119–124	0.4	11	52	162.7	484	29.2	156	93.7	566	29.9	NA	NA
3H-3, 20–23	1.0	11	52	173.5	485	29.1	209	93.6	NA	NA	NA	NA
3H-3, 140–143	0.7	11	52	182.0	485	29.0	175	94.0	NA	NA	NA	NA

Table T39 (continued).

Core, section, interval (cm)	Sample Type	Depth (mbsf)*	Depth (mcd)†	Salinity (ppt)	pH	Alkalinity (mM)	NH_4^+ (µm)	B (µm)	Ba (µm)	Ca (mM)
4H-1, 120–123	Rhizone	15.19	13.90	NA	7.6	2.6	72	786	0.8	10.8
4H-2, 38–42	Rhizone	15.87	14.58	NA	7.5	2.6	75	794	1.7	10.8
4H-2, 120–123	Rhizone	16.69	15.40	NA	7.5	2.6	77	787	0.8	10.8
4H-3, 20–23	Rhizone	17.19	15.90	NA	7.5	2.5	76	766	NA	10.2
4H-3, 108–111	Rhizone	18.07	16.78	NA	7.6	2.5	80	NA	NA	NA
8X-1, 144–151	Squeezer	32.91	34.35	NA	7.2	2.2	165	764	0.7	10.7
9X-1, 145–150	Squeezer	35.91	37.30	NA	NA	NA	NA	768	0.6	10.7

Notes: * = average depth of sampled interval, † = composite depth estimated from physical property data, after adjustments considering the NH_4^+ data. ‡ = collected and given to the chemistry laboratory without record. NA = not analyzed.

Core, section, interval (cm)	Fe (µm)	K (mM)	Mg (mM)	Mn (µm)	Na (mM)	S (mM)	Si (µm)	Sr (µm)	Cl^- (mM)	SO_4^{2-} (mM)	PO_4^{3-} (µm)	ZnAc PPT (color)
4H-1, 120–123	0.4	12	51	197.4	485	28.9	176	96.3	NA	NA	NA	NA
4H-2, 38–42	0.6	11	51	197.0	479	29.0	183	94.8	NA	NA	NA	NA
4H-2, 120–123	0.5	11	51	199.5	483	28.8	180	96.5	NA	NA	NA	NA
4H-3, 20–23	0.2	13	49	211.8	NA	27.4	145	92.9	NA	NA	NA	NA
4H-3, 108–111	NA	NA	NA	NA	NA	NA	NA	NA	NA	NA	NA	NA
8X-1, 144–151	146.8	11	49	99.6	488	27.2	187	97.4	567	26.8	0.1	NA
9X-1, 145–150	131.1	11	49	88.0	487	27.2	173	97.8	NA	NA	NA	NA

Table T40. Headspace methane concentrations, Holes M0002A, M0004A, and M0004C.

Core, section, interval (cm)	Depth (mbsf)	Depth (mcd)	Methane (ppmv)
302-M0002A-			
46X-2, 147–150	199.99	200.56	10*
49X-3, 148–151	213.15	215.47	12*
53X-3, 148–151	229.52	231.34	17
58X-2, 148–151	252.60	254.42	21*
61X-2, 0–3	264.13	266.01	19*
302-M0004A-			
7X-3, 0–3	281.55	281.75	14*
22X-1, 82–85	339.84	339.84	11*
23X-2, 146–150	344.59	344.59	140*
302-M0004C-			
8X-1, 139–144	32.85	34.29	10

Note: * = average value from two true replicates.

Table T41. Elemental contents of sediment samples, Holes M0002A, M0003A, M0004A, M0004B, and M0004C. (This table is available in an **oversized format.**)

Table T42. Relative mineral abundances in bulk sediment, Holes M0002A, M0003A, M0004A, M0004B, and M0004C. (This table is available in an **oversized format.**)

Table T43. Carbon and sulfur contents of bulk sediment, Holes M0002A, M0004A, M0004B, and M0004C.

Core, section, interval (cm)	Depth (mbsf)	Depth (mcd)	TC (wt%)	TS (wt%)	OC (wt%)	IC (wt%)	Notes
302-M0002A-							
3X-2, 124–133	9.29	13.83	0.20	0.28	0.19	0.01	
5X-2, 5–7	18.07	21.91	0.25	0.10	0.19	0.06	
6X-2, 52–54	23.40	25.06	0.30	0.41	0.21	0.09	
6X-2, 145–150	24.35	26.01	0.26	0.07	0.19	0.07	
8X-3, 50–52	34.11	38.68	0.51	0.11	0.28	0.24	
9X-2, 74–76	38.25	42.26	0.44	0.23	0.25	0.19	
10X-2, 72–74	43.23	46.74	0.26	0.08	0.22	0.04	
10X-2, 144–150	43.97	47.48	0.25	0.08	0.23	0.02	
12X-2, 56–58	52.09	55.03	0.35	0.10	0.34	0.01	
12X-2, 92–100	52.48	55.42	0.32	0.22	0.29	0.03	
15X-2, 25–27	66.77	66.77	0.37	0.21	0.28	0.09	
16X-2, 90–92	71.41	71.75	0.42	0.09	0.29	0.12	
16X-2, 144–150	71.97	72.31	0.34	0.07	0.33	0.01	
18X-2, 2–4	79.48	79.48	0.31	0.09	0.28	0.03	
18X-2, 138–145	80.87	80.87	0.28	0.07	0.27	0.02	
20X-2, 25–27	87.97	87.97	0.71	0.36	0.30	0.42	
21X-2, 25–27	92.97	92.97	0.32	0.16	0.29	0.03	
21X-2, 143–150	94.18	94.18	0.33	0.29	0.30	0.03	
23X-2, 25–27	101.59	101.59	0.37	0.09	0.28	0.09	
24X-2, 25–27	107.95	107.95	1.50	0.10	0.28	1.22	Apatite/CFA?
25X-2, 25–27	111.97	112.47	0.34	0.03	0.30	0.04	
27X-2, 25–27	121.96	121.96	0.44	0.07	0.22	0.22	
29X-2, 25–27	129.96	129.96	0.24	0.08	0.19	0.05	
30X-2, 25–27	134.97	134.97	0.25	0.21	0.25	0.00	
32X-2, 25–27	141.46	141.46	0.39	0.08	0.36	0.03	
33X-2, 25–27	145.97	146.77	0.95	0.10	0.22	0.73	Apatite/CFA?
34X-2, 25–27	150.76	150.76	0.36	0.12	0.21	0.15	
35X-2, 25–27	154.53	154.53	0.49	0.18	0.25	0.24	
37X-2, 68–70	165.70	164.70	0.10	0.19	0.10	0.01	
40X-2, 78–80	175.37	175.37	0.08	0.09	0.09	-0.00	
42X-2, 62–64	184.62	184.62	0.13	0.26	0.07	0.06	
46X-2, 64–66	199.15	199.72	3.61	12.64	3.57	0.05	High S
47X-2, 66–68	202.93	202.37	6.67	14.75	6.30	0.37	High S
50X-2, 60–62	217.12	220.00	2.85	12.30	2.76	0.09	High S
52X-2, 4–6	222.50	226.52	2.57	4.90	2.38	0.19	
53X-2, 80–82	227.33	229.15	3.02	5.91	2.81	0.21	
55X-2, 80–82	235.91	236.98	2.78	5.21	2.69	0.09	
302-M0004A-							
2X-2, 145–150	23.48	23.22	0.22	0.21	0.21	0.01	
6X-2, 145–151	276.48	276.48	3.43	6.57	3.39	0.04	
10X-2, 143–150	294.82	294.82	3.54	6.71	3.38	0.16	
19X-1, 144–151	322.01	322.01	1.83	6.83	1.77	0.06	
23X-1, 144–150	343.07	343.07	2.87	6.09	2.84	0.04	
30X-2, 143–152	383.29	383.29	3.12	9.31	3.04	0.08	
34X-2, 144–150	398.98	398.98	2.29	0.59	2.20	0.09	
34X-2, 144–150	398.98	398.98	2.31	0.63	2.20	0.11	Replicate
302-M0004B-							
1X-1, 127–137	11.32	11.48	0.23	0.08	0.20	0.03	
302-M0004C-							
1H-2, 64–66		2.16	0.22	0.09	0.18	0.05	
1H-2, 84–86	2.36	2.36	0.27	0.12	0.19	0.09	
2H-2, 64–66	6.15	5.50	0.22	0.09	0.17	0.05	
3H-2, 60–62	11.07	10.26	0.21	0.09	0.17	0.04	
4H-2, 64–66	16.12	14.83	0.21	0.10	0.19	0.02	
6X-2, 56–58	25.17	24.50	0.24	0.11	0.22	0.03	

Notes: TC = total carbon, TS = total sulfur, OC = organic carbon, IC = inorganic carbon. High TS content may affect the measured organic carbon content. CFA = carbonate fluorapatite.

Table T44. Amount and type of organic carbon in bulk sediment, Holes M0002A and M0004A. (See table note. Continued on next page.)

Core, section, interval (cm)	Top depth (mbsf)	Top depth (mcd)	TOC (wt%)	S1 (mg HC/g sed)	S2 (mg HC/g sed)	S3 (mg CO_2/g sed)	T_{max} (°C)	HI (mg HC/g C)	OI (mg CO_2/g C)
302-M0002A-									
1X-CC, 0–9	1.24	1.52	0.24	NA	NA	NA	NA	NA	NA
3X-CC, 3–11	11.72	16.26	0.18	NA	NA	NA	NA	NA	NA
4X-CC, 0–12	16.73	16.73	0.20	NA	NA	NA	NA	NA	NA
6X-CC, 0–17	26.62	28.28	0.18	NA	NA	NA	NA	NA	NA
7X-CC, 0–16	30.51	35.08	0.23	NA	NA	NA	NA	NA	NA
9X-CC, 0–47	41.70	45.77	0.24	NA	NA	NA	NA	NA	NA
10X-2, 138–144	43.91	47.42	0.30	0.15	0.27	0.49	476	92	166
12X-2, 86–92	52.41	55.35	0.32	0.12	0.24	0.33	477	75	103
12X-CC, 0–7	53.26	56.20	0.26	NA	NA	NA	NA	NA	NA
13X-CC, 0–18	56.59	59.53	0.29	0.17	0.25	0.94	609	86	323
14X-CC, 0–14	63.33	63.33	0.30	0.09	0.22	0.39	480	74	131
16X-2, 138–144	71.91	72.25	0.30	0.09	0.22	0.72	481	74	241
16X-CC, 0–19	72.44	72.78	0.28	NA	NA	NA	NA	NA	NA
17X-CC, 0–20	76.00	76.00	0.29	0.08	0.16	0.61	608	55	210
18X-1, 132–138	79.35	79.35	0.24	NA	NA	NA	NA	NA	NA
18X-CC, 0–15	80.08	80.08	0.29	0.06	0.18	0.32	477	61	109
19X-CC, 0–1	81.21	81.21	0.28	NA	NA	NA	NA	NA	NA
20X-CC, 0–9	90.93	90.93	0.26	NA	NA	NA	NA	NA	NA
21X-2, 137–143	94.11	94.11	0.33	0.10	0.29	0.45	475	88	137
21X-CC, 0–14	94.64	94.64	0.29	0.12	0.19	0.81	477	65	279
23X-1, 0–13	101.27	101.27	0.27	NA	NA	NA	NA	NA	NA
24X-CC, 0–23	110.80	110.80	0.34	0.10	0.25	0.59	475	74	175
27X-CC, 0–8	123.84	123.84	0.29	0.13	0.26	0.58	476	89	198
28X-CC, 0–10	127.49	127.49	0.38	0.08	0.23	0.30	479	60	79
29X-CC, 0–14	132.10	132.10	0.23	NA	NA	NA	NA	NA	NA
31X-CC, 0–15	136.13	139.13	0.19	NA	NA	NA	NA	NA	NA
32X-CC, 0–15	144.95	144.95	0.29	0.07	0.23	0.33	477	79	114
33X-CC, 0–20	147.97	148.77	0.29	0.10	0.21	0.27	473	71	92
34X-CC, 0–18	151.96	151.96	0.19	NA	NA	NA	NA	NA	NA
35X-CC, 0–8	158.83	158.83	0.22	NA	NA	NA	NA	NA	NA
36X-CC, 0–21	159.11	159.11	0.19	NA	NA	NA	NA	NA	NA
38X-CC, 0–11	171.76	171.76	0.10	NA	NA	NA	NA	NA	NA
39X-CC, 0–23	171.60	172.80	0.06	NA	NA	NA	NA	NA	NA
40X-CC, 0–12	178.30	178.30	0.09	NA	NA	NA	NA	NA	NA
41X-CC, 0–17	178.67	178.67	0.10	NA	NA	NA	NA	NA	NA
42X-CC, 0–16	187.33	187.33	0.10	NA	NA	NA	NA	NA	NA
44X-CC, 0–20	195.83	195.83	1.00	0.15	1.71	0.99	429	171	99
45X-CC, 0–18	197.33	197.33	0.72	0.17	0.79	0.60	420	110	84
46X-CC, 0–9	200.59	201.16	2.89	0.22	3.64	3.23	406	126	112
47X-CC, 0–19	207.40	206.84	2.09	0.29	2.15	2.11	388	103	101
48X-CC, 0–12	210.64	211.78	2.81	0.36	2.48	2.70	391	88	96
49X-CC, 0–16	215.42	217.74	2.55	0.26	2.41	1.83	398	94	72
50X-CC, 0–10	217.19	220.07	1.58	0.22	1.45	1.13	395	92	71
54X-CC, 0–7	230.48	232.50	2.33	0.47	3.29	1.60	385	141	69
55X-CC, 0–10	240.36	241.43	2.86	0.89	5.44	1.56	385	190	55
56X-CC, 0–30	243.09	244.91	2.93	0.68	4.41	1.84	388	151	63
57X-CC, 0–17	250.03	251.85	2.03	0.67	4.33	1.49	387	213	73
58X-CC, 0–11	254.77	256.59	3.15	0.95	7.63	1.96	395	243	62
59X-CC, 0–9	259.03	260.85	1.70	0.83	5.75	1.45	400	339	85
61X-CC, 0–16	265.37	267.25	2.31	0.70	5.00	1.75	386	217	76
62X-CC, 0–10	271.64	273.46	2.99	0.86	6.98	1.93	394	234	65
302-M0004A-									
4X-CC, 0–1	265.01	265.01	2.27	0.71	4.66	1.75	384	206	77
6X-CC, 0–18	278.69	278.69	2.70	0.86	6.90	1.69	388	255	63
8X-CC, 0–7	282.55	286.55	2.51	0.61	4.50	1.46	389	179	58
9X-CC, 0–9	287.62	287.62	2.61	0.62	6.31	1.71	387	242	66
10X-CC, 0–15	297.12	297.12	2.63	0.97	8.35	1.43	389	317	54
11X-CC, 0–23	302.62	302.62	4.23	0.55	5.67	2.38	385	134	56
12X-CC, 0–2	301.36	301.36	3.24	0.63	5.39	2.32	386	166	72
19X-CC, 0–16	323.62	323.62	1.51	0.61	3.32	0.81	372	219	54
20X-CC, 0–21	328.18	328.18	1.65	0.43	2.57	0.75	371	156	46
21X-CC, 0–20	332.76	332.76	0.90	0.47	1.89	0.45	368	210	50
22X-CC, 0–13	339.92	339.92	1.55	0.76	3.96	0.82	367	255	53
23X-CC, 0–22	345.56	345.56	2.46	0.92	6.07	0.96	371	247	39
27X-CC, 0–5	372.23	372.23	0.92	0.17	0.67	0.52	419	73	56
28X-CC, 0–5	377.01	377.48	1.58	0.24	1.75	0.57	418	111	36

Table T44 (continued).

Core, section, interval (cm)	Top depth (mbsf)	Top depth (mcd)	TOC (wt%)	S1 (mg HC/g sed)	S2 (mg HC/g sed)	S3 (mg CO_2/g sed)	T_{max} (°C)	HI (mg HC/g C)	OI (mg CO_2/g C)
302-M0002A-									
29X-CC, 0–12	377.06	379.06	2.06	0.12	2.62	0.67	421	127	32
30X-CC, 0–12	384.48	384.48	2.25	0.24	7.73	0.93	414	344	41
31X-CC, 0–55	383.48	384.98	2.00	0.32	6.78	0.87	412	340	44
32X-CC, 0–18	390.95	390.95	1.68	0.17	0.78	1.62	426	46	97
33X-CC, 0–15	394.08	394.08	1.54	0.13	0.61	1.62	423	40	105
35X-CC, 0–18	404.70	404.70	1.57	0.17	1.08	3.76	429	69	240
41X-CC, 0–5	424.81	424.81	0.91	0.08	0.99	0.23	421	109	25
42X-CC, 0–23	427.55	427.55	1.18	0.10	1.35	0.39	420	114	33

Note: TOC = total organic carbon, HI = hydrogen index, OI = oxygen index.

Table T45. Samples examined by scanning electron microscope.

Hole, section, interval (cm)	Macroscopic description	EDS peaks	Other analyses
302-			
M0002A-18X, 1, 143–150 cm	Rock fragment (sandy claystone?)	Al, Si, K, Fe	
M0002A-6X, CC, 0–3 cm	Mn-rich cemented conglomerate	Al, Si, K, Ca, Mn, Fe	XRD, XRF
M0004A-18X, CC	Dark layers—chert	Si, Fe	
M0004A-18X, CC	Light layers—chert	Si, Fe	
M0004A-15X, CC, cuttings	>64 µm grains, chert	Si	XRF
M0002A-40X, 2, 144–151 cm	Rock fragment (silty claystone?)	Al, Si, K, Fe, Ti	XRF
M0002A-1X, 2, 5 cm	Rock fragment (silty claystone?)	Al, Mg, Si, Cl, K, Mn, Fe	XRD, XRF
M0004A-28X, 1, 62–63 cm	Pyrite tubes	S, Fe	
M0002A-40X, 3, 43–45 cm	Red/Black "tubes"	Al, Mg, Si, K, Fe, Mn	
M0002A-28X, 1, 117–120 cm	Pyrite	S, Fe	
M0004A-28X, 2, 21–23 cm	Pyrite	S, Fe	
M0002A-40X, 3, 67–68 cm	Fe-rich "tubes"	Fe, Al, Si	
M0004A-27X, 4, 14–15 cm	Pyrite	S, Fe	

Notes: EDS = energy dispersive spectrometer. XRD = X-ray diffraction, XRF = X-ray fluorescence.

Table T46. Microbiology sample log.

Core, section, interval (cm)	Depth (mbsf)	Preservation method		
		Anaerobic (4°C)	Formalin (4°C)	Frozen (–80°C)
302-M0002A-				
3X-2, 140–145	12.07	X	X	X
6X-2, 140–145	28.50	X	X	X
10X-2, 138–144	47.07	X	X	X
12X-2, 86–92	54.72	X	X	X
16X-2, 138–144	71.81	X	X	X
18X-1, 132–138	72.45	X	X	X
21X-2, 137–143	93.87	X	X	X
23X-2, 108–114	101.93	X	X	X
24X-2, 138–144	103.20	X	X	X
27X-2, 140–144	122.61	X	X	X
30X-2, 139–144	130.21	X	X	X
33X-2, 139–144	142.03	X	X	X
37X-2, 139–144	164.82	X	X	X
40X-2, 139–144	169.09	X	X	X
56X-2, 145–152	241.74	X	X	X
302-M0003A-				
1H-1, 148–150	6.55	X		
2H-1, 148–150	9.29	X		
302-M0004A-				
6X-2, 140–145	270.47	X	X	X
10X-2, 137–143	293.83	X	X	X
19X-1, 142–144	321.43	X	X	
23X-1, 139–144	342.51	X		X
28X-1, 148–150	373.30	X		
34X-1, 142–144	398.41	X	X	